Mass Spectrometry-Based Approaches to Identify Novel Interaction Partners of the Tyrosine Phosphatase DEP-1

Dissertation

zur

Erlangung der naturwissenschaftlichen Doktorwürde
(Dr. sc. nat.)

vorgelegt der

Mathematisch-naturwissenschaftlichen Fakultät

der

Universität Zürich

von

Michael Simon Walser

aus

Teufen AR

Promotionskomitee

Prof. Dr. Alex Hajnal (Vorsitz)
Prof. Dr. Michael Hengartner
Prof. Dr. Gert Jansen
Prof. Dr. Fritz Müller

Zürich, 2013

Für Ärnschtu und Dädät
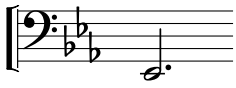
Zusammenfassung

Eine der wichtigsten post-transkriptionellen Protein-Modifikationen ist die reversible Phosphorylierung. Katalysiert durch Kinasen und Phosphatasen spielt die Phosphorylierung bzw. Dephosphorylierung von Proteinen eine bedeutende Rolle in der Regulation verschiedenster zellulärer Prozesse, wie z.B. in der Regulation des Zell-Zykluses, bei der Wachstumskontrolle, der Apoptose und in der Steuerung von Signalwegen. Eine abnormale Proteinphosphorylierung kann Ursache vieler verschiedener menschlicher Krankheiten sein, weshalb ein Verständnis dieser Modifikation von wichtiger Bedeutung ist.
Der stark konservierte EGFR/RAS/MAPK Signalweg ist der vermutlich am besten untersuchte Signaltransduktionsweg in der Zellbiologie. Er spielt eine bedeutende Rolle in verschiedensten Vorgängen der Entwicklung sowie bei der Entstehung von Krebs. Seine Aktivität wird durch Proteinphosphorylierung moduliert und durch ein komplexes Netzwerk negativer Regulatoren kontrolliert. Einer dieser Regulatoren ist die Protein Tyrosin Phosphatase DEP-1, welche den EGF Rezeptor und andere Rezeptor Tyrosin Kinasen dephosphoryliert. DEP-1 gehört somit zu den Tumorsuppressoren und ist in zahlreichen menschlichen Tumoren mutiert, wie z.B. in Schilddrüsen-, Darm-, Lungen-, Prostata- und Brustkrebs.
Das Ziel dieser Arbeit war, neue Interaktionspartner von DEP-1 im Nematoden *C. elegans* zu finden. Hierzu reinigte ich verschieden Varianten von markiertem DEP-1 aus *C. elegans* oder *E. coli* auf, und identifizierte mittels Massenspektrometrie die Proteine, welche an DEP-1 binden. Dabei entdeckte ich die β-Integrin Untereinheit PAT-3 als neues Substrat von DEP-1. Integrine sind heterodimere Membranproteine bestehend aus nicht-kovalent verbundenen α und β Untereinheiten, welche unter anderem für die Interaktion von Zellen mit der extrazellulären Matrix sowie für die Aktivierung zahlreicher Signalwege bedeutsam sind. Sie spielen eine Schlüsselrolle während der Entwicklung, der Immunabwehr, Blutstillung und der Krebsentstehung, und können somit Ursache vieler menschlicher Krankheiten sein.
Anhand verschiedener biochemischer Experimente konnte ich zeigen dass DEP-1 ein konserviertes NPxY Motiv von PAT-3 dephosphoryliert. DEP-1 hat somit eine regulatorische Rolle in der Integrin Aktivierung.
Ausserdem untersuchte ich die Interaktion von DEP-1 und PAT-3 *in vivo* während der Entwicklung der Vulva von *C. elegans*. Die Vulva ist ein 22-zelliges Organ, durch das der Hermaphrodit seine Eier ablegt. Sie wird von drei Vulvavorläuferzellen gebildet, deren Differenzierungen durch ein Zusammenspiel vom EGFR/RAS/MAPK, DELTA/NOTCH sowie dem WNT Signalweg gesteuert werden. Meine genetischen Experimente zeigten, dass DEP-1 das NPxY Motiv von PAT-3 dephosphoryliert, um die Integrine zu aktivieren. Als Folge davon inhibieren aktivierte Integrine den RAS/MAPK Signalweg in den sekundären Vulvavorläuferzellen.
Diese Ergebnisse zeigen eine bisher unbekannte Rolle von DEP-1 und den Integrinen in der Regulation des EGFR/RAS/MAPK Signalwegs, und tragen zu einem besseren Verständnis der Funktion und Regulierung der Integrine *in vivo* bei.

Summary

Reversible protein phosphorylation is one of the most important and well-studied post-translational modifications. Catalyzed by protein kinases and protein phosphatases, phosphorylation and dephosphorylation play a critical role in the regulation of many cellular processes, such as cell cycle, cell growth, apoptosis and signal transduction pathways. Abnormal protein phosphorylation can be a cause of human diseases, for which reason an understanding of this modification is of major importance.
The highly conserved EGFR/RAS/MAPK signaling pathway is probably the best characterized signal transduction pathway in cell biology and plays a crucial role in many developmental processes and cancer formation. Its activity is regulated through protein phosphorylation and controlled by a broad negative regulatory network that attenuates the different components of the EGFR/RAS/MAPK pathway. A member of this network is the density enhanced phosphatase DEP-1, which belongs to the receptor protein tyrosine phosphatases. It inhibits EGFR/RAS/MAPK signaling through dephosphorylation of the EGF receptor and thereby acts as a tumor suppressor. It has been found that DEP-1 is frequently deleted and mutated in various human cancers such as thyroid, colon, lung, pancreatic, and breast cancer.
In order to identify novel physiological substrates of DEP-1 in the nematode *C. elegans*, I performed affinity purifications of differently tagged versions of DEP-1 that were expressed in *C. elegans* or *E. coli*. Proteins that bound to DEP-1 were then identified by mass spectrometry. Thereby, the β-integrin subunit PAT-3 was found as a novel substrate of DEP-1. Integrins are non-covalently associated α/β heterodimers that mediate cell adhesions, make transmembrane connections to the cytoskeleton and activate many intracellular signaling pathways. Playing key roles in development, immune response, hemostasis and cancer formation, Integrins are at the heart of many human diseases.
By performing several biochemical experiments, I could show that DEP-1 binds to the evolutionary conserved NPXY motif of the PAT-3 cytoplasmic tail, the phosphorylation of which plays a regulatory role in integrin activation.
Furthermore, I investigated the interaction of DEP-1 and PAT-3 *in vivo* during development of the *C. elegans* hermaphrodite vulva. This simple egg-laying organ is formed by 22 cells and originates from three vulval precursor cells (VPCs), whose cell-fates are determined by the interplay of the EGFR/RAS/MAPK, DELTA/NOTCH, and WNT signaling pathways.
My genetic experiments could show that DEP-1 dephosphorylates the NPXY motif of PAT-3 to promote its activation. As a consequence, activated integrins inhibit the RAS/MAPK signaling pathway in the secondary VPCs.
Together, my results demonstrate a novel role of DEP-1 and the integrins during vulval development and give further insights into integrin regulation *in vivo*.

Contents

1

Introduction

1.1 The model organism *C. elegans*

Caenorhabditis elegans is a small, free-living, non-parasitic nematode that lives in nutrient- and microorganism-rich habitats such as compost, mushroom beds and garden soil where it feeds on bacteria and probably on other microorganisms (Wood, 1988). In Latin, the name of this approximately 1.3 mm-long roundworm means "recent" (*caeno*), "rod-like" (*rhabditis*) and "nice" (*elegans*): a newly discovered rod-like animal, which elegantly moves forward and backward in sinoidal waves.
In the early 70s, Sydney Brenner established *C. elegans* as a model organism to study various aspects of cell biology, developmental biology and behavior (Brenner, 1974). Nowadays, it is one of the most popular model organisms due to several attractive features, such as its short generation time, small size, cheap and space-saving maintenance, transparent body, the capability of keeping it frozen in -80°C indefinitely, and an invariant cell lineage.
The wild-type strain, named N2, was originally collected from compost near Bristol, England and defined as wild-type in the year 1965 (Wood, 1988). In the laboratory, the worms grow on agar plates seeded with genetically modified *E. coli* as food supply. The *E. coli* strain OP50 is more translucent than standard laboratory strains, facilitating the investigation of the worms under the microscope.
C. elegans has a short generation time, requiring 3.5 days going from the single-celled egg to adulthood (Fig. 1.1). After the embryo has hatched, the larva goes through four stages (L1 to L4) before becoming a mature adult. In response to overcrowding and in the absence of adequate food supply, *C. elegans* can undergo an alternative L3 stage, called dauer larva. This dauer larva can remain viable for as long as three months while it roams around in search of food.

In *C. elegans* there are two sexes, males and hermaphrodites (Fig. 1.2). The predominant sexual form is the hermaphrodite, which produces both sperm and eggs and has thus the ability of self-fertilization. Thus, in nature consist most populations of clones, meaning that the animals are the offspring of a single hermaphrodite. *C. elegans* is extremely fecund; one hermaphrodite can produce about 300 to 350 offspring by self-fertilization and even more if it mates with a male. These traits make it easy to produce numerous genotypes and phenotypes for genetic research (Ferguson and Horvitz, 1985; Tax et al., 1997).

The roundworm has five pairs of autosomes and one pair of sex chromosomes. In 1998 its genome was the first animal genome to be sequenced and comprises about 19'000 genes (*C. elegans* Sequencing Consortium, 1998). Approximately 35% of the *C. elegans* genes are closely related to human genes.
The gender of *C. elegans* is defined by the ratio of autosomal to sex-chromosomes: Hermaphrodites have two X-chromosomes, but can spontaneously generate X0 males by nondisjunction of the X-chromosome, which happens at a frequency of 0.1% (wormbook.org).
In 2002, Sydney Brenner (GB), H. Robert Horvitz (USA) and John E. Sulston (GB) received the Nobel Prize for Physiology and Medicine for their research in "genetic regulation of organ development and programmed cell death" in *C. elegans*.

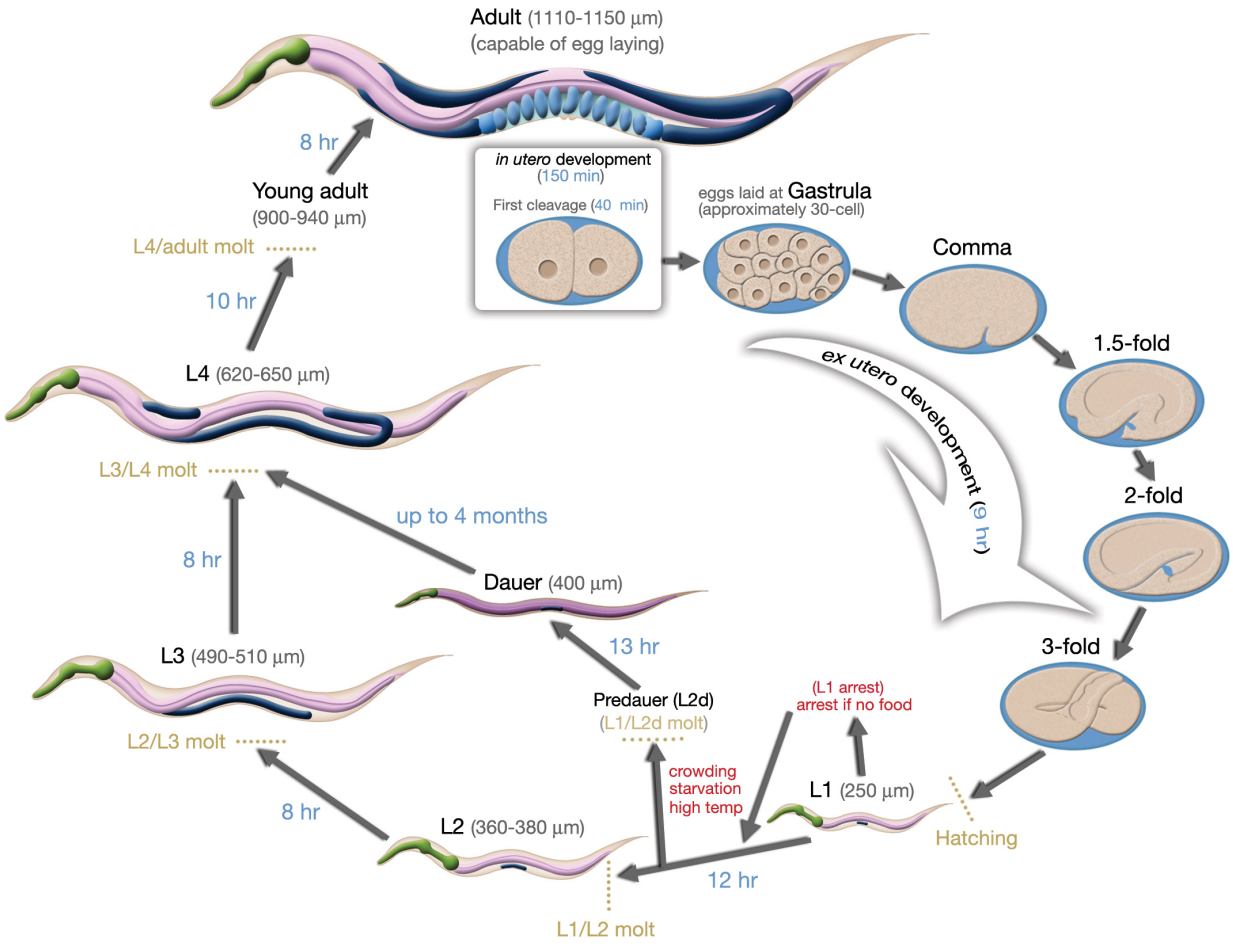

Figure 1.1 Life cycle of *C. elegans*.
After cleavage and embryogenesis there are four larval stages (L1 - L4) before the sexually mature adult is developped. Under crowded conditions and with limited food, the L1 larvae can enter an alternative developmental program called the dauer stage. (From www.wormatlas.org).

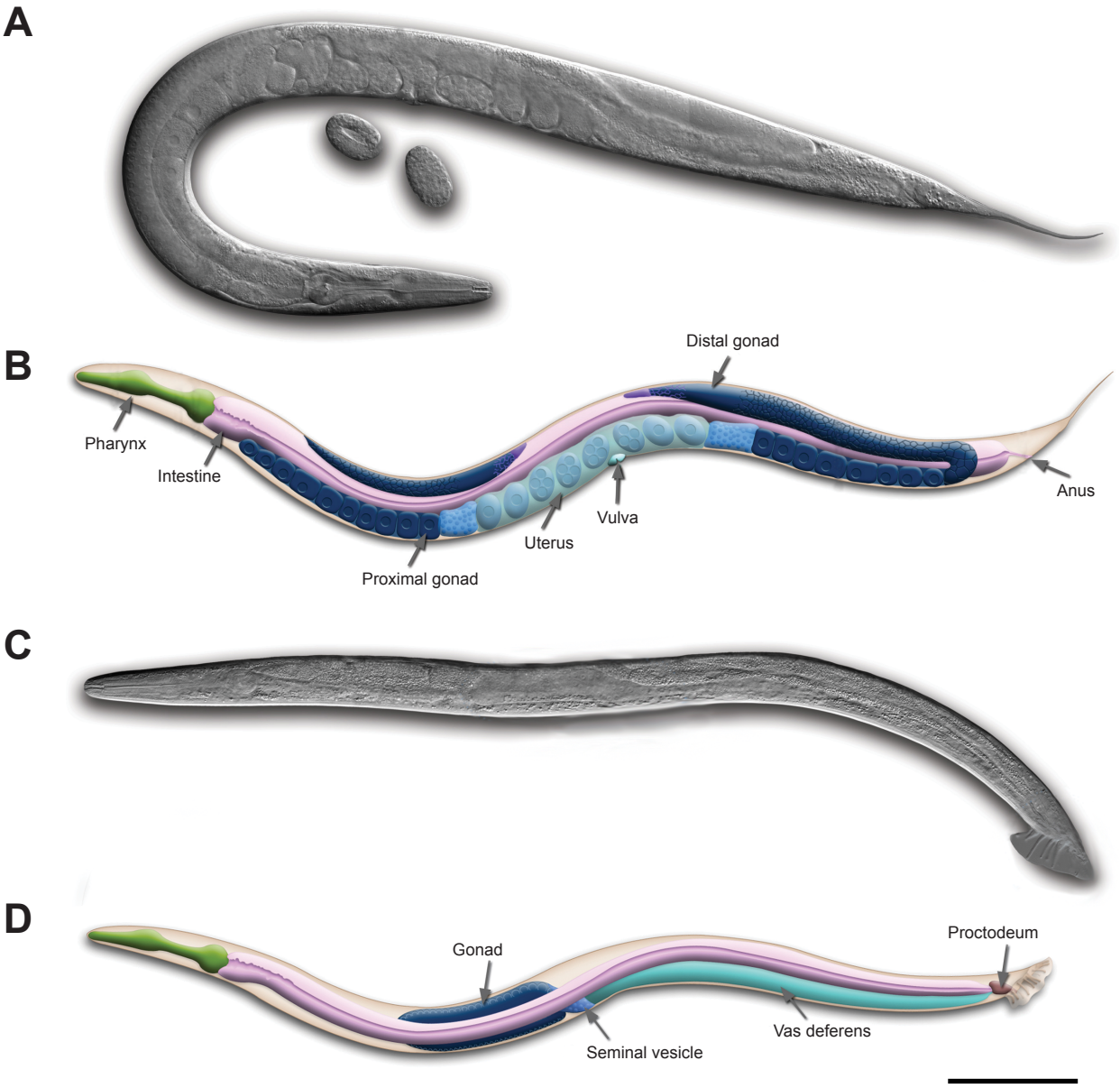

Figure 1.2 Sexes of *C. elegans*.
(**A**) Nomarski image of an adult hermaphrodite and (**B**) schematic drawing of its anatomical structures. (**C**) Nomarski image of an adult male and (**D**) schematic drawing of its anatomical structures, left lateral side. Scale bar represents 0.1 mm. (Adapted from www.wormatlas.org).

1.2 The vulva of *C. elegans*

The vulva of the hermaphrodite *C.elegans* is located on the ventral side of the mid section of the body, and consists of 22 cells forming a passage, through which sperm from males can enter and fertilized eggs can be laid (Fig. 1.2, 1.4 I). Vulval development occurs over a period of 20 hours and is one of the best-studied processes in animal development. The cells that form the vulva adopt an invariant pattern of cell fates, and disruption of this pattern by the creation of mutations within genes involved in vulval formation leads to the development of malformed vulvae. Vulval development is genetically amenable because mutations that affect vulval development are often viable and the corresponding phenotypes are easily discernable under the microscope making it a practical model to study organogenesis.
Since several evolutionary conserved signaling pathways such as the EGFR/RAS/MAPK, DELTA/NOTCH and Wnt pathways are involved, vulval development provides a simple model for the genetic and molecular analysis of pattern formation and organ morphogenesis during metazoan development (Horvitz and Sternberg, 1991).
Several human genes that play a key role in diseases such as Cancer or Alzheimer's have their *C.elegans* counterparts that control vulval development. Thus, the investigation of vulval development may lead to new effective therapeutic approaches for treating these diseases.

1.2.1 The vulval precursor cells

During the first larval stage, six equipotent vulval precursor cells (VPCs), termed P3.p through P8.p, are selected from 12 epithelial Pn.p cells, which are positioned along the ventral midline of the developing larva (Sulston and Horvitz, 1977). As a result of two signaling events, the VPCs adopt one of three different vulval fates at the early L3 stage (Fig. 1.3 A; Félix, 2012). The VPC fates differ in the cell lineage they produce: P6.p adopts a primary cell fate (1°) and divides three times to produce eight progeny cells that will form the inner part of the vulva. P5.p and P7.p adopt a secondary cell fate (2°) and undergo three rounds of cell divisions to produce seven progeny cells each, which will form the outer part of the vulva (Schindler and Sherwood, 2013; Sternberg and Horvitz, 1986; Sulston and White, 1980). The 1° and 2° fates are collectively referred to as vulval fates since only cells, which adopt a 1° or 2° fate contribute to the mature vulva. The other VPCs (P3.p, P4.p and P8.p) adopt a tertiary non-vulval cell fate (3°) and undergo one round of cell division before they fuse with the *hyp7*, the hypodermal syncytial cell that surrounds the VPCs.
In the late L3 and L4 stages, the descendants of the 1° and 2° cells undergo morphogenic movements and cell fusions to form a tube, consisting of seven toroidal rings that form the mature vulva (Schindler and Sherwood, 2013; Sharma-Kishore et al., 1999). During morphogenesis, the vulval cells also attach to the vulval muscles that control egg laying by regulating the opening of the vulva.

1.2.2 The inductive signal

At the beginning of the third larval stage (L3), the anchor cell (AC), a specialized cell in the somatic gonad, induces the underlying VPCs by secreting the epidermal growth factor (EGF) like ligand LIN-3 in a graded fashion (Fig. 1.3 B; Kornfeld, 1997; Sternberg and Han, 1998). All VPCs are equally competent to respond to the AC signal, but P6.p is closest to the AC. Therefore, P6.p receives the highest

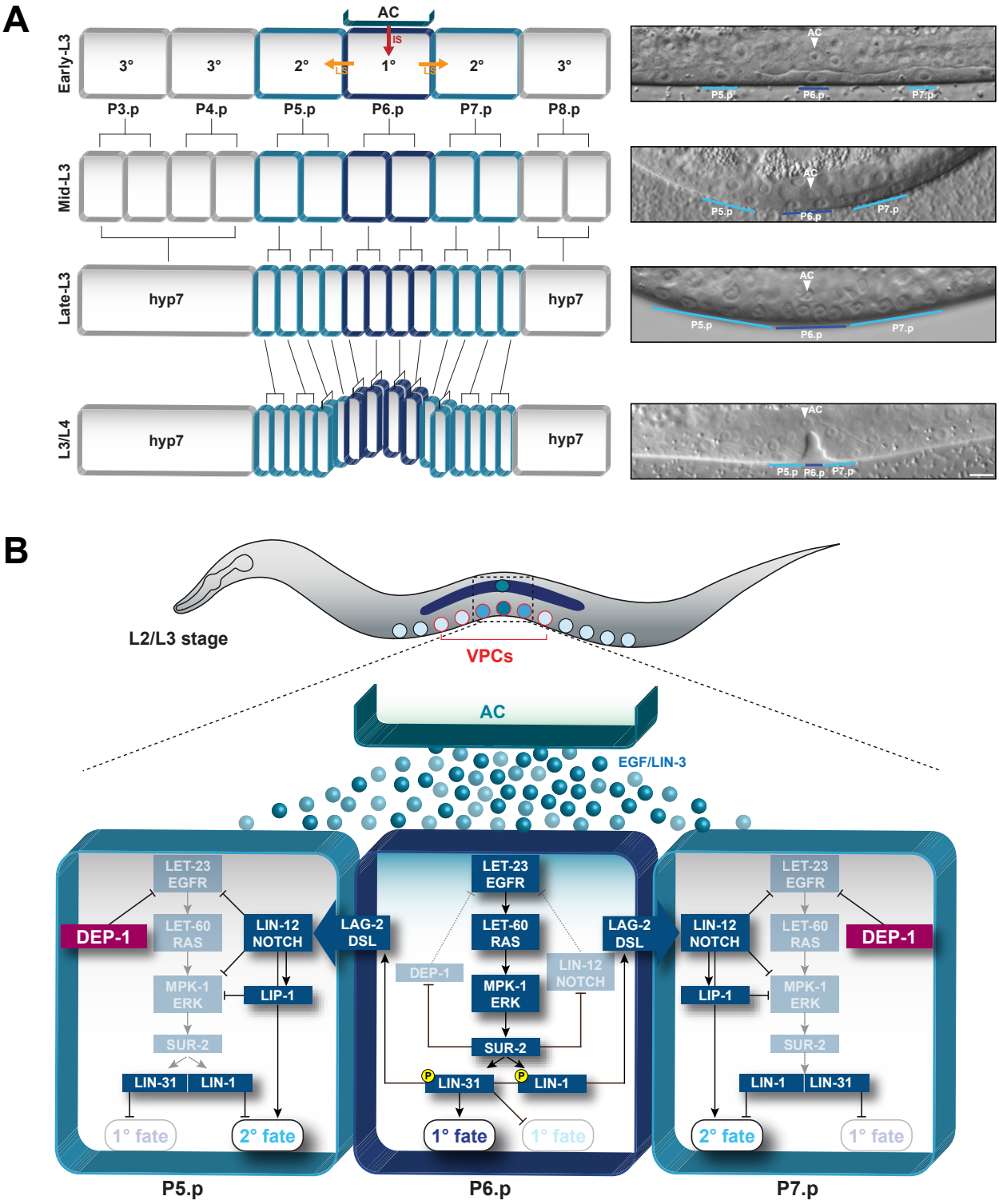

Figure 1.3 Vulval development.

(**A**) After the inductive signal (IS) is secreted by the anchor cell (AC), P6.p adopts the 1°Cell fate and divides three times to produce eight progeny cells. The lateral signal (LS) causes P5.p and P7.p to adopt the 2°Cell fate. They divide symmetrically twice, and once asymmetrically, to produce seven progeny cells. The other VPCs (P3.p, P4.p and P8.p) adopt the 3°Cell fate and fuse with the hypodermis (*hyp7*). (**B**) The AC triggers the evolutionarily conserved EGFR/RAS/MAPK pathway to specify the 1°Cell fate in P6.p. In addition, activation of LET-23/EGFR in P6.p also results in the production of a lateral signal via LIN-12/NOTCH that induces the adjacent VPCs (P5.p and P7.p) to adopt the 2°Cell fate. DEP-1 and LIP-1 block the transduction of the inductive AC signal in P5.p and P7.p.

possible level of inductive signal and thus adopts the 1° cell fate. P5.p and P7.p being further away from the AC receive lower levels and thereby adopt the 2° fate. P3.p, P4.p, and P8.p receive even less (or no) inductive signal, which results in the non-vulval 3° fate.
LIN-3/EGF binds to the EGF receptor tyrosine kinase (EGFR) homolog LET-23, which is initially expressed in all VPCs and activates the highly conserved EGFR/RAS/MAPK-pathway (Fig. 1.3 B; Sternberg and Han, 1998). LIN-1, an ETS domain containing transcription factor, is a crucial target of the EGFR/RAS/MAPK signaling pathway and acts as an inhibitor of vulval induction (Beitel et al., 1995). In the absence of the inductive signal, LIN-1 forms a hetero-dimer with LIN-31, a forkhead transcription factor, resulting in the inhibition of a vulval cell fate (Miller et al., 1993; Tan et al., 1998).
During vulval induction, LIN-1 and LIN-31 are both phosphorylated by MPK-1 in P6.p, leading to a disruption of the heterodimeric complex (Fig. 1.3 B). Thereafter, LIN-31 is able to induce the transcription of genes specific for 1° cell fate adoption, while LIN-1 is able to relief the VPC-wide *lag-2* repression in P6.p (Zhang and Greenwald, 2011). In P5.p and P6.p, the inhibitory effect of the hetero-dimer is overcome by the activation of several 2° cell fate specific target genes via the lateral signal (Félix, 2012).

1.2.3 The lateral signal

After P6.p has received the instructive signal from the AC, the lateral signal from P6.p activates the highly conserved LIN-12/NOTCH signaling pathway in the adjacent cells P5.p and P7.p to specify the 2°-1°-2° pattern of vulval cell fates (Sternberg, 1988; Wang and Sternberg, 2001; Yochem et al., 1988).
The high level of EGFR/RAS/MAPK signaling in P6.p down-regulates the LIN-12/NOTCH receptor via SUR-2, and reliefs the VPC-wide repression of LAG-2 by LIN-1 phosphorylation (Fig. 1.3 B; Shaye and Greenwald, 2002; Zhang et al., 2005). These ligands bind to the LIN-12/NOTCH receptor in P5.p and P7.p and activate the LIN-12/NOTCH pathway.
LIN-12/NOTCH signaling antagonizes the EGFR/RAS/MAPK activity by stimulating the transcription of various negative regulators such as *lip-1* and *lst-1 – lst-4* (Berset et al., 2001; Yoo et al., 2004). The outcome of this is a feedback loop where low EGFR/RAS/MAPK releases the LIN-12/NOTCH suppression by SUR-2. Beside this inhibition of the 1° cell fate in P5.p and P7.p, it has been suggested that LIN-12/NOTCH also plays an instructive role in specifying the 2° fate in these cells (Ambros, 1999; Sternberg and Horvitz, 1989).

1.2.4 The inhibitory signals

In addition to the inductive and the lateral signal, other signaling events impact on VPC fates. The synMuv (synthetic Multivulva) genes ensure that the distal VPCs P3.p, P4.p and P8.p adopt the tertiary (3°) non-vulval fate (Fig. 1.3 A; Fay and Yochem, 2007). They are grouped into three classes: *synMuvA*, *synMuvB*, and *synMuvC*. Most mutants of single *synMuv* genes do not exhibit defects during vulval development. However, a loss-of-function combination of *synMuv* class A with *synMuv* class B leads to a highly penetrant synthetic Muv phenotype (Fay and Yochem, 2007). Class C *synMuv* mutants elicit a Muv phenotype only in combination with a mutant of either class A or class B (Fay and Yochem, 2007). The *synMuv* genes repress *lin-39* in the distal VPCs that promotes their fusion to the hypodermal *hyp7* syncytium (Chen and Han, 2001). *hyp7* in turn represses the transcription of *lin-3* to prevent the VPCs from adopting a vulval cell fates (Cui et al., 2006).

1.3 Vulval induction index - a readout for RAS/MAPK signaling

All six VPCs have the equal developing potential to adopt one of the three vulval cell fates, and in wild-type animals, three out of the six VPCs are induced (vulval induction index = 3). However, in mutants where EGFR/RAS/MAPK signaling is elevated, e.g. in *let-60(gf)* animals, more than three VPCs are induced (vulval induction index of >3), resulting in a "multivulva" (Muv) phenotype (Félix, 2012).
Vice versa, when fewer than three cells are induced, the animals have a vulval induction index <3 and exhibit a "vulvaless" (Vul) phenotype. In these mutants, the progeny hatches and grows inside the hermaphrodite's body which is not able to lay eggs (Sternberg and Horvitz, 1986).
Hence, by counting the induced VPCs and by calculating the vulval induction index, it is possible to draw conclusions about the activity of EGFR/RAS/MAPK signaling in the different mutant backgrounds. This makes vulval development an excellent tool to study activities of signaling pathways.

1.4 Negative regulators of the EGFR/RAS/MAPK signaling pathway

1.4.1 Lateral signal induced phosphatase LIP-1

One of the target genes of the LIN-12/NOTCH pathway is the Lateral signal Induced Phosphatase-1 (LIP-1), a dual-specific phosphatase that inactivates the MAP kinase MPK-1 by dephosphorylation to inhibit 1° fate specification in P5.p and P7.p (Berset et al., 2001). *lip-1(lf)* animals contain higher levels of MAP kinase enzymatic activity, increasing the sensitivity of the VPCs toward the inductive signal. Since *lip-1(lf)* does not cause other defects in a wild-type background (Fig. 1.4 C), it is assumed that there are multiple LIN-12 target genes that act in a redundant manner (Berset et al., 2001).

1.4.2 Density enhanced phosphatase DEP-1

In a screen done in a sensitized *lip-1(lf)* background for genes that regulate the 1° versus 2° cell fate decision during vulval development, the receptor-type protein tyrosine phosphatase (R-PTP) DEP-1 was found (Berset, 2005). Further analyses have shown that DEP-1 negatively regulates LET-23 EGFR signaling in the vulva.
DEP-1::GFP is expressed at equal levels in P5.p, P6.p, and P7.p at the time of vulval induction. However, after the first round of cell division, DEP-1::GFP is down-regulated in the 1° lineage, but its expression persists in the 2° vulval cells until the L4 stage (Berset, 2005).
As in *lip-1(lf)* animals, vulval development appears normal in *dep-1(lf)* single mutants (Fig. 1.4 B). In contrast, *dep-1(lf);lip-1(lf)* double mutants show an adjacent primary fate (APF) phenotype, in which P5.p and P7.p descendants adopt a hybrid cell fate with 2° and 1° characteristics (Fig. 1.4 D, F, and H). In addition, *dep-1(lf);lip-1(lf)* animals exhibit a weak multivulva (Muv) phenotype due to an ectopic induction of P3.p, P4.p, or P8.p (Berset, 2005).
The transformation of cell fate can be visualized by analyzing the expression pattern of the 2° cell specific marker LIN-11::GFP, whose expression is absent or strongly reduced in most 2° cells of *dep-1(lf);lip-1(lf)* animals (Fig. 1.3 E and F).

DEP-1 (also known as PTPRJ, PTP-η or CD148) encodes a protein of 1367 amino acids and belongs to the class III R-PTP family (Hertog et al., 1999). Its expression is directly related to cell density – hence the name Density-Enhanced Phosphatase 1 (Östman et al., 1994).
Among the 100 PTPs encoded in the human genome 21 are R-PTPs, four of which are classified as class III. Characteristic for class III R-PTP, DEP-1 contains an intracellular catalytic tyrosine phosphatase domain, a single transmembrane domain, and multiple extracellular fibronectin type III repeats (Fig. 1.5 B). Furthermore, DEP-1 is highly glycosylated and contains multiple N-glycosylation sites in the extracellular region (Krueger et al., 1990; Matozaki et al., 1994; Thomas et al., 1994; Tonks, 2006).
The specificity for particular substrates of PTPs is a result of the configuration of the PTP active site. A characteristic of all members of the PTP family is the presence of a signature motif, [I/V] HCXXGXXR[S/T] (Fig. 1.5 C [1]), where the cysteine residue is essential for catalysis (Tonks, 2003).
In the intracellular COOH-terminal region, vertebrate PTPs share a common YxNΦ motif. The tyrosine of this motif can be phosphorylated to promote binding of Src-family kinases (Murata et al., 2010). Additionally, the phosphyorylated YxNΦ motifs serve as binding sites for the Src homology (SH) 2 domains. "Substrate-trapping" mutants of R-PTPs form stable complexes with receptor tyrosine kinases (RTKs), suggesting that RTKs are direct targets for R-PTP enzymatic activity (Flint et al., 1997; Jeon et al., 2012). However, this YxNΦ motif is not present in *C. elegans* DEP-1.

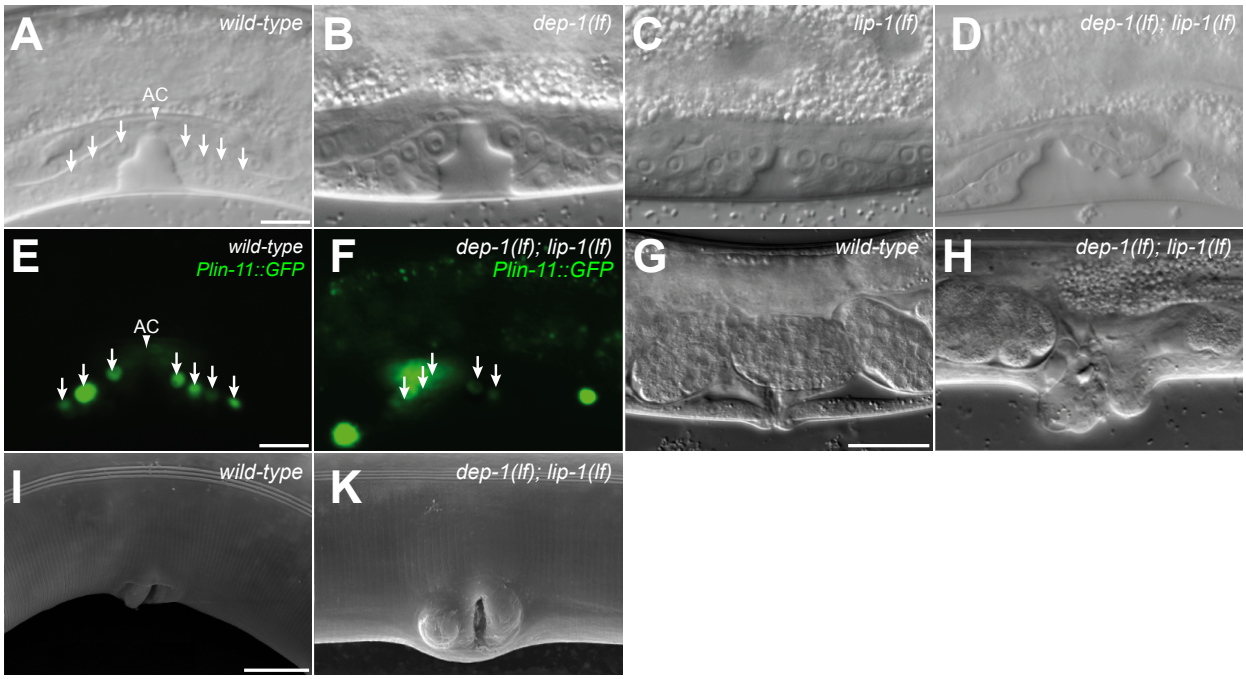

Figure 1.4 *dep-1(lf);lip-1(lf)* double mutants exhibit an adjacent primary fate phenotype.
Nomarski images of (**A**) wild-type, (**B**) *dep-1(lf);lip-1(lf)*, (**C**) *dep-1(lf)*, and (**D**) *lip-1(lf)* vulvae in L4 larvae. (**B**) In the *dep-1(lf);lip-1(lf)* mutant, the descendants of P7.p have detached from the cuticula and moved inward. (**E**) *Plin-11::GFP* expression in the P5.p and P7.p descendants of wild-type L4 larva and in *dep-1(lf);lip-1(lf)* mutants (**F**), in which *Plin-11::GFP* expression is strongly reduced. Adult vulvae of wild-type (**G**) and *dep-1(lf);lip-1(lf)* animals (**H**), exhibiting a protrusion of the vulva tissue, due to a mixed 1°/2°Cell fate of the P5.p and P7.p descendants. (**I**) Scanning electron micrographs of an adult vulva in a wild-type and (**K**) a *dep-1(lf);lip-1(lf)* double mutant. Arrows point to the *Plin-11::GFP* expressing vulval cells. AC: Anchor cell. Scale bars represent 10 µm.

DEP-1 tends to be expressed specifically at the apical surface of polarized cells, and it is most abundant in endothelial cells and various types of hematopoietic cells, but also in epithelial cells and fibroblasts (Autschbach et al., 1999; Borges et al., 1996; la Fuente-García et al., 1998; Östman et al., 1994; Tangye et al., 1998).
DEP-1 was found to be frequently deleted and mutated in various human cancers such as thyroid, colon, lung, pancreatic, and breast cancer (Iuliano et al., 2003; Ruivenkamp et al., 2002; Tonks, 2006; Trapasso et al., 2004). Furthermore, the mouse PTPRJ was found as the colon cancer susceptibility locus *Scc1* (Ruivenkamp et al., 2002), and it exhibits tumor-suppressor activity when ectopically overexpressed (Iuliano et al., 2003; Keane et al., 1996; Trapasso et al., 2000).
This growth inhibitory function of DEP-1 is consistent with the nature of some of its reported substrates (Fig. 1.5 D), namely a variety of growth factor receptors such as the epidermal growth factor receptor EGFR, the platelet-derived growth factor receptor (PDGFR), the vascular-endothelial growth factor receptor VEGFR, and the colony stimulating factor-1 receptor (MET), as well as Src family kinases (SFKs), ERK-1/2, and the p85 subunit of PI3K (Arora et al., 2011; Berset, 2005; Chabot et al., 2009; Grazia Lampugnani et al., 2003; Kappert et al., 2007; Palka, 2002; Sacco et al., 2009; Tarcic et al., 2009; Tsuboi et al., 2008; Zhu et al., 2008). Aberrations in their regulation is accountable for self-sufficiency cell growth, the first hallmark of cancer (Hanahan and Weinberg, 2011).
Known as other substrates of DEP-1 are proteins from the cell-cell junctional complexes including p120ctn, β-catenin and γ-catenin, occludin, and ZO-1, which might impact biological functions dependent on the loosening/strengthening of intercellular contacts (Holsinger et al., 2002; Palka, 2002; Sallee and Burridge, 2009). Finally, it has been reported that DEP-1 serves as a positive regulator of B-cell and macrophage immunoreceptor signaling and thrombocyte activation (Senis et al., 2009; Zhu et al., 2008). Together, these findings make DEP-1 a fascinating candidate for the development of innovative therapeutic strategies. For example, Takahashi et al. were able to induce ERK-1/2 dephosphorylation and inhibition of both *in vitro* cell growth and *in vivo* angiogenesis by using a monoclonal PTPRJ antibody (Takahashi, 2006).
The regulatory mechanisms controlling DEP-1 activity are largely unknown. However, two lingands have been identified in human cell culture experiments, namely thrombospondin 1 and syndecan-2 (Takahashi et al., 2012; Whiteford et al., 2011). Thrombospondin 1 is a trimeric glycoprotein that binds with high affinity to the extracellular part of DEP-1, resulting in increased catalytic activity of DEP-1 and thereby in inhibition of cell growth (Takahashi et al., 2012). Similarly, the heparan sulfat proteoglycan syndecan-2 binds to the extracellular part of DEP-1 to promote DEP-1 activity, which results in the stimulation of cell proliferation and cell growth (Whiteford et al., 2011).

1.4.3 The substrate trapping mutation D1241A

An essential step towards a complete understanding of the physiological function of the PTPs is the identification of their physiological substrates (Flint et al., 1997). Since the interaction between PTPs and their substrates are too weak to permit isolation of these complexes, the affinity for substrates has to be increased. By mutating the aspartic acid 1241 to an uncharged alanine (Fig. 1.5 C [2]), a decrease in negative charge at this position, as well as a conformation change forming a hydrophobic pocket that buries the pTyr of the substrate is induced (Jia et al., 1995), such that DEP-1 can covalently bind to its physiological substrates, but is unable to dephosphorylate the target efficiently. By this "substrate-trapping", the mutant DEP-1 and its substrate become locked in a stable "dead-end" complex.

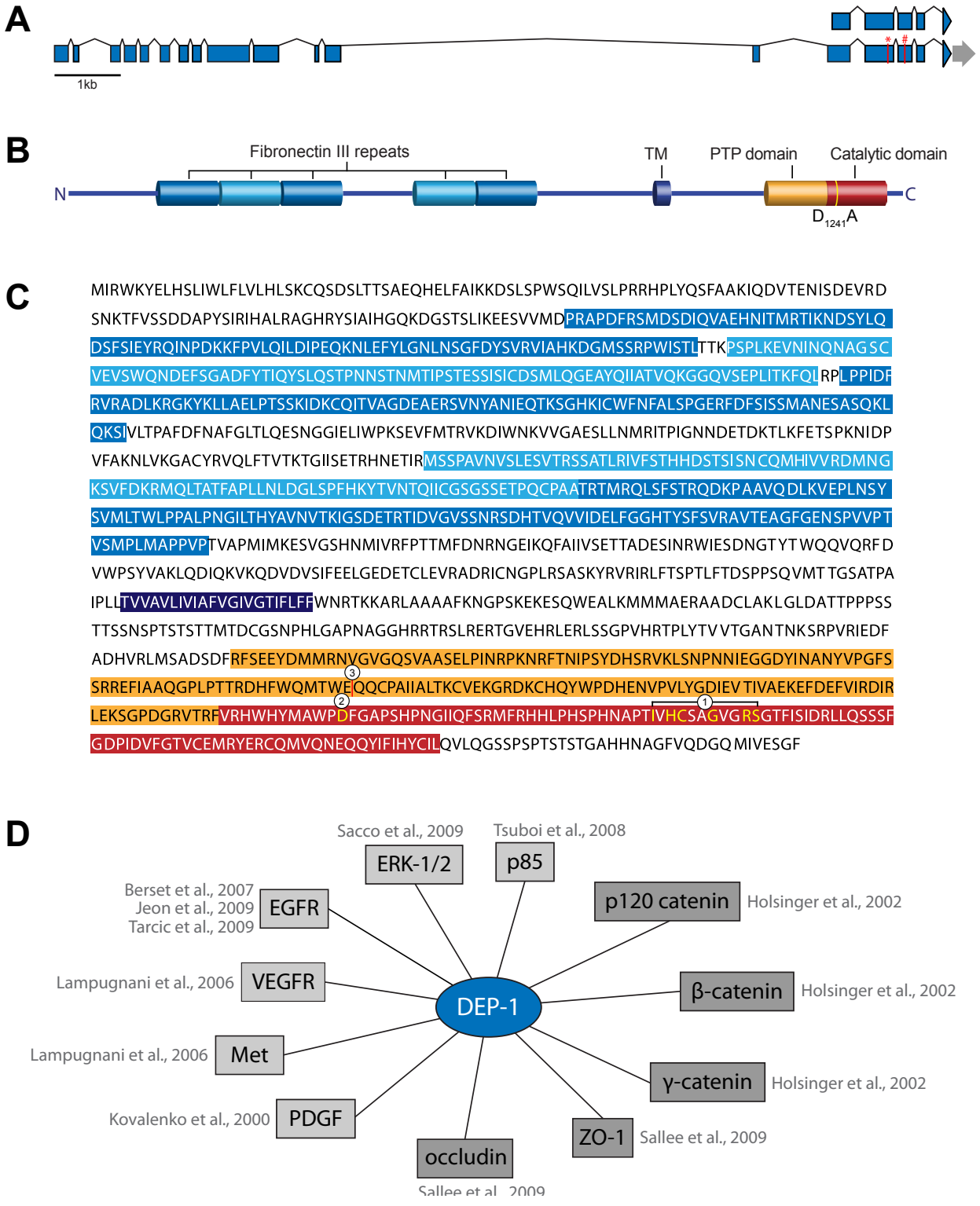

Figure 1.5 Density enhanced phosphatase DEP-1.
(**A**) Intron-exon structure of *C. elegans dep-1*. Asterisks indicates the stop mutation *zh34* and hash key indicates the substrate trapping mutation D1241A. (**B**) Domain structures of *C. elegans* DEP-1. (**C**) Protein sequence of *C. elegans* DEP-1. Fibronectin repeats, transmembrane-domain and catalytic domains are colour coded as in (**B**). The conserved [I/V]HCXXGXXR[S/T] motif is highlited and indicated with [1], the substrate trapping mutation D1241A with [2], and the stop mutation *zh34* with [3]. (**D**) Overview of the so far known substrates of DEP-1/PTPRJ/CD148. Scale bar represents 500 bp.

1.5 Integrins

The integrins, which are found on nearly all nucleated cells of multicellular animals, are a large family of cell adhesion molecules that form non-covalently associated α/β heterodimers (Hynes, 2002). The first integrin was identified 1986, and was named so because integrins serve to integrate the extracellular and intracellular environments. They do so by binding to ligands in the extra cellular matrix (ECM), such as fibronectin, vitronectin and collagen, and to cytoskeletal components and signaling molecules inside the cell (Hynes, 1992; Pytela et al., 1985; Springer, 1994; Tamkun et al., 1986; White et al., 2004). Integrins are especially important in areas that involve tissue growth or areas, in which cell attachment is necessary for proper function. Thus, embryonic development, angiogenesis and the immune system are critically dependent on integrins (Silva et al., 2008; Smith-Garvin et al., 2009; Spencer et al., 2004). Integrins are known to be involved in various disorders such as thrombosis, immune system disorders, infections, osteoporosis, and have been associated with a number of metastatic cancers (Coller and Shattil, 2008; Evans et al., 2009; Felding-Habermann, 2003; Hood and Cheresh, 2002; Lee et al., 2007; Stewart and Nemerow, 2007)

In vertebrates, at least 24 distinct α/β heterodimer combinations are formed by 18 α-subunits and 8 β-subunits, each of which can bind to a specific repertoire of cell-surface, ECM or soluble protein ligands (Fig. 1.6 A). Both α- and β-subunits are type I transmembrane glycoproteins with a large multidomain extracellular portion (>700 residues) and single spanning transmembrane domains. The α-chain is composed of a short cytoplasmic domain and a long extracellular domain composed of two calf domains followed by a thigh domain, and seven repeats constituting the β-propeller (Fig. 1.6 B). The β-chain has a longer cytoplasmic domain, four extracellular integrin epidermal growth factor-like domains (I-EGF), and an I-like domain inserted into the hybrid domain (Cox et al., 2010).

Integrins appear in three distinct conformations: a resting, closed conformation, an intermediate partially activated state, and a fully activated open, ligand-binding conformation (Fig. 1.6 C and D; Takagi et al., 2002; Xiao et al., 2004; Xiong et al., 2001). The regulation of integrin function occurs under tight spatial and temporal control of integrin affinity to extracellular ligands and is achieved by rapid, reversible changes in the confirmation of the extracellular domains of the integrin heterodimer, so-called "integrin activation" (Sims et al., 1991; Woodside et al., 2001).

Originally, it was thought that integrins are simply adhesion molecules and not true receptors because they have no homology to other known receptors and no evidence of intracellular signaling motifs (Cox et al., 2010). However, it has been found that signal transduction through the integrins can be conducted in either direction, which is referred to as either "inside-out" or "outside-in" signaling.
During "inside-out" signaling, intracellular activators, such as talin or kindlins, bind to the β-integrin cytoplasmic tail and cause a conformational change in the extracellular part of the integrins (Fig. 1.6 C) (Coller and Shattil, 2008). This results in increased affinity for extracellular ligands (integrin "activation") and controls adhesion strength and enables strong interactions between integrins and ECM proteins.
When integrins behave like traditional signaling receptors in transmitting information into cells by "outside-in" signaling, extracellular ligands bind to the α-I and β-I domains on the extracellular part of the integrins, resulting in conformation changes of the integrins (Fig. 1.6 D). Because many of the ligands are multivalent, this contributes additionally to integrin clustering.

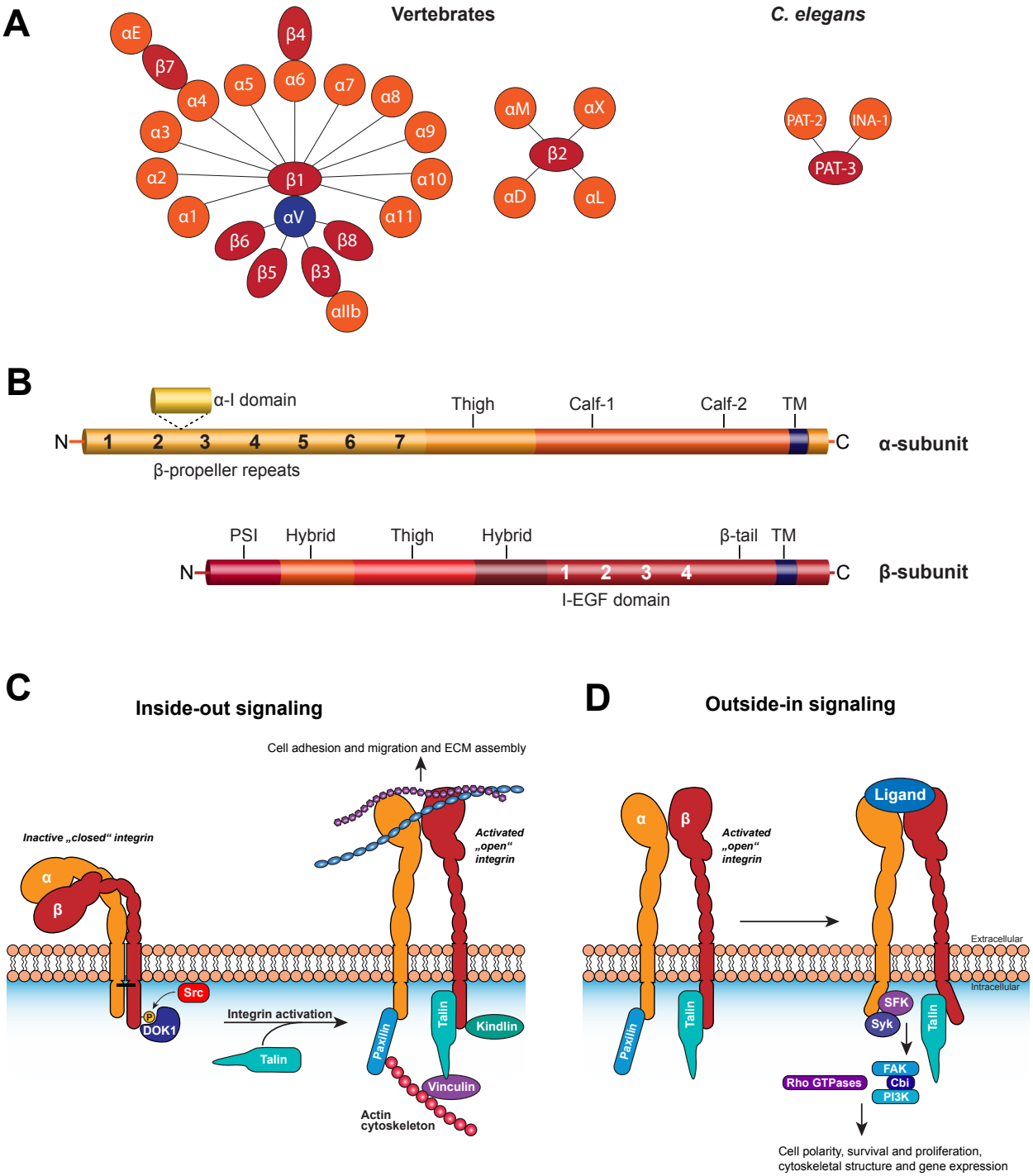

Figure 1.6 Integrins.

(**A**) Integrins are heterodimers comprising an α- and β-subunit. In vertebrates, 18 α-subunits and 10 β-subunits are known, in *C. elegans* two α-subunits and a single β-subunit. (Adapted from Cox et al, 2010). (**B**) Domain structures of vertebrate α- and β-Integrin subunits. (**C**) Potential mechanism regulating talin-mediated integrin activation. Resting integrins are held in a bent-inactive conformation. Talin binding to cytoplasmic integrin β tail induces conformational changes in the extracellular domain to form a high affinity receptor (inside-out signaling). Some of the structural proteins that couple the integrin and the actin cytoskeleton are shown. Src mediated tyrosine phosphorylation of integrin NPxY motifs, and competition with other β tail-binding proteins (e.g. DOK-1) may prevent integrin-talin interaction, so inhibiting integrin activation. (**D**) Binding of a ligand to activated integrin induces recruitment of additional signaling molecules (SFK and Syk) to the integrin tails, to activate downstream responses (e.g. over FAK/PI3K). This process is reffered to as outside-in signaling (Modified from Calderwood, 2004 and Lowell et al., 2011).

Although the two processes "outside-in" and "inside-out" signaling are separated, they are often closely linked. Thus, integrin activation can increase ligand binding, resulting in "outside-in" signaling, and conversely, ligand binding can generate signals that cause "inside-out" signaling (Shattil et al., 2010). Together, these two events lead to intracellular signals that control cell polarity, cytoskeletal structure, gene expression, cell survival and proliferation (Shattil et al., 2010).

1.5.1 Integrin cytoplasmic tails

The transmembrane helices and short cytoplasmic tails of both integrin subunits play a crucial role in coordinating the bidirectional signaling and the activation states of integrins (Liu et al., 2000; Shattil et al., 2010). The cytoplasmic tail of the α-subunits are between 15 and 78 amino acids long, and the cytoplasmic tails of the β-subunits contain between 46 and 68 amino acids. Since they do not have known enzymatic activity, they must interact with cytoplasmic signaling or adaptor proteins – there are at least 21 proteins known to bind to one or more integrin β tails – to affect or respond to the changing cellular activation state (Liu et al., 2000).

Both, the α- and β-cytoplasmic membrane-proximal tails, contain strong evolutionary conserved regions and play crucial roles in integrin activation (Fig. 1.7 A and B). Deletion of the cytoplasmic tail of the α-subunit, or of the conserved GFFKR sequence alone results in constitutive activation of the integrins, but a deletion that retains the GFFKR sequence does not (Lu and Springer, 1997; O'Toole et al., 1995; Ylänne et al., 1993). Similarly, a deletion of the membrane-proximal region of the β-cytoplasmic tail, activates integrins, but deletions that are closer to the C-terminal block integrin activation (Crowe et al., 1994; Hughes et al., 1995; Lu et al., 2001). Therefore, it is assumed that the membrane-proximal regions of the α- and β-cytoplasmic tails play a crucial role in integrin activation, probably by interacting with one another to stabilize an inactive conformation. On the one hand, the more distal regions of the β-cytoplasmic tails regulate activation through interactions with signaling proteins that might disrupt the membrane-proximal interaction, on the other, the membrane-distal α-sequences also regulate β-tail conformation and association with activator proteins in a cell-type specific manner (Calderwood, 2004).

Figure 1.7 Integrin cytoplasmic tails.
(**A**) Alignment of the amino acid sequences of *C. elegans* PAT-2 and human α6, α7, α3, α5, and α8 cytoplasmic tails. (**B**) Alignment of the amino acid sequences of *C. elegans* PAT-3 and human β2, β7, β1, β3, and β6 cytoplasmic tails. Conserved domains are highlighted in grey and yellow.

A central role for integrin activation is played by the NPxY (Asp-Pro-X-Tyr) motifs, C-terminal to the membrane-proximal region of the β-cytoplasmic tail (Fig. 1.7 B). Tyrosine phosphorylation of the NPxY motifs by the Src-family kinases reduces cell adhesion, leads to integrin displacement from focal adhesions, and is important in cell migration, hemostasis and transformation – indicating that phosphorylation of this Tyrosine may serve as an integrin activation "off switch" by interfering with required interactors (Datta et al., 2001; 2002; Johansson et al., 1994; Law et al., 1999; Sakai et al., 2001; 1998). In accordance to this, it was observed that when the Tyrosine in the first conserved NPxY motif was mutated to Alanine, the activation and structural changes of the integrins was strongly inhibited (Ulmer et al., 2001).
Tyrosine phosphorylation of the NPxY motif regulates the interaction of different phosphotyrosine binding (PTB) domain-containing proteins, such as the docking protein 1 (DOK1) and talin 1 (Fig 1.6 C) (Calderwood et al., 2003; Oxley et al., 2008). Talin is a major cytoskeletal actin-binding protein that binds with high affinity to the non-phosphorylated NPxY motif and plays a crucial role in integrin activation (Critchley, 2000; Tadokoro et al., 2003). On the other hand, DOK1 binds to the phosphorylated NPxY motif – further supporting the theory that Tyrosine phosphorylation of NPxY serves as a switch that controls, which of the alternating groups of PTB-containing proteins can bind to the integrins (Calderwood et al., 2003; Oxley et al., 2008).
The NPxY motifs are canonical signals for clathrin-mediated endocytosis of various surface receptors (Ohno et al., 1995), and several observations suggest that they are also involved in the regulation of integrin endocytosis. First, the β3-endonexin-mediated internalization of ligand-bound integrins is impaired when Y is substituted to A in the membrane proximal NPxY motif. Second, F to A substitutions in either one of the NPxY motifs of β2 integrins compromises their endocytosis. And third, clathrin-dependent integrin endocytosis in fibroblasts is reduced when Y is mutated to F in both NPxY motifs (Pellinen et al., 2008). Nevertheless, the exact pathways involved in the endocytosis of integrins are not clearly known and seem to vary between integrin heterodimers (Ramsay et al., 2007; Upla et al., 2004).

1.5.2 *C. elegans* integrins

In contrast to the numerous integrin subunits in vertebrates, *C. elegans* has only three integrins: Two α-subunits (INA-1 and PAT-2) and one β-subunit (PAT-3), providing an excellent model system for examining integrin function (Girard et al., 2007). Null alleles of *pat-2* and *pat-3* cause a "Paralyzed and Arrested at Two-fold" embryonic lethality phenotype (Pat), loss of *ina-1* (INtegrin alpha) results in a larval lethal phenotype (Baum and Garriga, 1997; Williams and Waterston, 1994).
PAT-3 is widely expressed in most tissues throughout development. PAT-3 expression can especially be observed in the body wall and sex muscles, along the intestinal tract, in the embryonic pharynx, the spermatheca, the uterus, the somatic gonad, the neurons, and the vulva (Gettner et al., 1995). Heterodimers of PAT-2/PAT-3 are expressed in many tissues, including the muscles and the somatic gonad, whereas INA-1/PAT-3 are localized mainly to migratory cells such as the distal tip cells (DTC) and the neurons (Cram et al., 2006; Lee et al., 2001; Meighan and Schwarzbauer, 2007).
It has been reported, that the integrins are also involved in vulval development: INA-1/PAT-3 play a key regulatory function during anchor cell invasion through the basal membrane by targeting the netrin receptor UNC-40 to the AC's plasma membrane (Hagedorn et al., 2009).
Several *pat-3* alleles including a null and a reduction-of-function mutation were found, all of which are positioned within the extracellular domain. Unfortunately, this limits the analysis of its intracellular function (Gettner et al., 1995).

61% of the PAT-3 protein sequence harbors similarity to the human β1 integrin, and shares many conserved motifs (see Fig. 1.7 B), such as the NPxY motifs. Mutations in the tyrosines of the NPxY motifs can rescue the embryonic lethality of the *pat-3(st564)* null allele, but display multiple mutant larval and adult phenotypes caused by defective integrin function, such as defects in DTC migration, ovulation, and muscle cell function (Lee et al., 2001; Xu et al., 2010).

1.6 Analyses of protein-protein interactions by mass spectrometry

1.6.1 Protein-protein interactions

Proteins are the workhorses of a cell and facilitate most processes, including gene expression, cell growth, proliferation, morphology, motility, nutrient uptake, signal transduction and apoptosis (Golemis and Adams, 2005). Protein expression is a highly dynamic process: Many proteins are expressed in a cell type-dependent manner, and cells respond to countless stimuli. Furthermore, a protein may interact only briefly with another protein just to modify it, for example a protein phosphatase that removes a phosphate from its target protein, which in turn may change protein-protein interactions.
This complexity makes it difficult to investigate and understand protein function in the proper biological context. However, information about these interactions is essential for a better understanding of the principles of cellular organization and diseases, and it is the basis for new therapeutic approaches (Li et al., 2012).

Protein-protein interactions can be classified based on their composition, affinity and lifetime as homo- and hetero-oligomeric complexes, and transient and permanent complexes, respectively (Ozbabacan et al., 2011).
In contrast to a permanent protein-protein interaction, which is usually very stable and thus only exists in its complexed form, a transient protein-protein interaction associates and dissociates *in vivo* (Nooren and Thornton, 2003). Transient interactions are, as the name implies, temporary in nature and typically require a set of conditions that promote their interaction. These can be phosphorylation, conformational changes or localization to discrete areas in the cells. Transient protein interactions are crucial for diverse biological processes, especially in the regulation of biochemical pathways and signaling cascades in the cells (Ozbabacan et al., 2011).

1.6.2 Identification of protein-protein interactions

One popular technique to determine and discover previously unknown physical interaction between two or more proteins is the pull-down assay. In this *in vitro* method, the target protein is tagged with an affinity tag (e.g. HA-, Strep-III-, or GST-tag) and expressed in *C. elegans* or *E. coli*. This "bait" is then captured by an immobilized affinity ligand specific for the tag, and incubated with a protein source that contains putative "prey" proteins, such as a cell lysate. The proteins that bind to the "bait" can then be detected by sodium dodecyl sulphate-polyacrylamide gel electrophoresis (SDS-PAGE), Western blot analysis, or mass spectrometry.

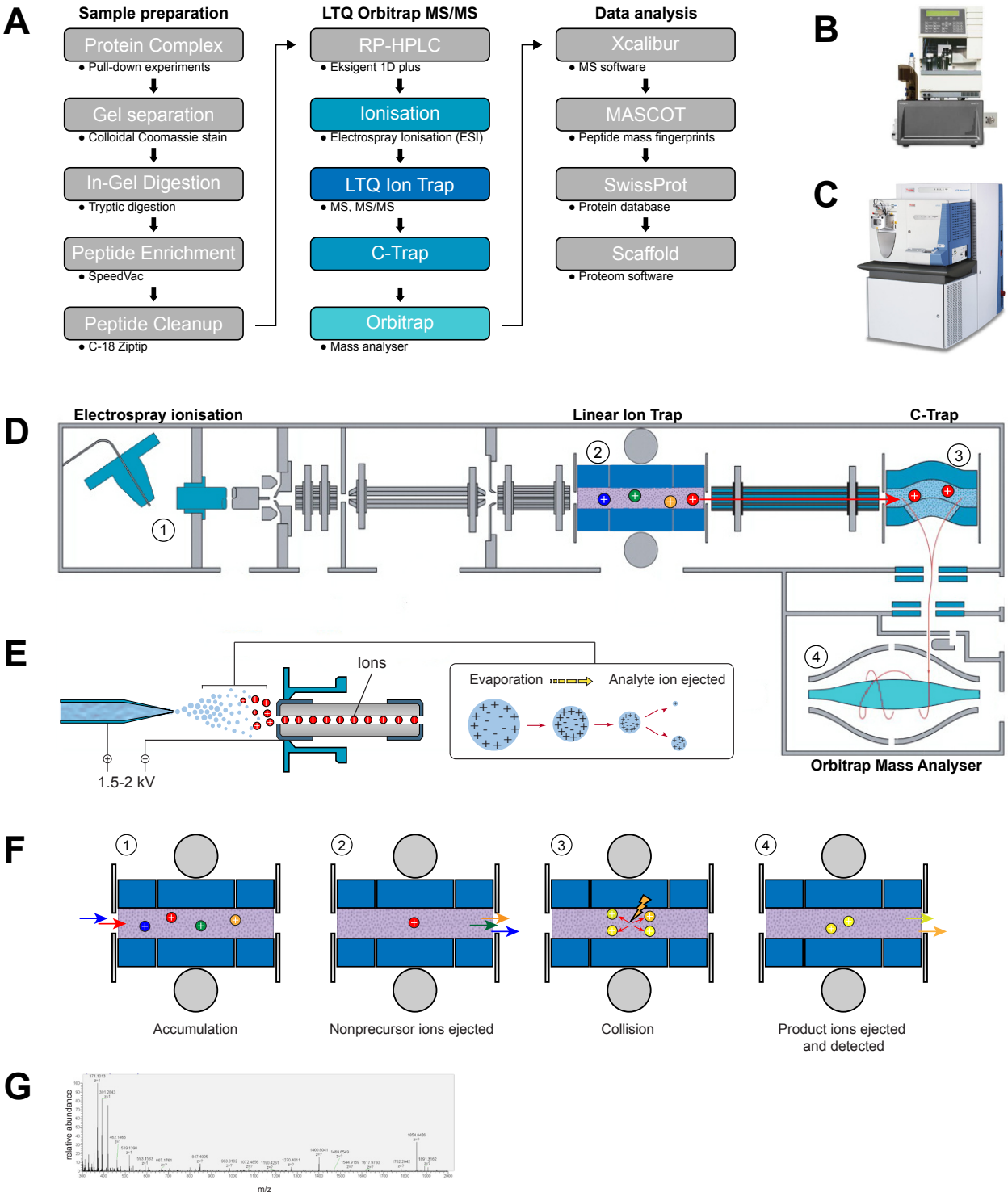

Figure 1.8 Protein identification by LC-MS/MS mass spectrometry.
(**A**) Workflow of sample preparation for MS analysis, measuring peptides in LTQ-Orbitrap LC-MS/MS, and data analysis by different softwares. (**B**) RP-HPLC (Eksigent 1 plus). (**C**) Mass spectrometer Thermo Scientific LTQ-Orbitrap. (**D**) Schematic of the LTQ-Orbitrap. Peptides are ionized by ESI [1] and move into the C-trap [3] via a quadrupole linear ion trap (LTQ) [2]. Ions are then injected into the orbitrap [4| where the m/z of the ions are detected. (**E**) Electrospray ionisation (ESI) and desorption of ions from solution. (**F**) During MS/MS, a limited m/z range including the precursor ions of interest are isolated by the LTQ [2]. After their fragmentation [3], the following fragment ions move to the C-trap and are analyzed in the orbitrap mass analyser. (**G**) Mass spectrum of a MS scan.

Tagging of proteins has the advantage that the tag can be systematically applied to any number of proteins. However, the tag modifies the protein, which may alter its activity. Also overexpression of the tagged protein might become a problem.
Another approach is to perform co-immunoprecipitation (Co-IP), where antibodies that bind specifically to the protein of interest are used to capture protein complexes. However, the main disadvantage is thereby, that high-quality antibodies are available only for a limited set of proteins (Mallick and Kuster, 2010).
In both approaches there is a high risk of non-specific co-purification. Therefore, it is essential to have the appropriate controls, and to further validate an identified interaction by other biochemical and genetic methods.

The characterization of protein-protein interactions by the above described methods helped to achieve a better understanding of how proteins function and what their biological function in the cell are. But until the late 1990's, protein function analyses were mainly focused on single proteins, so much, that the understanding of their function was fully limited to the knowledge of their interaction partners.
Thanks to the publication of the human genome and technological developments in mass spectrometry (MS) 15 years ago, it became possible to understand how proteins interact with each other and how they act in biological networks within the cell (Li et al., 2012). This was the birth of proteomics – the study of all proteins in a biological system. Nowadays proteomics spans diverse research topics, ranging from protein expression profiling analyzing signaling pathways and to developing protein biomarker assay systems (Mallick and Kuster, 2010).
The identification of protein complexes by proteomics has several advantages. First, interacting proteins can be purified under almost physiological conditions from an endogenous source, which limits artifacts. Second, functionally important protein modifications, such as phosphorylation or acetylation, can often be determined in the same context. And finally, protein complexes can generally easily be identified by mass spectrometry after either a solution digest or a one-dimensional SDS gel.

1.6.3 Sample preparation for mass spectrometry

Complex protein mixtures derived from pull-down assays present several problems in MS analysis. First, the mass spectra from complex mixtures are very difficult to fully analyze because of the overwhelming number of components. And second, the proteins are dissolved in buffers that contain chemicals that impair the MS results, e.g. detergents. To overcome these problems, the samples have to be prepared for their MS analysis by different techniques.
To reduce the complexity of the protein mixture, the proteins can be separated by SDS-PAGE according to their molecular weights and subsequently visualized by Colloidal Coomassie staining. The protein bands of interest are then excised and prepared for tryptic in-gel digestion (Fig. 1.8 A).
In the following preparation steps, the proteins in the gel pieces are de-stained and the disulphide bridges are irreversibly broken up by reduction and alkylation of the cystines and cysteines. The unfolded proteins are then cut enzymatically into a limited number of peptides by trypsin, a serine protease that cuts the peptide bond specifically at the carboxyl end of the basic amino acids arginine and lysine. After finishing the in-gel digestion, the peptides generated in this process are extracted from the gel matrix and resolved in an appropriate buffer that does not impact MS results.
Before the samples are ready for MS analysis, the peptide mixtures are desalted, purified and concen-

trated. This is achieved by C_{18} ZipTip purification, a process in which the peptides are passed through a reverse phase that contains linear aliphatic hydrocarbon of eighteen carbons (C_{18}), and washed with aqueous solution. Finally, the purified peptides are solved in proper mobile phases and ion-pairing reagents.
By doing these sample preparation steps, the problems mentioned above are solved: The samples become less complex, chemicals that impair MS analysis are gone, and the mixture contains roughly equal amounts of constituents. However, the sample preparation for MS-based analysis is a critical step, because it significantly impacts the quality and reproducibility of the MS results.

1.6.4 Mass spectrometry

Mass spectrometry (MS) is a sensitive and powerful analytical technique to detect, identify, and quantitate molecules based on their mass and charge (*m/z*). Originally developed almost 100 years ago, mass spectrometry was used to measure elemental atomic weights and the natural abundance of specific isotopes (Willard, 1988). Over time, a number of methods have been developed such as electrospray ionization (ESI) and matrix-assisted laser desorption/ionization (MALDI), which allows the collection of protein mass "fingerprints" that can be matched to proteins and peptides in databases to predict the identity of unknown proteins (Finehout and Lee, 2004). The sensitivity of current mass spectrometers allows one to detect analytes at concentrations in the attomolar range (10^{-15}; Sadiq et al., 2011).
A mass spectrometer consists of three major components (Fig. 1.8 D): First, an ion source produces gaseous ions from the studied substrate, second, a mass analyzer resolves the ions into their characteristic mass components according to their mass-to-charge (*m/z*) ratio, and third, a detector system detects the ions and records the relative abundance of each of the resolved ionic species.

1.6.5 RP-HPLC and ESI

In spite of the sample preparation mentioned above, the samples are still too complex for MS analysis and have to be further simplified before its introduction into the mass spectrometer. This is achieved by using reversed phase high-pressure liquid chromatography (RP-HPLC), where the liquid samples are separated according to their polarity, respectively their hydrophobicity (Fig. 1.8 B).
After RP-HPLC separation, the eluents are vaporized and ionized by electrospray ionization (ESI), which is especially useful for analyzing large biomolecules such as proteins, peptides and oligonucleotides (Chowdhury et al., 1990). The main advantage lies in the fact that ESI produces multiply charged ions with little or no fragmentation and it does not require heat or high vacuum.
During ESI, liquid sample is sprayed (nebulized) into a sharply pointed hollow metal tube, such as a syringe needle (Fig. 1.8 E). The tube outlet is connected to a high voltage power supply that charges the liquid at the needle tip, from which a jet of similarly charged liquid droplets is expelled. The electrostatic field causes further dissociation of the liquid droplets in the jet, resulting in a mist of fine droplets that evaporate to leave behind the highly charged analyte molecules for analyses. Eventually, the ions are ejected into the gas phase and pass through a capillary sampling entrance into the mass spectrometer.

1.6.6 LTQ Orbitrap LC-MS/MS

The mass spectrometer "LQT Orbitrap LC-MS/MS" (Fig. 1.8 C) consists of three main components: A linear ion trap for sample ionization, selection and fragmentation; an intermediate storage device (curved linear trap) that is required for short pulse injection; and an Orbitrap analyzer for Fourier transformation based analysis (Fig. 1.8 D).

After electrospray ionization, the ions first enter into the "linear trap quadrupole" ion trap (LTQ), which consists of four parallel rods arranged in a square (quadrupole; Fig. 1.7 D [2]). By applying voltages to the rods, electromagnetic fields are generated that determine which mass-to-charge ratio of ions can pass through the filter at a given time, and which specific ions are trapped (Fig. 1.8 F).

In the mass spectrometer "LTQ Orbitrap", the m/z is not only evaluated in the linear ion trap, but also in the "Orbitrap" mass analyzer. After passing the LTQ, the ions are stored intermediately in a curved linear trap (C-trap). Subsequently they are sent in the "Orbitrap" mass analyzer (Fig. 1.7 D [4]). The Orbitrap cell consists of an outer barrel-like electrode and a coaxial inner spindle-like electrode that form electrostatic fields. The ions are trapped in circular orbits because their electrostatic attraction to the inner electrode is balanced by centrifugal forces – they cycle around the inner electrode on elliptical trajectories. Additionally, the ions also move forward and back along the axis of the central electrode (z-axis), whereby their trajectories in space look like helices. The frequency of these harmonic oscillations along the z-axis depends only on the ion mass-to-charge ratio. Therefore, by measuring these oscillations and by using Fourier transformation, the *m/z* ratios of the ions can be determined. The entire process has to be performed under an extreme vacuum to remove contaminating non-sample ions, which can collide with sample ions and produce non-specific reaction products.

The mass spectrometer is connected to a computer with software that analyze the ion detector data and produces graphs that organize the detected ions by their individual *m/z* and relative abundance (Fig. 1.8 G). By processing these ions through databases, the identity of the molecule can be predicted, based on the m/z ratio.

The resulting molecular weight of the peptides measured by this described "full MS scan" is very valuable, but to identify the exact composition more structural information is needed. A technique that is commonly used to sequence proteins and oligonucleotides is multiple-stage MS (MS/MS, also known as tandem MS). Hereby, specific "precursor" ions are trapped in the LTQ and fragmented by colliding them with a stream of inert gas, a process known as collision induced dissociation (CID; Fig. 1.8 F [3-4]). The CID generates "product" ions out of the "precursor" ions, which can be in turn ejected from the LTQ, stored intermediately in the C-trap and analyzed in the Orbitrap mass analyzer.

1.6.7 Data analysis

The most common data representation of the MS analysis is the mass spectrum, which represents intensity vs. the m/z in a histogram (Fig. 1.8 G). These mass spectra are unique for each peptide, but its interpretation requires combined use of various procedures.

First, the mass spectra of the MS and MS/MS scans are compared against a library of mass spectra by using the software *Mascot*, whereby the amino acid sequences of the peptides are determined. In a second step, the sequences of the peptides are compared to protein databases (e.g. *SwissProt*) whereas the proteins corresponding to the peptides are identified. Finally, all data from the different MS experiments are compared by proteome software (e.g. *Scaffold*) and interpreted for their biological relevance.

2

Aim of this thesis

Reversible protein phosphorylation is one of the most important and well-studied post-translational modifications. Catalyzed by protein kinases and protein phosphatases, phosphorylation and dephosphorylation plays a critical role in the regulation of many cellular processes including cell cycle, growth, apoptosis and signal transduction pathway. About 30% of human proteins contain covalently bound phosphate, and abnormal protein phosphorylation can be a cause of many human diseases. Thus, it is of major importance to understand how phosphorylation regulates the function of proteins.
The physiological substrates of most protein phosphatases have not yet been identified, since the functional activity of phosphatases is complicated by the fact that animals mutant for a single phosphatase gene display no obvious phenotype, suggesting that most protein phosphatase act redundantly (Haj et al., 2003; Harroch et al., 2000). However, information about these interactions is essential for a better understanding of the principles of cellular organization and diseases, and it is the basis for new therapeutic approaches (Li et al., 2012).

The highly conserved EGFR/RAS/MAPK signaling pathway is probably the best characterized signal transduction pathway in cell biology and plays a crucial role in many developmental processes. Its dysregulation is common in many cancers as Ras is the most frequently mutated oncogene in human cancer and cancer formation.
EGFR/RAS/MAPK activity is regulated through protein phosphorylation and controlled by a broad negative regulatory network that attenuates the different components of this signaling pathway. A member of this network is the density enhanced phosphatase DEP-1, which belongs to the receptor protein tyrosine phosphatases. It inhibits EGFR/RAS/MAPK signaling through dephosphorylation of the EGF receptor and thereby acts as a tumor suppressor (Berset, 2005; Jeon and Zinn, 2009; Tarcic et al., 2009). In vertebrates, DEP-1 was found as the colon cancer susceptibility locus *Scc1* (Ruivenkamp et al., 2002), and it has been found that DEP-1 is frequently deleted and mutated in various human cancers such as thyroid, colon, lung, pancreatic, and breast cancer (Iuliano et al., 2003; Ruivenkamp et al., 2002; Tonks, 2006; Trapasso et al., 2004).
Many experiments were performed in cell culture to identify novel interactors of DEP-1. However, the lack of *in vivo* confirmation makes it difficult to estimate the physiological relevance during cell fate specification, pattern formation and tumorigenesis.
Thus, the specific aim of this thesis was to identify novel interactors of DEP-1 by a mass spectrometry-based approach, and to further elucidate their role *in vivo* during development of the *C. elegans* hermaphrodite vulva.

3

Projects

3.1 The *C. elegans* β-Integrin PAT-3 is a Substrate of the Tyrosine Phosphatase DEP-1

Manuscript in preparation

Michael Walser[1,2], Erika Fröhli[1], Paolo Nanni[3] and Alex Hajnal[1,4]

[1] Institute of Molecular Life Sciences, University of Zürich, Winterthurerstr. 190, Zürich CH-8057, Switzerland
[2] Molecular Life Science Zürich PhD program
[3] Functional Genomics Center Zürich, University of Zürich/ETH Zürich, Switzerland
[4] Corresponding author: alex.hajnal@imls.uzh.ch

Phone: +41 (0)44 635 48 54 Fax: +41 (0)44 635 68 98

Key words: DEP-1, *C. elegans*, vulval development, PAT-3, Integrin, NPxY, RAS signaling

Running title: *C. elegans* β-Integrin PAT-3 is a substrate of DEP-1

3.1.1 Abstract

Reversible protein phosphorylation is one of the most important and well-studied post-translational modifications and plays a critical role in the regulation of many cellular processes including cell cycle, growth, apoptosis and signal transduction pathway. The receptor protein tyrosine phosphatase DEP-1 inhibits EGFR/RAS/MAPK signaling through dephosphorylation of the EGF receptor. Moreover, DEP-1 regulates cell adhesion and motility, suggesting that DEP-1 has numerous physiological substrates.
In order to identify novel substrates of DEP-1, we have performed a mass spectrometry-based approach using a substrate-trapping DEP-1 mutant. In this manner, we identified the β-integrin subunit PAT-3 as a novel substrate of DEP-1. DEP-1 dephosphorylates one of the evolutionary conserved NPxY motifs of the PAT-3 cytoplasmic tail and thereby promotes PAT-3 activation. In the developing vulva, activated PAT-3 inhibits the RAS/MAPK signaling pathway in the secondary vulval cells. These results demonstrate a novel role of DEP-1 and integrins during regulation of RAS/MAPK signaling and give further insights into integrin regulation *in vivo*.

3.1.2 Introduction

Phosphorylation of proteins is a reversible post-translational modification and one of the most common modes of regulating protein functions (Hunter, 1999). Several components of the epidermal growth factor receptor (EGFR) signal transduction pathway are phosphorylated and activated when an EGF ligand binds to its receptor (Schlessinger, 2000). On the contrary, protein phosphatases attenuate the activity of EGFR/RAS/MAPK pathway by being part of a negative regulatory network. The genome of both vertebrates and invertebrates encode a large number of predicted phosphatase genes (Alonso et al., 2004), and disruption of their activities may lead to serious diseases and disorders (Kishihara et al., 1993; Li and Dixon, 2000; Shultz et al., 1993). The physiological substrates of most protein phosphatases have not yet been identified, as many of the experiments addressing this question were performed *in vitro* or by overexpression, which often impairs the substrate specification of phosphatases (Blanchetot et al., 2005; Hertog et al., 1999). However, the knowledge about physiological substrates of protein phosphatases is essential for a better understanding of the principles of cellular organization and diseases, and it is the basis for new therapeutic approaches (Li et al., 2012).

The Density Enhanced Phosphatase DEP-1 (also known as PTPRJ, PTP-η or CD148) belongs to the class III Receptor Protein Tyrosine Phosphatase (R-PTP) family (Hertog et al., 1999). As characteristical for R-PTP, DEP-1 contains an intracellular catalytic tyrosine phosphatase domain, a single transmembrane domain, and multiple extracellular fibronectin type III repeats. The mouse PTPRJ was found as the colon cancer susceptibility locus *Scc1* (Ruivenkamp et al., 2002), and it regulates cell motility and exhibits tumor-suppressor activity when ectopically overexpressed (Iuliano et al., 2003; Keane et al., 1996; Petermann et al., 2010; Trapasso et al., 2000). Moreover, DEP-1 was found to be frequently deleted and mutated in various human cancers such as thyroid, colon, lung, pancreatic, and breast cancer (Iuliano et al., 2003; Ruivenkamp et al., 2002; Tonks, 2006; Trapasso et al., 2004). The substrates of DEP-1 identified so far, namely a variety of growth factor receptors such as EGFR, PDGFR, VEGFR, MET, SFKs, ERK-1/2 and the p85 subunit of PI3K, as well as cell-cell junctional complexes including p120ctn, β-catenin and γ-catenin, occluding, and ZO-1, were analyzed almost exclusively in cell culture experiments (Arora et al., 2011; Berset, 2005; Chabot et al., 2009; Grazia Lampugnani et al., 2003; Kappert et al., 2007; Palka,

2002; Sacco et al., 2009; Tarcic et al., 2009; Tsuboi et al., 2008; Zhu et al., 2008). However, the lack of *in vivo* confirmation makes it difficult to estimate the physiological relevance during cell fate specification, pattern formation and tumorigenesis.

The development of the *C. elegans* hermaphrodite vulva serves as an excellent model to study evolutionary conserved signaling pathways like the RAS/MAPK, DELTA/NOTCH, and WNT-pathways and is one of the best-characterized models for organogenesis (Sternberg, 2005). In L2 larval stage, vulval development is induced when the gonadal anchor cell (AC) secretes the EGF-like growth factor LIN-3 in a graded fashion to the adjacent vulval precursor cells (VPCs) (Kornfeld, 1997; Sternberg and Han, 1998). All six VPCs, termed P3.p to P8.p, are equally competent to respond to this inductive AC signal, but P6.p is closest to the AC. Hence, P6.p receives the highest possible level of LIN-3 that activates the EGF receptor homolog LET-23 and thereby the RAS/MAPK pathway to specify the primary (1°) cell fate. Consequently, a lateral signal from P6.p is transduced by the DELTA/NOTCH signaling pathway to induce the secondary (2°) fate and to inactivate the EGFR/RAS/MAPK pathway in the neighboring VPCs P5.p and P7.p (Ambros, 1999; Berset et al., 2001; Chen and Greenwald, 2004; Yoo et al., 2004). The latter is achieved by the transcription of several negative regulators of the EGFR/RAS/MAPK signaling pathway in P5.p and P7.p, such as *dep-1, lip-1* and the *lst* genes (Berset, 2005; Berset et al., 2001; Yoo et al., 2004). After the vulval cell fates have been specified, the 1° VPC P6.p and the 2° VPCs P5.p and P7.p each go through three rounds of cell divisions to generate 22 cells that form the vulva. The remaining distal VPCs (P3.p, P4.p and P8.p) adopt the tertiary (3°) non-vulval cell fate, which divide once before they fuse with the surrounding hypodermis (*hyp7*).

Integrins, which are found on nearly all nucleated cells of multicellular animals, are a large family of cell adhesion molecules that form non-covalently associated α/β heterodimers. Both α- and β-subunits are type I transmembrane glycoproteins with a large multidomain extracellular portion, single spanning transmembrane domains, and short cytoplasmic tails (Hynes, 2002). In mammals, at least 24 distinct α/β heterodimer combinations are formed by 18 α-subunits and 8 β-subunits, each of which can bind to a specific repertoire of cell-surface, extra cellular matrix (ECM) or soluble protein ligands (Hynes, 1992; 2002). In addition to the regulation of cell adhesion events, integrins play critical roles in transducing signals in either direction, in what is referred to as either "inside-out" or "outside-in" signaling (Liu et al., 2000). In coordinating the bidirectional signaling and the activation states of the integrins, the transmembrane helices and short cytoplasmic tails of both subunits play a crucial role (Liu et al., 2000; Shattil et al., 2010).
Contrary to the numerous integrin subunits in vertebrates, *C. elegans* has only three integrins: Two α-subunits (INA-1 and PAT-2) and one β-subunit (PAT-3), providing an excellent model system for examining integrin function. Null alleles of *pat-2* and *pat-3* cause a "Paralyzed and Arrested at Two-fold" embryonic lethal phenotype (PAT), and loss of *ina-1* (INtegrin Alpha) results in larval lethality (Baum and Garriga, 1997; Williams and Waterston, 1994). PAT-3 is widely expressed in most tissues throughout development, especially in the body wall and sex muscles, along the intestinal tract, in embryonic pharynx, spermatheca, uterus, somatic gonad, neurons, and the vulva (Gettner et al., 1995). Furthermore, it has been shown that PAT-3 plays together with INA-1 a key regulatory function during anchor cell invasion through the basal membrane by targeting the netrin receptor UNC-40 to the AC's plasma membrane (Hagedorn et al., 2009).

In this study, we report the identification of the *C. elegans* β-integrin subunit PAT-3 in a mass spectrometry based approach as a novel substrate of the tyrosine phosphatase DEP-1. Using biochemical and genetic epistasis analyses, we found that DEP-1 dephosphorylates the highly conserved NPxY motif of the PAT-3 cytoplasmic tail to regulate its activity. Activated PAT-3 acts as a negative regulator of RAS/MAPK signaling during vulval development, most likely by inhibiting EGFR activation.

3.1.3 A mass spectrometry-based approach to find novel substrates of DEP-1

In order to identify novel substrates of *C. elegans* DEP-1, we performed a mass spectrometry-based approach in which proteins from pull-down experiments were analyzed by LC-MS/MS. The intracellular domain of DEP-1, which carries the substrate trapping mutation D1241A (Palka, 2002), was affinity-purified from *E. coli* using GST sepharose and used for pull-down experiments with total protein extract from mixed-staged *C. elegans* N2 (Fig. 3.1 A and B; Berset, 2005). To distinguish between proteins that remained bound specifically to the substrate trapping mutation and proteins that are not substrates of DEP-1, we also performed pull-down experiments with the wild-type intracellular domain (DEP-1intrawt) and with GST only (Fig. 3.1 C). Subsequently, protein complexes were separated by SDS-PAGE and stained with Colloidal Coomassie Blue, which led to the identification of three prominent protein bands with a molecular weight of 90.1 kD, 135.9 kD, and 174.4 kD, which were exclusively present in the DEP-1intraDA pull-downs (Fig. 3.1 D). After fragmentation of the SDS-gel (dotted lines in Fig. 3.1 D), proteins were processed for in-gel tryptic digestion and C18 ZipTip purification. Liquid chromatography and tandem mass spectrometry (LC-MS/MS) in conjunction with database searching against the *C. elegans* protein database finally led to the identification of 585 proteins, 97 of which were not present in the empty GST control (see section 3.1.9). Among the 43 proteins that bound exclusively to DEP-1intraDA, 99 peptides of the α-integrin subunit PAT-2 (MW=135.9 kD), and 54 peptides of the β-integrin subunit PAT-3 (MW=90.1 kD) were identified (Fig. 3.1 E), indicating an unambiguous identification of these proteins. Since it is unlikely that DEP-1 interacts with both the α and β integrin subunit, and because previously reportet data suggest a tyrosine phosphorylation dependent regulatory role of β-integrins (Calderwood, 2004), we focused our further studies on the examination of the interaction between DEP-1 and PAT-3.

3.1.4 DEP-1 binds to the NPxY motif of its substrate PAT-3

To confirm the binding of DEP-1intraDA to PAT-3, we performed co-immunoprecipitation (Co-IP) experiments using GST-purified DEP-1 and total protein extract from worms expressing PAT-3::GFP (*qyIs43*). Western blots against GFP showed a clear interaction between DEP-1intraDA and PAT-3::GFP, whereas no binding of DEP-1intrawt to PAT-3 was observed (Fig. 3.2 A).
Similar to these findings were the results from Co-IP experiments with protein extract from worms expressing PAT-2::GFP (*jeIs2222*). PAT-2::GFP clearly interacted with DEP-1intraDA, whereas only a very weak interaction with DEP-1intrawt was observed (data not shown).
To further test if this interaction is phosphorylation dependent, we added the PTP inhibitor sodium orthovanadate (Na_3VO_4; Huyer et al., 1997) to the protein extract that was subsequently used for Co-IP experiments. As expected, the interaction of DEP-1intraDA with PAT-3::GFP was completely inhibited in presence of sodium orthovanadate (Fig. 3.1 B). Thus, we conclude that the interaction of DEP-1 with its substrate PAT-3 is phosphorylation dependent.

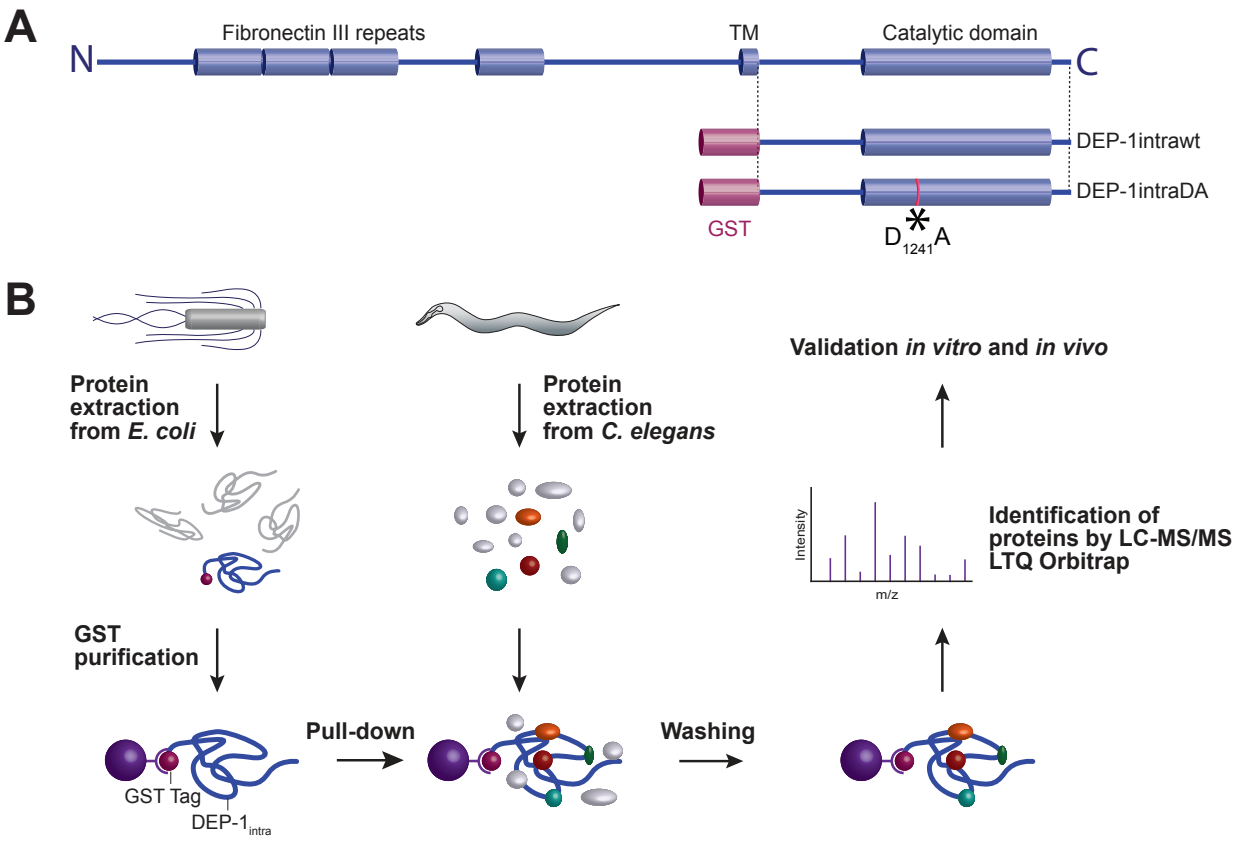

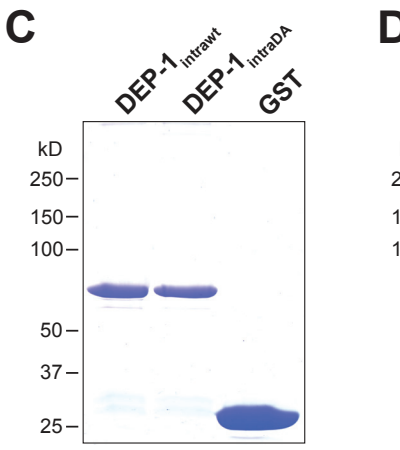

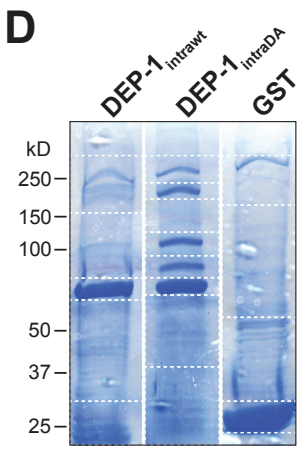

E

Identified Protein	DEP-1intrawt #1	#2	#3	DEP-1intraDA #1	#2	#3	MW (kD)
DEP-1	68	55	51	66	42	48	152.9
PAT-2	4	0	0	43	33	23	135.9
PAT-3	0	0	0	29	18	7	90.1
NID-1	2	2	0	25	16	0	174.4
PRP-8	0	3	0	12	16	0	272
RPS-6	0	10	7	8	15	8	28.1

Figure 3.1 Mass spectrometry-based approach to identify novel substrates of DEP-1.
(**A**) Domain structures of *C. elegans* DEP-1 and scheme of GST-tagged DEP-1intrawt and DEP-1intraDA fusion proteins. Asterisks indicates the substrate trapping mutation D1241A. (**B**) Workflow of GST purification, pull-down, and subsequent analysis by MS/MS. (**C**) Samples of purified DEP-1intrawt, DEP-1intraDA and GST were loaded on a SDS gel and stained with Coomassie Blue. (**D**) Samples after pull-down of N2 wild-type protein extract with purified GST::DEP-1 intrawt, GST::DEP-1intraDA, or GST were fractionated by SDS-PAGE and stained with Colloidal Coomassie Blue. Dashed lines indicate cutting lines of the SDS gel for subsequent tryptic in-gel digestion. (**E**) Top-six proteins that were identified by LC-MS/MS after pull-down experiments. Three independent purifications were analyzed (#1-3). Numbers indicate the quantity of identified peptides per protein. All listed proteins were not identified in the controls. P_{Min} protein = 95%; $\#_{Min}$ peptides = 2; P_{Min} peptide = 95%.

Since the catalytic phosphatase domain of DEP-1 is cytoplasmic, we assumed that the interaction with PAT-3 occurs over a cytoplasmic phospho-tyrosine. Thus, we focused our studies on the cytoplasmic tail of PAT-3, which contains three highly conserved tyrosines, namely Y772, Y792, and Y804 (Fig. 3.1 C). Y792 and Y804 belong to the two evolutionary conserved NPxY (Asp-Pro-X-Tyr) motifs, whose tyrosine phosphorylation are thought to activate integrins and to promote interactions with downstream signaling molecules (Calderwood et al., 2002; Chen et al., 1990; Lee et al., 2001). To determine if DEP-1 binds to one of these tyrosines, we generated *C. elegans* strains expressing ectopic PAT-3::GFP, in which the cytoplasmic tyrosines Y772, Y792, Y804, as well as the conserved threonins TTT796-798 were replaced

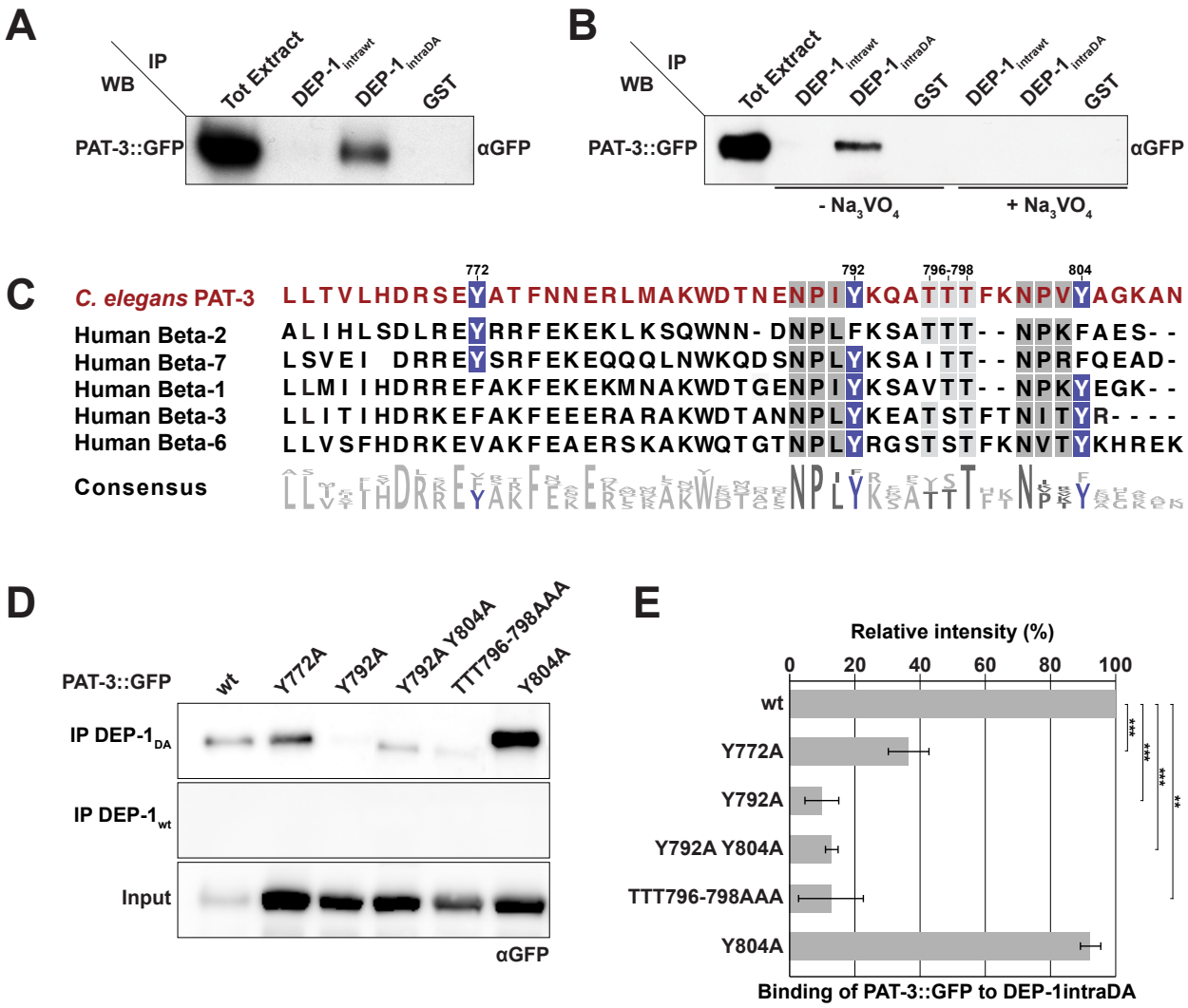

Figure 3.2 Interaction of PAT-3 with DEP-1 depends on NPxY phosphorylation.
(**A**) Co-IP confirms binding of DEP-1intraDA to PAT-3::GFP *in vitro*. (**B**) Interaction of DEP-1intraDA with PAT-3 is inhibited by the addition of 5 mM sodium orthovanadate (Na_3VO_4). (**C**) Alignment of the amino acid sequences of *C. elegans* PAT-3 and human β2, β7, β1, β3, and β6 cytoplasmic tails. Conserved tyrosines are highlited in purple and conserved NPxY domains are in grey. (**D**) Co-IP of DEP-1intra with different versions of PAT-3::GFP containing Tyr to Ala / Thr to Ala exchanges in the intracellular domain. (**E**) Quantification of the Co-IP experiments (relative intensity) that are shown in (**D**). All IPs were done in triplicates and normalized to the control Co-IP with wild-type PAT-3::GFP. Note that disruption of the Y792 in the first NPxY motif significantly diminishes binding to DEP-1. ** indicates a p-value≤0.005 and *** a p-value≤0.0005. Error bars report the standard error of the mean.

with alanine (Y772A, Y792A, Y792A Y804A, Y804A, and TTT796-798AAA). Co-IP experiments revealed that the interaction of DEP-1intraDA with PAT-3 containing the Y792A mutation (Y792A and Y792A Y804A) is significantly reduced (Fig. 3.1D and E). In contrast, the Y804A mutant did not affect the binding of DEP-1intraDA to PAT-3. Surprisingly, also the TTT796-798AAA mutation reduced significantly the interaction of PAT-3 with DEP-1intraDA. This might be caused by conformational changes that are induced by the replacement of the threonins TTT796-798 with alanines, leading to a disturbed interaction of DEP-1 with Y792 of the NPxY motif.
Taken together, our biochemical data indicate that DEP-1 dephosphorylates the tyrosine Y792, which is part of the first NPxY motif in the cytoplasmic tail of PAT-3.

3.1.5 PAT-3 is a negative regulator of RAS/MAPK signaling during vulval development

To further investigate the interaction between DEP-1 and PAT-3 *in vivo*, we examined the role of PAT-3 during *C. elegans* vulval development. Mutations in genes encoding components of signaling pathways that are involved during vulval development, such RAS/MAPK, NOTCH, and WNT pathways, change the patterning of the VPC fates. Mutations that hyperactivate the RAS/MAPK pathway, for example, cause the induction of more than three VPCs, resulting in a Multivulva phenotype (Félix, 2012). On the other hand, mutations that cause a decrease of RAS/MAPK signaling activity, lead to an induction of less than three VPCs and thus to a phenotype called Vulvaless. Thus, vulval induction by RAS/MAPK signaling can be quantified by counting the number of induced VPCs (Sternberg and Horvitz, 1986) and by determining the vulval index (VI).
dep-1(lf) single mutants develop a wild-type vulva due to redundancy of its phosphatase activity (Fig. 3.1 A; Berset, 2005). However, in the sensitized *let-60(gf)* background, in which the RAS/MAPK pathway is constitutively active because LET-60/RAS is hyperactivated (Ferguson and Horvitz, 1985), the role of DEP-1 as a negative regulator of RAS/MAPK signaling is evident. Compared to *let-60(gf)* single mutants (VI = 3.9), *dep-1(lf);let-60(gf)* double mutants exhibit highly increased vulval induction (VI = 5.5; Fig. 3.3 B, C and G; Berset, 2005). Thus, the sensitized *let-60(gf)* background enables the characterization of genes that influence RAS/MAPK signaling, which would otherwise not exhibit a vulval phenotype.
Loss-off PAT-2 or PAT-3 function results in strong "Paralyzed and Arrested at Two-fold" phenotypes, preventing an examination of their role when vulval development takes place. To overcome this problem, we reduced PAT-2 and PAT-3 function exclusively in the VPCs of *let-60(gf)* animals using the tissue-specific RNAi strain *let-60(gf);rde-1(ne219);zhEx418[lin-31::rde-1;myo-2::mCherry]* (Master thesis Anina Schneider). Compared to empty vector control treated animals, RNAi against both *pat-2* and *pat-3* increased the induction of VPCs significantly (Fig. 3.3 H). Furthermore, L4 larvae of *pat-2* and *pat-3* RNAi treated animals showed a similar adjacent primary fate (APF) phenotype as observed in *dep-1(lf);let-60(gf)* double mutants (Fig. 3.3 C-F; Berset, 2005).
To further determine the role of PAT-3 during vulval development, we disrupted *pat-3* function by a previously characterized dominant-negative construct (Lee et al., 2001), which was expressed under the vulval specific promoter of *lin-31* (Tan et al., 1998) in *let-60(n1046)* animals. In accordance with the RNAi results, animals expressing the dominant-negative PAT-3 showed significantly higher vulval induction compared to *let-60* animals control animals (Fig. 3.3 I).
In summary, these morphological changes in cell fate determination suggest that the PAT-2/PAT-3 integrins act as negative regulators of RAS/MAPK signaling during vulval development.

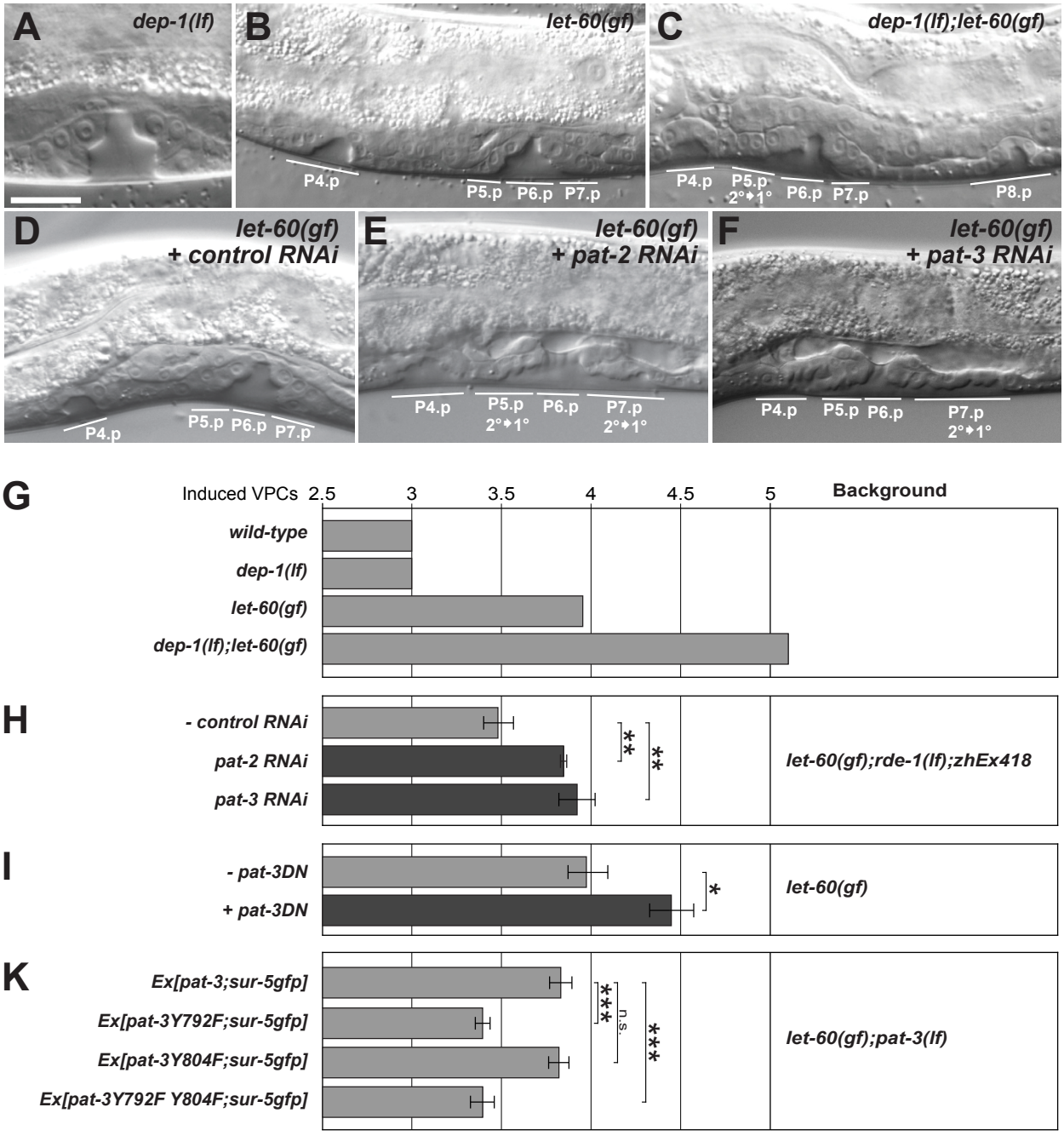

Figure 3.3 PAT-3 is a negative regulator of RAS/MAPK signaling during vulval development.
(**A**) Nomarski images of *dep-1(lf)* and (**B**) *let-60 ras (gf)* L4 larva. In *let-60(gf)* mutants, P5.p and P7.p have adopted the 2° fate, and their descendants remain attached to the cuticula, while some descendants of P4.p form an anterior pseudovulva. (**C**) *dep-1(lf);let-60(gf)* L4 larva exhibits 2°Cell fate transformation of P5.p in addition to the Muv phenotype. (**D-F**) RNAi in *let-60(gf);rde-1(ne219);zhEx418[lin-31::rde-1;myo-2::mCherry]* L4 larvae against empty vector control (**D**), *pat-2* (E), and *pat-3* (**F**). *pat-2i* and *pat-3i* cause similar cell fate transformation as in *dep-1(lf);let-60(gf)* animals. (**G**) Vulval induction is not altered in *dep-1(lf)* animals. However, *dep-1(lf)* increases the enhanced vulval induction of *let-60(gf)* animals in L4 staged animals. (**H**) RNAi against *pat-2* and *pat-3* enhances vulval induction of *let-60(gf);rde-1(ne219);zhEx418[lin-31::rde-1;myo-2::mCherry]* L4 larvae. (**I**) Vulval specific expression of dominant negative PAT-3 also increases vulval induction of *let-60(gf)* animals. (**K**) Extrachromosomal expression of PAT-3 containing Y792A transition decreases vulval induction of *let-60(gf);pat-3(lf)* animals. In contrast, expression of Y804F mutant PAT-3 does not alter vulval induction of *let-60(gf);pat-3(lf)* animals. * indicates a p-value≤0.05, ** a p-value≤0.005, and *** p-value≤0.0005. Error bars report the standard error of the mean. Scale bar represents 10 μm.

3.1.6 The influence of PAT-3 on RAS/MAPK signaling is regulated by the NPxY motif

Phosphorylation of cytoplasmic NPxY motifs is thought to be a switch mechanism for the control of integrin receptor activation (Oxley et al., 2008). Since our biochemical data indicated that DEP-1 binds to the first NPxY motif, we next investigated if tyrosine phosphorylation of Y792 regulates the inhibitory function of PAT-3 on RAS/MAPK signaling during vulval development. As reported previously, animals expressing PAT-3 with mutated NPxY motifs (*pat-3Y792F*, *pat-3Y804F*, and *pat-3Y792F*) rescue the embryonic lethality of *pat-3(st564)* null mutants and generate viable and fertile progeny (Lee et al., 2001). Thus, we analyzed these *pat-3* mutant constructs in the sensitized *pat-3(lf);let-60(gf)* background to examine the level of induced VPCs. As expected, the Y792 mutation causes a significant decrease of vulval induction, whereas the Y804 mutation did not show an alteration in induced vulval cells (Fig. 3.3 K). We therefore conclude that dephosphorylation of Y792 by DEP-1 activates PAT-3 to inhibit RAS/MAPK signaling during vulval development.

3.1.7 DEP-1 co-localizes with LET-23 and PAT-3 during vulval development

We next examined the expression pattern and subcellular localization of DEP-1, LET-23 and PAT-3 during vulval development. Therefore, we generated a functional endogenous DEP-1::mCherry reporter line by *MosTic* integration (Robert et al., 2009; see section 3.2.10) that was analyzed by confocal spinning disc microscopy. Expression of DEP-1::mCherry could be observed on the apical plasma membrane as well as in intracellular punctae of the VPC at the Pn.px and Pn.pxx larval stages (3.4 A' and B'). Similar results were observed with an endogenous DEP-1::GFP reporter line (see section 3.2.11), which was able to rescue the adjacent primary fate (APF) phenotype of *dep-1(lf);lip-1(lf)* animals. DEP-1::mCherry, which is slightly enhanced in the 2° lineage, partially co-localized with LET-23::GFP in punctate structure near the plasma membrane of both Pn.px and Pn.pxx staged animals (Fig. 3.4 A'' and B'').

As reported previously, a translational PAT-3::GFP reporter that is co-expressed with genomic INA-1, was expressed during vulval development within the AC, the basolateral side of the VPCs, as well as in neighboring somatic gonad (Hagedorn et al., 2009). Further expression studies together with DEP-1::mCherry revealed that DEP-1::mCherry partially co-localized with PAT-3::GFP at the basolateral side and in intracellular punctae of 2° VPCs of Pn.px (Fig. 3.4 C'') and Pn.pxx larvae (Fig. 3.4 D''). In later stages, namely in early L4 (Fig. 3.4 E'') and late L4 larvae (3.4 F''), DEP-1::mCherry expression and its co-localization with PAT-3::GFP was predominantly observed at the apical side of the 2° VPCs, but only rarely in intracellular punctae.

Finally, we tested if DEP-1 regulates the subcellular localization of PAT-3 and LET-23 in the VPCs. As mentioned before, PAT-3::GFP expression is usually seen at the basolateral side of the VPCs, whereas expression at the apical side is detected rarely. However, in *dep-1(lf)* mutants an enhanced apical accumulation of PAT-3::GFP in punctate structure was observed, indicating that DEP-1 might be involved in the regulation of integrin trafficking (Fig. 3.4 G and H). In contrast, no misexpression of LET-23::GFP could be observed in *dep-1(lf)* mutants (data not shown).

Taken together, these results indicate that DEP-1 interacts not only *in vitro* with its substrates LET-23 and PAT-3, but also *in vivo* during vulval development. In addition, our data suggest that DEP-1 might have a regulatory function to control endocytosis and trafficking of PAT-3.

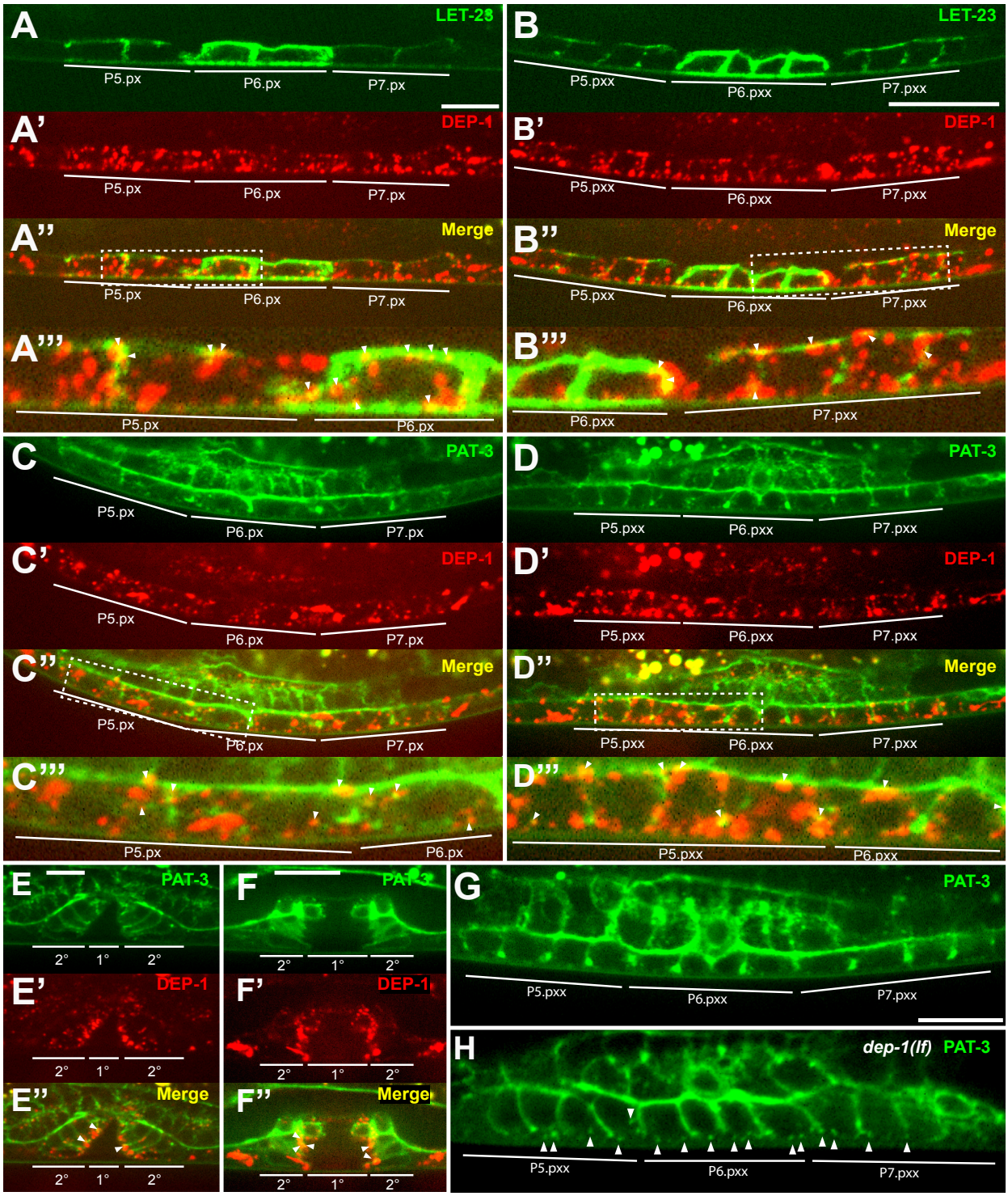

Figure 3.4 DEP-1 co-localizes with PAT-3 and LET-23 during vulval development.
(**A-B**) Expression of LET-23::GFP and DEP-1::mCherry at the Pn.px stage (**A**) and at the Pn.pxx stage (**B**). (**A**" and **B**") Merged images whereas details (dashed squares) are shown in (**A**"' and **B**"'). Arrow heads point at intracellular punctae containing both DEP-1::mCherry and LET-23::GFP. (**C-F**) Expression of PAT-3::GFP and DEP-1::mCherry at the Pn.px stage (**C**), at the Pn.pxx stage (**D**), after invagination (**E**) and at L4 christmas tree stage (**F**). (**C**"-**F**") Merged images whereas details (dashed squares) are shown in (**C**"') and (**D**"'). Arrow heads point at intracellular punctae containing both DEP-1::mCherry and PAT-3::GFP. (**G** and **H**) Expression of PAT-3::GFP in Pn.pxx stage. (**H**) In *dep-1(lf)* mutants, more PAT-3::GFP is expressed at the apical side, indicated by arrow heads. All images are z-projections (average intensity) of spinning-confocal z-stacks. Scale bar represents 10 µm.

3.1.8 Discussion

Activated integrins negatively regulate RAS/MAPK signaling during vulval development

Tyrosine phosphorylation by kinases and the subsequent dephosphorylation by phosphatases are key mechanisms that regulate intracellular signal transduction required for organogenesis. During *Caenorhabditits elegans* vulval development, the receptor protein tyrosine phosphatase DEP-1 (PTPRJ, PTP-η or CD148) inhibits EGFR/RAS/MAPK signaling in the secondary vulval cells through dephosphorylation of the EGF receptor. In order to identify novel physiological substrates of DEP-1, we performed pull-down experiments with the intracellular domain of DEP-1 containing the substrate trapping mutation D1241A and whole protein extract of *C. elegans*. Proteins that bound to DEP-1 were then identified by LC-MS/MS mass spectrometry. Among 43 proteins that bound solely to DEP-1intraDA, the β-integrin subunit PAT-3 was found.

PAT-3 binds almost exclusively to DEP-1 containing the substrate-trapping mutation D1241A that allows the catalytically inactive DEP-1 to remain bound to its phosphorylated substrate (Palka, 2002), but not to wild-type DEP-1. Together with the observation that the interaction of PAT-3 and DEP-1intraDA is completely inhibited in presence of the phosphatase inhibitor sodium orthovanadate, these data suggests that PAT-3 interacts with DEP-1 in a phosphorylation-dependent manner.

Our further biochemical results give evidence that DEP-1 dephosphorylates the tyrosine Y792 of the PAT-3 cytoplasmic tail, which is part of the evolutionary conserved NPxY motif. Phosphorylation of the NPxY motifs by Src-family kinases is essential for integrin activation and promotes the interaction with competing integrin-binding proteins, such as talin and DOK-1 (Oxley et al., 2008).

Talin, a major cytoskeletal protein that binds with high affinity to non-phosphorylated NPxY, triggers integrin activation (Critchley, 2000; Tadokoro et al., 2003). Moreover, it provides a mechanical link between integrins and the actin cytoskeleton, and induces conformational changes in the extracellular domain of the integrins (Ye et al., 2010). However, phosphorylation of the NPxY motif decreases binding of talin while increasing binding of DOK-1, which both inhibit integrin activation (Calderwood et al., 2003).

Results from cell culture experiments give evidence for this integrin activation "off switch", since NPxY phosphorylation reduces cell adhesion, leads to integrin displacement from focal adhesions, and affects cell migration, hemostasis and transformation (Datta et al., 2001; 2002; Johansson et al., 1994; Law et al., 1999; Sakai et al., 2001; 1998). Also data from *C. elegans* integrins highlight the important role of NPxY phosphorylation. *C. elegans* expressing PAT-3 with disrupted NPxY motifs are viable (Lee et al., 2001), but they display aberrant distal tip cell migration and ovulation, and defects in muscle cell formation and tail morphogenesis (Xu et al., 2010). This further suggests that NPxY motifs play important roles in the tissue-specific function of integrins.

Functional studies of NPxY motifs in mice showed that disruption of the NPxY motifs impairs the proliferation and survival of mouse embryonic fibroblasts (Hirsch et al., 2002). Furthermore, other data revealed that aberrant NPxY motifs in mouse β1 or β3 integrins affect integrin functions and platelet aggregation (Law et al., 1999), or cause bleeding defects and embryonic lethality (Chen et al., 2006).

In summary, numerous data indicate that phosphorylation of the NPxY motifs is crucial for integrin regulation, but its importance *in vivo* remains to be further determined.

Activated integrins negatively regulate RAS/MAPK signaling during vulval development

Vulval development of *C. elegans* provides a convenient model to study the functions of DEP-1 and PAT-3 *in vivo*. Our data reveal that vulval-specific knockdown of the integrin subunits *pat-2* and *pat-3* by RNAi or by expression of a dominant negative form of *pat-3* results in the enhancement of the multivulva phenotype of *let-60(gf)* animals, suggesting that integrins inhibit RAS/MAPK signaling in the secondary VPCs. Additionally, knockdown of *pat-2* and *pat-3* in *let-60(gf)* mutants results in a similar adjacent primary fate (APF) phenotype as it is observed in *dep-1(lf);let-60(gf)* double mutants (Berset, 2005). This transformation of the 2° cell fate into 1° fate with mixed 1° and 2° characteristics in P5.p and P7.p descendants further supports a negative regulatory function of the integrins during vulval development (Fig. 3.5).

The inhibitory effect of PAT-3 on RAS/MPK signaling can be activated when the tyrosine Y792 is mutated to phenylalanine, which mimics the enhanced dephosphorylation caused by *dep-1(gf)*. Interestingly, this is the same tyrosine being part of the regulatory NPxY motif, which has been identified to be the binding site of DEP-1 in our biochemical experiments. Hence, we have both *in vitro* and *in vivo* evidence that DEP-1 dephosphorylates PAT-3 at the first NPxY motif, which further supports the model that phosphorylation of the NPxY motifs plays a regulatory function in integrin activation.

The molecular mechanisms of how PAT-2/PAT-3 negatively inhibits RAS/MAPK signaling are not yet known. It also remains to be elucidated if the integrins negatively regulate the activity of the EGF receptor LET-23 themselves, or if the inhibitory effect of integrins concerns more downstream components of the RAS/MAPK signaling pathway, such as RAS/LET-60 (Fig. 3.5).

Since the cytoplasmic tails of integrins have no homology to other intracellular signaling motifs known (Cox et al., 2010), it is likely that the inhibitory effect on RAS/MAPK signaling is achieved indirectly over one or several of the numerous adaptor proteins that are known to bind to integrin β-tails (Fig. 3.5 protein "X"; Liu et al., 2000).

One of the most important adaptor protein is talin, which binds with high affinity to the non-phosphorylated NPxY motif and plays a crucial role in integrin activation (Critchley, 2000; Tadokoro et al., 2003). *C. elegans* talin (TLN-1, UNC-35) co-localizes with PAT-2 and PAT-3 (Moulder et al., 1996) and plays a central role in regulating distal tip cell migration. Furthermore, reduction of talin expression causes severe defects in gonad formation, disrupted oocyte maturation, and contractile muscle cells showed disorganization of the actin cytoskeleton leading to complete paralysis, a phenotype that was also observed with depletion of *pat-2* and *pat-3*. (Cram et al., 2003). Thus, it would be conceivable that the inhibitory effect of PAT-2/PAT-3 on RAS/MAPK signaling observed in this study might be acting indirectly via talin/UNC-35.

However, there are also other possibilities of how integrins can collaborate with EGFR or other growth factor receptors (GFR). First, it has been reported that the signaling function of integrins depends on intracellular signal molecules, which are shared with other growth factor signaling pathways, for example Shc, Src family kinases, RAS-MAPK, JNK, PKC and PI3K (Clark and Brugge, 1995; Fantl et al., 1993; Howe et al., 1998; Schlaepfer and Hunter, 1998; Schwartz et al., 1995). Furthermore, focal adhesion kinase (FAK) is associated with both, integrin signaling and several different signaling proteins (Mitra and Schlaepfer, 2006). However, loss of *kin-32*/FAK did not alter the vulval induction of *let-60(gf)* animals (PhD thesis of Itay Naktimon, table 1), indicating that FAK is not involved in regulating RAS/MAPK signaling during vulval development.

Second, integrins mutually collaborate with GFR to create an environment in which the GFRs can properly interact with downstream signaling molecules (Yamada and Even-Ram, 2002). This crosstalk

may involve direct induction of EGFR phosphorylation by integrin binding, signal amplification of GF-induced receptor activation by integrin-ECM ligation, or physical interaction between the receptors (Giancotti and Tarone, 2003).
Third, integrins mediate direct activation of GFRs, including direct interaction between the receptors. αVβ3 and β1 for example associate with EGFR on the membrane, and the clustering of the two receptor types triggers transactivation (Moro, 2001). Forth, many growth factors activate the expression of integrins, which in turn may further activate signaling by GFRs, such as the hepatocyte growth factor, which increases selectively the expression of α2 and α3 integrins (Chiu et al., 2002).
In most of these cases, integrins appear to function as positive regulators of GFR signaling. However, there are also mechanisms described in which integrins negatively regulate GFR signaling. One example is the α1β1 mediated activation of the T cell protein tyrosine phosphatase TCPTP, which induces dephosphorylation of EGFR, VEGFR2, and PDGFRβ to attenuate their activity (Mattila et al., 2008; 2010; 2005).

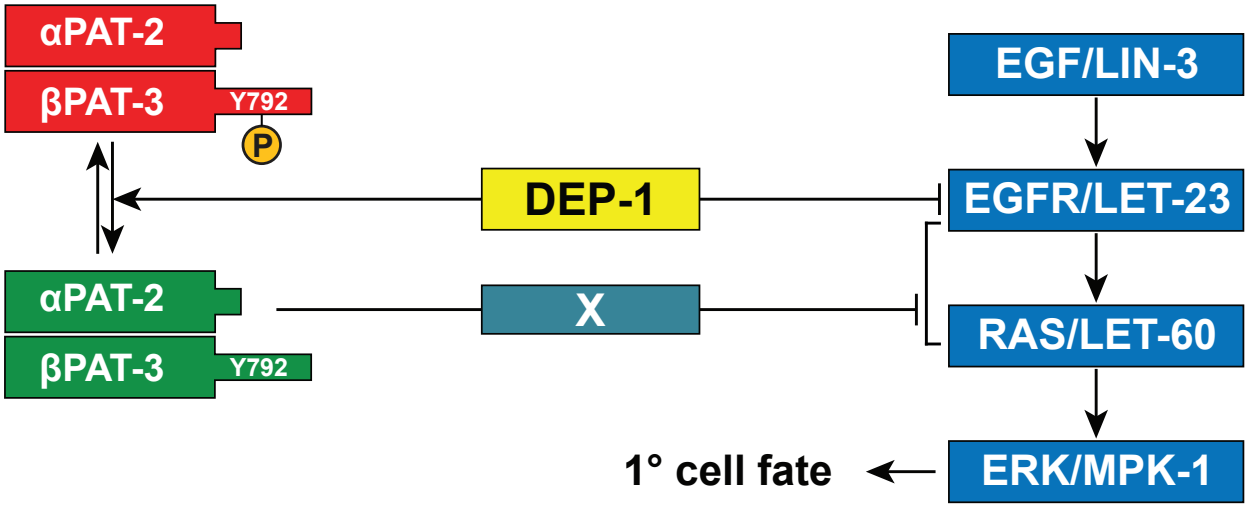

Figure 3.5 A model for PAT-3/PAT-2 and DEP-1 function during vulval development.
EGF activates the EGFR/RAS/MPK signaling pathway to induce 1° cell fate specific gene expression. DEP-1 blocks the transduction of the inductive signal by dephosphorylating the EGFR LET-23. In addition, DEP-1 dephosphorylates the cytoplasmic tail of β integrin PAT-3 (Y702) to activate the integrin heterodimers PAT-2/PAT-3, which in turn negatively regulate RAS/MPK signaling.

NPxY motifs are involved in PAT-3 trafficking

The expression pattern of PAT-3::GFP and DEP-1::mCherry give further evidence that DEP-1 and PAT-3 do not only interact *in vitro*, but also *in vivo* during vulval development. Furthermore, co-localization of DEP-1 with both LET-23 and PAT-3 is observed in similar subcellular regions, namely in intracellular punctae as well as at the membrane, suggesting that all three transmembrane protein might interact with each other in a complex inside the cells. However, this hypothesis remains to be elucidated.
In addition, the examination of the expression pattern of PAT-3::GFP indicates that DEP-1 not only activates PAT-3, but also might regulate its subcellular localization. While PAT-3::GFP expression is

normaly seen at the basolateral side of the VPCs, loss off *dep-1* enhances apical accumulation of PAT-3::GFP, suggesting induced endocytosis of PAT-3 in *dep-1(lf)* mutants. We have to admit that these changes in subcellular localization are very weak and due to the limits of optical resolution we have not yet been able to quantify these changes.
However, it is known that integrins are constantly internalized and recycled back to the plasma membrane in most cell types (Pellinen, 2006) to control integrin-dependent cell adhesion, spreading and migration, as well as cancer cell invasion (Margadant et al., 2011). Both clathrin-mediated endocytosis and clathrin-independent internalization of integrins have been demonstrated for integrins.
The NPxY motifs are canonical signals for clathrin-mediated endocytosis of various surface receptors (Ohno et al., 1995), and several observations suggest that they are also involved in the regulation of integrin endocytosis. First, the β3-endonexin-mediated internalization of ligand-bound integrins is impaired when Y is substituted to A in the membrane proximal NPxY motif. Second, F to A substitutions in either one of the NPxY motifs of β2 integrins compromises their endocytosis. And third, clathrin-dependent integrin endocytosis in fibroblasts is reduced when Y is mutated to F in both NPxY motifs (Pellinen et al., 2008).
Nevertheless, the exact pathways involved in the endocytosis of integrins are not clearly known and seem to vary between integrin heterodimers (Ramsay et al., 2007; Upla et al., 2004). Moreover, it remains unclear how the individual NPxY motifs regulate integrin trafficking, and through which proteins this is achieved.

Several studies based on cell-culture experiments investigated the manifold functions of integrins and DEP-1, and showed that both seem to participate in a large number of protein-protein interactions. However, only some of these interactions have been observed *in vitro*, and the lack of *in vivo* confirmation makes it difficult to estimate the physiological relevance of many observations (Ivaska and Heino, 2011).
Our data describe a novel connection between integrins and RAS/MAPK, which both are of central importance during developmental processes and cancer formation. Moreover, our results established vulval development as a system to study the role of integrin activity during developmental processes, and to analyze the connection to the RAS/MAPK signaling pathway *in vivo*.

3.1.9 Proteins identified by GST::DEP-1 pull-down experiments and MS/MS analyses

Gene name	Accession Number		pTB29_20101117	pTB29_20101101	pTB29_20101220	pTB30_20101117	pTB30_20101101	pTB30_20101220	pGEX_20101117	pGEX_20101101	pGEX_20101220	Protein Abundance (ppm)
pat-2	P34446	Integrin alpha pat-2 (Paralyzed arrest at two-fold protein 2)	4	0	0	43	33	23	0	0	0	58.8
pat-3	Q27874	Integrin beta pat-3 (Paralyzed arrest at two-fold protein 3)	0	0	0	29	18	7	0	0	0	42
nid-1	C7FZU3	Protein F54F3.1b, partially confirmed by transcript evidence	2	2	0	25	16	0	0	0	0	63.8
prp-8	P34369	Pre-mRNA-splicing factor 8 homolog	0	3	0	12	16	0	0	0	0	65.6
rps-6	Q9NEN6	40S ribosomal protein S6	0	10	7	8	15	8	0	0	0	2440
K12D12.1	Q23670	Probable DNA topoisomerase 2	0	2	0	8	9	0	0	0	0	111
puf-12	Q09622	Pumilio domain-containing protein 12	0	0	2	7	5	0	0	0	0	107
vit-4	P18947	Vitellogenin-4	0	0	0	7	4	2	0	0	0	570
apl-1	Q10651	Beta-amyloid-like protein	0	0	0	6	5	0	0	0	0	8.26
F08D12.1	P91240	Signal recognition particle 72 kDa protein homolog	0	0	0	6	0	0	0	0	0	134
rpl-16	Q27389	60S ribosomal protein L13a	9	5	0	5	9	5	0	0	0	2404
eft-1	Q23463	Elongation factor protein 1, confirmed by transcript evidence	0	0	5	5	5	4	0	0	0	70.8
avr-15	Q95PJ6	Protein R11G10.1b, confirmed by transcript evidence	0	0	0	4	2	0	0	0	0	4.21
mcm-5	Q21902	DNA replication licensing factor mcm-5	2	0	2	4	0	3	0	0	0	69.5
C13B9.3	Q09236	Probable coatomer subunit delta (Delta-coat protein)	2	2	0	4	0	0	0	0	0	164
eif-3	O02328	Eukaryotic translation initiation factor 3 subunit C	0	0	0	4	0	0	0	0	0	169
kin-19	P42168	Casein kinase I isoform alpha	0	0	0	4	0	0	0	0	0	160
sym-1	Q93374	Protein C44H4.3	0	0	0	4	0	0	0	0	0	52.2
Q95XR0	Q95XR0	Putative uncharacterized protein	2	0	0	3	5	2	0	0	0	289
pro-3	Q9NEU2	Protein SDA1 homolog	0	0	2	3	3	2	0	0	0	24.6
mrs-1	Q20970	Methionyl-tRNA synthetase, cytoplasmic	0	0	0	3	2	2	0	0	0	120
F58G11.2	P90897	Putative uncharacterized protein F58G11.2	0	0	5	3	0	0	0	0	0	74.9
cnx-1	P34652	Calnexin homolog	0	0	0	3	0	0	0	0	0	72.6
F14B4.3	Q27493	Protein F14B4.3, partially confirmed by transcript evidence	0	0	0	3	0	0	0	0	0	31.7
math-33	O45623	Protein H19N07.2a, confirmed by transcript evidence	0	0	0	3	0	0	0	0	0	71.3
ngp-1	Q56VZ2	Protein T19A6.2c, confirmed by transcript evidence	0	0	0	3	0	0	0	0	0	63.3
T05E11.3	Q22235	Protein T05E11.3a, confirmed by transcript evidence	0	0	0	3	0	0	0	0	0	448
rpl-11.2	Q19162	Ribosomal protein, large subunit protein 11.2	4	4	5	2	5	3	0	0	0	808
car-1	Q9XW17	Protein Y18D10A.17, confirmed by transcript evidence	3	0	3	2	3	3	0	0	0	524
C18B2.3	Q18074	Putative uncharacterized protein	2	3	0	2	3	2	0	0	0	153
rpt-2	O16368	Probable 26S protease regulatory subunit 4	0	2	0	2	2	0	0	0	0	535
K04C2.2	Q21210	Putative uncharacterized protein	0	0	0	2	2	0	0	0	0	65.5
his-24	P10771	Histone H1.1	0	0	0	2	0	2	0	0	0	596
rsp-1	Q23121	Probable splicing factor, arginine/serine-rich 1 (CeSRp75) (RNA-binding protein srp-5)	0	0	2	2	0	0	0	0	0	199
abcf-3	Q20306	Putative uncharacterized protein	0	0	0	2	0	0	0	0	0	96
ama-1	P16356	DNA-directed RNA polymerase II subunit RPB1 (RNA polymerase II subunit B1)	0	0	0	2	0	0	0	0	0	66.1
npp-13	Q9BKT9	Nuclear pore complex protein protein 13, isoform a	0	0	0	2	0	0	0	0	0	102
nsf-1	Q09EE7	Protein H15N14.2b, confirmed by transcript evidence	0	0	0	2	0	0	0	0	0	90.8
nst-1	Q21086	Guanine nucleotide-binding protein-like 3 homolog (Nucleostemin-1)	0	0	0	2	0	0	0	0	0	108
pgl-1	Q304E5	P granule abnormality protein 1, isoform b	0	0	0	2	0	0	0	0	0	97.2
rpb-2	Q10578	RNA polymerase II subunit B2	0	0	0	2	0	0	0	0	0	59.4
tps-2	O45380	Trehalose-6-phosphate synthase 2	0	0	0	2	0	0	0	0	0	27.2
unc-54	Q09981	UNC-45	0	0	0	2	0	0	0	0	0	2658
ZK550.3	O62512	Protein ZK550.3, partially confirmed by transcript evidence	0	0	0	2	0	0	0	0	0	40
Y37E3.8	Q9BKU5	Putative uncharacterized protein	0	4	3	0	5	0	0	0	0	2162
Y62H9A.6	Q9XWT3	Protein Y62H9A.6, confirmed by transcript evidence	0	0	2	0	3	0	0	0	0	565
Y54G2A.2	Y54G2A.2	Protein Y54G2A	0	0	0	0	3	0	0	0	0	
ivd-1	O44446	Isovaleryl-CoA dehydrogenase ivd-1	0	0	0	0	2	2	0	0	0	389
rps-5	P49041	40S ribosomal protein S5	4	4	3	0	2	0	0	0	0	1535
F55A12.5	O01756	Putative uncharacterized protein	3	0	0	0	2	0	0	0	0	28.3
rpl-15	P91374	60S ribosomal protein L15	0	5	0	0	2	0	0	0	0	2131

F44E5.1	Q9XU97	Protein F44E5.1, confirmed by transcript evidence	0	0	0	0	2	0	0	0	0	709
F45H10.2	O45525	Protein F45H10.2, confirmed by transcript evidence	0	0	0	0	2	0	0	0	0	271
F46F11.1	P91309	Inositol hexakisphosphate and diphosphoinositol-pentakisphosphate kinase	0	0	0	0	2	0	0	0	0	18.6
imb-4	Q23089	Importin beta family protein 4, isoform a	0	0	0	0	2	0	0	0	0	46.7
R09F10.8	Q23031	Putative uncharacterized protein	0	0	0	0	2	0	0	0	0	8.03
rpl-38	O17570	60S ribosomal protein L38	0	0	0	0	2	0	0	0	0	1169
plp-1	Q94230	Pur alpha like protein protein 1, confirmed by transcript evidence	0	0	0	0	0	4	0	0	0	468
cey-1	O62213	Protein F33A8.3, confirmed by transcript evidence	0	0	0	0	0	3	0	0	0	1132
K01G5.5	O17919	Putative H/ACA ribonucleoprotein complex subunit 4	0	0	0	0	0	3	0	0	0	245
ret-1	A5JYU4	Protein W06A7.3f	0	0	0	0	0	3	0	0	0	69.1
Y62H9A.3	Q9XWT5	Protein Y62H9A.3, confirmed by transcript evidence	0	0	0	0	0	3	0	0	0	12.9
cdc-48.1	P54811	Transitional endoplasmic reticulum ATPase homolog 1	3	0	3	0	0	2	0	0	0	436
rab-11.1	O01803	Rab family protein 11.1	2	3	0	0	0	2	0	0	0	226
C46G7.2	O02141	Putative uncharacterized protein	0	3	0	0	0	2	0	0	0	211
ran-1	O17915	GTP-binding nuclear protein ran-1 (Ras-related nuclear protein 1)	0	2	0	0	0	2	0	0	0	831
sqd-1	Q8MXR6	Homologous to drosophila sqd (Squid) protein protein 1	0	2	0	0	0	2	0	0	0	1530
C05G5.4	P53596	Succinyl-CoA synthetase subunit alpha	0	0	0	0	0	2	0	0	0	1365
C10G11.7	P91027	Putative uncharacterized protein	0	0	0	0	0	2	0	0	0	547
imp-2	P49049	Intramembrane protease 2	0	0	0	0	0	2	0	0	0	76.7
R04D3.3	Q21713	Protein R04D3.3 , partially confirmed by transcript evidence	0	0	0	0	0	2	0	0	0	1.15
rpt-5	O76371	Proteasome regulatory particle, atpase-like protein 5	0	0	0	0	0	2	0	0	0	834
let-711	Q20937	Lethal protein 711, partially confirmed by transcript evidence	2	2	0	0	0	0	0	0	0	26.9
tag-18	Q22508	Temporarily assigned gene name protein 18	2	2	0	0	0	0	0	0	0	131
asp-1	Q9TVS4	Aspartic protease 1	2	0	0	0	0	0	0	0	0	1290
cey-2	P91306	Y-box protein 2, confirmed by transcript evidence	2	0	0	0	0	0	0	0	0	490
cox-2	P24894	Cytochrome c oxidase subunit 2	2	0	0	0	0	0	0	0	0	74.2
D2045.2	Q18983	Protein D2045.2, partially confirmed by transcript evidence	2	0	0	0	0	0	0	0	0	37.2
npp-8	Q95Y15	Nuclear pore complex protein protein 8, isoform b	2	0	0	0	0	0	0	0	0	21.8
pat-4	Q9TZC4	Paralysed arrest at two-fold protein 4, confirmed by transcript evidence	2	0	0	0	0	0	0	0	0	67
R13H4.2	A5Z2W3	Protein R13H4.2a, confirmed by transcript evidence	2	0	0	0	0	0	0	0	0	35.1
rps-30	Q18231	Ribosomal protein, small subunit protein 30, confirmed by transcript evidence	0	2	2	0	0	0	0	0	0	154
larp-1	D5MCN1	Larp (Rna binding la related protein) homolog protein 1	0	2	0	0	0	0	0	0	0	304
dpy-11	Q9UAV4	Dumpy : shorter than wild-type protein 11	0	2	0	0	0	0	0	0	0	135
F25H2.2	Q93566	Protein F25H2.2, confirmed by transcript evidence	0	2	0	0	0	0	0	0	0	1.91
F55C5.8	Q20822	Probable signal recognition particle 68 kDa protein (SRP68)	0	2	0	0	0	0	0	0	0	106
gfi-1	Q94246	Gei-4(Four) interacting protein protein 1	0	2	0	0	0	0	0	0	0	60.9
his-2	P08898	Histone H3	0	2	0	0	0	0	0	0	0	187
ift-74	Q18106	Ift (Chlamydomonas intraflagellar transport) homolog protein 74	0	2	0	0	0	0	0	0	0	
K07H8.10	O45181	Putative uncharacterized protein	0	2	0	0	0	0	0	0	0	230
rop-1	Q27274	60 kDa SS-A/Ro ribonucleoprotein homolog	0	2	0	0	0	0	0	0	0	74.8
dhs-3	A5JYX4	Protein T02E1.5a, confirmed by transcript evidence	0	0	2	0	0	0	0	0	0	104
F23B12.4	A8WHS3	Protein F23B12.4a, confirmed by transcript evidence	0	0	2	0	0	0	0	0	0	10.2
kin-3	P18334	Casein kinase II subunit alpha	0	0	2	0	0	0	0	0	0	220
mcm-7	O16297	Yeast mcm (Licensing factor) related protein 7	0	0	2	0	0	0	0	0	0	39.1
tag-174	Q20779	Probable cytochrome c oxidase subunit 6A	0	0	2	0	0	0	0	0	0	379
tba-4	Q20409	Protein F44F4.11, partially confirmed by transcript evidence	0	0	2	0	0	0	0	0	0	426
ubl-1	P37165	Ubiquitin-like protein 1-40S ribosomal protein S27a	0	0	2	0	0	0	0	0	0	592
atp-3	P91283	Atp synthase subunit protein 3, isoform a, confirmed by transcript evidence	6	6	6	0	2	9	0	0	2	1538
trap-3	Q95XS1	Translocon-associated protein protein 3, confirmed by transcript evidence	0	0	0	0	0	0	0	0	2	295
rpl-10	Q09533	60S ribosomal protein L10 (QM protein homolog)	10	12	9	12	11	9	0	2	0	2038
Y25C1A.5	Q9TYL9	Coatomer subunit beta (Beta-coat protein)	0	0	4	7	3	5	0	2	0	127
eif-3.B	Q9XWI6	Eukaryotic translation initiation factor 3 subunit B (eIF3b)	0	0	2	6	0	3	0	2	0	100
egl-45	P34339	Egg-laying defective protein 45 (Eukaryotic translation initiation factor 3 subunit 10)	2	2	0	4	0	3	0	2	0	208
alg-1	B6VQ75	Protein F48F7.1b	0	0	4	3	2	2	0	2	0	72.5
Y59A8A.3	Q9GRZ9	Protein Y59A8A.3, confirmed by transcript evidence	0	0	2	3	0	4	0	2	0	362
rps-24	Q1XFY9	Ribosomal protein, small subunit protein 24	0	3	6	2	4	5	0	2	0	2060
lmp-1	Q11117	LAMP family protein lmp-1	2	2	2	2	0	0	0	2	0	139
imb-5	Q965V4	Importin beta family protein 5	0	0	4	2	0	0	0	2	0	45.7
dnj-29	Q9U1V9	Protein Y63D3A.6b, confirmed by transcript evidence	0	0	0	2	0	0	0	2	0	73.6

npp-9	Q21021	Protein F59A2.1a, confirmed by transcript evidence	0	0	0	2	0	0	0	2	0	217
rskn-2	Q18846	PRibosomal protein S6 kinase alpha-5 homolog	0	0	0	2	0	0	0	2	0	45.8
spl-1	Q9Y194	Sphingosine-1-phosphate aldolase	0	0	0	2	0	0	0	2	0	95.9
rpl-32	Q22716	Protein T24B8.1a, confirmed by transcript evidence	2	0	2	0	3	3	0	2	0	2363
rps-27	Q9TXP0	40S ribosomal protein S27	0	0	0	0	2	2	0	2	0	191
unc-116	P34540	Kinesin heavy chain (Uncoordinated protein 116)	0	3	2	0	2	0	0	2	0	179
rpl-25.1	P48162	60S ribosomal protein L23a 1	0	0	0	0	2	0	0	2	0	1316
tba-3	P91910	Tubulin alpha-3 chain (Mechanosensory abnormality protein 12)	0	0	0	0	2	0	0	2	0	
prmt-1	Q9U2X0	Protein Y113G7B.17, confirmed by transcript evidence	2	0	0	0	0	0	0	2	0	446
Y57G11C	O18239	Putative uncharacterized protein Y57G11C.15	2	0	0	0	0	0	0	2	0	190
nuo-1	Q17880	Protein C09H10.3, confirmed by transcript evidence	0	2	2	0	0	0	0	2	0	249
gst-16	Q93698	Protein F37B1.5, partially confirmed by transcript evidence	0	2	0	0	0	0	0	2	0	24.4
rla-2	Q9U1X9	Protein Y62E10A.1, confirmed by transcript evidence	0	0	2	0	0	0	0	2	0	5637
Y67H2A.5	Q95PZ1	Protein Y67H2A.5, confirmed by transcript evidence	0	0	2	0	0	0	0	2	0	670
acdh-11	Q3T978	Protein Y45F3A.3b, confirmed by transcript evidence	0	0	0	0	0	0	0	2	0	68.6
acs-11	Q20264	Fatty acid coa synthetase family protein 11, partially confirmed by transcript evidence	0	0	0	0	0	0	0	2	0	294
acs-5	Q9XWD1	Protein Y76A2B.3, confirmed by transcript evidence	0	0	0	0	0	0	0	2	0	83.7
arp-1	Q9NA98	Protein Y53F4B.22, confirmed by transcript evidence	0	0	0	0	0	0	0	2	0	202
C34F11.3	D7SFL2	Putative uncharacterized protein	0	0	0	0	0	0	0	2	0	170
clp-1	P34308	Calpain clp-1	0	0	0	0	0	0	0	2	0	203
D1005.1	P53585	Probable ATP-citrate synthase	0	0	0	0	0	0	0	2	0	152
dpf-3	O44987	Dipeptidyl peptidase four (Iv) family protein 3	0	0	0	0	0	0	0	2	0	40.1
emb-8	Q09590	NADPH--cytochrome P450 reductase	0	0	0	0	0	0	0	2	0	75.9
F07A11.2	Q19130	Protein F07A11.2a, confirmed by transcript evidence	0	0	0	0	0	0	0	2	0	22.6
gsk-3	Q9U2Q9	Glycogen synthase kinase-3	0	0	0	0	0	0	0	2	0	177
gsnl-1	Q21253	Gelsolin-like protein 1	0	0	0	0	0	0	0	2	0	136
gsp-1	Q27497	Serine/threonine-protein phosphatase PP1-alpha	0	0	0	0	0	0	0	2	0	202
H03A11.2	Q9XTW1	Protein H03A11.2, partially confirmed by transcript evidence	0	0	0	0	0	0	0	2	0	48.1
haf-4	Q9TZD9	Half transporter (Pgp related) protein 4	0	0	0	0	0	0	0	2	0	56.1
hpo-29	Q8WTL6	Putative uncharacterized protein	0	0	0	0	0	0	0	2	0	
immt-1	Q22505	Putative uncharacterized protein	0	0	0	0	0	0	0	2	0	294
nduf-5	Q9N3D9	Putative uncharacterized protein	0	0	0	0	0	0	0	2	0	453
npl-4.2	O01894	Putative uncharacterized protein	0	0	0	0	0	0	0	2	0	37.2
pod-2	Q9GZI3	Polarity and osmotic sensitivity defect protein 2, isoform a	0	0	0	0	0	0	0	2	0	57.6
ppw-1	O02095	Paz/piwi domain-containing protein 1	0	0	0	0	0	0	0	2	0	34.9
ppw-2	Q9N585	Paz/piwi domain-containing protein 2	0	0	0	0	0	0	0	2	0	29.4
R02D3.1	O44503	Putative uncharacterized protein R02D3.1	0	0	0	0	0	0	0	2	0	179
ran-3	Q18211	Regulator of chromosome condensation (RCC1 homolog)	0	0	0	0	0	0	0	2	0	182
rpn-5	Q19324	Proteasome regulatory particle, non-atpase-like protein 5	0	0	0	0	0	0	0	2	0	223
tag-320	Q11067	Probable protein disulfide-isomerase A6	0	0	0	0	0	0	0	2	0	415
tba-1	O18688	Protein F26E4.8, confirmed by transcript evidence	0	0	0	0	0	0	0	2	0	573
ttr-2	P34500	Transthyretin-like protein 2	0	0	0	0	0	0	0	2	0	364
ttr-24	Q9XXR4	Protein Y51A2D.9, confirmed by transcript evidence	0	0	0	0	0	0	0	2	0	119
Y71H10B.1	Q86MI3	Putative uncharacterized protein	0	0	0	0	0	0	0	2	0	74
Y71H2AR.1	Q9BL27	Putative uncharacterized protein	0	0	0	0	0	0	0	2	0	184
ZK669.4	Q23571	Protein ZK669.4, confirmed by transcript evidence	0	0	0	0	0	0	0	2	0	174
ZK829.7	Q23624	Protein ZK829.7, confirmed by transcript evidence	0	0	0	0	0	0	0	2	0	175
ZK836.2	Q23629	Probable 2-oxoglutarate dehydrogenase E1 component DHKTD1 homolog	0	0	0	0	0	0	0	2	0	117
cyp-25a5	O44485	Cytochrome p450 family protein 25A5	0	0	0	0	0	0	0	2	0	
rps-25	P52821	40S ribosomal protein S25	2	2	6	2	5	6	0	2	2	2175
B0303.3	P34255	Uncharacterized protein B0303.3	0	0	3	2	4	3	0	2	2	426
rpl-31	Q9U332	60S ribosomal protein L31	0	0	3	0	2	2	0	2	2	864
nduf-7	Q94360	NADH-ubiquinone oxidoreductase 20 kDa subunit	0	0	0	0	0	0	0	2	2	
Y71F9AL.17	Q9N4H7	Putative uncharacterized protein	4	0	0	10	4	5	0	3	0	145
T22D1.4	Q9GZH4	Putative uncharacterized protein	0	3	2	2	0	0	0	3	0	198
rpl-35	P34662	60S ribosomal protein L35	0	3	3	0	2	2	0	3	0	4176
let-805	Q9UB28	Myotactin form B	0	0	0	0	2	0	0	3	0	87.1
alh-12	Q7Z1Q2	Aldehyde dehydrogenase protein 12, isoform b	0	0	0	0	0	0	0	3	0	391
apb-1	Q9N4F3	APB-1 protein, isoform a	0	0	0	0	0	0	0	3	0	122

C32F10.8	O01685	Putative uncharacterized protein C32F10.8	0	0	0	0	0	0	0	3	0	417
C41G7.9	B3WFW9	Protein C41G7.9a, confirmed by transcript evidence	0	0	0	0	0	0	0	3	0	277
drp-1	Q8WQC9	Dynamin related protein protein 1, isoform b	0	0	0	0	0	0	0	3	0	76.2
F42G9.1	P49595	Probable protein phosphatase 2C F42G9.1	0	0	0	0	0	0	0	3	0	137
F52E4.5	Q20675	Putative uncharacterized protein	0	0	0	0	0	0	0	3	0	131
glh-1	P34689	ATP-dependent RNA helicase glh-1	0	0	0	0	0	0	0	3	0	119
H19N07.1	O45622	Protein H19N07.1a, confirmed by transcript evidence	0	0	0	0	0	0	0	3	0	176
haf-9	O44897	Half transporter (Pgp related) protein 9, isoform a	0	0	0	0	0	0	0	3	0	74.2
M106.4	Q09580	Glutamine amidotransferase	0	0	0	0	0	0	0	3	0	98.7
mvk-1	Q9N4Z7	Putative uncharacterized protein	0	0	0	0	0	0	0	3	0	
oig-2	Q9XWM1	Protein Y38F1A.9, partially confirmed by transcript evidence	0	0	0	0	0	0	0	3	0	179
pdi-3	O17908	CeERp57	0	0	0	0	0	0	0	3	0	1362
R06C7.1	Q21770	Germ cell-expressed protein R06C7.1	0	0	0	0	0	0	0	3	0	42.2
rnr-1	Q03604	Ribonucleotide reductase large subunit	0	0	0	0	0	0	0	3	0	69.1
rps-21	P49197	40S ribosomal protein S21	0	0	0	0	0	0	0	3	0	2616
T20B3.1	Q9XUN8	Protein T20B3.1, confirmed by transcript evidence	0	0	0	0	0	0	0	3	0	49.2
tax-6	Q0G819	Protein C02F4.2c, partially confirmed by transcript evidence	0	0	0	0	0	0	0	3	0	101
Y67D2.3	Q9BKQ9	Putative uncharacterized protein	0	0	0	0	0	0	0	3	0	262
fbp-1	Q9N2M2	Fructose-1,6-biphosphatase protein 1	3	0	4	2	0	3	0	3	2	690
rpn-3	Q04908	26S proteasome regulatory subunit rpn-3	0	0	0	2	0	2	0	3	2	306
F38E11.5	Q20168	Probable coatomer subunit beta' (Beta'-coat protein))	2	0	3	6	0	5	0	3	3	217
F59C6.5	Q93831	Protein F59C6.5, confirmed by transcript evidence	0	0	0	0	0	0	0	3	3	405
vit-1	P55155	Vitellogenin-1	7	4	7	39	30	13	0	4	0	715
abcf-2	Q9XTD9	Protein T27E9.7, confirmed by transcript evidence	2	2	0	3	0	0	0	4	0	112
Y46G5A.4	Q9U2G0	Putative U5 small nuclear ribonucleoprotein 200 kDa helicase (EC 3.6.4.13)	0	5	0	2	3	0	0	4	0	56.4
ears-1	Q23315	Protein ZC434.5, confirmed by transcript evidence	2	0	0	2	2	3	0	4	0	
pyr-1	Q18990	Protein D2085.1, partially confirmed by transcript evidence	0	2	0	2	0	0	0	4	0	103
crt-1	P27798	Calreticulin	0	2	0	0	2	0	0	4	0	3113
nmt-1	P46548	Myristoyl-CoA:protein N-myristoyltransferase	2	3	0	0	0	0	0	4	0	163
msp-10	P05634	Major sperm protein 10/36/56/76 (MSP)	0	2	2	0	0	0	0	4	0	56.8
rpl-36	P49181	60S ribosomal protein L36	0	0	3	0	0	0	0	4	0	1493
cyn-15	Q9U1Q3	Protein Y87G2A.6, confirmed by transcript evidence	0	0	0	0	0	0	0	4	0	47.1
F55H12.4	P90889	Protein F55H12.4, confirmed by transcript evidence	0	0	0	0	0	0	0	4	0	72.9
iff-2	Q20751	Eukaryotic translation initiation factor 5A-2	0	0	0	0	0	0	0	4	0	643
lrp-1	Q04833	Low-density lipoprotein receptor-related protein (LRP)	0	0	0	0	0	0	0	4	0	16.1
T04A8.7	Q22137	Protein T04A8.7a, confirmed by transcript evidence	0	0	0	0	0	0	0	4	0	143
ZC416.6	O44183	Putative uncharacterized protein ZC416.6	0	0	0	0	0	0	0	4	0	16.5
egl-4	O76360	cGMP-dependent protein kinase egl-4	3	2	3	8	4	2	0	5	0	113
ars-2	O01541	Alanyl-tRNA synthetase, cytoplasmic	2	2	2	5	2	0	0	5	0	292
alh-3	Q19428	Protein F36H1.6, confirmed by transcript evidence	0	0	0	4	0	0	0	5	0	412
R05F9.6	Q21742	Putative uncharacterized protein	4	3	0	3	0	2	0	5	0	378
ddb-1	Q21554	DNA damage-binding protein 1	2	0	0	0	2	0	0	5	0	32.1
grs-1	Q10039	Glycyl-tRNA synthetase	0	2	0	0	0	0	0	5	0	344
fars-1	Q86B36	Phenylalanyl amino-acyl trna synthetase protein 1, isoform b	0	0	0	0	0	0	0	5	0	
pars-1	Q22620	Prolyl trna synthetase protein 1, isoform a	0	0	0	0	0	0	0	5	0	
spc-1	Q21408	Spectrin protein 1	0	0	0	0	0	0	0	5	0	295
unc-18	P34815	Putative acetylcholine regulator unc-18	0	0	0	0	0	0	0	5	0	65
unc-22	D3YT57	unc-22	0	0	0	0	0	0	0	5	0	132
unc-70	E0AHA7	Uncoordinated protein 70, isoform c	0	0	0	0	0	0	0	5	0	181
unc-89	O01761	Muscle M-line assembly protein unc-89	0	0	0	0	0	0	0	5	0	64.7
W09C5.8	Q9U329	Protein W09C5.8, confirmed by transcript evidence	0	0	2	0	0	0	0	5	2	354
uba-1	C1P636	Protein C47E12.5c, confirmed by transcript evidence	5	5	0	4	0	2	0	6	0	335
eel-1	Q9GUP2	Enhancer of efl-1 mutant phenotype protein 1	0	0	0	0	0	0	0	6	0	42.1
gspd-1	Q27464	Glucose-6-phosphate 1-dehydrogenase	0	0	0	0	0	0	0	6	0	123
vrs-2	Q9U1Q4	Valyl-tRNA synthetase	4	0	3	8	0	2	0	7	0	209
tsn-1	Q19328	Tudor staphylococcal nuclease homolog protein 1	4	0	6	4	2	7	0	7	0	697
gsy-1	Q9U2D9	Probable glycogen [starch] synthase	0	2	0	4	0	0	0	7	0	223
lev-11	Q22866	Tropomyosin isoforms a/b/d/f (Levamisole resistant protein 11)	13	7	0	7	0	4	0	8	8	7575
npp-12	P91495	Nuclear pore complex protein protein 12	2	0	0	0	0	0	0	10	0	51.6

ketn-1	A7DT47	Kettin (Drosophila actin-binding) homolog protein 1	0	0	0	0	0	0	0	13	0	134
nmy-1	Q20641	Non-muscle myosin protein 1	0	0	0	2	0	0	0	17	2	114
fasn-1	P91871	Protein F32H2.5, partially confirmed by transcript evidence	9	7	0	12	8	0	0	21	0	147
dhc-1	Q19020	Dynein heavy chain, cytoplasmic (Dynein heavy chain, cytosolic) (DYHC)	0	8	0	0	4	0	0	29	0	65.1
gcn-1	B3CJ34	Putative uncharacterized protein	16	14	0	20	21	0	0	42	0	75.2
T08G11.1	Q8T3D2	Protein T08G11.1b, partially confirmed by transcript evidence	0	2	0	0	0	0	0	55	0	69.1
clu-1	P34466	Protein KIAA0664 homolog	2	3	3	7	4	5	2	0	0	116
F54F11.2	B6VQ96	Protein F54F11.2b, partially confirmed by transcript evidence	0	0	0	3	0	0	2	0	0	127
got-2	Q17994	Aspartate aminotransferase	2	0	2	2	0	0	2	0	0	
asp-4	Q21966	Protein R12H7.2, confirmed by transcript evidence	2	0	0	2	0	0	2	0	0	588
tag-241	D3KFS7	Protein C34E11.3a	0	0	0	2	0	0	2	0	0	
rpl-37a	Q9U2A8	60S ribosomal protein L37a	0	0	3	0	3	0	2	0	0	83.8
rpl-26	Q19869	60S ribosomal protein L26	0	5	3	0	2	0	2	0	0	1712
aldo-2	P46563	Fructose-bisphosphate aldolase 2	2	0	0	0	0	2	2	0	0	2697
Y53G8AL.2	Q9N3H3	Putative uncharacterized protein	0	0	0	0	0	2	2	0	0	285
F44G3.2	O45518	Protein F44G3.2, confirmed by transcript evidence	5	0	4	0	0	0	2	0	0	96.6
goa-1	P51875	Guanine nucleotide-binding protein G(o) subunit alpha	2	0	2	0	0	0	2	0	0	115
F23B12.5	Q19749	Pyruvate dehydrogenase complex component E2	2	0	0	0	0	0	2	0	0	593
sdz-8	P90780	Protein C55A6.5, partially confirmed by transcript evidence	2	0	0	0	0	0	2	0	0	144
sod-2	P31161	Superoxide dismutase	0	3	0	0	0	0	2	0	0	210
R09B3.3	O45713	Protein R09B3.3 , confirmed by transcript evidence	0	0	2	0	0	0	2	0	0	5025
bre-1	Q18801	**GDP-mannose 4,6 dehydratase 1**	0	0	0	0	0	0	2	0	0	2.11
C24A3.2	Q18124	Putative uncharacterized protein	0	0	0	0	0	0	2	0	0	35.1
cyn-7	P52015	Peptidyl-prolyl cis-trans isomerase 7	0	0	0	0	0	0	2	0	0	2407
cyt-1	P41956	Succinate dehydrogenase cytochrome b560 subunit, mitochondrial	0	0	0	0	0	0	2	0	0	
eif-3	O61820	Eukaryotic translation initiation factor 3 subunit E	0	0	0	0	0	0	2	0	0	174
F32A7.5	P91859	Protein F32A7.5a, partially confirmed by transcript evidence	0	0	0	0	0	0	2	0	0	229
let-70	P35129	Ubiquitin-conjugating enzyme E2 2	0	0	0	0	0	0	2	0	0	332
lpd-9	D5MCR9	Protein T21C9.5b, confirmed by transcript evidence	0	0	0	0	0	0	2	0	0	123
ndk-1	Q93576	Protein F25H2.5, confirmed by transcript evidence	0	0	0	0	0	0	2	0	0	
srs-2	Q18678	Serine--tRNA ligase	0	0	0	0	0	0	2	0	0	300
T08H10.1	Q22352	Putative uncharacterized protein T08H10.1	0	0	0	0	0	0	2	0	0	296
ttr-41	Q86NH9	Putative uncharacterized protein	0	0	0	0	0	0	2	0	0	281
ubc-9	Q95017	Ubiquitin-conjugating enzyme E2 9	0	0	0	0	0	0	2	0	0	142
W09H1.5	O45903	Probable trans-2-enoyl-CoA reductase 1	0	0	0	0	0	0	2	0	0	71
rpl-17	Q9BL19	60S ribosomal protein L17	0	5	4	0	4	7	2	0	2	1932
hpo-18	O16298	Putative uncharacterized protein	0	0	0	0	2	0	2	0	2	
pmt-2	Q22993	Putative uncharacterized protein	0	0	0	0	0	0	2	0	2	556
nra-4	Q8ITW0	Putative uncharacterized protein	2	3	0	5	0	2	2	2	0	
lrs-1	Q09996	Leucyl-tRNA synthetase	0	3	0	3	0	2	2	2	0	161
csq-1	Q20203	Protein F40E10.3, confirmed by transcript evidence	0	0	0	2	0	0	2	2	0	250
cpl-1	O45734	Protein T03E6.7, confirmed by transcript evidence	2	4	0	0	3	5	2	2	0	589
ril-1	O17694	Protein C53A5.1, confirmed by transcript evidence	0	0	0	0	3	0	2	2	0	437
ZK1073.1	O02485	Uncharacterized protein ZK1073.1	0	0	0	0	0	2	2	2	0	212
his-11	P04255	Histone H2B 1	0	2	0	0	0	0	2	2	0	426
nrs-1	Q19722	Asparaginyl-tRNA synthetase	0	2	0	0	0	0	2	2	0	311
cct-5	P47209	T-complex protein 1 subunit epsilon	0	0	0	0	0	0	2	2	0	723
F45H10.3	O02267	Protein F45H10.3, confirmed by transcript evidence	0	0	0	0	0	0	2	2	0	436
hsp-4	P20163	Heat shock 70 kDa protein D	0	0	0	0	0	0	2	2	0	440
rrt-1	Q19825	Probable arginyl-tRNA synthetase	0	0	0	0	0	0	2	2	0	146
spg-7	Q9N3T5	Spg (Spastic paraplegia) protein 7	0	0	0	0	0	0	2	2	0	115
T20B12.7	P41847	Anamorsin homolog (Fe-S cluster assembly protein DRE2 homolog)	0	0	0	0	0	0	2	2	0	379
Y39B6A.3	A5HWB2	Protein Y39B6A.3b, confirmed by transcript evidence	0	0	0	0	0	0	2	2	0	9.24
T14G10.5	Q22498	Probable coatomer subunit gamma	4	4	2	4	3	4	2	2	2	158
F43E2.7	O02093	Putative uncharacterized protein F43E2.7	2	0	3	0	0	2	2	2	2	255
R53.4	Q22021	Putative ATP synthase subunit f, mitochondrial	0	3	3	0	3	2	2	2	3	386
mmcm-1	Q23381	MethylmalonylCoA mutase homolog 1	0	0	0	3	0	0	2	3	0	205
krs-1	Q22099	Lysyl-tRNA synthetase	0	0	0	2	0	0	2	3	0	280
par-5	P41932	14-3-3-like protein 1 (Partitioning defective protein 5)	3	3	0	0	0	2	2	3	0	1754

C30F12.7	Q95YD8	Putative uncharacterized protein	3	0	0	0	0	0	2	3	0	175
rpa-2	O01504	60S acidic ribosomal protein P2	2	0	4	0	0	0	2	3	0	138
paa-1	Q09543	Protein phosphatase PP2A regulatory subunit A	0	4	0	0	0	0	2	3	0	432
K02F3.2	Q21153	Probable calcium-binding mitochondrial carrier K02F3.2	0	0	0	0	0	0	2	3	0	138
sqv-4	Q19905	UDP-glucose 6-dehydrogenase (Squashed vulva protein 4)	0	0	0	0	0	0	2	3	0	181
trap-4	Q9U238	Protein Y56A3A.21, confirmed by transcript evidence	0	0	0	0	0	0	2	3	0	360
trs-1	P52709	Threonyl-tRNA synthetase	0	0	0	0	0	0	2	3	0	165
F36A2.7	P90860	Protein F36A2.7, confirmed by transcript evidence	0	0	0	0	2	2	2	3	2	1020
asb-1	Q20053	Protein F35G12.10, confirmed by transcript evidence	0	3	0	0	0	2	2	3	2	138
vit-3	Q9N4J2	Vitellogenin-3	7	3	2	25	17	5	2	4	0	595
K07C5.4	Q21276	Uncharacterized NOP5 family protein K07C5.4	5	5	10	15	12	11	2	4	0	411
alh-13	P54889	Aldehyde dehydrogenase family 13	0	0	3	4	0	0	2	4	0	104
rpl-27	P91914	60S ribosomal protein L27	0	4	8	2	5	5	2	4	0	2873
ads-1	O45218	Alkyldihydroxyacetonephosphate synthase	2	0	2	0	0	0	2	4	0	128
R05H10.5	O62327	Probable glutathione peroxidase	0	0	0	0	0	0	2	4	0	236
hrp-2	Q9NLD1	Protein F58D5.1a, confirmed by transcript evidence	3	5	0	3	0	0	2	4	2	386
pab-1	Q9U302	Protein Y106G6H.2a, confirmed by transcript evidence	13	13	2	13	0	3	2	5	0	840
laf-1	Q4W5R4	Lethal and feminizing protein 1, confirmed by transcript evidence	8	15	2	12	0	4	2	5	0	171
cpt-1	Q9U2F2	Protein Y46G5A.17, confirmed by transcript evidence	0	0	6	6	0	2	2	5	0	51.3
rps-13	P51404	40S ribosomal protein S13	2	6	2	4	6	2	2	5	0	2561
gst-29	Q9NAB1	Protein Y53F4B.32, confirmed by transcript evidence	6	8	2	2	3	2	2	5	0	26.2
F58F9.7	Q20992	Acyl-coenzyme A oxidase	0	0	0	0	0	0	2	5	0	84.2
rps-17	O01692	40S ribosomal protein S17	2	4	4	0	4	3	2	5	2	3320
lec-3	Q09581	32 kDa beta-galactoside-binding lectin lec-3	0	0	0	0	0	0	2	6	0	419
nex-2	Q27512	Protein T07C4.9a, confirmed by transcript evidence	0	0	0	0	0	0	2	6	0	64.8
cgh-1	Q95YF3	ATP-dependent RNA helicase cgh-1	4	6	5	5	3	5	2	6	2	265
ers-1	O62431	Probable glutaminyl-tRNA synthetase	2	2	3	8	4	4	2	7	0	213
nol-5	O45012	Putative uncharacterized protein	2	4	8	5	2	8	2	7	0	353
C14C10.5	Q17971	Protein C14C10.5, partially confirmed by transcript evidence	0	0	0	0	0	0	2	7	0	42.5
cpt-2	Q17831	Protein R07H5.2a, confirmed by transcript evidence	0	0	0	0	0	0	2	7	0	136
pdi-2	Q17770	Protein disulfide-isomerase 2	0	0	0	0	0	0	2	7	0	3642
W06H3.3	Q9XXN1	Protein W06H3.3 , partially confirmed by transcript evidence	0	0	2	3	0	0	2	8	0	119
frs-2	Q19713	Phenylalanyl-tRNA synthetase beta chain	2	2	0	0	0	0	2	8	0	181
F20D6.11	Q19655	Putative uncharacterized protein	0	0	0	0	0	0	2	8	0	130
T23E7.2	O17338	Putative uncharacterized protein	3	4	0	9	4	2	3	0	0	397
cpn-3	O01542	Calponin protein 3	2	2	3	0	2	2	3	0	0	2021
F27D4.1	Q93615	Probable electron transfer flavoprotein subunit alpha	0	0	0	0	0	3	3	0	0	903
B0250.5	Q9XTI0	Probable 3-hydroxyisobutyrate dehydrogenase	0	0	0	0	0	2	3	0	0	262
mdt-28	A8WHP8	Protein W01A8.1c, confirmed by transcript evidence	0	0	2	0	0	0	3	0	0	258
C50F7.4	P53589	Succinyl-CoA synthetase beta chain	0	0	0	0	0	0	3	0	0	246
cpz-1	O01850	Cathepsin Z-like enzyme cpz-1	0	0	0	0	0	0	3	0	0	189
cts-1	P34575	Probable citrate synthase	0	0	0	0	0	0	3	0	0	1582
F32D1.5	O16294	Guanosine 5'-monophosphate oxidoreductase	0	0	0	0	0	0	3	0	0	434
iff-1	P34563	Eukaryotic translation initiation factor 5A-1	0	0	0	0	0	0	3	0	0	882
pfn-1	Q9XW16	Profilin-1	0	0	0	0	0	0	3	0	0	804
vha-14	P34462	V-type proton ATPase subunit D	0	0	0	0	0	0	3	0	0	476
rpl-10a	Q9N4I4	60S ribosomal protein L10a	3	4	4	6	4	6	3	0	2	2038
rpl-20	O44480	60S ribosomal protein L18a	0	7	4	4	3	7	3	0	2	2610
acdh-3	O44549	Putative uncharacterized protein	5	2	3	4	0	3	3	2	0	705
his-1	P62784	Histone H4	0	2	3	2	2	0	3	2	0	681
rpt-3	P46502	Probable 26S protease regulatory subunit 6B	0	0	0	2	0	2	3	2	0	370
gst-23	P91505	Glutathione s-transferase protein 23, partially confirmed by transcript evidence	2	2	0	2	0	0	3	2	0	NA
rpl-25	Q20647	60S ribosomal protein L23a 2	0	6	4	0	4	3	3	2	0	2133
rpl-28	Q21930	60S ribosomal protein L28	3	2	3	0	3	2	3	2	0	2695
rps-28	Q95Y04	40S ribosomal protein S28	0	2	0	0	3	0	3	2	0	2729
gst-24	Q93694	Protein F37B1.1, confirmed by transcript evidence	0	4	0	0	2	0	3	2	0	47.2
rpa-1	P91913	60S acidic ribosomal protein P1 (Ribosomal protein large subunit P1)	3	0	0	0	0	3	3	2	0	139
gpdh-2	A7LPE6	Protein K11H3.1d, confirmed by transcript evidence	0	0	0	0	0	3	3	2	0	474
unc-87	P37806	Protein unc-87 (Uncoordinated protein 87)	0	2	0	0	0	2	3	2	0	626

hgo-1	Q9Y041	Homogentisic acid oxidase	0	0	0	0	0	0	3	2	0	222
T12D8.10	Q69ZI6	Protein T12D8.10, confirmed by transcript evidence	0	0	0	0	0	0	3	2	0	263
gpb-1	P17343	Guanine nucleotide-binding protein subunit beta-1	0	0	0	0	0	2	3	2	2	345
acdh-10	Q22347	Probable medium-chain specific acyl-CoA dehydrogenase 10,	5	0	2	4	0	0	3	2	3	451
rpt-6	Q9XTT9	Protein Y49E10.1, confirmed by transcript evidence	0	0	0	2	2	0	3	3	0	282
R04F11.2	Q21732	Protein R04F11.2, confirmed by transcript evidence	0	0	4	0	2	2	3	3	0	1053
eif-3	Q95QW0	Eukaryotic translation initiation factor 3 subunit L (eIF3l)	2	0	2	0	0	0	3	3	0	
rme-1	Q86S80	Receptor mediated endocytosis protein 1, isoform f	2	0	0	0	0	0	3	3	0	182
mbf-1	Q9XTV4	Protein H21P03.1, confirmed by transcript evidence	0	0	0	0	0	0	3	3	0	432
Y38F2AR.9	Q95XS2	Putative uncharacterized protein	0	0	0	0	0	0	3	3	0	53.5
rps-23	Q19877	40S ribosomal protein S23	2	2	4	3	5	4	3	3	2	2491
T09A5.11	P45971	Oligosaccharyl transferase 48 kDa subunit	3	3	4	2	2	3	3	3	2	177
rps-22	O17218	Ribosomal protein, small subunit protein 22, isoform a,	2	4	10	0	6	3	3	3	2	2759
rpl-23	P48158	60S ribosomal protein L23	0	2	6	2	4	4	3	3	3	2135
cand-1	Q9XTJ0	Protein Y102A5A.1, partially confirmed by transcript evidence	5	4	4	5	3	3	3	4	0	123
tag-203	O44985	Temporarily assigned gene name protein 203	0	0	0	3	0	0	3	4	0	75.7
ucr-2.2	Q22370	Protein T10B10.2, confirmed by transcript evidence	0	0	0	0	0	0	3	4	0	472
rpl-13	P91128	60S ribosomal protein L13	8	10	3	4	7	4	3	4	2	2209
rps-10	O01869	Ribosomal protein, small subunit protein 10	4	4	5	2	2	3	3	4	3	2017
alh-8	P52713	Malonate-semialdehyde dehydrogenase	2	4	2	3	2	3	3	5	0	1955
rpl-3	P50880	60S ribosomal protein L3	11	15	5	13	15	4	3	5	2	2393
sip-1	Q20363	Stress-induced protein 1	0	2	0	0	0	3	3	5	3	2326
drs-1	Q03577	Aspartyl-tRNA synthetase	5	0	6	4	2	6	3	6	0	255
cct-4	P47208	T-complex protein 1 subunit delta	0	0	0	0	0	0	3	6	0	857
acs-4	Q20121	Fatty acid coa synthetase family protein 4, confirmed by transcript evidence	4	2	4	9	0	5	3	6	2	148
cct-7	Q9TZS5	Chaperonin containing tcp-1 protein 7, isoform a, confirmed by transcript evidence	2	2	2	0	0	3	3	6	2	476
C28H8.3	Q09475	Uncharacterized helicase C28H8.3	3	2	3	6	0	2	3	7	0	87.2
R12C12.1	Q21962	Putative uncharacterized protein	0	0	3	5	3	2	3	7	0	210
sdhb-1	Q09545	Succinate dehydrogenase	0	3	0	0	0	0	3	7	0	340
R05D3.9	P34542	Uncharacterized protein R05D3.9	0	0	0	0	0	0	3	7	0	52.6
rps-18	O18240	Protein Y57G11C.16, confirmed by transcript evidence	2	7	6	3	6	4	3	7	3	4920
rpl-22	P52819	60S ribosomal protein L22	0	7	13	7	11	8	3	8	2	3299
rpn-1	Q9GZH5	Proteasome regulatory particle, non-atpase-like protein 1	3	2	9	11	5	5	3	9	5	255
nuo-5	Q9N4Y8	Nadh ubiquinone oxidoreductase protein 5, isoform a	2	4	5	10	2	7	3	12	3	540
W07E11.1	Q22275	Protein W07E11.1, partially confirmed by transcript evidence	2	5	0	0	0	0	3	18	2	111
myo-5	Q21'000	Putative uncharacterized protein	4	3	0	3	0	0	3	19	2	141
vha-8	Q95X44	Vacuolar h atpase protein 8	3	4	0	3	0	3	4	0	0	1473
fmo-2	Q21310	Flavin monooxygenase	2	0	0	2	0	2	4	0	0	3.83
rpn-6	Q20938	Probable 26S proteasome regulatory subunit rpn-6.1	0	0	2	2	0	0	4	0	0	302
rpt-4	O17071	Proteasome regulatory particle ATPase-like protein 4	0	0	2	0	2	0	4	0	0	494
rpt-1	Q18787	Proteasome 26S subunit ATPase 2	0	0	0	0	0	0	4	0	0	322
C04C3.3	O44451	Pyruvate dehydrogenase E1 component subunit beta	3	2	0	4	0	3	4	0	2	499
fib-1	Q22053	rRNA 2'-O-methyltransferase fibrillarin	5	4	3	7	6	6	4	2	0	712
rab-1	Q9UAQ6	Rab family protein 1	4	5	0	3	0	4	4	2	0	758
W08E12.7	Q9N5B3	Putative uncharacterized protein	0	0	0	0	0	0	4	2	0	1063
rps-26	O45499	40S ribosomal protein S26	4	3	3	4	5	3	4	2	2	1335
rpl-19	O02639	60S ribosomal protein L19	9	6	4	4	12	5	4	3	0	3055
tag-210	P91917	Putative GTP-binding protein tag-210	3	0	3	0	0	4	4	3	0	476
rpl-14	Q9XVE9	Protein C04F12.4, confirmed by transcript evidence	0	5	5	4	5	4	4	3	2	3227
cco-2	P55954	Cytochrome c oxidase subunit 5A, mitochondrial (Cytochrome c oxidase polypeptide Va)	0	0	2	0	0	2	4	3	2	916
rps-7	Q23312	40S ribosomal protein S7	2	5	11	8	11	6	4	4	0	2334
tufm-1	Q19072	Elongation factor Tu	4	4	0	6	5	2	4	4	0	330
hsp-12.2	P34328	Heat shock protein Hsp-12.2	0	0	0	0	0	0	4	4	0	412
vig-1	O16646	Vig (Drosophila vasa intronic gene) ortholog protein 1	5	7	7	6	5	4	4	4	2	1843
ldh-1	Q27888	L-lactate dehydrogenase	4	6	0	6	2	6	4	4	2	279
let-767	C1P622	Lethal protein 767, isoform b, confirmed by transcript evidence	2	2	2	2	0	7	4	4	2	184
gst-6	P91252	Probable glutathione S-transferase 6	2	4	0	0	2	0	4	4	2	122
K08E3.5	Q69Z13	Protein K08E3.5f, confirmed by transcript evidence	0	0	0	0	0	0	4	4	2	345
T22F3.3	Q86NC1	Phosphorylase	6	3	3	9	7	2	4	5	0	970

mca-3	Q95XP6	Putative uncharacterized protein	2	0	0	8	0	0	4	5	0	153
rps-2	P51403	40S ribosomal protein S2	2	9	8	4	7	3	4	5	0	2158
T25B9.9	Q17761	6-phosphogluconate dehydrogenase	0	4	0	2	0	0	4	5	0	557
rpn-2	Q18115	26S proteasome non-ATPase regulatory subunit 1	4	3	3	10	4	5	4	5	2	184
ucr-2.1	Q9BI61	Protein VW06B3R.1b, confirmed by transcript evidence	2	4	4	2	0	0	4	5	2	968
aldo-1	P54216	Fructose-bisphosphate aldolase 1	5	3	4	4	2	2	4	5	3	2067
hel-1	Q18212	Spliceosome RNA helicase DDX39B homolog	0	0	2	0	2	3	4	5	3	337
rpl-24.1	O01868	60S ribosomal protein L24	0	7	0	4	10	8	4	6	0	3526
tcp-1	P41988	T-complex protein 1 subunit alpha	0	4	4	2	2	0	4	6	0	472
rps-8	P48156	40S ribosomal protein S8	6	11	7	11	11	9	4	6	3	2237
rps-19	O18650	40S ribosomal protein S19	4	7	7	0	6	5	4	6	3	2483
F47B10.1	P53588	Succinyl-CoA synthetase beta-A chain	5	4	5	2	5	6	4	7	2	695
irs-1	Q21926	Isoleucyl-tRNA synthetase	4	2	3	9	0	3	4	8	0	122
cat-2	O61235	Catalase-2	0	0	0	0	0	2	4	8	0	3.23
rpl-21	P34334	60S ribosomal protein L21	2	6	3	5	8	5	4	8	3	2356
Y37E3.17	Q6AW03	Putative uncharacterized protein	0	2	0	7	0	0	4	10	3	310
cdc-48	P54812	Transitional endoplasmic reticulum ATPase homolog 2	5	2	5	9	4	6	4	11	2	436
unc-15	P10567	Paramyosin (Uncoordinated protein 15)	3	6	5	12	5	5	4	17	6	2391
F22F7.1	Q9GZE9	Putative uncharacterized protein	0	0	0	0	0	0	5	0	0	201
dim-1	Q18066	Disorganized muscle protein 1 (2D-page protein spot 8)	0	0	0	0	0	4	5	0	2	594
rps-14	P48150	40S ribosomal protein S14	2	4	5	4	6	3	5	3	0	1597
cth-1	O45391	Protein F22B8.6, confirmed by transcript evidence	2	0	0	2	0	0	5	3	0	71.2
rpl-6	P47991	60S ribosomal protein L6	7	11	9	6	8	7	5	3	2	2295
acdh-7	Q22781	Acyl coa dehydrogenase protein 7, confirmed by transcript evidence	5	2	3	3	0	4	5	3	2	600
R05G6.7	Q21752	Probable voltage-dependent anion-selective channel	0	6	2	0	5	8	5	3	2	2361
rpl-8	Q9XVF7	60S ribosomal protein L8	5	10	6	9	5	8	5	3	3	1650
unc-60	Q07750	Actin-depolymerizing factor 1, isoforms a/b (Uncoordinated protein 60)	2	3	0	0	0	0	5	3	3	1788
rps-9	Q20228	40S ribosomal protein S9	0	9	5	4	6	4	5	4	0	2186
glrx-10	Q9N456	Glutaredoxin protein 10	3	4	5	2	5	2	5	4	4	684
F41C3.5	P52717	Uncharacterized serine carboxypeptidase F41C3.5	4	4	3	0	2	3	5	5	0	630
gst-38	O45451	Protein F35E8.8, confirmed by transcript evidence	2	3	0	3	0	0	5	5	2	8.02
asb-2	Q19126	Atp synthase b homolog protein 2	4	6	2	5	0	6	5	5	4	557
phb-1	Q9BKU4	Mitochondrial prohibitin complex protein 1 (Prohibitin-1)	3	2	6	2	3	6	5	5	4	1108
rpl-7	O01802	60S ribosomal protein L7	8	10	6	8	8	13	5	5	5	2403
atp-5	Q17763	Protein C06H2.1, confirmed by transcript evidence	10	8	7	3	2	5	5	5	5	1427
T02G5.7	Q22101	Putative uncharacterized protein	0	0	0	3	0	0	5	6	0	480
glb-1	P30627	Globin-like protein	0	2	2	0	2	0	5	6	0	653
sams-1	O17680	PS-adenosylmethionine synthase 1	2	0	0	0	0	2	5	6	0	672
act-5	O45815	Protein T25C8.2, confirmed by transcript evidence	6	4	3	4	4	2	5	6	5	1298
imb-3	Q9N5V3	Importin beta family protein 3, confirmed by transcript evidence	5	5	7	9	4	9	5	7	0	121
LLC1.3	O17953	Protein LLC1.3a, confirmed by transcript evidence	2	3	0	5	0	0	5	7	0	984
cct-8	Q9N358	T-complex protein 1 subunit theta (TCP-1-theta) (CCT-theta)	4	2	3	2	0	2	5	7	0	473
F53A2.7	O45552	Protein F53A2.7, confirmed by transcript evidence	4	0	3	3	0	3	5	7	2	1165
prdx-2	A8DYR6	Peroxiredoxin protein 2	5	7	5	4	6	2	5	9	2	2916
rps-20	Q8WQA8	Protein Y105E8A.16, confirmed by transcript evidence	3	4	3	0	6	3	5	10	3	3421
vha-15	Q22494	Vacuolar proton pump subunit H 2	5	5	2	7	6	4	5	10	5	416
hsp-60	P50140	Chaperonin homolog Hsp-60, mitochondrial (Heat shock protein 60)	0	0	0	0	0	0	5	11	0	2423
alh-9	P46562	Putative aldehyde dehydrogenase family 7 member A1 homolog	3	3	0	3	2	0	5	11	3	601
cct-6	P46550	T-complex protein 1 subunit zeta	4	6	0	0	0	0	5	12	2	472
T25F10.6	Q23050	Putative uncharacterized protein T25F10.6	6	3	0	9	0	2	5	15	4	1392
T22B11.5	O61199	Alpha-ketoglutarate dehydrogenase	10	7	14	17	8	12	5	16	5	530
rpl-9	Q95Y90	60S ribosomal protein L9	2	10	5	7	9	4	6	2	0	2896
asg-2	Q18803	Probable ATP synthase subunit g 2	7	5	3	0	3	3	6	2	3	481
phb-2	P50093	Mitochondrial prohibitin complex protein 2 (Prohibitin-2)	4	5	4	5	4	5	6	3	5	604
R07H5.8	Q93934	Protein R07H5.8, confirmed by transcript evidence	2	2	0	3	0	2	6	4	2	1017
acp-6	Q9GUF2	Acid phosphatase family protein 6, confirmed by transcript evidence	8	2	3	6	2	5	6	4	3	220
fum-1	O17214	Probable fumarate hydratase	2	2	0	2	0	0	6	5	0	934
D2063.3	Q6EZG4	Putative uncharacterized protein	2	0	0	2	0	0	6	5	0	93.7
rpl-30	Q9XWS4	Protein Y106G6H.3, confirmed by transcript evidence	4	3	5	0	5	2	6	5	0	1099

sodh-1	Q17334	Alcohol dehydrogenase 1 (Sorbitol dehydrogenase family protein 1)	3	6	4	4	3	3	6	6	2	1763
rps-15	Q9XVP0	40S ribosomal protein S15	3	7	7	5	8	4	6	6	3	2721
rpl-33	P49180	60S ribosomal protein L35a	2	6	6	0	3	2	6	6	5	2326
C16A3.10	Q18040	Probable ornithine aminotransferase	7	4	3	6	5	3	6	7	3	730
rps-12	P49196	40S ribosomal protein S12	0	3	5	0	2	5	6	8	6	900
rpl-4	O02056	60S ribosomal protein L4	17	18	10	22	19	13	6	9	6	2708
gst-41	Q966G8	Glutathione s-transferase protein 41	5	13	4	3	6	4	6	10	4	29.9
rps-1	P48154	40S ribosomal protein S3a	9	10	12	12	13	7	6	11	2	2661
F57B10.3	O44742	Cofactor-independent phosphoglycerate mutase	0	4	3	2	2	2	6	11	3	705
Y43F4B.5	O45934	Protein Y43F4B.5a, confirmed by transcript evidence	0	0	0	0	0	0	6	11	4	330
cct-2	P47207	T-complex protein 1 subunit beta	2	0	0	2	0	2	6	12	0	444
Y71H10A.1	Q9TZL8	6-phosphofructokinase	3	4	4	11	4	6	6	12	2	280
gdh-1	Q23621	Glutamate dehydrogenase	5	6	5	6	3	6	6	16	7	
F17C11.9	P54412	Probable elongation factor 1-gamma (EF-1-gamma) (eEF-1B gamma)	3	0	0	0	0	0	7	3	0	937
rps-11	Q20206	Protein F40F11.1, confirmed by transcript evidence	2	5	8	5	8	6	7	4	3	1776
gpd-1	P04970	Glyceraldehyde-3-phosphate dehydrogenase 1	6	6	2	6	3	6	7	7	0	756
K08D12.3	Q966I7	Putative uncharacterized protein	0	0	0	0	0	0	7	7	2	328
rpa-0	Q93572	60S acidic ribosomal protein P0	8	5	8	6	3	10	7	8	7	2663
C37E2.1	Q93353	Isocitric dehydrogenase subunit beta	5	5	4	3	0	5	7	10	5	338
enol-1	Q27527	2-phospho-D-glycerate hydro-lyase	4	12	3	6	7	2	7	11	0	4422
rpl-7A	Q966C6	60S ribosomal protein L7a	8	12	9	12	7	10	7	11	5	2015
vha-12	Q19626	Vacuolar proton pump subunit B	6	6	4	7	5	4	7	12	4	1979
pccb-1	Q20676	Putative uncharacterized protein	5	6	5	9	5	0	7	17	4	846
pam-1	Q20627	Puromycin-sensitive aminopeptidase protein 1, isoform a	6	3	3	7	7	5	7	18	3	418
gei-7	Q10663	Bifunctional glyoxylate cycle protein (Gex-3-interacting protein 7)	19	5	10	23	16	13	7	18	6	777
F58F12.1	Q09544	ATP synthase subunit delta, mitochondrial (F-ATPase delta subunit)	2	3	0	3	0	2	8	3	3	1959
rpl-18	O45946	60S ribosomal protein L18	7	12	6	9	10	9	8	5	0	3797
mdh-1	Q9UAV5	Malate dehydrogenase	5	3	3	4	3	0	8	5	0	2090
rpl-12	P61866	60S ribosomal protein L12	3	5	4	6	4	3	8	6	2	3385
F43G9.1	Q93714	Probable isocitrate dehydrogenase	7	5	6	3	3	6	8	7	0	802
cct-3	Q9N4J8	Putative uncharacterized protein	2	2	0	3	0	3	8	8	0	385
rps-4	Q9N3X2	40S ribosomal protein S4	11	19	16	22	16	19	8	9	2	2657
Y69A2AR	Q95XJ0	ATP synthase gamma chain	8	9	8	11	9	7	8	9	4	1322
C44B7.10	Q18599	Putative uncharacterized protein	9	9	8	9	9	7	8	9	5	2154
rps-16	Q22054	40S ribosomal protein S16	9	9	10	8	12	11	8	9	8	2456
acdh-12	Q19057	Acyl coa dehydrogenase protein 12, isoform a	0	2	0	0	0	0	8	10	4	491
T08B2.7	Q9BIC3	Putative uncharacterized protein	3	2	15	14	11	11	8	12	5	479
gst-39	Q9NAB0	Protein Y53F4B.33, confirmed by transcript evidence	16	14	7	9	6	4	8	12	7	109
F49E2.2	A6ZJ46	Protein F49E2.2c, partially confirmed by transcript evidence	5	8	0	7	0	0	8	13	4	58.9
hsp-3	P27420	Heat shock 70 kDa protein C	6	7	0	6	0	3	8	15	4	1510
pyk-1	B7WNA0	Protein F25H5.3e, partially confirmed by transcript evidence	4	4	0	4	0	0	8	16	0	443
W10C8.5	O45011	Putative uncharacterized protein	3	4	3	3	0	0	9	9	3	306
ucr-1	P98080	Ubiquinol-cytochrome-c reductase complex core protein 1	7	10	6	8	7	9	9	11	7	1192
fln-1	D0IMZ5	FLN-1 protein, isoform a, partially confirmed by transcript evidence	7	3	9	17	4	12	9	16	4	343
tct-1	Q93573	Translationally-controlled tumor protein homolog (TCTP)	2	6	5	2	0	2	10	0	2	3680
gst-27	Q9NAB3	Protein Y53F4B.30, confirmed by transcript evidence	15	7	5	8	7	3	10	10	4	355
mlc-1	P19625	Myosin regulatory light chain 1	5	6	6	6	7	5	10	10	6	2151
aco-1	Q23500	Probable cytoplasmic aconitate hydratase (Aconitase)	6	6	6	9	3	4	10	19	5	882
gst-26	Q9NAB4	Protein Y53F4B.29, confirmed by transcript evidence	9	8	6	6	4	4	11	7	5	318
inf-1	P27639	Eukaryotic initiation factor 4A (eIF-4A)	9	7	3	9	6	5	11	10	5	735
F01G4.6	P40614	Phosphate carrier protein, mitochondrial (PTP)	9	7	10	11	8	8	11	12	9	613
rpl-5	P49405	60S ribosomal protein L5	10	15	8	16	12	11	11	13	8	3694
rack-1	Q21215	Guanine nucleotide-binding protein subunit beta-2-like 1	8	10	7	7	7	9	11	14	3	2329
gst-13	Q22814	Protein T26C5.1, confirmed by transcript evidence	16	18	10	7	13	8	11	16	11	136
tkt-1	O17759	Protein F01G10.1, confirmed by transcript evidence	10	4	4	6	0	3	11	19	3	1834
T25G3.4	P90795	Probable glycerol-3-phosphate dehydrogenase	7	5	3	7	0	3	11	20	2	159
F46H5.3	Q10454	Probable arginine kinase F46H5.3 (AK) (EC 2.7.3.3)	7	7	6	6	4	5	12	8	4	4094
C08H9.2	Q17832	Protein C08H9.2a, confirmed by transcript evidence	4	5	9	13	6	7	12	11	2	583
rps-0	P46769	40S ribosomal protein SA	10	11	10	11	9	10	12	12	8	2456

gst-4	Q21355	Glutathione S-transferase 4	11	16	6	6	13	5	12	13	6	83
F45D11.15	Q9N2K4	Putative uncharacterized protein	8	12	7	8	5	4	12	15	0	716
mlc-3	P53014	Myosin, essential light chain (Myosin light chain alkali)	13	12	6	6	7	8	12	16	11	7584
vha-13	Q9XW92	Vacuolar proton pump subunit alpha	7	7	0	5	0	2	12	17	6	2335
aco-2	P34455	Probable aconitate hydratase (Aconitase)	12	8	13	18	10	10	12	19	8	1933
gpd-2	P17329	Glyceraldehyde-3-phosphate dehydrogenase 2 (GAPDH-2)	9	9	6	10	5	4	13	10	6	2973
rps-3	P48152	40S ribosomal protein S3	10	13	11	14	12	12	13	10	8	2815
hsp-6	P11141	Heat shock 70 kDa protein F, mitochondrial	4	5	0	5	0	0	13	14	4	1261
chc-1	P34574	Probable clathrin heavy chain 1	20	11	8	29	16	9	13	15	5	247
5C820	Q9GQ62	5C820	4	8	5	0	5	2	14	14	8	342
gst-28	Q9NAB2	Protein Y53F4B.31, confirmed by transcript evidence	17	12	6	18	12	8	14	16	6	174
sca-1	Q9XU13	Protein K11D9.2b, confirmed by transcript evidence	18	10	8	21	12	9	14	21	4	634
dep-1	**Q20120**	**Protein F44G4.8a, partially confirmed by transcript evidence**	**68**	**55**	**51**	**66**	**42**	**48**	**14**	**23**	**3**	1.16
eat-6	P90735	Protein B0365.3, confirmed by transcript evidence	18	10	11	23	12	13	14	24	5	426
idh-1	Q21032	Isocitrate dehydrogenase	8	9	0	9	6	0	15	10	0	1244
gst-36	Q09607	Probable glutathione S-transferase gst-36	14	16	9	9	8	10	15	11	9	375
mdh-1	O02640	Probable malate dehydrogenase	11	9	7	10	4	8	15	15	7	2090
pcca-1	Q19842	Propionyl-CoA carboxylase alpha chain	16	8	8	26	12	10	15	18	3	902
ahcy-1	P27604	Adenosylhomocysteinase (AdoHcyase)	10	12	8	13	9	8	16	11	6	4696
sdha-1	Q09508	Succinate dehydrogenase	8	10	2	8	0	5	16	16	9	635
tba-2	P34690	Tubulin alpha-2 chain	14	18	12	19	17	15	17	17	5	874
gst-20	O01987	Protein Y48E1B.10 gst-20	16	23	13	12	19	11	17	18	10	266
pyc-1	O17732	Pyruvate carboxylase 1	11	11	8	26	15	10	17	19	2	327
ant-1	O45865	Protein T27E9.1a, confirmed by transcript evidence	12	18	15	16	18	19	18	23	15	819
daf-21	Q18688	Heat shock protein 90 (Abnormal dauer formation protein 21)	20	15	18	30	17	25	19	29	10	1522
hsp-1	P09446	Heat shock 70 kDa protein A	13	16	9	15	2	13	20	28	13	2550
gst-5	Q09596	Probable glutathione S-transferase 5	19	23	14	15	18	15	21	19	14	199
gst-7	P91253	Probable glutathione S-transferase 7	23	23	14	13	18	16	21	24	18	778
W05G11.6	O44906	Putative uncharacterized protein W05G11.6	22	17	13	20	2	12	22	32	6	1439
tbb-2	P52275	Tubulin beta-2 chain (Beta-2-tubulin)	19	24	16	31	21	25	23	21	10	1372
gst-1	P10299	Glutathione S-transferase P	22	24	21	21	17	21	24	23	18	690
eef-2	P29691	Elongation factor 2 (EF-2)	20	6	10	26	19	16	24	34	13	7.81
vit-5	P06125	Vitellogenin-5	69	50	42	167	129	85	24	47	9	750
gst-10	Q9N4X8	Glutathione S-transferase P 10	25	25	17	16	24	20	25	28	20	215
R11A5.4	O02286	Protein R11A5.4a, confirmed by transcript evidence	19	22	14	22	3	13	25	34	19	1849
atp-2	P46561	ATP synthase subunit beta, mitochondrial	26	21	18	29	17	21	26	24	18	6267
eft-3	P53013	Elongation factor 1-alpha (EF-1-alpha)	19	22	21	20	21	16	28	27	15	3510
act-1	P10983	Actin-1/3	25	25	18	29	21	18	29	23	17	2359
H28O16.1	Q9XXK1	ATP synthase subunit alpha, mitochondrial	26	26	24	32	25	18	31	38	25	6282
myo-1	P02567	Myosin-1 (Lethal protein 75)	30	14	7	39	17	11	32	67	27	
myo-3	P12844	Myosin-3 (Myosin heavy chain A)	37	10	2	49	8	7	35	44	14	489
vit-2	P05690	Vitellogenin-2	78	54	55	184	123	86	37	55	14	1514
myo-2	P12845	Myosin-2 (Myosin heavy chain C)	33	21	2	50	24	12	39	79	31	570
vit-6	P18948	Vitellogenin-6	102	68	87	227	177	152	56	82	33	1565
myo-4	P02566	Myosin-4 (Myosin heavy chain B) (Uncoordinated protein 54)	130	71	69	162	62	85	126	175	113	

Table 1 Proteins that were identified by LC-MS/MS analyses after GST::DEP-1 pull-down experiments.
LC-MS/MS analyses identified 585 proteins. Every pull-down was done in triplicates. The numbers represent the peptides that were detected. Min. Protein Probability = 95%; Min. Number of Peptides = 2. Values from „Protein abundance“ correspond to the „*C.elegans* PaxDB integrated dataset“ (www.pax-db.org).

3.1.10 Materials and methods

C. elegans methods and strains

The strains used for the experiments and crosses were derivates of Bristol strain N2 of *Caenorhabditis elegans*. The animals were cultivated under standard conditions at 20°C as described in (Brenner, 1974). Unless noted otherwise, the mutations used have been described previously and are listed below by their linkage group. Standard methods were used to construct double mutants. The vulval index (VI) was scored at the L4 larval stage using Nomarski optics as described (Berset et al., 2001). For Nomarski analysis, animals were mounted on 4% agarose pads in M9 solution containing 20 mM tetramisole hydrochloride.

The alleles used are LGII: *dep-1(zh34)* (Tarcic et al., 2009), *unc-4(e120)* (Brenner, 1974), *rrf-3(pk1426)* (Simmer et al., 2002), *ttTi25067* (*dep-1* transposon insertion) (Université Lyon 1, Villeurbanne, France). LGIII: *unc-119(e2498)* (Maduro and Pilgrim, 1995), *unc-119(ed3)* (Maduro and Pilgrim, 1995), u*nc-119(ed4)* (Maduro and Pilgrim, 1995), *pat-3(st564)* (Williams and Waterston, 1994), *glp-1(q339)* (Troemel et al., 1999). LGIV: *lip-1(zh15)* (Berset et al., 2001), *let-60(n1046)* (Ferguson and Horvitz, 1985). LGV: *rde-1(ne219)* (Pavelec et al., 2009), *nid-1(cg119)* (Trzebiatowska et al., 2008),

The integrated transgenic arrays are: LGII: *zhIs70[dep-1::gfp::unc-119(+)],zhIs71[dep-1::mCherry:: unc-119(+)]*. LGIV: *qyIs15[zmp-1>HA-ßtail]* (Hagedorn et al., 2009), *zhIs038[let-23::GFP; unc-119(+)]* (Haag et al., unpublished data). LG unknown: *qyIs43 [pat-3::GFP + ina-1(genomic) + unc-119(+)]* (Hagedorn et al., 2009), *zhIs020[peft-3::taptag::dep-1 extracellular domain / unc-119(+)],qyIs110(egl-17>dnPat-3)* (Hagedorn et al., 2009), *jeIs2222[pat-2::GFP rol-6(su1006)]* (Meighan and Schwarzbauer, 2007).

The transgenic arrays /transgene, cotransformation marker) were: *zhEx418[lin-31::rde-1, myo-2::mCherry], zhEx419[pat-3::gfp Y792A Y804A], zhEx420[pat-3::gfp Y772A], zhEx432[pat-3::gfp Y772A Y804A], zhEx456[pat-3::gfp Y792A,], zhEx457[pat-3::gfp Y804A], zhEx458[pat-3::gfp TTT796-798AAA], zhEx477[dep-1::mCherry], zhEx524[pat-3::gfp,myo-2::mCherry], zhEx528[pat-3::gfp Y804A, myo-2::mCherry], mwEx31[pat-3 Y804F]* (Lee et al., 2001), *mwEx32[pat3 Y792F Y804F]* (Lee et al., 2001).

GST pull-down experiments for LC-MS/MS analyses

The intracellular domain of DEP-1 (wild-type and D1241A) was cloned into the BamHI site of the *E. coli* expression vector pGEX-2TK (Pharmacia) as described by Berset et al. (2005). Recombinant proteins were affinity-purified on glutathione Sepharose according to the manufacturer's protocol, except that protein expression was induced in BL21 bacteria at 18°C, and fusion proteins were washed in 20 mM NaP pH=8.0, 250 mM NaCl, 1% Triton-X. Approximately 50 µg of each DEP-1 fusion protein (wild-type/D1241A) and 100 µg of GST as a negative control were used for each binding reaction. To prepare N2 worm extract, mixed-stage liquid cultures were cleaned by sucrose flotation, resuspended in lysis buffer (100 mM Tris pH=8.0, 150 mM NaCl, 1 mM EDTA, 1 mM DTT, 0.5% NP-40, 1x protease inhibitor cocktail; Roche), shock frozen in liquid nitrogen, and homogenized in a mixer mill (MM300; Retsch). Thawed worm extract was then centrifuged for 10 min at 4°C and 10'000g to remove insoluble components. About 2.5 mg of total protein extract was used for each reaction. Binding was performed at 4°C over night, followed by three washes with lysis buffer. Bound proteins were eluted by boiling the beads for 5 min in 30 µl of laemmli buffer and separated on a 4-15% linear gradient SDS-gel (Biorad Nr. 161-1104), followed by Colloidal Coomassie Blue staining according the manufacturer's protocol (Roti Blue; Roth).

In-gel digestion and protein identification by LTQ-Orbitrap

Differential protein bands were excised with a scalpel into small pieces and prepared for in-gel tryptic digestion. Thereby the gel pieces were washed and dehydrated three times in 50% Acetonitrile and dried in speedvac. 10 mM DTT (in 25 mM Ammonium bicarbonate pH=8.0) was added to cover gel pieces and incubated for 45 min at 56°C. After DTT was removed, 50 mM IAM (in 25 mM Ammonium bicarbonate pH=8.0) was added to cover gel pieces and incubated for 1 hour at room temperature in the dark. IAM was removed and gel pieces were washed twice with 50% Acetonitrile before dried in Speed Vac. 25 mM Ammonium bicarbonate pH=8.0 containing 50 ng trypsin was added to be absorbed by the gel pieces and incubated over night at 37°C. To extract the peptides, gel pieces were incubated three times for 15 min with 50% Acetonitrile / 5% TFA and once with 100% Acetonitrile. The peptides were speedvac dried before resuspended in 5 µl of 3% Acetonitrile/0.1% formic acid. Samples were desalted with C18 ZipTip® (Millipore) according to the manufacturer's protocol before being analyzed on a calibrated LTQ-Orbitrap mass spectrometer (Thermo Scientific). Desalted peptides were resovled in 15 µl of 3% Acetonitrile/0.2% formic acid and loaded on a 10 cm fused silica column packed with 3 µm 200 Å pore size C18 resin. Peptides were eluted from the column via an ACN gradient of 5-45% (v/v) over 80 min and 40-80% ACN over the subsequent 15 min in a buffer containing 0.2% formic acid (v/v) at a flow rate of 200 nl/min.

The range of MS scan was m/z 450-1500. LC-MS/MS spectra were exported to the MASCOT generic format (mgf) and proteins were identified by searching the MASCOT database search engine version 2.2 (Perkins et al., 1999). The MASCOT search parameters were as follows: set-off threshold at 0.05 in the expectation value cutoff, peptide tolerance at 5 ppm, MS/MS tolerance at 0.8 Da, peptide charge of 2+ or 3+, trypsin as enzyme allowing up to one missed cleavage, carbamidomethylation on cysteines as a fixed modification and oxidation on methionine as a variable modification. Only peptides with a maximum of 2 (3 for semi-tryptic digest) missed cleavage sites were allowed in database searches. Further comparisons of the proteins were performed using Scaffold 3.0 (Proteome Software).

GST pull-down experiments for Western blot experiments

Approximately 10 µg of purified GST::DEP-1 (wild-type and D1241A) and 40 µg of GST (negative control) were incubated with ca. 800 µg total worm extract over night at 4°C for each binding reaction. Followed by washing with lysis buffer (see above), bound proteins were eluted by boiling the beads for 5 min in Laemmli buffer. GFP tagged proteins were detected on Western blots of 10% acrylamide gels with monoclonal anti-GFP antibody (Roche, Cat. No. 11 814 460 001). For phosphatase inhibitor experiments, 5 mM Na_3VO_4 was added to the lysis buffer.

Endogenous dep-1::mCherry reporter

An endogenous single copy reporter of *dep-1::mCherry* was created by *MosTIC* insertion as reported by Robert et al., (2009). The repair templates were cloned by PCR fusion of the last 1.8 kb of the *dep-1* locus to *mCherry*, followed by 500 bp of the *dep-1* 3' UTR, the *C. briggsae unc-119* rescue construct, and 1.9 kb of the genomic *dep-1* downstream region. The final construct was subcloned into pGEM®-T Easy (Promega) and 50 ng/µl of the created plasmid (pMW28) was micro-injected together with 50 ng of the Mos1-transposase pJL43.1, 2.5 ng of *myo-2::mCherry*, 5 ng of pCFJ104, and 10 ng of pGH8 into the Mos insertion line *ttTi25067; unc-119(e2498)*. *MosTIC* engineered animals were identified by screening the F2 progeny for crawlers that lost the *myo-2::mCherry* marker, and confirmed by sequencing.

RNAi

RNAi was performed by feeding worms with dsRNA-producing *E. coli* as described by Kamath et al., (2001) with the following modifications: The worms were synchronized with hypochloride solution, and L1 larvae (P0) were placed on growth media plates and allowed to grow at 20°C. The F2 generation was then analyzed. 3 mM IPTG was added to the agar to induce the expression of dsRNA.

3.1.11 Acknowledgements

We wish to thank all members of the Hajnal laboratory, Fritz Müller and Michael Hengartner for critical input and support into this work. We are especially grateful to Franziska Pfistner and Daniel Widmer for their input and comments on the manuscript. We thank the Functional Genomic Center Zurich FGCZ, particularly Claudia Fortes and Bernd Roschitzki for their assistance with the MS analyses. We thank Werner Boll for his help with the spinning confocal microscope. We thank David Sherwood for the *pat-3::gfp* reporter; Myeongwoo Lee for the *pat-3* NPxY mutants; J. Ahringer for RNAi clones; to Andrew Fire for GFP vectors; the "Biology of *Caenorhabditis elegans*" Facility - CNRS UMS 3421 for sending the MosInsertion strain *ttTi25067*; and the *Caenorhabditis elegans* Genetic Center for some of the strains used. This work was supported by grants from the Swiss National fond SNF to A.H and the Kanton Zürich.

3.1.12 References

Alonso, A., Sasin, J., Bottini, N., Friedberg, I., Friedberg, I., Osterman, A., Godzik, A., Hunter, T., Dixon, J., and Mustelin, T. (2004). Protein tyrosine phosphatases in the human genome. Cell 117, 699–711.

Ambros, V. (1999). Cell cycle-dependent sequencing of cell fate decisions in Caenorhabditis elegans vulva precursor cells. Development 126, 1947–1956.

Arora, D., Stopp, S., Böhmer, S.-A., Schons, J., Godfrey, R., Masson, K., Razumovskaya, E., Rönnstrand, L., Tänzer, S., Bauer, R., et al. (2011). Protein-tyrosine phosphatase DEP-1 controls receptor tyrosine kinase FLT3 signaling. J. Biol. Chem. 286, 10918–10929.

Baum, P.D., and Garriga, G. (1997). Neuronal migrations and axon fasciculation are disrupted in ina-1 integrin mutants. Neuron 19, 51–62.

Berset, T.A. (2005). The *C. elegans* homolog of the mammalian tumor suppressor Dep-1/Scc1 inhibits EGFR signaling to regulate binary cell fate decisions. Genes & Development 19, 1328–1340.

Berset, T., Hoier, E.F., Battu, G., Canevascini, S., and Hajnal, A. (2001). Notch inhibition of RAS signaling through MAP kinase phosphatase LIP-1 during *C. elegans* vulval development. Science 291, 1055–1058.

Blanchetot, C., Chagnon, M., Dubé, N., Hallé, M., and Tremblay, M.L. (2005). Substrate-trapping techniques in the identification of cellular PTP targets. Methods 35, 44–53.

Brenner, S. (1974). The genetics of Caenorhabditis elegans. Genetics 77, 71–94.

Calderwood, D.A. (2004). Integrin activation. J. Cell. Sci. 117, 657–666.

Calderwood, D.A., Fujioka, Y., de Pereda, J.M., García-Alvarez, B., Nakamoto, T., Margolis, B., McGlade, C.J., Liddington, R.C., and Ginsberg, M.H. (2003). Integrin beta cytoplasmic domain interactions with phosphotyrosine-binding domains: a structural prototype for diversity in integrin signaling. Proc. Natl. Acad. Sci. U.S.a. 100, 2272–2277.

Calderwood, D.A., Yan, B., de Pereda, J.M., Alvarez, B.G., Fujioka, Y., Liddington, R.C., and Ginsberg, M.H. (2002). The phosphotyrosine binding-like domain of talin activates integrins. J. Biol. Chem. 277, 21749–21758.

Chabot, C., Spring, K., Gratton, J.-P., Elchebly, M., and Royal, I. (2009). New role for the protein tyrosine phosphatase DEP-1 in Akt activation and endothelial cell survival. Molecular and Cellular Biology 29, 241–253.

Chen, H., Zou, Z., Sarratt, K.L., Zhou, D., Zhang, M., Sebzda, E., Hammer, D.A., and Kahn, M.L. (2006). In vivo beta1 integrin function requires phosphorylation-independent regulation by cytoplasmic tyrosines. Genes & Development 20, 927–932.

Chen, N., and Greenwald, I. (2004). The lateral signal for LIN-12/Notch in *C. elegans* vulval development comprises redundant secreted and transmembrane DSL proteins. Developmental Cell 6, 183–192.

Chen, W.J., Goldstein, J.L., and Brown, M.S. (1990). NPxY, a sequence often found in cytoplasmic tails, is required for coated pit-mediated internalization of the low density lipoprotein receptor. J. Biol. Chem. 265, 3116–3123.

Chiu, S.-J., Jiang, S.-T., Wang, Y.-K., and Tang, M.-J. (2002). Hepatocyte growth factor upregulates alpha2beta1 integrin in Madin-Darby canine kidney cells: implications in tubulogenesis. J. Biomed. Sci. 9, 261–272.

Clark, E.A., and Brugge, J.S. (1995). Integrins and signal transduction pathways: the road taken. Science 268, 233–239.

Cox, D., Brennan, M., and Moran, N. (2010). Nat Rev Drug Discov 2010 Cox. 1–17.

Cram, E.J., Clark, S.G., and Schwarzbauer, J.E. (2003). Talin loss-of-function uncovers roles in cell contractility and migration in *C. elegans*. J. Cell. Sci. 116, 3871–3878.

Critchley, D.R. (2000). Focal adhesions - the cytoskeletal connection. Curr. Opin. Cell Biol. 12, 133–139.

Datta, A., Shi, Q., and Boettiger, D.E. (2001). Transformation of chicken embryo fibroblasts by v-src uncouples beta1 integrin-mediated outside-in but not inside-out signaling. Molecular and Cellular Biology 21, 7295–7306.

Datta, A., Huber, F., and Boettiger, D. (2002). Phosphorylation of beta3 integrin controls ligand binding strength. J. Biol. Chem. 277, 3943–3949.

Fantl, W.J., Johnson, D.E., and Williams, L.T. (1993). Signalling by receptor tyrosine kinases. Annu. Rev. Biochem. 62, 453–481.

Ferguson, E.L., and Horvitz, H.R. (1985). Identification and characterization of 22 genes that affect the vulval cell lineages of the nematode Caenorhabditis elegans. Genetics 110, 17–72.

Félix, M.-A. (2012). Caenorhabditis elegans vulval cell fate patterning. Phys Biol 9, 045001.

Gettner, S.N., Kenyon, C., and Reichardt, L.F. (1995). Characterization of beta pat-3 heterodimers, a family of essential integrin receptors in *C. elegans*. J. Cell Biol. 129, 1127–1141.

Giancotti, F.G., and Tarone, G. (2003). Positional control of cell fate through joint integrin/receptor protein kinase signaling. Annu. Rev. Cell Dev. Biol. 19, 173–206.

Grazia Lampugnani, M., Zanetti, A., Corada, M., Takahashi, T., Balconi, G., Breviario, F., Orsenigo, F., Cattelino, A., Kemler, R., Daniel, T.O., et al. (2003). Contact inhibition of VEGF-induced proliferation requires vascular endothelial cadherin, beta-catenin, and the phosphatase DEP-1/CD148. J. Cell Biol. 161, 793–804.

Hagedorn, E.J., Yashiro, H., Ziel, J.W., Ihara, S., Wang, Z., and Sherwood, D.R. (2009). Integrin Acts Upstream of Netrin Signaling to Regulate Formation of the Anchor Cell•s Invasive Membrane in *C. elegans*. Developmental Cell 17, 187–198.

Hertog, den, J., Blanchetot, C., Buist, A., Overvoorde, J., van der Sar, A., and Tertoolen, L.G. (1999). Receptor protein-tyrosine phosphatase signalling in development. Int. J. Dev. Biol. 43, 723–733.

Hirsch, E., Barberis, L., Brancaccio, M., Azzolino, O., Xu, D., Kyriakis, J.M., Silengo, L., Giancotti, F.G., Tarone, G., Fässler, R., et al. (2002). Defective Rac-mediated proliferation and survival after targeted mutation of the beta1 integrin cytodomain. J. Cell Biol. 157, 481–492.

Howe, A., Aplin, A.E., Alahari, S.K., and Juliano, R.L. (1998). Integrin signaling and cell growth control. Curr. Opin. Cell Biol. 10, 220–231.

Hunter, T. (1999). 1-s2.0-S0092867400816888-main. Cell 100, 113–127.

Huyer, G., Liu, S., Kelly, J., Moffat, J., Payette, P., Kennedy, B., Tsaprailis, G., Gresser, M.J., and Ramachandran, C. (1997). Mechanism of inhibition of protein-tyrosine phosphatases by vanadate and pervanadate. J. Biol. Chem. 272, 843–851.

Hynes, R.O. (1992). Integrins: versatility, modulation, and signaling in cell adhesion. Cell 69, 11–25.

Hynes, R.O. (2002). Integrins: bidirectional, allosteric signaling machines. Cell 110, 673–687.

Iuliano, R., Trapasso, F., Le Pera, I., Schepis, F., Samà, I., Clodomiro, A., Dumon, K.R., Santoro, M., Chiariotti, L., Viglietto, G., et al. (2003). An adenovirus carrying the rat protein tyrosine phosphatase eta suppresses the growth of human thyroid carcinoma cell lines in vitro and in vivo. Cancer Res. 63, 882–886.

Ivaska, J., and Heino, J. (2011). Cooperation between integrins and growth factor receptors in signaling and endocytosis. Annu. Rev. Cell Dev. Biol. 27, 291–320.

Johansson, M.W., Larsson, E., Lüning, B., Pasquale, E.B., and Ruoslahti, E. (1994). Altered localization and cytoplasmic domain-binding properties of tyrosine-phosphorylated beta 1 integrin. J. Cell Biol. 126, 1299–1309.

Kamath, R.S., Martinez-Campos, M., Zipperlen, P., Fraser, A.G., and Ahringer, J. (2001). Effectiveness of specific RNA-mediated interference through ingested double-stranded RNA in Caenorhabditis elegans. Genome Biol. 2, RESEARCH0002.

Kappert, K., Paulsson, J., Sparwel, J., Leppänen, O., Hellberg, C., Östman, A., and Micke, P. (2007). Dynamic changes in the expression of DEP-1 and other PDGF receptor-antagonizing PTPs during onset and termination of neointima formation. Faseb J. 21, 523–534.

Keane, M.M., Lowrey, G.A., Ettenberg, S.A., Dayton, M.A., and Lipkowitz, S. (1996). The protein tyrosine phosphatase DEP-1 is induced during differentiation and inhibits growth of breast cancer cells. Cancer Res. 56, 4236–4243.

Kishihara, K., Penninger, J., Wallace, V.A., Kündig, T.M., Kawai, K., Wakeham, A., Timms, E., Pfeffer, K., Ohashi, P.S., and Thomas, M.L. (1993). Normal B lymphocyte development but impaired T cell maturation in CD45-exon6 protein tyrosine phosphatase-deficient mice. Cell 74, 143–156.

Kornfeld, K. (1997). Vulval development in Caenorhabditis elegans. Trends Genet. 13, 55–61.

Law, D.A., DeGuzman, F.R., Heiser, P., Ministri-Madrid, K., Killeen, N., and Phillips, D.R. (1999). Integrin cytoplasmic tyrosine motif is required for outside-in alphaIIbbeta3 signalling and platelet function. Nature 401, 808–811.

Lee, M., Cram, E.J., Shen, B., and Schwarzbauer, J.E. (2001). Roles for beta(pat-3) integrins in development and function of Caenorhabditis elegans muscles and gonads. J. Biol. Chem. 276, 36404–36410.

Li, L., and Dixon, J.E. (2000). Form, function, and regulation of protein tyrosine phosphatases and their involvement in human diseases. Semin. Immunol. 12, 75–84.

Li, M., Wu, X., Wang, J., and Pan, Y. (2012). Towards the identification of protein complexes and functional modules by integrating PPI network and gene expression data. BMC Bioinformatics 13, 109.

Liu, S., Calderwood, D.A., and Ginsberg, M.H. (2000). Integrin cytoplasmic domain-binding proteins. J. Cell. Sci. 113 (Pt 20), 3563–3571.

Maduro, M., and Pilgrim, D. (1995). Identification and cloning of unc-119, a gene expressed in the Caenorhabditis elegans nervous system. Genetics 141, 977–988.

Margadant, C., Monsuur, H.N., Norman, J.C., and Sonnenberg, A. (2011). Mechanisms of integrin activation and trafficking. Curr. Opin. Cell Biol. 23, 607–614.

Mattila, E., Auvinen, K., Salmi, M., and Ivaska, J. (2008). The protein tyrosine phosphatase TCPTP controls VEGFR2 signalling. J. Cell. Sci. 121, 3570–3580.

Mattila, E., Marttila, H., Sahlberg, N., Kohonen, P., Tähtinen, S., Halonen, P., Perälä, M., and Ivaska, J. (2010). Inhibition of receptor tyrosine kinase signalling by small molecule agonist of T-cell protein tyrosine phosphatase. BMC Cancer 10, 7.

Mattila, E., Pellinen, T., Nevo, J., Vuoriluoto, K., Arjonen, A., and Ivaska, J. (2005). Negative regulation of EGFR signalling through integrin-alpha1beta1-mediated activation of protein tyrosine phosphatase TCPTP. Nat. Cell Biol. 7, 78–85.

Meighan, C.M., and Schwarzbauer, J.E. (2007). Control of *C. elegans* hermaphrodite gonad size and shape by vab-3/Pax6-mediated regulation of integrin receptors. Genes & Development 21, 1615–1620.

Mitra, S.K., and Schlaepfer, D.D. (2006). Integrin-regulated FAK-Src signaling in normal and cancer cells. Curr. Opin. Cell Biol. 18, 516–523.

Moro, L. (2001). Integrin-induced Epidermal Growth Factor (EGF) Receptor Activation Requires c-Src and p130Cas and Leads to Phosphorylation of Specific EGF Receptor Tyrosines. Journal of Biological Chemistry 277, 9405–9414.

Moulder, G.L., Huang, M.M., Waterston, R.H., and Barstead, R.J. (1996). Talin requires beta-integrin, but not vinculin, for its assembly into focal adhesion-like structures in the nematode Caenorhabditis elegans. Mol. Biol. Cell 7, 1181–1193.

Ohno, H., Stewart, J., Fournier, M.C., Bosshart, H., Rhee, I., Miyatake, S., Saito, T., Gallusser, A., Kirchhausen, T., and

Bonifacino, J.S. (1995). Interaction of tyrosine-based sorting signals with clathrin-associated proteins. Science 269, 1872–1875.

Oxley, C.L., Anthis, N.J., Lowe, E.D., Vakonakis, I., Campbell, I.D., and Wegener, K.L. (2008). An integrin phosphorylation switch: the effect of beta3 integrin tail phosphorylation on Dok1 and talin binding. J. Biol. Chem. 283, 5420–5426.

Palka, H.L. (2002). Hepatocyte Growth Factor Receptor Tyrosine Kinase Met Is a Substrate of the Receptor Protein-tyrosine Phosphatase DEP-1. Journal of Biological Chemistry 278, 5728–5735.

Pavelec, D.M., Lachowiec, J., Duchaine, T.F., Smith, H.E., and Kennedy, S. (2009). Requirement for the ERI/DICER complex in endogenous RNA interference and sperm development in Caenorhabditis elegans. Genetics 183, 1283–1295.

Pellinen, T. (2006). Integrin traffic. J. Cell. Sci. 119, 3723–3731.

Pellinen, T., Tuomi, S., Arjonen, A., Wolf, M., Edgren, H., Meyer, H., Grosse, R., Kitzing, T., Rantala, J.K., Kallioniemi, O., et al. (2008). Integrin trafficking regulated by Rab21 is necessary for cytokinesis. Developmental Cell 15, 371–385.

Petermann, A., Haase, D., Wetzel, A., Balavenkatraman, K.K., Tenev, T., Gührs, K.-H., Friedrich, S., Nakamura, M., Mawrin, C., and Böhmer, F.-D. (2010). Loss of the Protein-Tyrosine Phosphatase DEP-1/PTPRJ Drives Meningioma Cell Motility. Brain Pathology 21, 405–418.

Ramsay, A.G., Keppler, M.D., Jazayeri, M., Thomas, G.J., Parsons, M., Violette, S., Weinreb, P., Hart, I.R., and Marshall, J.F. (2007). HS1-associated protein X-1 regulates carcinoma cell migration and invasion via clathrin-mediated endocytosis of integrin alphavbeta6. Cancer Res. 67, 5275–5284.

Robert, V.J.P., Katic, I., and Bessereau, J.-L. (2009). Mos1 transposition as a tool to engineer the Caenorhabditis elegans genome by homologous recombination. Methods 49, 263–269.

Ruivenkamp, C.A.L., van Wezel, T., Zanon, C., Stassen, A.P.M., Vlcek, C., Csikós, T., Klous, A.M., Tripodis, N., Perrakis, A., Boerrigter, L., et al. (2002). Ptprj is a candidate for the mouse colon-cancer susceptibility locus Scc1 and is frequently deleted in human cancers. Nat. Genet. 31, 295–300.

Sacco, F., Tinti, M., Palma, A., Ferrari, E., Nardozza, A.P., van Huijsduijnen, R.H., Takahashi, T., Castagnoli, L., and Cesareni, G. (2009). Tumor Suppressor Density-enhanced Phosphatase-1 (DEP-1) Inhibits the RAS Pathway by Direct Dephosphorylation ofERK1/2 Kinases. J. Biol. Chem. VOL.284, pp.22048–pp.22058.

Sakai, T., Jove, R., Fässler, R., and Mosher, D.F. (2001). Role of the cytoplasmic tyrosines of beta 1A integrins in transformation by v-src. Proc. Natl. Acad. Sci. U.S.a. 98, 3808–3813.

Sakai, T., Zhang, Q., Fässler, R., and Mosher, D.F. (1998). Modulation of beta1A integrin functions by tyrosine residues in the beta1 cytoplasmic domain. J. Cell Biol. 141, 527–538.

Schlaepfer, D.D., and Hunter, T. (1998). Integrin signalling and tyrosine phosphorylation: just the FAKs? Trends Cell Biol. 8, 151–157.

Schlessinger, J. (2000). Cell signaling by receptor tyrosine kinases. Cell 103, 211–225.

Schwartz, M.A., Schaller, M.D., and Ginsberg, M.H. (1995). Integrins: emerging paradigms of signal transduction. Annu. Rev. Cell Dev. Biol. 11, 549–599.

Shattil, S.J., Kim, C., and Ginsberg, M.H. (2010). The final steps of integrin activation: the end game. Nat. Rev. Mol. Cell Biol. 11, 288–300.

Shultz, L.D., Schweitzer, P.A., Rajan, T.V., Yi, T., Ihle, J.N., Matthews, R.J., Thomas, M.L., and Beier, D.R. (1993). Mutations at the murine motheaten locus are within the hematopoietic cell protein-tyrosine phosphatase (Hcph) gene. Cell 73, 1445–1454.

Simmer, F., Tijsterman, M., Parrish, S., Koushika, S.P., Nonet, M.L., Fire, A., Ahringer, J., and Plasterk, R.H.A. (2002). Loss of the putative RNA-directed RNA polymerase RRF-3 makes *C. elegans* hypersensitive to RNAi. Curr. Biol. 12, 1317–1319.

Sternberg, P.W., and Han, M. (1998). Genetics of RAS signaling in *C. elegans*. Trends Genet. 14, 466–472.

Sternberg, P.W., and Horvitz, H.R. (1986). Pattern formation during *C. elegans* vulval induction. Cell 44, 761–772.

Sternberg, P.W. (2005). Vulval development. WormBook 1–28.

Tadokoro, S., Shattil, S.J., Eto, K., Tai, V., Liddington, R.C., de Pereda, J.M., Ginsberg, M.H., and Calderwood, D.A. (2003). Talin binding to integrin beta tails: a final common step in integrin activation. Science 302, 103–106.

Tan, P.B., Lackner, M.R., and Kim, S.K. (1998). MAP kinase signaling specificity mediated by the LIN-1 Ets/LIN-31 WH transcription factor complex during *C. elegans* vulval induction. Cell 93, 569–580.

Tarcic, G., Boguslavsky, S.K., Wakim, J., Kiuchi, T., Liu, A., Reinitz, F., Nathanson, D., Takahashi, T., Mischel, P.S., Ng, T., et al. (2009). An Unbiased Screen Identifies DEP-1 Tumor Suppressor as a Phosphatase Controlling EGFR Endocytosis. Current Biology 19, 1788–1798.

Tonks, N.K. (2006). Protein tyrosine phosphatases: from genes, to function, to disease. Nat. Rev. Mol. Cell Biol. 7, 833–846.

Trapasso, F., Iuliano, R., Boccia, A., Stella, A., Visconti, R., Bruni, P., Baldassarre, G., Santoro, M., Viglietto, G., and Fusco, A. (2000). Rat protein tyrosine phosphatase eta suppresses the neoplastic phenotype of retrovirally transformed thyroid cells through the stabilization of p27(Kip1). Molecular and Cellular Biology 20, 9236–9246.

Trapasso, F., Yendamuri, S., Dumon, K.R., Iuliano, R., Cesari, R., Feig, B., Seto, R., Infante, L., Ishii, H., Vecchione, A., et al. (2004). Restoration of receptor-type protein tyrosine phosphatase eta function inhibits human pancreatic carcinoma cell growth in vitro and in vivo. Carcinogenesis 25, 2107–2114.

Troemel, E.R., Sagasti, A., and Bargmann, C.I. (1999). Lateral signaling mediated by axon contact and calcium entry regulates asymmetric odorant receptor expression in *C. elegans*. Cell 99, 387–398.

Trzebiatowska, A., Topf, U., Sauder, U., Drabikowski, K., and Chiquet-Ehrismann, R. (2008). Caenorhabditis elegans teneurin, ten-1, is required for gonadal and pharyngeal basement membrane integrity and acts redundantly with integrin ina-1 and dystroglycan dgn-1. Mol. Biol. Cell 19, 3898–3908.

Tsuboi, N., Utsunomiya, T., Roberts, R.L., Ito, H., Takahashi, K., Noda, M., and Takahashi, T. (2008). The tyrosine phosphatase CD148 interacts with the p85 regulatory subunit of phosphoinositide 3-kinase. Biochem. J. 413, 193.

Upla, P., Marjomäki, V., Kankaanpää, P., Ivaska, J., Hyypiä, T., Van Der Goot, F.G., and Heino, J. (2004). Clustering induces a lateral redistribution of alpha 2 beta 1 integrin from membrane rafts to caveolae and subsequent protein kinase C-dependent internalization. Mol. Biol. Cell 15, 625–636.

Williams, B.D., and Waterston, R.H. (1994). Genes critical for muscle development and function in Caenorhabditis elegans identified through lethal mutations. J. Cell Biol. 124, 475–490.

Xu, X., Ahn, J.H., Tam, P., Yu, E.J., Batra, S., Cram, E.J., and Lee, M. (2010). Analysis of conserved residues in the beta-pat-3 cytoplasmic tail reveals important functions of integrin in multiple tissues. Dev. Dyn. 239, 763–772.

Yamada, K.M., and Even-Ram, S. (2002). Integrin regulation of growth factor receptors. Nat. Cell Biol. 4, E75–E76.

Ye, F., Hu, G., Taylor, D., Ratnikov, B., Bobkov, A.A., McLean, M.A., Sligar, S.G., Taylor, K.A., and Ginsberg, M.H. (2010). Recreation of the terminal events in physiological integrin activation. J. Cell Biol. 188, 157–173.

Yoo, A.S., Bais, C., and Greenwald, I. (2004). Crosstalk between the EGFR and LIN-12/Notch pathways in *C. elegans* vulval development. Science 303, 663–666.

Zhu, J.W., Brdicka, T., Katsumoto, T.R., Lin, J., and Weiss, A. (2008). Structurally distinct phosphatases CD45 and CD148 both regulate B cell and macrophage immunoreceptor signaling. Immunity 28, 183–196.

3.2 Additional experiments

3.2.1 Optimizing the preparation of *C. elegans* protein extract

An efficient and gentle preparation of protein extract is one of the basic steps during biochemical experiments. Several methods are known to extract proteins from a tissue, such as repeated freezing and thawing, sonication, mechanical disruption, or permeabilization by organic solvents. The method of choice depends on how robust the tissue is and how fragile the proteins are. Since the extraction process releases proteases that start digesting the proteins in solution, it is essential to slow down proteolysis by adding protease inhibitors and to perform protein extraction under cooled conditions.

The tough cuticle of *C. elegans*, which is composed primarily of collagens, highly cross-linked cuticle, and surface glycoproteins (Page and Johnstone, 2007), complicates protein extraction. In our laboratory, proteins have been so far extracted from worms by dounce homogenization (Fig. 3.6 A). Thereby, animals were mechanically disrupted by shear stresses that were generated by up- and down movements of a pestle in a glass mortar. However, the yield of protein extract obtained by this method was very low because only adult animals are disrupted, whereas the majority of larvae stayed intact (Fig. 3.6 B). In addition, the handling of the dounce homogenizer was exhausting and made it impossible to extract proteins at constant chilled temperatures.

To achieve a disruption of worms in all larval stages and to increase the yield of protein extract, we tried to grind *C. elegans* in a MixerMill (Fig. 3.6 C). Thereby, animals were suspended in lysis buffer and drop wise shock frozen in liquid nitrogen. The frozen droplets were then transferred to a grinding beaker containing a small steel ball (Fig. 3.6 C), which was pre-chilled in liquid nitrogen. By shaking the grinding beaker in a MixerMill with a frequency of 30 Hz, the frozen worms were grinded to a fine powder.

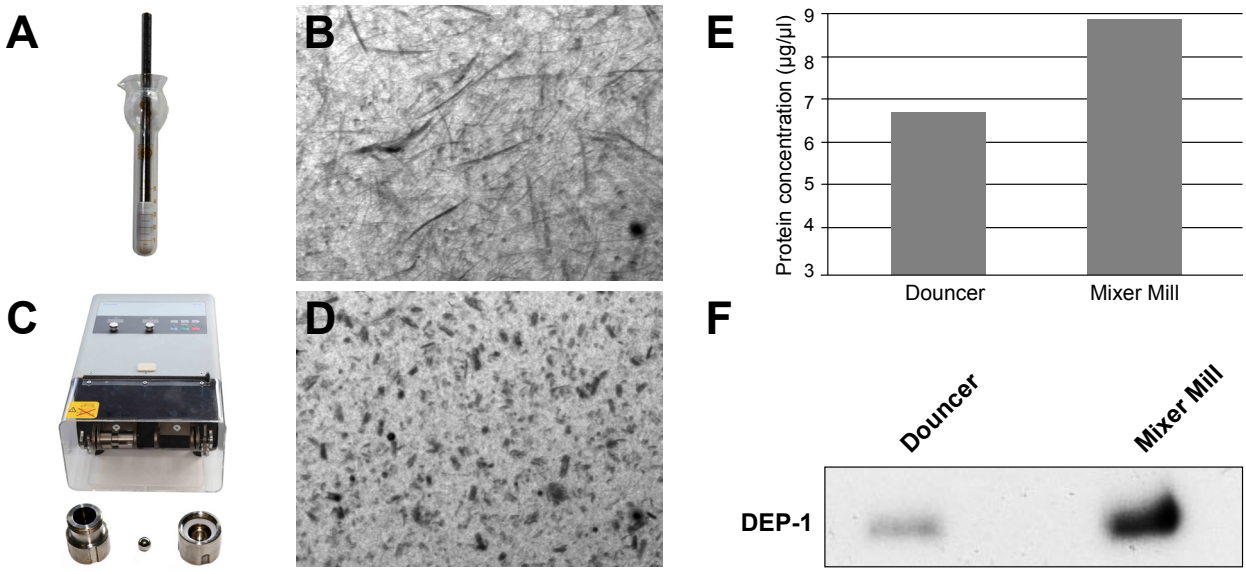

Figure 3.6 Preparation of *C. elegans* protein extract.
(**A**) Traditional protein extraction was performed by homogenizing worms in a dounce homogenizer. (**B**) Disruption of worms after dounce homogenization (150x up and down). (**C**) Grinding of frozen worms in a MixerMill (3x 2min at 30 Hz) results in a much more efficient disruption of worms (**D**). (**E**) Protein concentration of total protein extract obtained by dounce homogenization or MixerMill grinding. (**F**) Immunoblot of total protein extract from DEP-1full::HS animals using anti-HA antibodies. Protein extract was either obtained by dounce homogenization or MixerMill grinding.

After slow thawing of the powder at 4°C and subsequent centrifugation in a cool centrifuge, the whole worm protein extract was obtained.

By applying this new method, the efficiency of protein extraction could be improved notably. No intact animals could be recognized after MixerMill homogenization (Fig. 3.6 D), and the concentration of total protein extract was clearly enhanced (Fig. 3.6 E). Also the yield of membrane-bound DEP-1 was increased (Fig. 3.6 F). Furthermore, this method allowed a sample preparation at constant temperatures below 4°C, preventing a protein degradation.

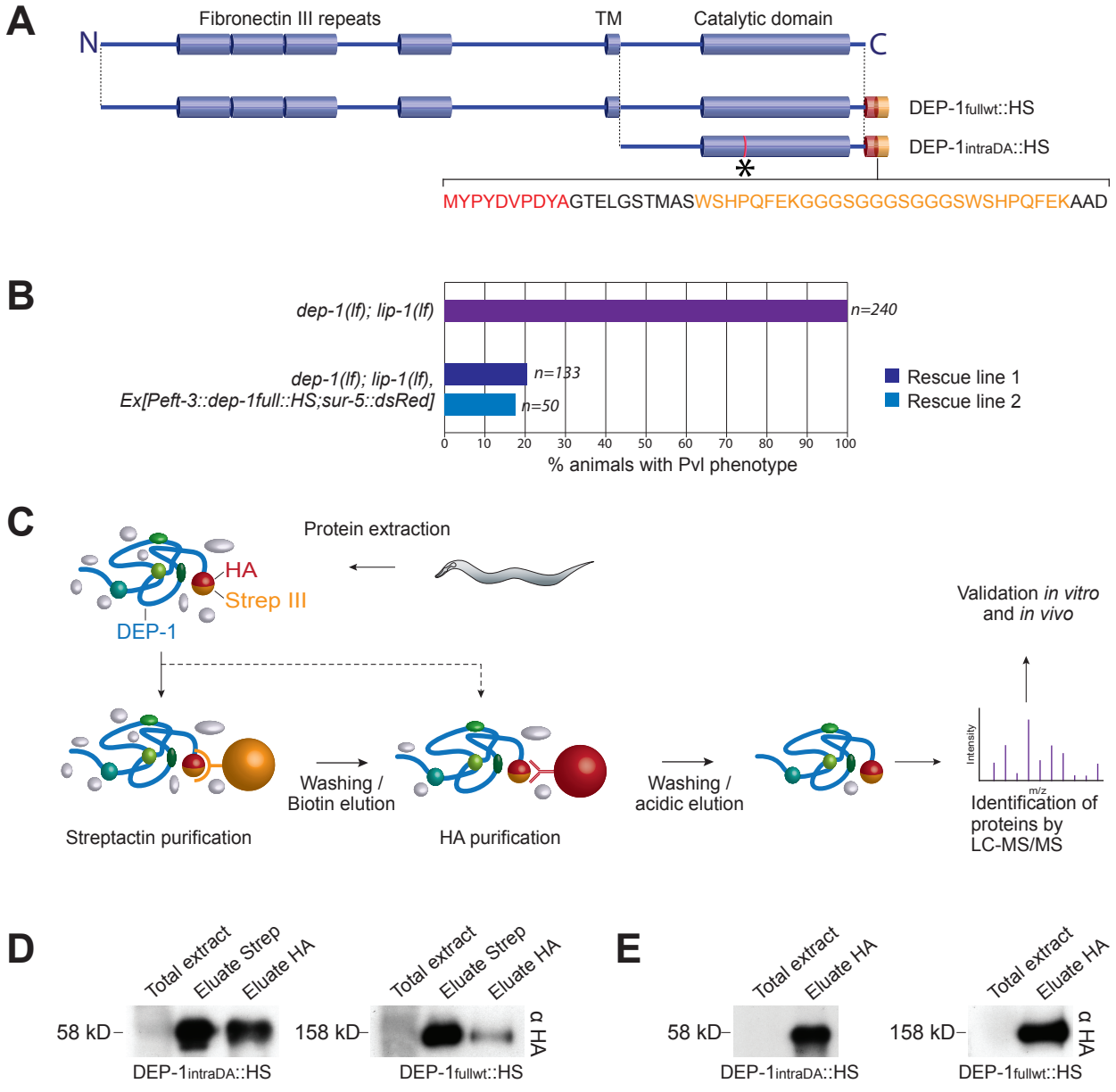

Figure 3.7 StrepTactin-HA affinity-purification of DEP-1.

(**A**) Domain structures of *C. elegans* DEP-1 and scheme of Hemaglutinin-StrepTactin-III (HS)-tagged DEP-1fullwt and DEP-1intraDA fusion proteins. Asterisks indicates the substrate trapping mutation D1241A. Amino acid sequence of the HS tag is indicated. (**B**) *Peft-3::dep-1full::HS* was co-injected with *sur-5::dsRed* in *dep-1(lf);lip-1(lf)* animals. Two lines of animals carring the extrachromosomal arrays rescued the Pvl phenotype. (**C**) Workflow of StrepTactin-HA double- and HA single purification with subsequent analysis by MS/MS. (**D**) Eluates of the StrepTactin-HA double purification and (**E**) of HA single purification were analyzed on an immunoblot using antiHA antibodies.

3.2.2 StrepTactin-HA double affinity-purification of DEP-1::HS

To purify DEP-1 together with its physiological interaction partners we initially used the tandem affinity-purification TAP-tag system (Puig et al., 2001). However, this system was not working in our hands (C. Walser, T. Schmid, M. Walser, data not shown) for which reason we decided to use the small double-affinity HA-Strep-III-tag (HS) that was recently developed at the ETH (Fig. 3.7 A, Glatter et al., 2009). The StrepTactin-haemagglutinin (SH) double purification enables a pure sample preparation with very little contaminant protein present, which allows to analyze the entire affinity-purified sample by a reversed-phase liquid chromatography unit coupled to a mass spectrometer in one single step (Glatter et al., 2009). A further advantage of the HS tag is its smaller size of the HS tag (5 kD) compared to the TAP-tag (21 kD). In our approach, the HA-Strep-III-tag was cloned to the C-terminus of full-length DEP-1 (DEP-1 full::HS / pMW4, Fig. 3.7 A) and to the DEP-1 intracellular domain containing the substrate-trapping mutation D1241A in the phosphatase domain (DEP-1intraDA::HS / pMW5), which allows the catalytically inactive enzyme to remain bound to its phosphorylated substrate (Palka, 2002). Since DEP-1 is expressed only in a few cells and therefore belongs to lower abundant proteins (1.16 ppm; www.pax-db.org), we over-expressed DEP-1::HS under the ubiquitous *eft-3* promoter. Otherwise, we would not have been able to purify an adequate amount of tagged proteins. By integrating the plasmids pMW4 and pMW5 into the genome of *C. elegans* by ballistic transformation, we obtained the two transgenic strains *zhIs27[Peft-3::dep-1full::HS;unc-119(+)]* and *zhIs28[Peft-3::dep-1intraD1241A::HS;unc-119(+)]*.

To test the functionality of *Peft-3::dep-1full::HS* (pMW4), we micro-injected this construct together with the co-injection marker *sur-5::dsRed* into *dep-1;lip-1(lf)* animals, which show typically a strong Pvl-phenotype (Fig. 3.7B). Since *Peft-3::dep-1full::HS* was able to rescue the Pvl phenotype of *dep-1;lip-1(lf)* animals, we concluded that this construct was functional.

For the double affinity-purification of DEP-1::HS, proteins were extracted from *zhIs27* and *zhIs28* animals by MixerMill grinding and incubated during a first purification step with StrepTactin-sepharose (Fig. 3.7 C). After several washing steps, purified DEP-1::HS was eluted with Biotin and incubated in a second purification step with monoclonal anti-HA agarose conjugate. Further washing steps followed before the double affinity-purified DEP-1::HS was eluted under acidic conditions. In order to identify contaminants that were not eliminated during washing procedures (e.g. proteins that bound to the Strep-Tactin sepharose and/or to the HA-agarose), we made mock purifications using protein extract of wild-type N2 animals.

The progress of the two purification steps was monitored by Western blot analyses, where the eluates of the different purification steps were loaded on a SDS-gel and immunoblotted with antibodies against HA (Fig. 3.7 D).

3.2.3 LC-MS/MS analysis of StrepTactin-HA purified DEP-1::HS

Western blot analyses indicated a very low yield of StrepTactin-HA purified DEP-1, especially from DEP-1 fullwt::HS (Fig. 3.7 D). Thus, we performed the tryptic digestion directly in the sample (in-solution digestion) instead of first separating the proteins by SDS-PAGE and performing an in-gel tryptic digestion (see 3.1.3). After ZipTip purification, the prepared samples were analyzed by LC-MS/MS. In total, 42 proteins were identified (Fig. 3.8 A), of which DEP-1 was the most abundant protein. Thus, we concluded that the SH double affinity-purification was working. However, the low yield of SH-purified DEP-1 made it impossible to pull-down an adequate amount of interacting proteins that can be detected by LC-MS/MS.

3.2.5 HA single purification of DEP-1::HS

To increase the yield of purified DEP-1 and thereby the amount of proteins interacting with DEP-1::HS, we decided to omit the StrepTactin purification and to perform only a single HA-purification (Fig. 3.7 C, dashed arrow). Furthermore, we tested if an increase of total *C. elegans* protein extract could enlarge the yield of purified DEP-1::HS. Thus, we incubated equilibrated monoclonal anti-HA agarose conjugate with 35 mg, 70 mg or 100 mg of total extract (Fig. 3.8 E) that derived from *zhIs27* and *zhIs28* animals. After intensive washing steps, purified DEP-1::HS was eluted under acidic conditions and further processed for LC-MS/MS analyses.

3.2.6 LC-MS/MS analysis of HA purified DEP-1::HS

Western blot analyses of HA-purified DEP-1 revealed that the yield of DEP-1::HS could be increased significantly by performing only HA-single purification (Fig. 3.7 E). This enlarged yield of DEP-1 resulted in a three-fold increase of proteins that were identified by LC-MS/MS. Among the 332 proteins that were identified in two independent LC-MS/MS experiments, 27 proteins were found exclusively in the DEP-1intraDA::HS fraction (Fig. 3.8 A).

However, not only an omission of the StrepTactin purification could increase the number of identified proteins but also the amount of protein extract that was used for the HA-purification, since an enhancement of protein extract from 35 mg to 100 mg resulted in the identification of 1.3 times more proteins (Fig. 3.8 E).

Taken together, these findings indicate that an increase of the yield of purified DEP-1::HS could improve the quality of the mass spectrometry results, and that the amount of purified DEP-1 is crucial for the successful identification of DEP-1 interactors by LC-MS/MS.

3.2.4 Proteins identified by DEP-1::HS pull-down experiments and MS/MS analyses

Gene name	Accession number		dep1intra_1_20101011	dep1intra_2_20101011	dep1full_1_20101011	dep1full_2_20101011	N2_1_20101011	N2_2_20101011	Protein Abundance (ppm)
dep-1	Q20120	Density enhanced phosphatase	21	15	28	36	0	0	1.16 ppm
vit-1	P55155	Vitellogenin-1	4	2	0	2	0	0	715 ppm
pcca-1	Q19842	Propionyl-CoA carboxylase alpha chain	4	0	3	2	0	0	902 ppm
lact-9	O62481	Protein LACT-9, isoform a	3	0	1	2	0	0	14.3 ppm
rps-12	P49196	40S ribosomal protein S12	3	0	1	0	0	0	900 ppm
chc-1	P34574	Probable clathrin heavy chain 1	3	0	0	0	0	0	247 ppm
sca-1	Q9XTG6	Calcium ATPase	3	0	0	0	0	0	634 ppm
lec-2	Q20684	Protein LEC-2, isoform a	2	6	2	0	0	0	630 ppm
M28.5	Q21568	NHP2-like protein 1 homolog	2	1	1	0	0	0	1259 ppm
ahcy-1	P27604	Adenosylhomocysteinase	2	1	0	2	0	0	4696 ppm
F46H5.3	Q10454	Probable arginine kinase F46H5.3 (AK) (EC 2.7.3.3)	2	1	0	0	0	0	4094 ppm
eat-6	P90735	Protein EAT-6	2	0	1	1	0	0	426 ppm
dld-1	O17953	Dihydrolipoyl dehydrogenase	2	0	1	0	0	0	
inf-1	P27639	Eukaryotic initiation factor 4A (eIF-4A)	2	0	0	0	0	0	735 ppm

vha-12	Q19626	Probable V-type proton ATPase subunit B	2	0	0	0	0	0	1979 ppm
gdh-1	Q23621	Glutamate dehydrogenase	2	0	0	0	0	0	
lys-7	O16202	Protein LYS-7	1	3	0	1	0	0	74.6 ppm
act-5	O45815	Protein ACT-5	1	3	0	1	0	0	1298 ppm
rps-28	Q95Y04	40S ribosomal protein S28	1	2	1	0	0	0	2729 ppm
vit-5	P06125	Vitellogenin-5	1	2	0	0	0	0	750 ppm
phb-1	Q9BKU4	Mitochondrial prohibitin complex protein 1	1	0	2	0	0	0	1108 ppm
lpd-5	Q9N4L8	Protein LPD-5	1	0	1	2	0	0	653 ppm
B0513.4	O45227	Protein B0513.4, isoform a	1	0	0	3	0	0	107 ppm
rpl-15	P91374	60S ribosomal protein L15	1	0	0	2	0	0	2131 ppm
vab-10	O18290	Protein ZK1151.1a	0	15	0	1	0	0	60.1 ppm
Y43F8B.1	B7FAR9	Protein Y43F8B.1, isoform d	0	12	0	0	0	0	82.3 ppm
nmy-2	Q19658	Protein F20G4.3	0	6	0	0	0	0	81.6 ppm
atn-1	Q23158	Protein ATN-1, isoform a	0	6	0	0	0	0	179 ppm
deb-1	P19826	Vinculin (P107B)	0	5	0	0	0	0	200 ppm
C39D10.7	Q18529	Protein C39D10.7	0	5	0	0	0	0	30.0 ppm
gei-15	Q21482	Putative uncharacterized protein	0	5	0	0	0	0	214 ppm
hmg-11	Q22204	High mobility group protein I alpha	0	5	0	0	0	0	895 ppm
lfi-1	Q23081	Lin-5 (Five) interacting protein protein 1	0	5	0	0	0	0	334 ppm
D1086.10	B1Q273	Protein D1086.10, isoform c	0	4	0	0	0	0	129 ppm
grd-5	O16462	Protein GRD-5	0	3	0	2	0	0	728 ppm
C08A9.10	Q27GT6	Protein C08A9.10	0	3	0	1	0	0	7.04 ppm
C14F11.4	B3WFT8	Protein C14F11.4, isoform a	0	3	0	0	0	0	71.2 ppm
hmg-12	O45912	High mobility group protein I beta	0	3	0	0	0	0	358 ppm
fipr-21	Q20277	Protein FIPR-21	0	3	0	0	0	0	168 ppm
W03F8.10	Q7YZM5	Putative uncharacterized protein	0	3	0	0	0	0	256 ppm
W03F11.1	O01780	Protein W03F11.1	0	2	0	1	0	0	21.9 ppm
F19C7.1	Q19591	Protein F19C7.1	0	2	0	1	0	0	88.1 ppm
lam-1	O44565	Protein LAM-1	0	2	0	0	0	0	106 ppm
ZK484.3	O44895	Protein ZK484.3	0	2	0	0	0	0	228 ppm
ttr-51	O62289	Protein TTR-51	0	2	0	0	0	0	638 ppm
W01F3.2	O62390	Protein W01F3.2	0	2	0	0	0	0	26.2 ppm
emb-9	P17139	Collagen alpha-1(IV) chain	0	2	0	0	0	0	12.4 ppm
ifa-4	P90900	Intermediate filament protein ifa-4 (Cel IF A4)	0	2	0	0	0	0	235 ppm
mlc-4	Q09510	Probable myosin regulatory light chain	0	2	0	0	0	0	268 ppm
C18B2.3	Q18074	Protein C18B2.3	0	2	0	0	0	0	153 ppm
ZK84.1	Q23635	Protein ZK84.1	0	2	0	0	0	0	82.2 ppm
gfi-1	Q94246	Protein GFI-1	0	2	0	0	0	0	60.9 ppm
unc-95	Q9NEZ5	Protein UNC-95	0	2	0	0	0	0	104 ppm
K07H8.10	O45181	Protein K07H8.10	2	1	2	0	0	1	230 ppm
rpl-17	Q9BL19	60S ribosomal protein L17	2	1	1	1	0	1	1932 ppm
C25A1.6	Q9XVR8	Putative H/ACA ribonucleoprotein complex subunit 3-like protein	2	2	1	1	0	2	379 ppm
W01D2.1	O62388	Ribosomal protein L37	3	1	4	4	0	3	1314 ppm
eef-2	P29691	Elongation factor 2 (EF-2)	5	2	3	4	1	0	7.81 ppm
rps-0	P46769	40S ribosomal protein SA	4	2	2	4	1	0	2456 ppm
gpd-2	P17329	Glyceraldehyde-3-phosphate dehydrogenase 2	3	2	2	2	1	0	2973 ppm
rpl-9	Q95Y90	60S ribosomal protein L9	3	1	1	1	1	0	2896 ppm
alg-2	O16720	Protein ALG-2, isoform a	3	0	1	0	1	0	67.2 ppm
anc-1	Q9N4M4	Nuclear anchorage protein 1	2	6	0	0	1	0	294 ppm
sqd-1	Q8MXR6	Protein SQD-1, isoform a	2	1	3	1	1	0	1530 ppm
aco-2	P34455	Probable aconitate hydratase, mitochondrial	2	1	2	1	1	0	1933 ppm
hil-3	Q19743	Histone H1.3	2	0	2	0	1	0	168 ppm
mdh-1	Q9UAV5	Malate dehydrogenase	2	0	1	0	1	0	2090 ppm
hsp-3	P27420	Heat shock 70 kDa protein C	2	0	0	0	1	0	1510 ppm
ucr-2.2	Q22370	Protein UCR-2.2	2	0	0	0	1	0	472 ppm
T23E7.2	O17338	Putative uncharacterized protein	1	4	4	0	1	0	397 ppm
rps-20	Q8WQA8	Protein RPS-20	1	3	1	2	1	0	3421 ppm
ZC373.2	Q23258	Protein ZC373.2	1	2	0	0	1	0	230 ppm
sdha-1	Q09508	Succinate dehydrogenase	1	1	2	0	1	0	635 ppm

W09D12.1	Q23227	Protein W09D12.1	1	1	2	0	1	0	22.8 ppm
D1054.11	Q18947	Protein D1054.11	1	1	0	3	1	0	186 ppm
dlst-1	O45148	Protein DLST-1	1	0	1	2	1	0	
rack-1	Q21215	Guanine nucleotide-binding protein subunit beta-2-like 1	1	0	1	2	1	0	2329 ppm
ifb-1	Q19289	Intermediate filament protein ifb-1	0	16	0	0	1	0	1291 ppm
ifa-1	D2Y8W0	Protein F38B2.1d	0	13	0	0	1	0	413 ppm
hpo-34	Q6A2D2	Protein HPO-34	0	12	0	0	1	0	
hil-4	O17536	Histone H1.4 (Histone H1-like protein 4)	0	5	0	0	1	0	122 ppm
ZK1321.4	Q9XTP9	Protein ZK1321.4a	0	4	0	0	1	0	207 ppm
lam-2	Q18823	Laminin-like protein lam-2	0	3	0	0	1	0	152 ppm
mlc-5	Q9XVI9	Protein MLC-5	0	3	0	0	1	0	
tag-18	Q22508	Protein TAG-18	0	2	0	0	1	0	131 ppm
ifd-1	Q86DC6	Intermediate filament protein ifd-1	0	2	0	0	1	0	66.2 ppm
H03A11.2	Q9XTW1	Protein H03A11.2	0	2	0	0	1	0	48.1 ppm
K07C5.4	Q21276	Uncharacterized NOP5 family protein K07C5.4	5	0	4	2	1	1	411 ppm
K06G5.1B	Q5WRM0	Protein K06G5.1	4	3	3	2	1	1	320 ppm
rps-1	P48154	40S ribosomal protein S3a	4	1	3	4	1	1	2661 ppm
asp-6	O01530	Aspartic protease 6 (EC 3.4.23.-)	3	4	5	1	1	1	961 ppm
rpl-11.2	Q19162	Protein RPL-11.2	3	2	1	1	1	1	808 ppm
hil-2	P15796	Histone H1.2 (Histone H1-like protein 2)	2	4	2	1	1	1	275 ppm
isp-1	O44512	Cytochrome b-c1 complex subunit Rieske, mitochondrial (EC 1.10.2.2)	2	3	2	2	1	1	458 ppm
T09B4.5	O02155	Protein T09B4.5, isoform a	2	2	2	1	1	1	156 ppm
rpl-31	Q9U332	60S ribosomal protein L31	2	1	2	1	1	1	864 ppm
cey-4	Q9XTJ6	Protein Y39A1C.3	2	0	4	2	1	1	927 ppm
F53F4.10	Q20719	Probable NADH dehydrogenase	1	2	2	1	1	1	413 ppm
Y63D3A.7	Q9XWG2	Protein Y63D3A.7	1	1	0	2	1	1	287 ppm
lec-1	O45904	Protein LEC-1, isoform b	0	3	1	0	1	1	1421 ppm
tag-61	O45865	Protein ANT-1.1, isoform a	5	2	4	4	1	2	1798 ppm
clec-265	Q21471	Protein CLEC-265	4	1	2	3	1	2	13.1 ppm
rpl-33	P49180	60S ribosomal protein L35a	3	1	2	1	1	2	2326 ppm
D1054.10	Q18943	Protein D1054.10	2	2	1	2	1	2	267 ppm
rps-25	P52821	40S ribosomal protein S25	2	1	2	1	1	2	2175 ppm
rpl-41	P48166	60S ribosomal protein L44 (L41)	2	1	2	0	1	2	2062 ppm
T04A8.6	Q22135	Protein T04A8.6	2	0	2	2	1	2	68.0 ppm
C56G2.7	Q09289	Proteasomal ubiquitin receptor ADRM1 homolog	2	0	1	2	1	2	702 ppm
F58F12.1	Q09544	ATP synthase subunit delta	1	2	2	2	1	2	1959 ppm
rps-27	Q9TXP0	40S ribosomal protein S27	1	2	1	3	1	2	191 ppm
Y54F10AM.5	Q9BL03	Protein Y54F10AM.5	1	1	1	1	1	2	367 ppm
aly-1	Q17561	Protein ALY-1	1	0	3	0	1	2	120 ppm
R12E2.13	O61793	Protein R12E2.13	1	0	1	2	1	2	89.4 ppm
his-1	P62784	Histone H4	6	7	3	2	1	3	681 ppm
pqn-53	Q21793	Protein PQN-53, isoform a	4	1	3	0	2	0	69.6 ppm
asp-1	Q9TVS4	Aspartic protease 1	4	1	1	5	2	0	1290 ppm
LLC1.2	O17954	Protein LLC1.2, isoform a	2	3	4	2	2	0	117 ppm
Y34B4A.6	Q95Y29	Protein Y34B4A.6	2	2	2	2	2	0	174 ppm
C08F11.11	O62053	UPF0375 protein C08F11.11	1	1	2	1	2	0	137 ppm
hrpf-1	Q8MQG5	Putative uncharacterized protein W02D3.11	1	0	1	0	2	0	83.0 ppm
sodh-1	Q17334	Alcohol dehydrogenase 1	1	0	0	0	2	0	1763 ppm
ketn-1	A7DT47	Kettin (Drosophila actin-binding) homolog protein 1	0	42	0	0	2	0	134 ppm
flu-2	Q18026	Kynureninase	0	4	0	2	2	0	
myo-5	Q21'000	Protein MYO-5	0	0	0	0	2	0	141 ppm
tba-2	P34690	Tubulin alpha-2 chain	4	2	3	5	2	1	874 ppm
asp-2	Q86NE0	Protein ASP-2, isoform b	3	3	4	2	2	1	202 ppm
ucr-2.1	Q9BI61	Protein VW06B3R.1b	3	1	3	2	2	1	968 ppm
let-2	P17140	Collagen alpha-2(IV) chain	2	6	2	2	2	1	18.6 ppm
htz-1	Q27511	Histone H2A.V (H2A.F/Z)	2	2	2	2	2	1	1163 ppm
Y67D2.3	Q9BKQ9	Protein Y67D2.3	2	1	1	2	2	1	262 ppm
nduf-5	Q9N3D9	Protein NDUF-5	1	2	2	2	2	1	453 ppm
ile-1	P90913	ERGIC-53-like protein	1	1	0	6	2	1	149 ppm

ZC412.10	A8WHT2	Protein ZC412.10	0	0	0	2	2	1	NA
F45H10.3	O02267	Protein F45H10.3	4	5	1	2	2	2	436 ppm
rps-10	O01869	Protein RPS-10	4	4	3	4	2	2	2017 ppm
rps-17	O01692	40S ribosomal protein S17	4	2	3	3	2	2	3320 ppm
rpl-5	P49405	60S ribosomal protein L5	4	2	1	3	2	2	3694 ppm
rla-1	P91913	60S acidic ribosomal protein P1	3	3	3	2	2	2	4729 ppm
cey-2	P91306	Protein CEY-2	3	1	2	4	2	2	490 ppm
perm-2	O44145	Protein PERM-2	2	2	2	2	2	2	
dpy-17	Q20778	Protein DPY-17	2	1	2	1	2	2	15.9 ppm
gln-1	Q95YD1	Protein GLN-1	2	1	0	3	2	2	32.4 ppm
hsp-1	P09446	Heat shock 70 kDa protein A	5	8	7	3	2	3	2550 ppm
rps-6	Q9NEN6	40S ribosomal protein S6	3	4	4	6	2	3	2440 ppm
ubl-1	P37165	Ubiquitin-like protein 1-40S ribosomal protein S27a	3	2	3	4	2	3	592 ppm
hpo-18	O16298	Protein HPO-18	2	4	3	1	2	3	
perm-4	O44144	Protein PERM-4	2	3	0	5	2	3	
rps-21	P49197	40S ribosomal protein S21	1	1	2	4	2	3	2616 ppm
mdh-2	O02640	Probable malate dehydrogenase, mitochondrial (EC 1.1.1.37)	5	2	3	2	3	0	
rps-22	O17218	Protein RPS-22, isoform a	3	2	2	3	3	0	2759 ppm
mig-6	O76840	Papilin (Abnormal cell migration protein 6)	2	13	2	2	3	0	155 ppm
enol-1	Q27527	Enolase	2	1	2	0	3	0	4422 ppm
lec-6	Q9N384	Protein LEC-6	1	1	1	1	3	0	737 ppm
nmy-1	Q20641	Protein NMY-1	0	9	0	0	3	0	114 ppm
lev-11	Q27249	Tropomyosin isoforms c/e	0	6	0	0	3	0	7575 ppm
vig-1	O16646	Vig (Drosophila vasa intronic gene)	3	2	1	3	3	1	1843 ppm
tbb-2	P52275	Tubulin beta-2 chain (Beta-2-tubulin)	10	6	5	8	3	2	1372 ppm
rps-2	P51403	40S ribosomal protein S2	7	6	3	5	3	2	2158 ppm
his-3	P09588	Histone H2A	5	4	4	4	3	2	372 ppm
pab-1	Q9U302	Protein PAB-1, isoform a	5	4	2	5	3	2	840 ppm
rps-7	Q23312	40S ribosomal protein S7	5	2	3	4	3	2	2334 ppm
rpl-23	P48158	60S ribosomal protein L23	4	1	2	3	3	2	2135 ppm
rpl-32	Q22716	Protein RPL-32, isoform a	3	4	2	5	3	2	2363 ppm
F49E2.5	D0VWM5	Protein F49E2.5, isoform k	3	3	2	1	3	2	456 ppm
cey-1	O62213	Protein CEY-1	3	2	3	2	3	2	1132 ppm
rps-5	P49041	40S ribosomal protein S5	3	2	2	2	3	2	1535 ppm
rpl-10	Q09533	60S ribosomal protein L10 (QM protein homolog)	3	1	4	6	3	2	2038 ppm
rps-9	Q20228	40S ribosomal protein S9	3	1	2	3	3	2	2186 ppm
Y66H1A.4	Q9TYK1	Probable H/ACA ribonucleoprotein complex subunit 1-like protein	2	1	3	2	3	2	345 ppm
rpl-7	O01802	60S ribosomal protein L7	6	3	3	4	3	3	2403 ppm
rps-14	P48150	40S ribosomal protein S14	5	5	5	3	3	3	1597 ppm
rpl-30	Q9XWS4	Protein RPL-30, isoform a	4	0	1	3	3	3	1099 ppm
rps-30	Q18231	Protein RPS-30	3	4	3	2	3	3	154 ppm
rpl-25.1	P48162	60S ribosomal protein L23a 1	2	3	2	3	3	3	1316 ppm
rpl-24.1	O01868	60S ribosomal protein L24	6	1	5	5	3	4	3526 ppm
rpl-14	Q9XVE9	Protein RPL-14	3	3	3	3	3	5	3227 ppm
cbd-1	O45599	Protein CBD-1	4	10	2	13	3	14	17.7 ppm
pqn-22	O02143	Prion-like-(Q/n-rich)-domain-bearing protein protein 22	0	19	0	0	4	0	218 ppm
C44B7.10	Q18599	Protein C44B7.10	5	1	2	2	4	1	2154 ppm
rps-18	O18240	Protein RPS-18	3	5	3	4	4	1	4920 ppm
rps-16	Q22054	40S ribosomal protein S16	5	3	5	3	4	2	2456 ppm
rpl-19	O02639	60S ribosomal protein L19	4	2	2	2	4	2	3055 ppm
rpl-20	O44480	60S ribosomal protein L18a	3	3	2	2	4	3	2610 ppm
rps-11	Q20206	Protein RPS-11	7	4	5	5	4	4	1776 ppm
rpl-3	P50880	60S ribosomal protein L3	5	4	3	4	4	4	2393 ppm
rps-26	O45499	40S ribosomal protein S26	5	3	5	3	4	4	1335 ppm
rps-19	O18650	40S ribosomal protein S19	4	5	4	5	4	4	2483 ppm
rpl-35	P34662	60S ribosomal protein L35	4	4	4	4	4	4	4176 ppm
his-24	P10771	Histone H1.1	3	5	4	3	4	4	596 ppm
rps-24	Q1XFY9	Protein RPS-24	3	2	2	4	4	4	2060 ppm
his-11	P04255	Histone H2B 1	3	7	5	5	4	5	426 ppm

rpl-4	O02056	60S ribosomal protein L4	9	7	3	7	4	7	2708 ppm
vit-6	P18948	Vitellogenin-6	12	5	2	8	5	0	1565 ppm
rps-15	Q9XVP0	40S ribosomal protein S15	6	4	4	5	5	1	2721 ppm
fib-1	Q22053	rRNA 2'-O-methyltransferase fibrillarin	5	3	4	3	5	1	712 ppm
rps-13	P51404	40S ribosomal protein S13	3	4	2	3	5	1	2561 ppm
rpl-13	P91128	60S ribosomal protein L13	5	4	3	6	5	2	2209 ppm
atp-4	O16517	Protein ATP-4	4	5	4	6	5	2	2175 ppm
lys-1	O62415	Protein LYS-1	3	3	3	3	5	2	148 ppm
rpl-27	P91914	60S ribosomal protein L27	2	3	3	5	5	2	2873 ppm
rla-2	Q9U1X9	Protein RLA-2	7	5	6	6	5	3	5637 ppm
rps-3	P48152	40S ribosomal protein S3	6	3	5	6	5	3	2815 ppm
rpl-10	Q9N4I4	60S ribosomal protein L10a	4	4	4	3	5	3	2038 ppm
rpl-12	P61866	60S ribosomal protein L12	4	5	3	4	5	4	3385 ppm
rpl-36	P49181	60S ribosomal protein L36	3	4	4	5	5	5	1493 ppm
unc-15	P10567	Paramyosin (Uncoordinated protein 15)	0	24	1	1	6	1	2391 ppm
rps-23	Q19877	40S ribosomal protein S23	4	5	4	4	6	2	2491 ppm
Y69A2AR.18	Q95XJ0	Protein Y69A2AR.18, isoform a	4	2	6	5	6	2	1322 ppm
rpl-21	P34334	60S ribosomal protein L21	6	5	5	4	6	3	2356 ppm
R09H10.5	Q21884	Protein R09H10.5	5	2	4	5	6	3	70.4 ppm
unc-87	P37806	Protein unc-87 (Uncoordinated protein 87)	1	19	1	2	6	3	626 ppm
rpl-22	P52819	60S ribosomal protein L22	6	4	8	6	6	4	3299 ppm
prdx-2	A8DYR6	Peroxiredoxin protein 2	6	3	4	6	6	4	2916 ppm
mlc-2	P19626	Myosin regulatory light chain 2	3	7	5	5	6	4	2051 ppm
rpl-28	Q21930	60S ribosomal protein L28	8	7	5	6	6	5	2695 ppm
rpl-37	Q9U2A8	60S ribosomal protein L37a	5	3	4	5	6	5	83.8 ppm
rpl-8	Q9XVF7	60S ribosomal protein L8	7	5	8	5	6	6	1650 ppm
rpl-25.2	Q20647	60S ribosomal protein L23a 2	5	4	7	5	6	7	2133 ppm
ifb-2	Q19286	Intermediate filament protein ifb-2	0	7	0	0	7	0	533 ppm
F40F4.6	Q20219	Protein F40F4.6	11	3	8	0	7	1	223 ppm
T25C12.3	Q22774	Protein T25C12.3	11	6	8	7	7	3	233 ppm
atp-3	P91283	Protein ATP-3, isoform a	8	6	9	6	7	6	1538 ppm
rpa-0	Q93572	60S acidic ribosomal protein P0	9	7	6	8	7	8	2663 ppm
rpl-18	O45946	60S ribosomal protein L18	7	6	5	7	8	4	3797 ppm
rps-4	Q9N3X2	40S ribosomal protein S4	12	8	7	11	8	7	2657 ppm
rpa-2	O01504	60S acidic ribosomal protein P2	7	7	8	8	8	8	138 ppm
rpl-26	Q19869	60S ribosomal protein L26	7	5	6	8	8	8	1712 ppm
atp-5	Q17763	Protein ATP-5	10	5	10	8	8	9	1427 ppm
unc-52	B6VQ97	Protein ZC101.2d	1	27	7	13	9	0	71.9 ppm
lev-11	Q22866	Tropomyosin isoforms a/b/d/f	0	12	0	2	9	2	7575 ppm
eft-3	P53013	Elongation factor 1-alpha (EF-1-alpha)	7	4	5	8	9	3	3510 ppm
dim-1	Q18066	Disorganized muscle protein 1	8	9	6	5	9	4	594 ppm
H27A22.1	O17912	Protein H27A22.1a	13	6	9	5	9	9	8.86 ppm
rps-8	P48156	40S ribosomal protein S8	10	8	7	10	9	10	2237 ppm
H28O16.1	Q9XXK1	ATP synthase subunit alpha	6	7	6	8	10	4	6282 ppm
T25F10.6	Q23050	Protein T25F10.6, isoform a	1	27	4	4	10	4	1392 ppm
rpl-6	P47991	60S ribosomal protein L6	9	6	7	10	10	7	2295 ppm
act-1	P10983	Actin-1	8	15	6	7	10	7	2359 ppm
atp-2	P46561	ATP synthase subunit beta, mitochondrial (EC 3.6.3.14)	10	8	9	8	10	9	6267 ppm
mlc-3	P53014	Myosin, essential light chain (Myosin light chain alkali)	5	11	12	10	12	9	7584 ppm
rpl-7A	Q966C6	60S ribosomal protein L7a	14	7	11	11	13	7	2015 ppm
myo-3	P12844	Myosin-3 (Myosin heavy chain A) (MHC A)	0	38	2	3	25	3	489 ppm
let-75	P02567	Myosin-1	0	50	0	4	29	2	603 ppm
myo-2	P12845	Myosin-2 (Myosin heavy chain C) (MHC C)	1	49	1	9	31	4	570 ppm
unc-54	P02566	Myosin-4	15	104	21	53	102	47	2658 ppm

Table 2 Proteins that were identified by LC-MS/MS analyses after DEP-1::HA pull-down experiments.
LC-MS/MS analyses identified 246 proteins. Every pull-down was done in dublicate. The numbers represent the peptides that were detected. Min. Protein Probability = 95%; Min. Number of Peptides = 2. Values from „Protein abundance“ correspond to the „*C.elegans* PaxDB integrated dataset“ (www.pax-db.org).

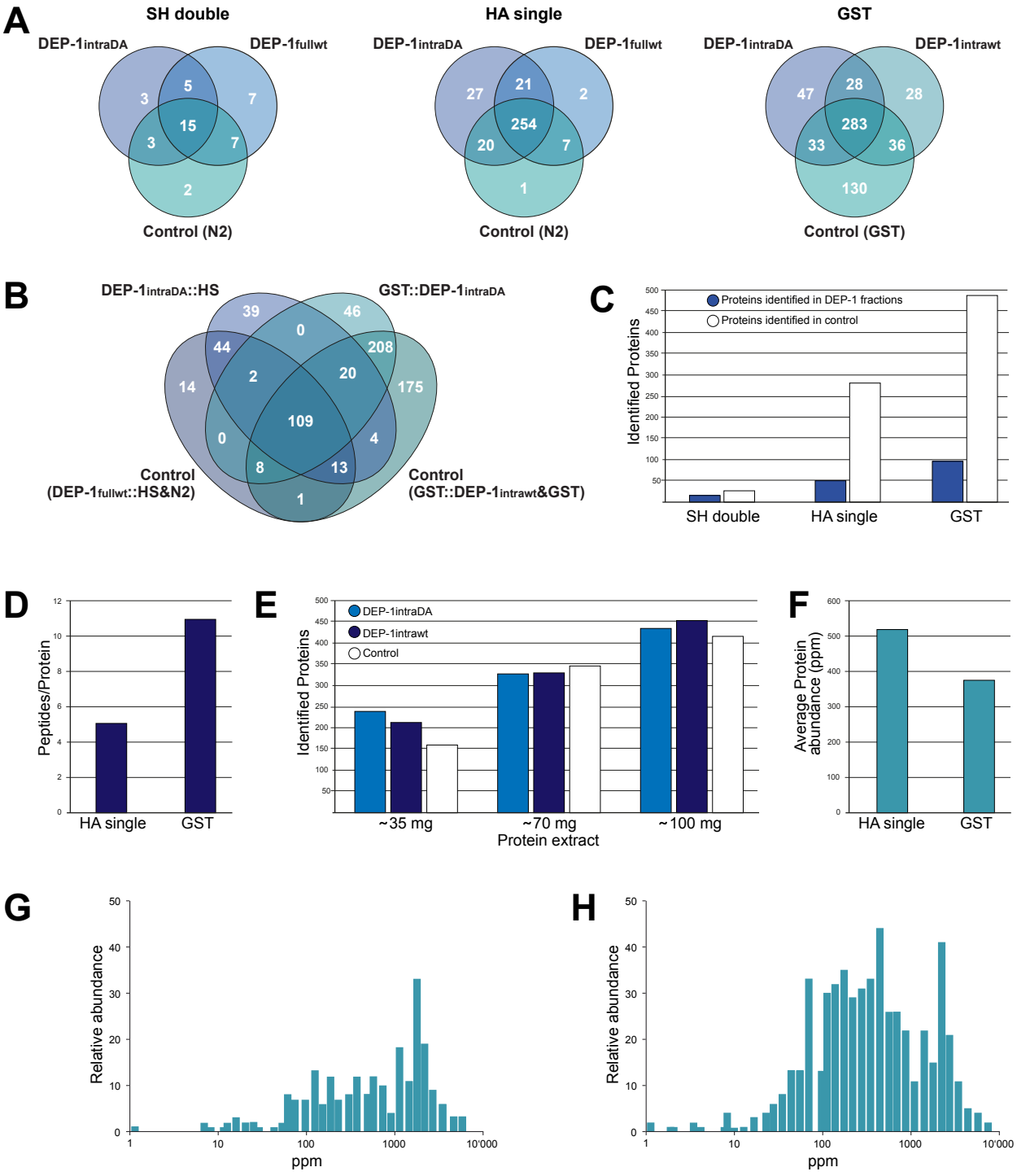

Figure 3.8 Comparison of LC-MS/MS results after HA- and GST pull-down experiments.
(**A**) Number of proteins identified by LC-MS/MS analyses after StrepTactin-HA double purification, HA single purification, and GST-purification. (**B**) Overlap of proteins identified by LC-MS/MS analyses after HA single purification and GST-purification of DEP-1intraDA. (**C**) Number of proteins identified by LC-MS/MS analyses after StrepTactin-HA double purification, HA single purification, and GST-purification. (**D**) Average number of peptides corresponding to one protein identified by LC-MS/MS analyses after HA single and GST-purification. (**E**) Influence of amount of protein extract on the number of identified proteins by LC-MS/MS analyses of HA-purified proteins. (**F**) Average abundance of the proteins identified by LC-MS/MS analyses after HA single- and GST-purification. (**G**) Relative protein abundance of proteins identified by LC-MS/MS analyses after HA single purification and (**H**) GST purification. Protein abundance was calculated from *C. elegans* PaxDB integrated dataset. P_{Min} protein = 95%, $\#_{Min}$ peptides = 2; P_{Min} peptide = 95%.

3.2.7 Comparison of LC-MS/MS results after HA- and GST pull-down experiments

LC-MS/MS analyses of HA- and GST-purified DEP-1 led to the identification of total 683 proteins. Surprisingly, no proteins were identified which bound to both DEP-1intraDA::HS and GST::DEP-1 intraDA but not to the controls (Fig 3.8 B), although in both methods the intracellular domain of DEP-1 was purified. However, the vast majority of identified proteins were found in one or both of the control fractions, indicating that the HA-purified DEP-1::HS still contained numerous contaminants that were not identified by analyzing the HA-controls.
Further comparison of the LC-MS/MS data of the three different purification methods (SH-double purification, HA-single purification, and GST-purification) revealed that the amount of purified DEP-1 affects the number of identified proteins significantly (Fig. 3.8 C, D). Moreover, the confidence of proteins identified by LC-MS/MS could be enhanced by increasing the yield of purified DEP-1, represented by the number of peptides belonging to a protein (Fig. 3.8 E). And in addition, higher amounts of purified DEP-1 led to the identification of more proteins that are less abundant (Fig. 3.8 F-H). Thus, our data suggest that the yield of purified DEP-1 affects not only the quantity of proteins identified by LC-MS/MS but also their quality.

3.2.8 Production of polyclonal DEP-1 antibodies

An alternative way to identify novel interaction partners of DEP-1 would be to perform co-immunoprecipitation experiments, in which antibodies binding specifically to DEP-1 are used to capture the protein complex. Since there were no *C. elegans* DEP-1 antibodies available, we produced polyclonal DEP-1 antibodies that are directed against the intracellular domain of GST-tagged DEP-1.
Therefore, the GST-tagged intracellular domain of DEP-1 (GST::DEP-1intra, pTB29) was expressed in *E. coli* BL21 and purified using GST-sepharose (Fig. 3.9 B). After elution from the sepharose, the purified DEP-1 was used for the immunization of the two rabbits 006-9AB-1D2 and 006-9AC-B07 at the institute of laboratory animal sciences, whose sera were received after three months (Fig. 3.9 A step 1).
The rabbit sera contained a large diversity of antibodies that would affect the quality of immunohistochemical experiments. Thus, we affinity-purified the DEP-1 specific antibodies from the sera by a HiTrap NHS-activated column that was previously packet with GST::DEP-1 (Fig. 3.9 A step 2). Antibodies specific for GST::DEP-1 were retained in the column, whereas other antibodies were washed away. After washing, the antibodies could be eluted under acidic and basic conditions. A Ponceau-stained dot blot enabled the identification of the fractions containing the eluted antibodies (Fig. 3.9 C).
The affinity-purified antibodies contained not only DEP-1, but also GST-specific antibodies. Thus, we performed a second affinity-purification with another HiTrap NHS-activated column that was packed with GST (Fig. 3.9 A step 3). The eluates from the first affinity-purification were passed through the GST column, whereas only the GST but not the DEP-1 specific antibodies were retarded. Finally, the affinity-purified antibodies were aliquoted and stored at -80°C.

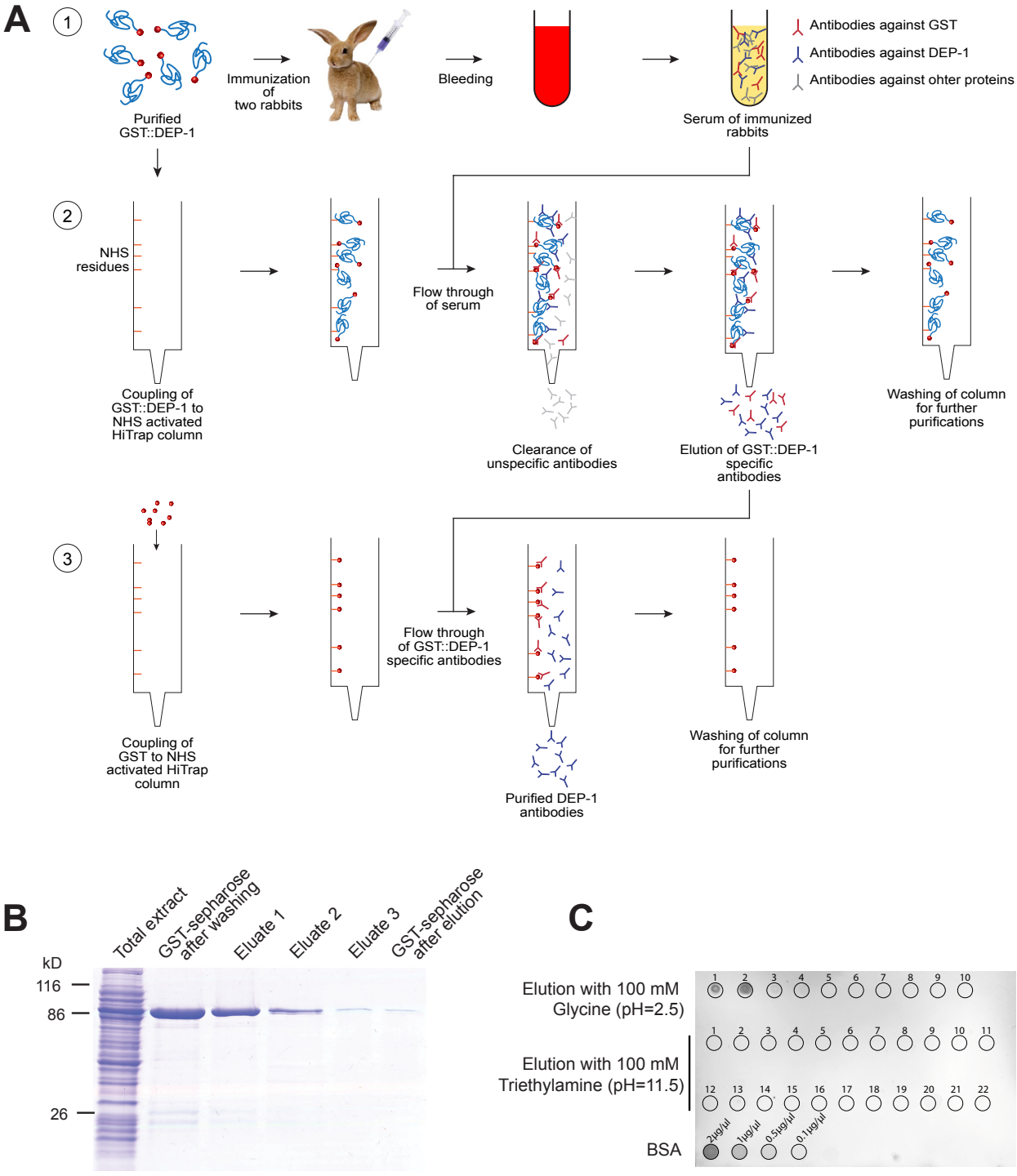

Figure 3.9 Workflow of the production of polyclonal DEP-1 antibodies.
(**A**) Immunization [1] of rabbits with purified GST::DEP-1intra. After 3 months, the rabbits were bleeded to optain the sera. [2] First affinity-purification with NHS activated HiTrap column coupled with purified GST::DEP-1. After flow through of the serum, unspecific antibodies were washed off the column, whereas antibodies specific for GST::DEP-1 remained bound to the column before they were eluted with 100 mM Glycine (pH=2.5) and 100 mM Triethylamine (pH=11.5). [3] Second affinity-purification with NHS activated HiTrap column coupled with purified GST. Flow through of the eluted antibodies resulted in the separation of DEP-1 and GST-specific antibodies. (**B**) Monitoring of the GST::DEP-1 purification by SDS-PAGE and Coomassie Blue staining. (**C**) Ponceau-stained DotBlot allowed the identification of the fractions containing DEP-1 antibodies after elution with 100 mM Glycine (pH=2.5) and 100 mM Triethylamine (pH=11.5) during affinity-purification.

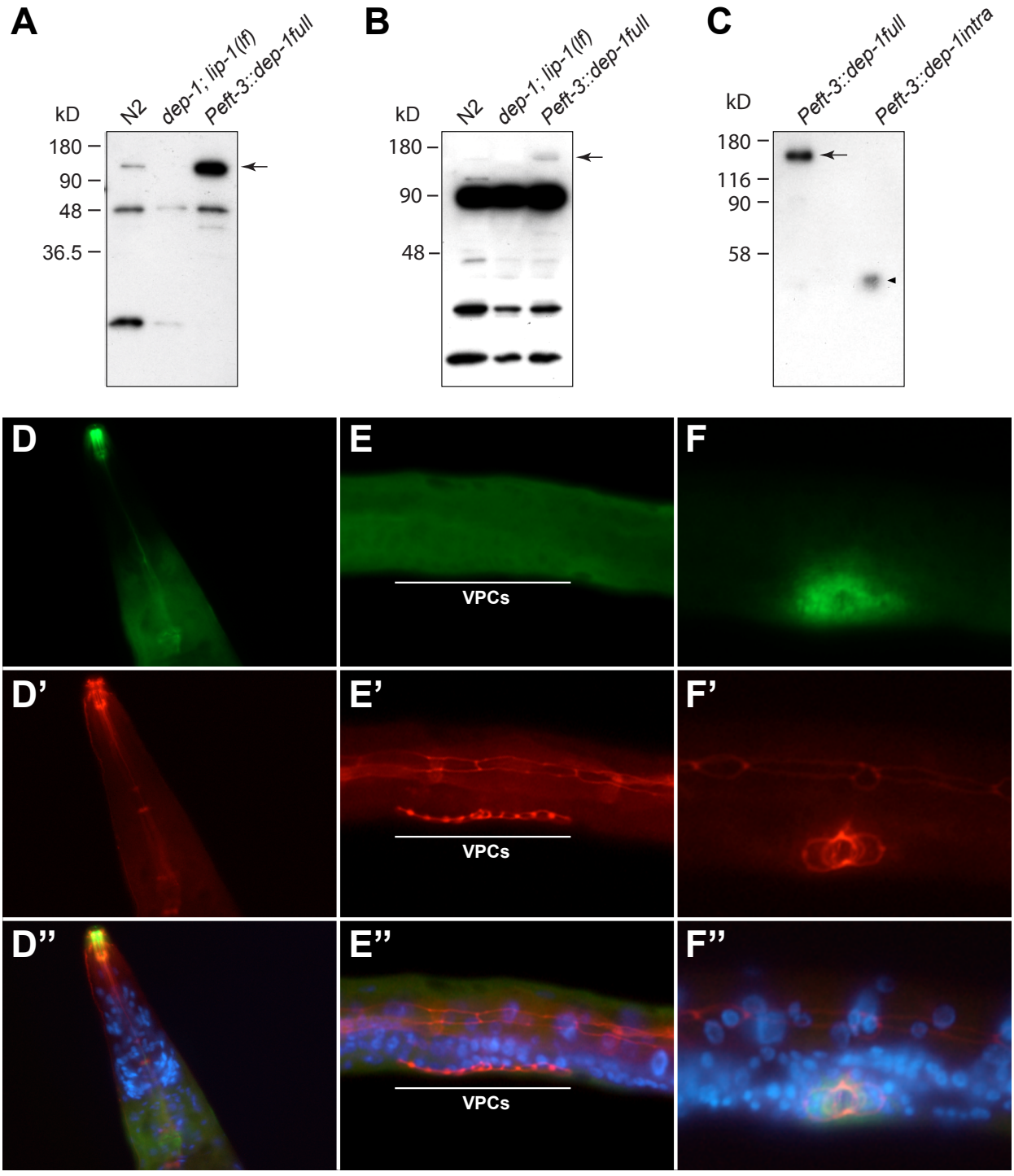

Figure 3.10 Polyclonal DEP-1 antibodies.
(**A**) Total protein extract of 50 worms (wild-type N2, *dep-1(lf);lip-1(lf)*, and *Peft-3::dep-1full::HS*) boiled in 50 µl of SDS loading buffer was analyzed on Western blot using polyclonal antibodies against DEP-1. Arrow indicates the signal corresponding to DEP-1. (**B**) Same as in (**A**) with the difference that protein extraction was performed by dounce homogenization. (**C**) Eluates of StrepTactin-purified DEP-1full::HS and DEP-1intra::HS were stained with DEP-1 antibodies. Arrow indicates the signal corresponding to DEP-1full and arrowhead indicates DEP-1intra. (**D-F**) Immunostainings of *C. elegans* using polyclonal DEP-1 antibodies and (**D'-F'**) monoclonal AJM-1 antibodies which stain the cell-junctions. (**D"-F"**) Merged images of DEP-1 and AJM-1 images with DAPI staining of the nuclei (blue). (**D**) Head of an adult animal, (**E**) mid region of a larva in the Pn.pxx stage, and (**F**) vulva of a L4 larva.

3.2.9 Examination of polyclonal DEP-1 antibodies

The specificity of the affinity-purified DEP-1 antibodies was examined by immunoblots in which protein extracts of N2, *dep-1(lf);lip-1(lf)*, and *Peft-3::dep-1full::HS* animals were analyzed (3.10 A and B). Our results indicated that DEP-1 was weakly stained in N2 animals, not observable in *dep-1(lf);lip-1(lf)* mutants, and clearly visible in animals that expressed DEP-1 under the ubiquitous promoter *eft-3*. However, only the purified antibodies of the rabbit 006-9AC-B07 but not of 006-9AB-1D2 recognized DEP-1 (Fig. 3.10 A and B, data not shown). Since StrepTactin-purified DEP-1full::HS and DEP-1intraD1241A::HS also were recognized by the produced polyclonal DEP-1 antibodies, we assumed that they were functional and specific for DEP-1 (Fig. 3.10 C).
Additionally, we tested if the polyclonal DEP-1 antibodies also work for *C. elegans* immunostaining. Thereby, fixed and permeabilized worms were incubated with polyclonal DEP-1 as well as αAJM-1 antibodies that stain the cell junctions of the VPCs. After DNA staining with Hoechst dye, the animals were mounted on coverslips and analyzed by fluorescence microscopy. A weak and diffuse signal of stained DEP-1 could be observed in some neurons of the head (Fig. 3.10 D) and in the vulva of a few animals of L4 larval stage (Fig. 3.10 F). However, no DEP-1 expression in the VPCs could be detected in Pn.pxx larvae (Fig. 3.10 E). Since we did not further optimize the immunostaining with αDEP-1 antibodies, we are not yet able to determine if they would be functional for *C. elegans* immunostaining.

3.2.10 Generation of endogenous DEP-1 reporters by using *MosTIC*

Until recently, the expression of transgenes in *C.elegans* was limited to the introduction of extrachromosomal repetitive structures, which behave like additional chromosomes in the cells. Since the sequences present on these structures are often overexpressed whereas they are silenced in the germline (Kelly et al., 1997; Stinchcomb et al., 1985), the translated proteins are usually not expressed in physiological conditions.
In 2009, a novel transgene-instructed genome engineering technique called *MosTIC* (*Mos1* excision-induced transgene-instructed gene conversion) has been reported, allowing the generation of endogenous reporters in *C. elegans* (Robert et al., 2009). *MosTIC* is initiated by the mobilization of *Mos1*, a 1.3 kb DNA transposon that was isolated from *Drosophila mauritiana* (Jacobson and Hartl, 1985; Jacobson et al., 1986), which was inserted by its controlled mobilization into the genome of *C. elegans* (Fig. 3.11 A). By expressing the *Mos* transposase in the germline, the *Mos1* insertion is re-excised from the genomic loci and thereby causing a double-strand break (DSB). This DSB is naturally repaired by recombination using homologous chromosome as repair template. However, the recombination machinery can also recognize extrachromosomal transgenic repair templates, in which a transgene of interest (e.g. *gfp* or *mCherry*) is flanked by two "arms" homologous to the genomic region broken by *Mos1* excision (Robert et al., 2009). The homologous recombination with such a transgene allows to generate single copy transgenes at a defined locus in the genome.
The strain *ttTi25065* contains a *Mos1* insertion in the *dep-1 3'UTR*, enabling the generation of an endogenous *dep-1::gfp* or *dep-1::mCherry* reporter. To establish the *MosTIC* technique in our laboratory, we tested three different approaches.

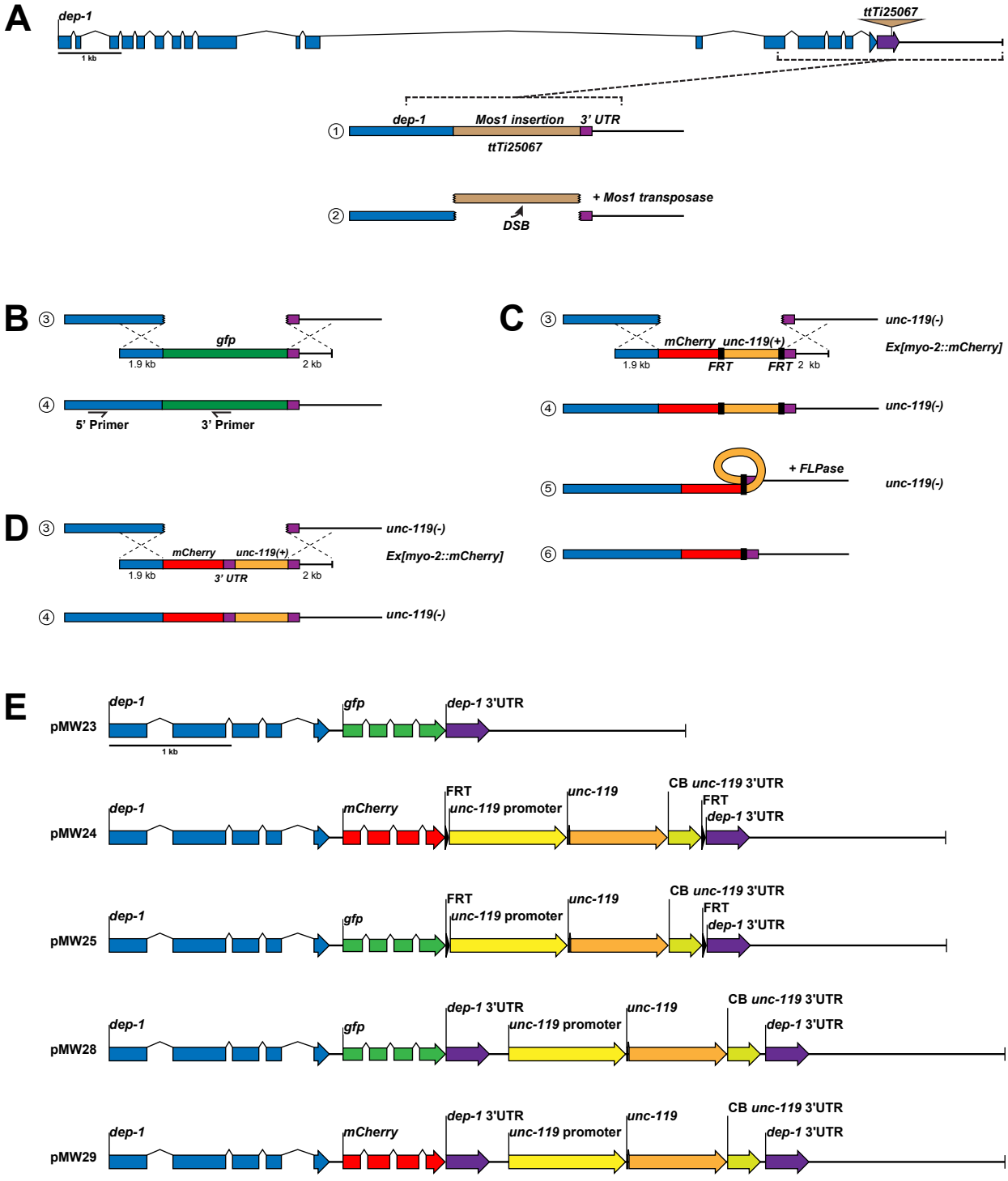

Figure 3.11 Creation of endogenous DEP-1 reporters by *MosTIC*.
(**A**) Intron exon structure of *dep-1* and position of the Mos1 transposon insertion *ttTi25067*. In presence of the Mos1 transposase [2], the Mos1 transposon is mobilized and generates a double-strand break (DSB) at the excision site. The DSB is repaired by homologous recombination [3, 4] using a transgenic repair template, in which *gfp* (**B**) or *mCherry* (**C and D**) is flanked by 2 kb of genomic DNA. (**C**) In the repair template pMW24 an *unc-119* rescue construct is flanked by FRT sites. After repair by transgene instructed gene conversion [4], addition of FLPase excises the *unc-119* rescue construct [5, 6]. (**D**) *mCherry* is fused to the *dep-1 3'UTR*, followed by an *unc-119* rescue construct. (**E**) Design of the *MosTIC* repair templates pMW23, pMW24, pMW25, pMW28, and pMW29.

Strategy A

To insert a GFP tag at the 3' end of the *dep-1* locus, we generated a repair template (pMW23) in which the coding sequence of *gfp* is flanked by the last 1.9 kb of the *dep-1* locus and by 2 kb of the *dep-1* 3' genomic region respectively (Fig. 3.11 B). This repair template was micro-injected together with the germline specific transposase (*Pglh-2::MosTase*) and the co-injection-marker *Pmyo-3::mCherry* into young adult worms homozygous for the *Mos1* insertion *ttTi25065* to generate extrachromosomal transgenes. Thereafter, each P0 animal was transferred to an individual plate and kept at 20°C to give rise to F2-F3 progeny.

The identification of transgenic animals in which the GFP has been integrated into the genome occurred via a PCR-based screen (Fig. 3.11 B). Thereby, the genomic DNA was extracted form half of a plate containing F2-F3 progeny and tested by PCR for positive integrants. In case of a positive test, the remaining half of animals could be sub-pooled and subsequently analyzed by further rounds of PCR-screenings, until the animals homozygous for the integrated transgene were identified (for details see Fig. 4 of Robert et al., 2009). However, the PCR-screening did not lead to the identification of animals in which the GFP -tag was integrated into the *dep-1* locus.

Strategy B

As in strategy A, the coding sequence of *gfp/mCherry* was flanked by the last 1.9 kb of the *dep-1* locus and by 2 kb of the *dep-1* 3' genomic region, respectively. In addition, the repair constructs pMW24 and pMW25 contained the *C. briggsae unc-119* rescue sequence that is flanked by two flippase recognition targets (FRT; Fig. 3.11 C, E). These repair templates were micro-injected together with the germline specific transposase (*Pglh-2::MosTase*), and the co-injection-marker *Pmyo-3::mCherry* into *ttTi25065;unc-119(lf)* animals. Thereafter, each P0 animal was transferred to an individual plate and kept at 20°C to give rise to progeny. The F2-F3 progeny was screened for animals that both lost the extrachromosomal repair template and displayed a rescue of the paralyzed Unc phenotype. Thereby, a strain in which *mCherry::FRT::unc-119(+)::FRT* was integrated in the locus of *dep-1* could be isolated.

Next, we tried to excise the *unc-119* rescuing sequence from the obtained transgenic animals by FLP-FRT site directed recombination. Adding of flippase (FLPase), which recognizes the FRT sites that are flanking *unc-119(+)*, catalyzed a recombination between the two identical but oppositely oriented FRT repeats (Fig. 3.11 C step 5) to excise *unc-119(+)* out of the genome and thereby in animals that show the Unc phenotype again.

We first expressed the FLPase under the heat specific promoter *Phsp-16-48* and made two heat-shock treatments (2x 30min at 33°C with an interval of 16 hours). This led to the identification of ten animals that showed an Unc phenotype, indicating that the FRT-flanked *unc-119* rescuing construct was excised. However, all progeny of these animals exhibited a non-Unc phenotype, why we hypothesized that the *unc-119* rescuing construct was only excised in the somatic cells but not in the germline.

For a stronger expression of the FLPase in the germline, we expressed the FLPase under the two promoters *Pglh-2* and *Peft-3*. However, expression of *Pglh-2::FLPase* (pMW26) or *Peft-3::FLPase* (pMW27) did not result in the identification of animals showing an Unc phenotype.

Strategy C

In the strain received from Strategy B, in which *mCherry::FRT::unc-119(+)::FRT* was integrated into the locus of *dep-1*, the *unc-119* rescue construct disrupted the *dep-1 3'UTR*. Thus, we made new rescue constructs in which the *dep-1 3'UTR* was cloned in front of the *C. briggsae unc-119* rescue sequence without

being flanked by FRT sites (Fig. 3.11 D, E). By micro-injecting the repair template pMW28 or pMW29 together with the germline specific transposase (*Pglh-2::MosTase*) and the co-injection-markers *Pmyo-2::mCherry*, *Pmyo-3::mCherry*, and *Prab-3::mCherry* into *ttTi25065;unc-119(lf)* animals, we were able to receive the *MosTIC* engineered strains *zhIs70* (*dep-1::gfp*) and *zhIs71* (*dep-1::mCherry*).

3.2.11 Comparison of DEP-1 reporter lines

In our laboratory, four different reporter lines have been generated to explore the expression pattern of DEP-1, namely a transcriptional and an extrachromosomal translational DEP-1::GFP reporter (Berset, 2005), as well as two *MosTic* engineered lines in which a GFP or mCherry tag was introduced directly into the endogenous *dep-1* locus.

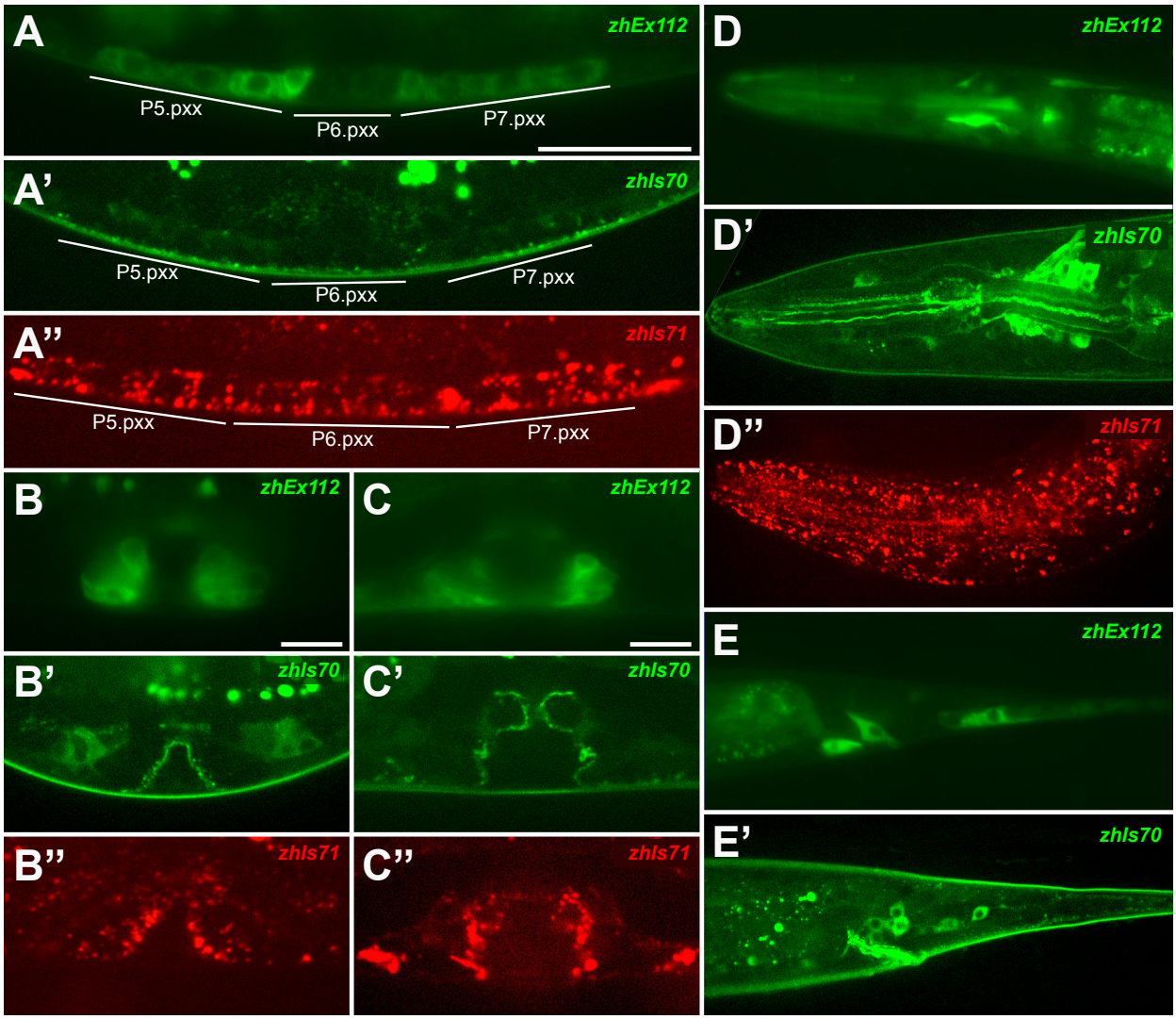

Figure 3.12 Comparison of DEP-1 reporters.
Expression of DEP-1 in Pn.pxx stage (**A-A"**), in early L4 stage (**B-B"**), in late L4 stage (**C-C"**), in the head region (**D-D"**), and in the tail region (**E-E'**). (**A-E**) Extrachromosomal translational *dep-1::gfp* reporter line *zhEx112*. (**A'-E'**) *MosTIC* engineered endogenous *dep-1::gfp* reporter line *zhIs70*. (**A"-D"**) *MosTIC* engineered endogenous *dep-1::mCherry* reporter line *zhIs71*. Except for (**A-E**), all images are z-projections (average intensity) of spinning-confocal z-stacks. Scale bar represents 10 µm.

The extrachromosomal translational DEP-1::GFP reporter line *zhEx112* indicated that DEP-1 is downregulated in the 1° lineage, whereas expression was persistent in the 2° vulval cells until the L4 stage (Fig. 3.12 A-C; Berset, 2005). Most of the DEP-1::GFP fusion protein was expressed intracellularly and in the endoplasmatic reticulum (ER), but not at the cell membrane as it is expected for a transmembrane protein. A similar expression pattern was observed by analysis of a transcriptional *Pdep-1::gfp* reporter (Berset, 2005).
As described in section 3.2.7, we created two DEP-1 reporter lines *zhIs70* (DEP-1::GFP) and *zhIs71* (DEP-1::mCherry) by *MosTIC*. Since APF phenotype of *dep-1(lf);lip-1(lf)* animals was rescued by DEP-1::GFP *zhIs70*, we assume that the tagged *dep-1* is functional. In the Pn.pxx stage of *zhIs70* animals, DEP-1::GFP is weakly expressed at the apical side of the VPCs and in the cytoplasm of the 2° lineage (Fig. 3.12 A'), whereas no cytoplasmic expression could be observed in the 1° lineage.
In the VPCs of L4 larvae, DEP-1::GFP was expressed at the apical side of the VPCs, but also in intracellular punctae of the 2° lineage (Fig. 3.12 B' and C'). In addition, DEP-1::GFP expression was found in numerous neurons in the head (Fig. 3.12 D'), in the rectal cells, and in the dorso-rectal and lumbar ganglions (Fig. 3.12 E').
Similar to the expression of DEP-1::GFP in the line *zhIs70* was the expression pattern of DEP-1::mCherry in *zhIs71* animals. However, cytoplasmic expression of DEP-1::mCherry was strongly enhanced in both the 1° and 2° VPCs of Pn.pxx larvae (Fig. 3.12 A''). Furthermore, DEP-1::mCherry expression was more dotted in the head region (Fig. 3.12 D'') compared to DEP-1::GFP (*zhIs70*). Though, in the vulva of L4 larvae, the expression patterns of both *MosTic* engineered reporters looked similarly, namely at the apical membrane with some intracellular punctae in the 2° lineage (Fig. 3.12 B'' and C'').

3.2.12 Analysis of vulval morphogenesis in *dep-1(lf)* mutants

After induction of the vulval cell fates, the VPCs undergo a phase of morphogenetic changes to form the adult vulva. Thereby, the vulval cells invaginate and move from the ventral midline toward the dorsal uterus (Fig. 3.13 A). At the same time, the cells extend circumferentially toward the vulval midline to form a stack of seven toroid-shaped cells surrounding a central lumen (Sharma-Kishore et al., 1999). These morphogenetic movements are controlled by LET-502, which induces actomyosin-mediated contraction of the apical lumen in the secondary toroids to generate a dorsal pushing force (Farooqui et al., 2012).
The role of actin assembly during vulval morphogenesis can be examined by the analysis of filamentous actin (F-actin), visualized by the reporter *Pdlg-1::LifeAct::gfp* (Farooqui et al., 2012). During vulval development, LifeAct::GFP is expressed in the VPCs of Pn.pxx stage larvae, already before morphogenic movements take place. Particularly, LifeAct::GPF is upregulated in P6.p descendants VulF and VulE as well as in the outer descendants VulA and VulB of P5.p and P7.p (Fig. 3.13 B and D).
The fact that DEP-1::GFP is expressed reciprocally to LifeAct::GFP (downregulation in the primary lineage and upregulation in the inner descendants of P5.p and P7.p), led to the hypothesis that DEP-1 is involved in controlling actin activity during vulval morphogenesis (Fig. 3.13 B,C). This assumption was further supported by the identification of the integrin β-subunit PAT-3 as a substrate of DEP-1, since it has been reported that integrins play a crucial role in cell adhesion and migration by providing transmembrane links between the extracellular matrix and the actin cytoskeleton (Zaidel-Bar et al., 2007).

To investigate if DEP-1 affects the assembly of filamentous actin, we compared the expression of LifeAct::GFP in the VPCs of wild-type and *dep-1(lf)* animals in the Pn.pxx stage and in L4 vulvae (Fig. 3.13 D-G). Thereby, we analyzed fluorescence images taken by a standard fluorescence microscope and a spinning-disc microscope. However, we were not able to observe an alteration in the expression of LifeAct::GFP in the VPCs of *dep-1(lf)* animals, neither in the inner descendants of P5.p and P7.p during Pn.pxx stage, nor in the vulva of L4 larvae. Together with the fact that vulval morphogenesis development is not obviously altered in *dep-1(lf)* mutants, we conclude that DEP-1 is not involved in controlling morphogenetic movements during vulval development by regulating actin assembly via the integrins.

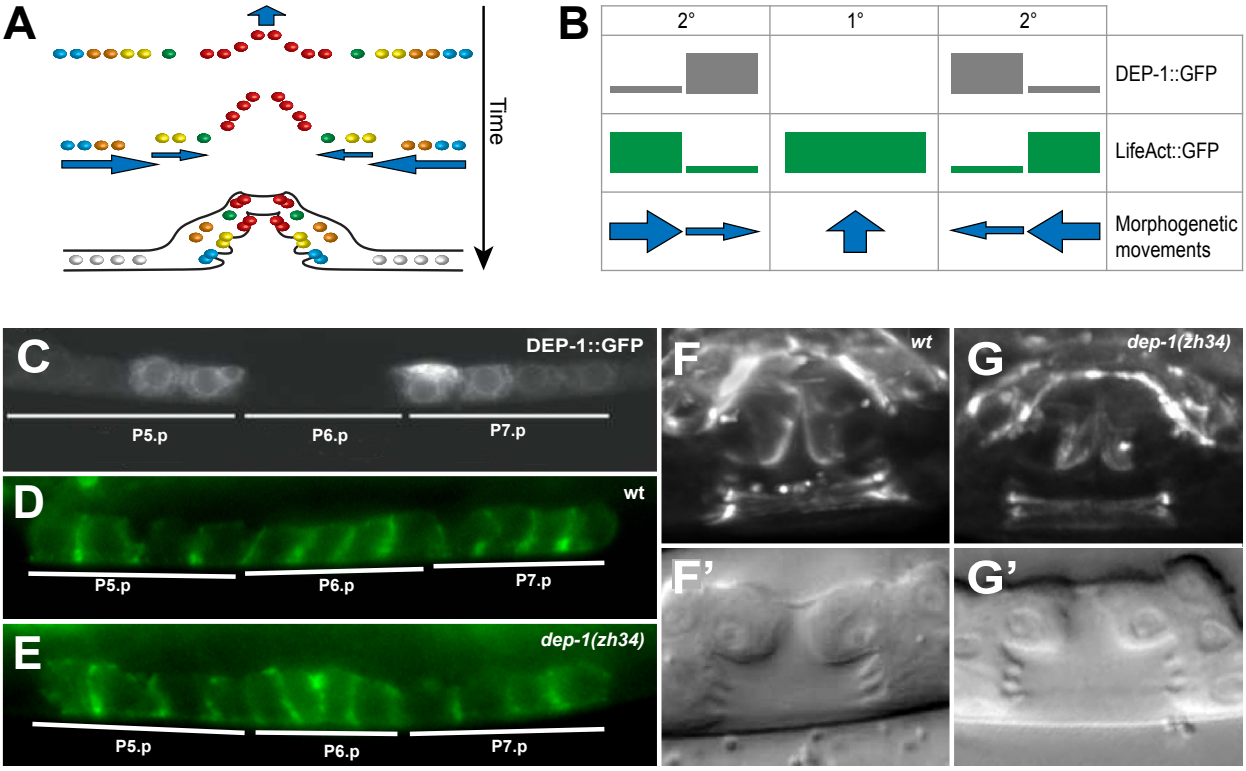

Figure 3.13 Analysis of LifeAct::GFP in *dep-1(lf)* mutants.
(**A**) Morphogenetic changes form the vulva. VPCs invaginate and move dorsal from the ventral midline toward the dorsal uterus. (**B**) Schematic intensity of DEP-1::GFP and LifeAct::GFP expression during Pn.pxx stage larvae. Blue arrows represent schematic intensities of morphogenetic movements taking place during further vulval development. (**C**) Expression of the translational DEP-1::GFP reporter *zhEx112* (adapted from Berset et al., 2005). (**D**) Expression of LifeAct::GFP in a wild-type and (**E**) a *dep-1(lf)* Pn.pxx stage larva. (**F**) LifeAct::GFP expression in a wild-type and (**G**) a *dep-1(lf)* L4 larva. Maximum intensity projections of z-stacks. (**F'** and **G'**) Corresponding Nomarski images.

3.2.13 Nidogen-1 – another putative substrate of DEP-1

Among the proteins that were identified by LC-MS/MS after pull-down of N2 protein extract with GST-purified DEP-1intraDA was Nidogen (NID-1; Fig. 3.1). NID-1 (entactin) is a 174.4 kD glycoprotein that consists of two amino (G1 and G2) and one carboxyl (G3) terminal globular domains that are connected by a rod domain composed primarily of endothelial growth factor (EGF) repeats (Fox et al., 1991; Kang and Kramer, 2000). Being a major constituent of basement membrane, NID-1 forms a complex with col-

lagen and laminin-1 (Aumailley et al., 1993). Nevertheless, loss of *nid-1* results in viable animals that are fertile and that display no overt abnormal phenotypes (Kang and Kramer, 2000).
To examine the role of NID-1 during vulval development, we first created the transcriptional *Pnid-1::gfp* reporter line *zhEx479*. In three-fold staged embryos, *Pnid-1::gfp* expression could be observed predominantly in the body wall muscle cells (Fig. 3.14 B'). In L4 larvae, strong expression of *Pnid-1::gfp* was observed in developing somatic structures of the gonad and in numerous neurons (Fig. 3.14 A'). However, significant *Pnid-1::gfp* expression was neither observed in the VPCs of animals in the Pn.pxx stage nor in the vulva of early and late L4 larvae (Fig. 3.14 C'-E'), which is contradictory to the findings of Kang and Kramer (2000). By immunostaining of worms with anti-NID-1 antibodies, a strong NID-1 accumulation was reported to be seen in the vulva of late L3 to L4 stage larvae (Kang and Kramer, 2000). Since no further information about VPC specific expression has been reported, the examination of a translational NID-1::GFP would be needed. Such a reporter line would also allow verifying the interaction of DEP-1intraDA with NID-1 by performing co-immunoprecipitation experiments.
We next tested if *nid-1* affects RAS/MAPK signaling during vulval development. If so, we would expect to see that *nid-1(lf)* shows the same adjacent primary fate phenotype in the sensitized *lip-1(lf)* background as it is observed in *dep-1(lf);lip-1(lf)* animals. However, no alterations in vulval morphology could be observed in *nid-1(lf);lip-1(lf)* double mutants.
Since we could neither observe an expression of *Pnid-1::gfp* in the VPCs, nor had *nid-1(lf)* an effect on vulval development in the sensitized *lip-1(lf)* background, we did not further analyze this candidate.

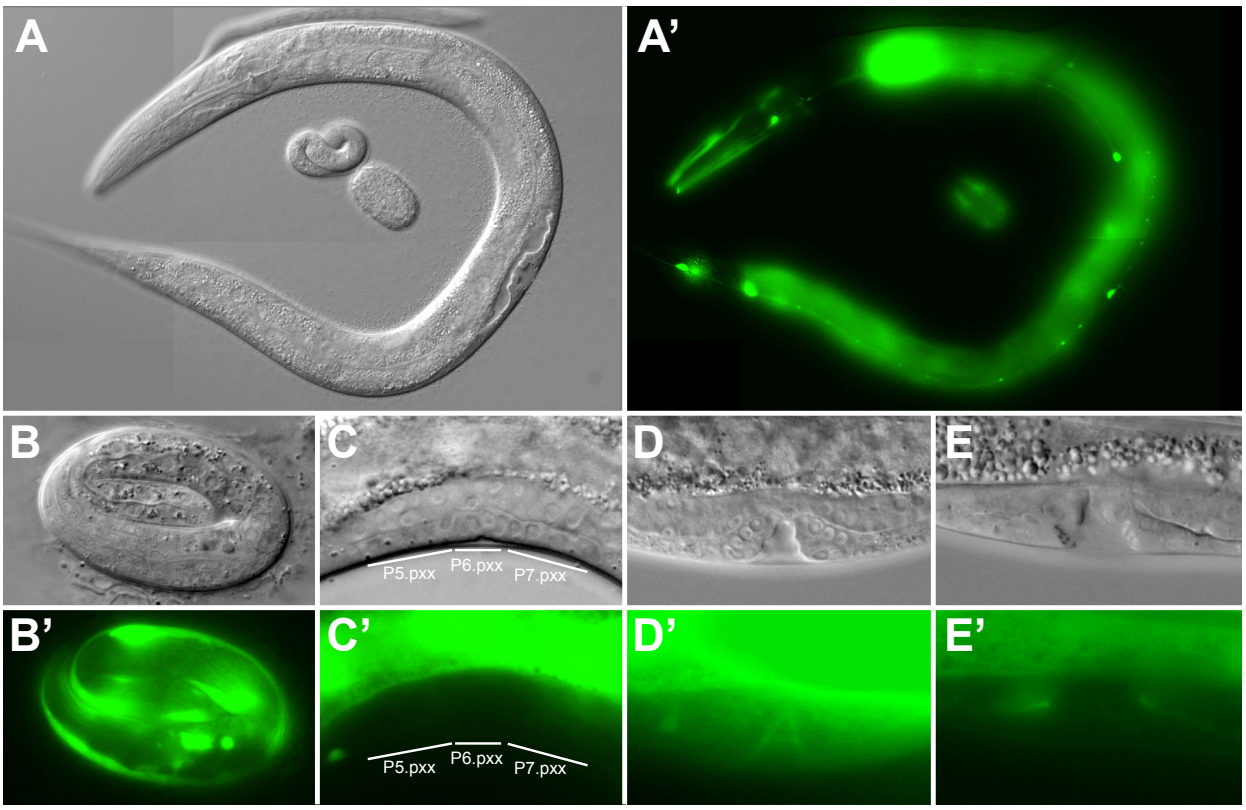

Figure 3.14 Expression pattern of NID-1::GFP.
Expression of an extrachromosomal transcriptional *Pnid-1::gfp* reporter in a L4 larva (**A'**), in a three-fold-staged embryo (**B'**), in a Pn.pxx staged larva (**C'**), in an early L4 staged larva (**D'**), and in a late L4 staged larva (**E'**). (**A-E**) Corresponding Nomarsky images.

3.3 A conserved function of *C. elegans* CASY-1 calsyntenin in associative learning

Several studies have shown that *C. elegans* is a convenient model to study genes implicated in associative memory (Mohri et al., 2005; Rose and Rankin, 2006; Saeki et al., 2001; Zhang et al., 2005). By using different sensory neurons and integrating interneurons, nematodes can learn about mechanosensory input (Rose and Rankin, 2001), chemosensory input (Morrison et al., 1999; Wen et al., 1997), and thermosensory input (Mori, 1999) to approach or avoid tastes, odors or temperatures that predict the presence or absence of food.

In collaboration with Andreas Papassotiropoulos, Dominique de Quervain, and Frédéric Hoerndli, we analyzed the associative learning behavior of *C. elegans* mutants lacking genes that were identified in a genome-wide screen for gene variants associated with human episodic memory performance (Papassotiropoulos et al., 2006).

My own contribution to this manuscript

In order to test the associative learning behavior of different mutants in *C. elegans*, I established the "gustatory" NaCl chemotaxis assay (Saeki et al., 2001) in our laboratory. This behavior test is based on the observation that wild-type worms display a strong attraction to 25 mM NaCl. However, when worms are starved on plates that contain NaCl, the chemotaxis towards NaCl decreases dramatically (Saeki et al., 2001). In contrast to wild-type worms, *casy-1(tm718)* mutants did not show an aversion but only a partial decline in their attraction towards NaCl when they were starved in the presence of NaCl (Fig. 3 A of the manuscript Hoerndli et al., 2009). Hence, the NaCl chemotaxis assay enables the characterization of learning-deficient mutants, and thereby in a further understanding of genes involved in associative learning behavior.

OPEN ACCESS Freely available online

PLoS one

A Conserved Function of *C. elegans* CASY-1 Calsyntenin in Associative Learning

Frédéric J. Hoerndli[1,2¤], Michael Walser[1], Erika Fröhli Hoier[1], Dominique de Quervain[4,5], Andreas Papassotiropoulos[2,3], Alex Hajnal[1]*

1 Institute of Zoology, University of Zürich, Zürich, Switzerland, **2** Division of Molecular Psychology, University of Basel, Basel, Switzerland, **3** Life Science Training Facility, Biozentrum, University of Basel, Basel, Switzerland, **4** Division of Psychiatry Research, University of Zürich, Zürich, Switzerland, **5** Center for Integrative Human Physiology, University of Zürich, Zürich, Switzerland

Abstract

Background: Whole-genome association studies in humans have enabled the unbiased discovery of new genes associated with human memory performance. However, such studies do not allow for a functional or causal testing of newly identified candidate genes. Since polymorphisms in Calsyntenin 2 (CLSTN2) showed a significant association with episodic memory performance in humans, we tested the *C. elegans* CLSTN2 ortholog CASY-1 for possible functions in the associative behavior of *C. elegans*.

Methodology/Principal Findings: Using three different associative learning paradigms and functional rescue experiments, we show that CASY-1 plays an important role during associative learning in *C. elegans*. Furthermore, neuronal expression of human CLSTN2 in *C. elegans* rescues the learning defects of *casy-1* mutants. Finally, genetic interaction studies and neuron-specific expression experiments suggest that CASY-1 may regulate AMPA-like GLR-1 glutamate receptor signaling.

Conclusion/Significance: Our experiments demonstrate a remarkable conservation of the molecular function of *Calsyntenins* between nematodes and humans and point at a role of *C. elegans casy-1* in regulating a glutamate receptor signaling pathway.

Citation: Hoerndli FJ, Walser M, Fröhli Hoier E, de Quervain D, Papassotiropoulos A, et al. (2009) A Conserved Function of *C. elegans* CASY-1 Calsyntenin in Associative Learning. PLoS ONE 4(3): e4880. doi:10.1371/journal.pone.0004880

Editor: Brian D. McCabe, Columbia University, United States of America

Received September 4, 2008; **Accepted** February 6, 2009; **Published** March 16, 2009

Funding: This work was supported by grants from the Swiss National Science Foundation to A. P., D.Q. and A. H. and by the Kanton of Zürich. The funders had no role in study design, data collection and analysis, decision to publish, or preparation of the manuscript.

Competing Interests: The authors have declared that no competing interests exist.

* E-mail: ahajnal@zool.uzh.ch

¤ Current address: Department of Biology, University of Utah, Salt Lake City, Utah, United States of America

Introduction

The cellular and molecular mechanisms underlying learning and memory are the focus of intense research. Although many new components have been described that are conserved across different animal species, the exact mechanisms by which synaptic strength is regulated remain elusive [1] . Long-term potentiation (LTP) and depression (LTD), which are a key mechanisms underlying memory formation, involve plastic changes in synaptic strength through modulation of AMPA Glutamate receptor currents [2]. One frequently used mechanism by which neurons modulate synaptic strength is through the regulation of the number of neurotransmitter receptors at the surface of synapses [3]. Intracellular trafficking, exo- and endocytosis of receptors as well as surface dynamics also play important roles in regulating the exact number of receptors at the synapse [2,4]. However, the exact mechanisms by which this is achieved are not completely understood.

Studies in both invertebrates and vertebrates have identified several genes and signaling pathways important for learning and memory. From this work it appears that many of the memory-related molecular mechanisms are conserved across different species. Despite the obvious differences in learning and memory tasks performed by different species and the anatomical differences between their nervous systems, recent human genetic studies suggest that genetic variability in the orthologs of related signaling molecules known from studies in model organisms contributes to inter-individual memory differences in humans [5]. Therefore, genes associated with human episodic memory identified in whole-genome association studies could provide new insights into the mechanisms underlying memory formation and storage.

Recently, an unbiased genome-wide screen for human hippocampus-dependent, episodic memory, which studied more than 500000 single nucleotide polymorphisms (SNPs), resulted in the identification of *CLSTN2* (encoding calsyntenin 2) as a memory-related human gene [6]. Specifically, *C* allele carriers of a common T→C substitution within *CLSTN2* had better episodic memory performance than *TT* genotype carriers in a verbal delayed recall task, which was performed by 341 Swiss young adults (median age 22 years). The better performance of the *C* allele carriers was observed 5 min and 24 h after learning, whereas immediate recall performance was similar between genotype groups, indicating that *CLSTN2* is related to hippocampus-dependent memory performance and that the findings were not biased by possible

differences in motivation, attention and working memory performance between groups. This association was not replicated in a second population of middle-aged participants from the US, which may be partially attributed to differences in ethnicity, in mean age between study populations, or in differences between cognitive tasks used [6]. However, a recent independent study in

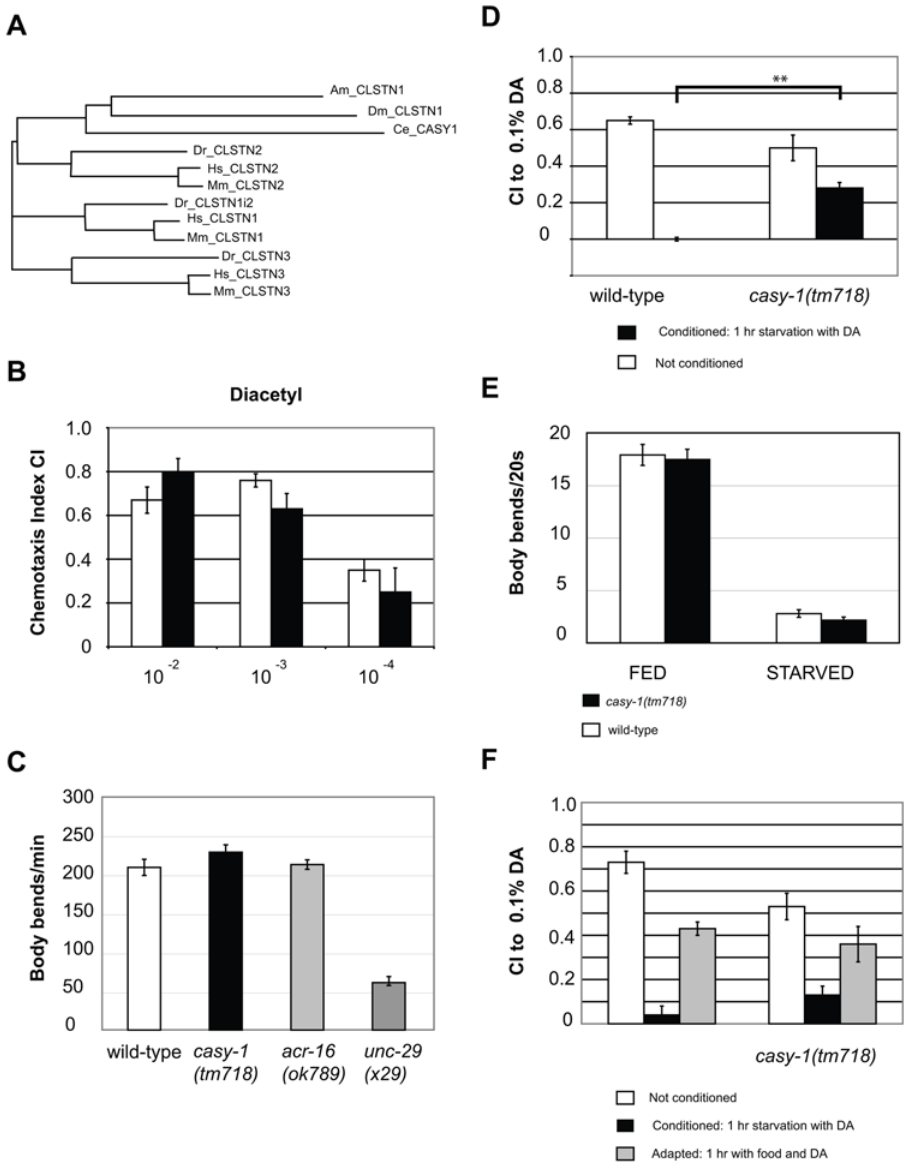

Figure 1. Olfactory associative learning defects in *casy-1(tm718)* mutants. (A) Rooted tree diagram showing the sequence similarities between the invertebrate and the three classes of vertebrate calsyntenins. The protein sequences of CLSTN1, CLSTN2 and CLSTN3 from *Homo sapiens* (*Hs*), *Mus musculus* (*Mm*), *Danio rerio* (*Dr*) and the single calsyntenins from *Drosophila melanogaster* (*Dm*), *Apis mellifera* (*Am*) and *Caenorhabditis elegans* (*Ce*) were aligned using the ClustalX program, and a rooted tree was drawn using PHYLIP. Note that the invertebrate calsyntenins and the vertebrate CLSTN2 proteins originate from a common branch. (B) Chemotaxis of wild-type and *casy-1(tm718)* worms towards 10^{-2}, 10^{-3} and 10^{-4} fold dilution of Diacetyl in 100% EtOH(V/v) assay in the absence of conditioning. The assays were repeated on three different days using one plate for each condition and were quantified using the chemotaxis Index CI (CI = (worms in DA - worms at EtOH)/ total number of worms, see methods). Error bars indicate the standard error of mean. White bars: wild-type N2, Black bars: *casy-1(tm718)*. (C) Swimming assay of *casy-1(tm718)*, wild-type, nicotinic Acetylcholine-receptor *acr-16* knock out (*ok789*) and levamisole acetylcholine-receptor *unc-29* subunit knock-out (*x29*). Number of body bends per minute counted manually, and blinded to the respective genotypes (N = 20). (D) Chemotaxis of starvation conditioned wild-type and *casy-1(tm718)* animals. The experiment was repeated on three separate days with six replicates per assay. The results of a Student t-test are indicated as * = $p<0.05$ and ** = $p<0.01$. (E) Food sensing assay. Locomotion rate of wild-type and *casy-1(tm718)* worms in body bends/20 seconds of worms transferred from a food plate to another food plate (FED), or worms allowed to starve on an empty agar plate for 1 hr (STARVED). White bars: wild-type, Black bars: *casy-1(tm718)*. (F) Adaptation assay. Comparison of the chemotaxis Index CI of wild-type and *casy-1(tm718)* to 0.1% DA after starving for 1 hour without DA (White bars), with 100% DA (Black Bars) and on food for 2 hours with 100% DA (Grey bars). Assays were repeated on two different days using 3 replicates per condition. For the complete dataset of the behavioral assays, see Table S1.
doi:10.1371/journal.pone.0004880.g001

adolescents replicated the beneficial effect of the *CLSTN2 C* allele on verbal recall [7].

Even though there exists no direct equivalent of human episodic memory in the small nematode *C. elegans*, several forms of associative behaviour and long-term memory have been observed in this model organism [8–11]. For example, *C. elegans* is capable of pairing food deprivation sensation with olfactory cues [12], gustatory cues [9] and the temperature of its environment [11] by using different sensory neurons and integrating interneurons. Essentially, this type of learning is akin to some classical conditioning paradigms such as conditioned taste aversion (CTA) where an unconditioned stimulus (US) is paired with a conditioned stimulus (CS) [13]. Moreover, *C. elegans* is capable of distinguishing multiple cues based on past experience using a serotonin dependent mechanism [8]. Together with an easily modifiable genetic background and many available knock-out alleles, *C. elegans* allows a fast and systematic way to analyze genes implicated in associative memory.

Taking advantage of the fact that the *C. elegans* genome encodes only one *CLSTN* gene (*casy-1*) homologous to vertebrate CLSTN2 and that a knock-out allele is available, we show that *casy-1* plays an important role in associative learning in both thermotaxis and chemotaxis conditioning paradigms. While this work was in progress, an independent study has identified *casy-1* in a forward genetic screen for behavioural mutants [14]. In addition to the reported behavioural defects of *casy-1* mutants, we show here that the pan-neuronal expression of human CLSTN2 rescues the chemotaxis conditioning defect of *casy-1(tm718)*, thus demonstrating a strong conservation between CLSTN2 and *casy-1* at the level of their molecular function. Finally, we describe a putative mechanism for CASY-1 in regulating associative behaviour via glutamate receptor signalling based on neuron-specific rescue experiments and on the genetic interaction between *casy-1* and the glutamate receptor subunit *glr-1*.

Results and Discussion

The *C. elegans* genome encodes a single CLSTN2 ortholog *casy-1*

To test a causal relationship between CLSTN2 function and learning and memory, we searched the genomes of invertebrate model organisms for CLSTN2 orthologs. While vertebrate genomes typically encode three *Calsyntenin* family members, the genomes of invertebrates like *Drosophila melanogaster* and *C. elegans* contain only a single *Calsyntenin* gene (Fig. 1A). Protein sequence alignment of the three vertebrate Calsyntenin family members with the invertebrate Calsyntenins indicates that the single *C. elegans* homolog CASY-1 as well as *Drosophila* Calsyntenin are most similar to vertebrate CLSTN2 (Fig. 1A).

CLSTN2 is a type I transmembrane protein with two extracellular calcium-binding cadherin domains and two intracellular kinesin light chain-binding domains [15,16]. These domains are conserved in all three Calsyntenin family members including *C. elegans* CASY-1 [15]. Similar to mammalian Calsyntenins, a transcriptional *casy-1* reporter is expressed in many head nerve ring neurons, some of which send processes into the ventral nerve cord (Fig. 2A and data not shown). Moreover, a GFP-tagged CASY-1 protein was reported to localize at synapses (Duan and Hedgecock, personal communication). Given the sequence similarity between human CLSTN2 and *C. elegans* CASY-1 and their neuronal expression in both organisms, we asked whether the *casy-1* gene might function in regulating associative learning in *C. elegans*. The *casy-1* deletion mutant *tm718* (kindly provided by S. Mitani) contains a 601 bp deletion in exon 4, creating a frameshift followed by a premature stop codon. The *tm718* allele results in the production of a protein truncated at position 117 that lacks most of the extracellular and the entire intracellular domain. We observed no obvious anatomical, behavioral or locomotory defects in naive *casy-1(tm718)* animals (Fig. 1B,C). Moreover, *casy-1(tm718)* animals appear healthy and are fertile.

Behavioral defects in *C. elegans casy-1* mutants

To test associative learning in *C. elegans*, we used three established context-dependent behavioral paradigms that are based on olfactory, gustatory and thermosensory starvation conditioning, respectively [11,17]. The chemotaxis of naive *casy-1(tm718)* animals to three different volatile attractants was comparable to the response of the wild-type strain (Fig. 1B and Fig. S1). We thus investigated the olfactory associative learning capacity of *casy-1(tm718)* animals by testing their ability to reverse the attraction to an odorant after associating this odorant with a

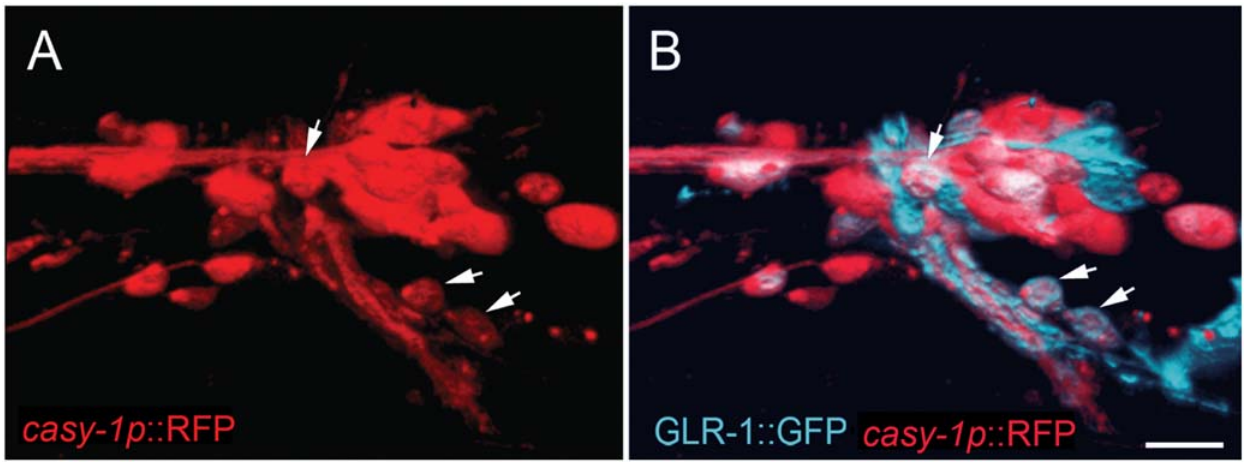

Figure 2. Expression pattern of a transcriptional *casy-1* reporter. (A) Expression of the *casy-1p*::RFP transcriptional reporter (red) and (B) a GLR-1::GFP translational reporter (blue) [22] in the nerve ring of an adult animal. A 3D reconstruction of confocal sections through the left hemisphere is shown (see methods). The two arrowheads in the bottom right corner point at RMDDL and SMDDL and the arrowhead in the top half points at SMDVL, which co-express *casy-1p*::RFP and GLR-1::GFP. Anterior is left and ventral is bottom. Scale bar in (B) is 10 µm.
doi:10.1371/journal.pone.0004880.g002

negative stimulus such as starvation (*see methods*). After starvation conditioning, the chemotaxis index (CI) of unconditioned controls and conditioned animals was compared in a quantitative chemotaxis assay [17]. Unconditioned wild-type and *casy-1(tm718)* animals both displayed strong chemotaxis to 0.1% diacetyl (DA, Fig. 1D), indicating that *casy-1(tm718)* mutants have no sensory defects in DA olfaction under these conditions. After a one hour starvation period in the presence of DA, wild-type animals did not show any attraction to DA, while *casy-1(tm718)* mutants were still significantly attracted by DA (CI = 0.3, $p<0.01$ using a Student t-test, 6 replicates repeated three times), albeit less efficiently than unconditioned control animals (Fig. 1D). The behavioral difference between wild-type and *casy-1(tm718)* animals is not due to a defect in food detection, since we observed normal slowing of *casy-1(tm718)* locomotion compared to wild-type, when animals were deprived of food and replaced on a new bacterial lawn (Fig.1E) [18].

To investigate the possibility that the chemotactic association defect of *casy-1(tm718)* could be due to adaptation (i.e. a decrement in response due to sensory fatigue that cannot be dishabituated [19]) rather than to an associative learning defect, we pre-exposed both strains to concentrated DA in the presence of abundant food before measuring their CI to 0.1% DA (gray bars in Fig. 1F). DA-adapted wild–type and *casy-1(tm718)* animals showed a similar partial reduction in their CI to DA , indicating that *casy-1(tm718)* mutants can adapt to high concentrations of DA. We thus conclude that a loss of *casy-1* function predominantly reduces associative learning without significantly impairing olfactory adaptation.

Next, we tested the performance of *casy-1(tm718)* mutants in an "gustatory" NaCl chemotaxis conditioning paradigm [9]. Wild-type worms display a strong attraction to 25 mM NaCl that is reversed when worms are first starved in the presence of NaCl in liquid cultures for 1 hour (Fig. 3A) [9]. Unconditioned *casy-1(tm718)* worms displayed a chemotaxis index (CI) that was similar to naive wild-type animals. However, when starved in the presence of NaCl *casy-1(tm718)* mutants did not show an aversion but only a partial decline in their attraction towards NaCl (Fig. 3A).

To test the associative behavior in the context of a third sensory system, we examined the performance of *casy-1(tm718)* mutants in a thermotaxis conditioning paradigm. Wild-type animals typically migrate towards the temperature at which they had been previously fed, but they avoid this temperature after a 3 hour starvation period [11]. We used a modified version of this conditioning paradigm by training groups of worms at specific temperatures and placing them on thin agar plates with a steep temperature gradient to measure their Thermotaxis Index (TTI) [20]. Wild-type worms grown at 15°C showed a TTI close to zero after 3 hours of starvation conditioning at 15°C, whereas *casy-1(tm718)* animals continued to exhibit significant albeit reduced thermotaxis to 15°C after starvation conditioning at this temperature (Fig. 3B).

In conclusion, *casy-1(tm718)* mutants exhibit strong associative learning defects in the context of three different sensory stimuli with no sensory impairment of the naive animals when compared to wild-type. These results point at a central function of CASY-1 in promoting associative learning downstream of different sensory stimuli.

Expression of human CLSTN2 rescues the behavioral defects of *casy-1* mutants

To confirm that the olfactory and thermotaxis association defects observed in *tm718* animals are due to the loss of *casy-1* function, we introduced a *casy-1* minigene composed of 5 kb of 5′ regulatory sequences fused to 3 kb cDNA of the long *casy-1* isoform (B0034.3a) and 3 kb of 3′ non-coding sequences into *casy-1(tm718)* animals. A transgenic line carrying the *casy-1* minigene on an extrachromosomal array (*zhE242.1[casy-1 minigene]*) was tested in the olfactory and thermotaxis conditioning paradigms. We calculated a learning index (%LI) as the difference between the CI or TTI of unconditioned and conditioned animals divided by the CI or TTI, respectively, of the unconditioned animals [8] (see methods). In both paradigms, the transgenic animals showed

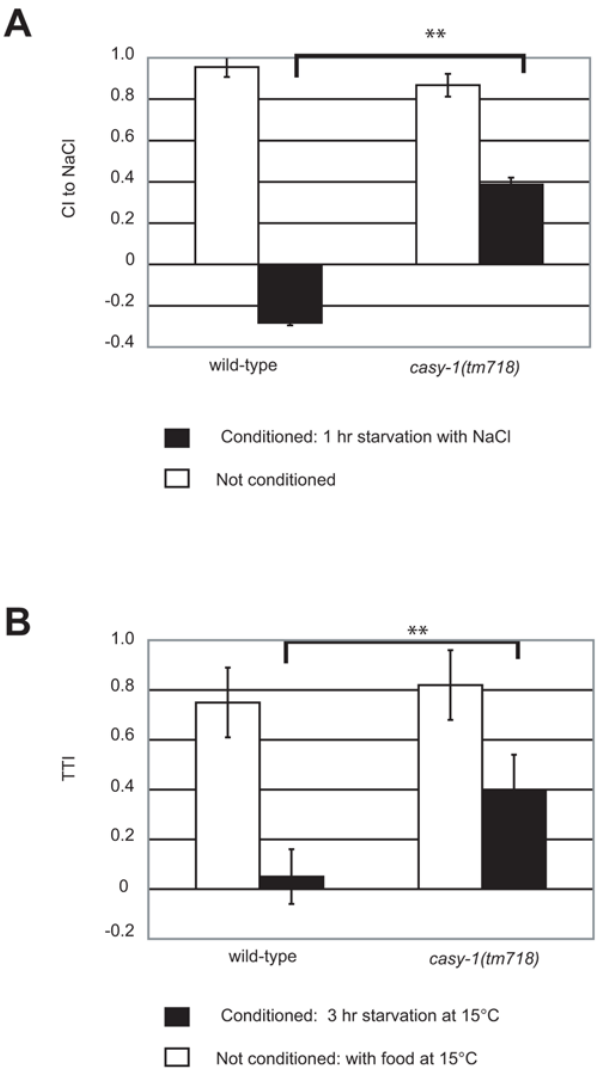

Figure 3. NaCl chemotaxis and thermotaxis associative learning defects in *casy-1(tm718)* mutants. (A) Chemotaxis of starvation conditioned wild-type (N2) and *casy-1(tm718)* worms to 25 mM NaCl. The chemotaxis index was calculated as CI = (worms at NaCl - worms at neutral)/ total number of worms. The experiment was repeated on three separate days with three replicates per assay. Error bars indicate the standard error of mean. (B) Thermotaxis association experiments with wild-type and *casy-1 (tm718)* animals. The thermotaxis index was calculated as TTI = (worms on the cold side of the plate – worms on the warm side)/ total worms in the assay. The experiment was repeated on three separate days. Error bars indicate the standard error of mean. In (A) and (B), the results of a Student t-test are indicated as * = $p<0.05$ and ** = $p<0.01$. For the complete dataset, see Table S1.
doi:10.1371/journal.pone.0004880.g003

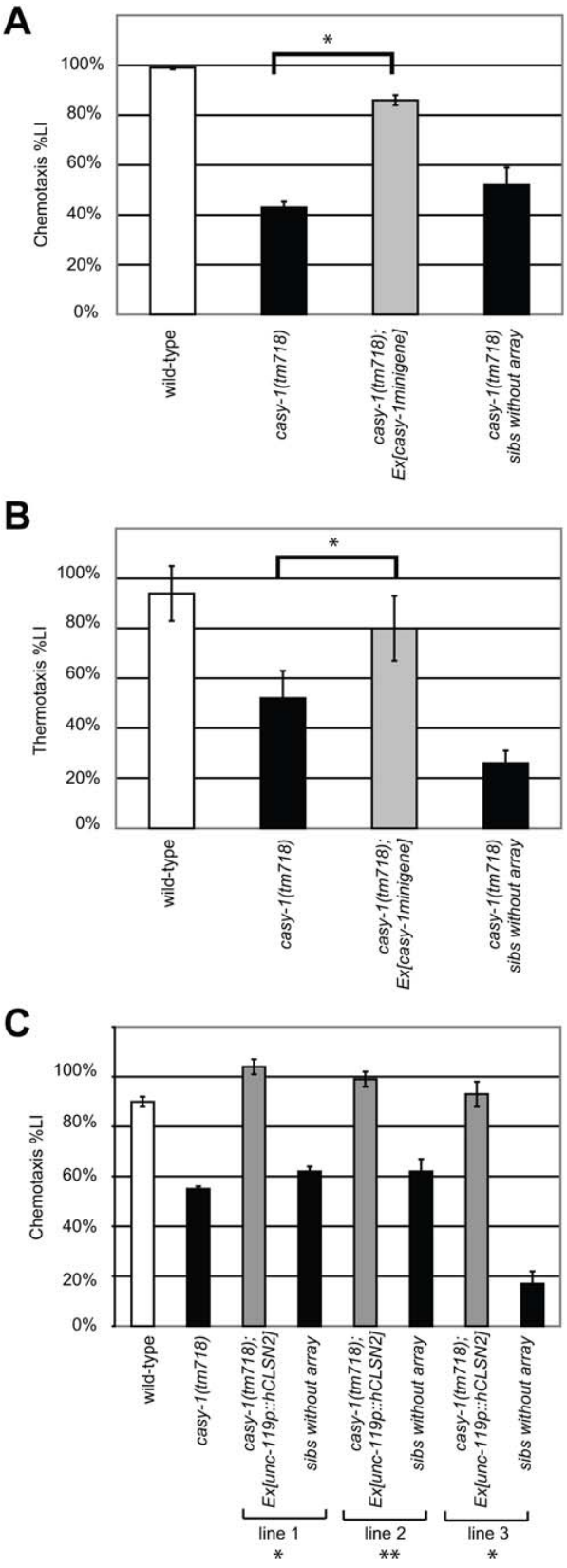

Figure 4. Rescue of the *casy-1(tm718)* behavioral defect with *C. elegans casy-1* and human *clstn2* transgenes. (A) Rescue of the chemotaxis and (B) thermotaxis conditioning defects with a *casy-1* minigene. Results obtained with one (*zhEx242.1*) of four transgenic lines are shown. To quantify the rescue, we defined a % Learning Index as %LI = 100 · (CI of naive worms - CI of conditioned worms)/ CI of naive worms) and analogous for the TTI. As controls, *casy-1(tm718)* animals that had lost the GFP-labeled extrachromosomal rescuing array (*casy-1(tm718)* sibs without array) were included with the transgenic animals in the assay, and their %LI was scored in parallel with the %LI of the transgenic animals. (C) Rescue of the *casy-1(tm718)* chemotaxis conditioning defects by expression of human CLSTN2 cDNA under control of the neuronal *unc-119* promoter and the *casy-1* 3′UTR. The results obtained with three independent lines *zhEx282.1* to *zhEx282.3* are shown. In (C), Student t-test LIs from *casy-1(tm718)* were compared to LIs of the rescue lines. For the complete dataset, see Table S1 and Fig. S2.

doi:10.1371/journal.pone.0004880.g004

significant rescue of the %LI, while their non-transgenic siblings (*casy-1(tm718)* sibs without array) that were simultaneously scored on the same assay plates exhibited behavioral defects comparable to the parental *casy-1(tm718)* strain (Fig. 4A, B).

To test the functional conservation between human CLSTN2 and *C. elegans* CASY-1 at the molecular level, we expressed human CLSTN2 cDNA under the control of the pan-neuronal *unc-119* promoter and with the *C. elegans casy-1* 3′UTR in place of the CLSTN2 3′UTR in *casy-1(tm718)* mutants and measured the %LI of CLSTN2 transgenic animals using the olfactory conditioning assay. All three transgenic lines that were tested showed a significant rescue of the behavioral defects (Fig. 4C). Control transgenic animals carrying the *unc-119* promoter-*casy-1* 3′UTR vector lacking the CLSTN2 cDNA insert exhibited no significant increase in the %LI when compared to non-transgenic *casy-1(tm718)* animals (Fig. S2). Thus, human CLSTN2 can functionally replace *C. elegans* CASY-1 in an associative learning paradigm.

CASY-1 acts in a GLR-1 Glutamate receptor pathway

Human CLSTN1 and CLSTN2 form a complex with the MINT2/X-11-like neuronal adaptor protein and kinesin light chain (KLC1), suggesting a function for CLSTNs in the transport or sorting of synaptic vesicles [15,16,21]. Since mutations in the *C. elegans* ortholog of Mint2 (*lin-10*) cause defects in the clustering of the AMPA-type glutamate receptor subunit GLR-1 at the synapses of ventral cord interneurons and LIN-10 can bind to the PDZ binding motif at the C-terminus of GLR-1 [22], we hypothesized that CASY-1 might regulate the synaptic function or transport of GLR-1. Even though we did not observe a significant mislocalization of a translational GLR-1::GFP reporter in ventral cord motorneurons of *casy-1(tm718)* mutants (data not shown), *glr-1(n2461)* mutants showed similar association defects in the olfactory conditioning assays as *casy-1(tm718)* mutants (Fig. 5A). Notably, GLR-1 has been previously shown to be important for olfactory assocation and critical for long-term memory in *C. elegans* [23,24]. To test a possible function of CASY-1 in a GLR-1 signaling pathway, we examined the genetic interaction between *casy-1(tm718)* and *glr-1(n2461)*. We found no further reduction in the %LI in the *casy-1(tm718); glr-1(n2461)* double loss-of-function mutant compared to either single mutant, suggesting that *casy-1* and *glr-1* may act in the same pathway regulating olfactory conditioning (Fig. 5A). We thus tested if increased levels of GLR-1 could rescue the behavioral defects of *casy-1(tm718)* mutants. For this purpose, we introduced a rescuing multicopy extrachromosomal array containing a 6 kb fragment spanning the *glr-1* locus (*zhEx243.1[glr-1(+)]*) into the *casy-1(tm718)* background. *casy-1(tm718); zhEx243.1[glr-1(+)]* animals showed a similar %LI in the olfactory conditioning assay as wild-type animals

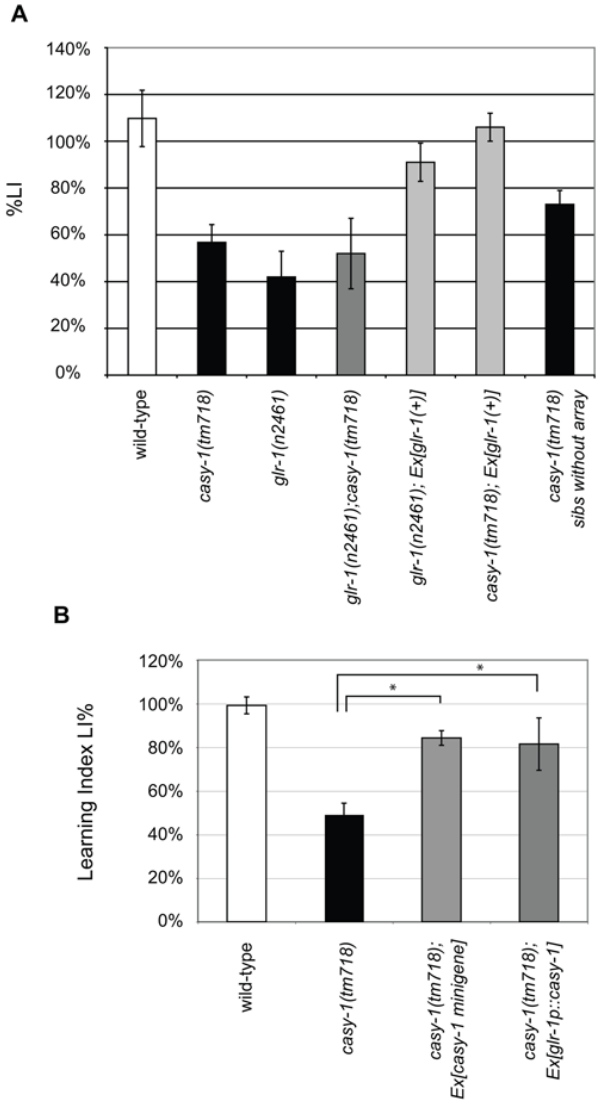

Figure 5. Genetic interaction between *casy-1* and the *glr-1* glutamate receptor signaling pathway. (A) Chemotaxis conditioning assays with *casy-1(tm718) and glr-1(n2461)* single and the double mutants and rescue of *casy-1(tm718)* conditioning defects by overexpression of *glr-1* using the *zhEx243.1* array. (B) Rescue of the *casy-1(tm718)* conditioning defects by expression of *casy-1* cDNA under control of the *glr-1* promoter. The average %LI of four independent lines is shown. Two of the lines showed a complete and two lines a partial rescue of the %LI. For comparison, the data for the *casy-1* minigene rescue experiment from fig. 4 A are shown. The scoring and quantifications were done as described in the legend to [Fig. 4]. For the complete dataset, see Table S1.
doi:10.1371/journal.pone.0004880.g005

(Fig. 5A). Thus, increasing the GLR-1 gene dosage can compensate for the behavioral defects of *casy-1(tm718)* mutants, suggesting that CASY-1 positively regulates GLR-1 signaling during olfactory conditioning.

Some of the head neurons expressing the *casy-1* transcriptional reporter also expressed the *glr-1::gfp* reporter (Fig. 2B). Strongest co-expression was seen in the RMDD, SMDD, RMD and SMDV motor/interneurons that regulate head turning, and weaker *casy-1p::rfp* expression was observed in the *glr-1*-positive AVE command interneurons (not visible in Fig. 2B). We therefore tested if expression of *casy-1* under control of the *glr-1* promoter was sufficient to rescue the olfactory learning defects of *casy-1 (tm718)* mutants. In two out of four lines tested, the DA starvation conditioning defect was completely and in the remaining two lines weakly rescued (Fig. 5B and Table S1). Thus, *casy-1* acts at least in part in *glr-1* positive neurons during olfactory associative learning. It is interesting to note that Ikeda et al.[14] found that during salt chemotaxis conditioning, expression of *casy-1* in *glr-1* positive neurons was not sufficient to rescue the associative learning defects. Accordingly, a recent study by Kano et al. [25] showed that associative learning as well as short-term memory using the salt chemotaxis conditioning paradigm are not *glr-1* dependent. Thus, *casy-1* may perform another, *glr-1* independent function during gustatory (salt) chemotaxis learning, as *casy-1* may act in multiple, distinct pathways depending on the type of sensory inputs that need to be associated with the starvation signal.

Conclusions

In summary, our study reveals an important role of *C. elegans casy-1 calsyntenin* in associative learning in response to different environmental stimuli. It should be noted that in all the association assays shown, the behavior of conditioned *casy-1(tm718)* mutants still significantly differed from the naive controls (i.e. the %LI of *casy-1* mutants was always greater than 0), indicating that loss of *casy-1* function does not result in a complete loss of all associative behavior. Thus, there must exist multiple parallel pathways controlling associative learning in *C. elegans*. For example, components of the insulin signaling pathway have been implicated in salt chemotaxis learning, and *casy-1* was found to act in parallel to the insulin pathway during salt chemotaxis learning [14].

Finally, we demonstrate that the molecular function of human CLSTN2 and *C. elegans* CASY-1 is conserved, as human Calsyntenin-2 can functionally replace CASY-1 during olfactory learning. Given the relatively large evolutionary distance between these two species and the anatomical dissimilarity of their nervous systems, this degree of conservation at the molecular level is remarkable. Thus, Calsyntenin might be a key component of conserved molecular pathways regulating different aspects of learning and memory in diverse species.

Methods

Strains were maintained and grown according to standard procedures [26]. Wild-type refers to *C. elegans* Bristol, variety N2. *casy-1(tm718)* mutants were kindly provided by the Mitani Lab and backcrossed three times before use in all assays. All transgenic animals were generated by microinjection of the indicated DNAs into the syncytial gonads as described. Alleles and transgenes used: LGI: *unc-29(x29)* (kind gift of A.V. Maricq); LGII: *casy-1(tm718)*; LGIII: *glr-1(n2461)*; LGV: *acr-16(ok789)*; transgenes: *zhEx242.1[-casy-1 minigene; sur-5::gfp]*, *zhEx243.1[glr-1(+), lin-48 ::gfp]*, *zhEx282.1 to 282.3[unc-119p::*CLSTN2*::casy-1 3′UTR, sur-5::gfp]*, *zhEx285.1 to zhEx285.3[unc-119p::no insert::casy-1 3′UTR, sur-5::gfp]*, *zhEx245[casy-1p::rfp]*, *nuIs24[glr-1::gfp]*, *Ex[glr-1p::casy-1]*.

PCR fusion constructs

All DNA fragments were amplified using proof reading polymerase from *C. elegans* genomic DNA or total N2 cDNA. Individual fragments were fused by PCR fusion [27]. A 6 kb genomic *glr-1* fragment was amplified (forward: 5′-ccggtcatacgggagataga-3′, reverse: 5′- taaattttcctgggggcttc-3′) to generate *zhEx243.1*. 5 kb of the 5′ UTR region of *casy-1* (forward outer: 5′- ggatattggtcaccttcccta-3′,

nested forward: 5′- ttctagattattctgacaaccatttg-3′, reverse: 5′-cgagcag-catggtgatgtttg-3′) were fused to 2995 bp *casy-1* cDNA (B0034.3a, 5′ fusion primer: 5′-actcacgcacacaaaaccaatcatgcgaactgcgtactttatttttgtc-3′, reverse: 5′- ggagggagtcatgaatgttga-3′) and 1.6 kb of 3′UTR (forward 3′UTR: 5′-gttcgtttgacaagccgttt-3′, nested forward 3′UTR: 5′- agccgtttggtttttcaatg-3′, cDNA fusion primer: 5′- aattccttcagg-catgttgc-3′). This PCR construct was used together with the transformation marker *sur-5::gfp* to generate *zhEx242.1*. Details on the construction of the *glr-1p::casy-1*, the *casy-1p::rfp* and the *unc-119p*::CLSTN2::*casy-1 3′UTR* rescue and control (without insert) constructs are available upon request.

Olfactory conditioning

All assays were conducted with 50–200 well-fed synchronized young adult worms, using 10 cm Petri CTX agar dishes (2% agar, 5 mM KPO_4 pH = 6.0, 1 mM $CaCl_2$, 1 mM $MgSO_4$). Except for agar composition, chemotaxis assays were performed as described previously [17]. Adaptation and starvation conditioning assays were performed as previously described [12], except that animals were washed three times with M9 buffer (22 mM KH_2PO_4, 22 mM Na_2HPO_4, 85 mM NaCl, 1 mM $MgSO_4$) for 20 min each, resulting in 1 hour pre-starvation before the olfactory conditioning was performed.

NaCl conditioning

Salt chemotaxis and salt chemotaxis learning assays were assessed as described before with some modifications [28,29],. Briefly, synchronized and well-fed young adult nematodes were washed 3 times in CTX buffer. 100–200 worms were placed at the intersection of a four-quadrant CTX plate to test chemotaxis and liquid was removed with a tissue paper. Chemotaxis plates were prepared one day in advance. Pairs of opposite quadrants of four-quadrant Petri plates (Falcon X plate, Becton Dickinson Labware) were filled with 16 ml buffered agar (2% agar, 5 mM KPO_4 pH 6, 1 mM $CaCl_2$ and 1 mM $MgSO_4$), either containing 25 mM NaCl or not. Adjacent quadrants were connected with a thin layer of molten agar 1 h before the assay. The chemotaxis index was calculated 10 min after the worms were placed on the CTX plates: (A–C)/ total number of worms), where A is the number of worms at the quadrants with, and C is the number of worms at the quadrants without NaCl.

For NaCl chemotaxis learning assays, the collected nematodes were transferred after the washing procedure into 30 ml CTX buffer containing 20 mM NaCl for 1 h at room temperature [14], and chemotaxis was tested immediately afterwards. All experiments were performed in triplicates at least three times.

Thermotaxis conditioning

We created a thermotaxis setup as described previously using a steep thermal gradient on a thin agar plate [20]. A 2–3 mm thick CTX agar plate 130 mm long 90 mm wide was rested on heated and cooled metal blocks, respectively, such that 13°C was measured at one end and 33° at the other end of the plate. 200–400 worms were spotted along the 22°C isothermic line measured shortly before applying the worms. The worms were then left to migrate for 45 min. At the end of the assay, the plate was separated into a cold region and a warm region along the 22°C isothermic line, and the worms were immediately counted to determine the TTI as described [20].

Microscopy

For the image shown in Fig. 2, animals were anesthetized with 10 mM NaN_3 and mounted in M9 buffer on 3% agarose pads. Optical sections through the left hemisphere were recorded on a Leica SP2 confocal microscope using a 63× N.A. 1.4 objective and a z-step size of 0.73 µm. 3D reconstructions were generated using the volocity 2.3. software package (Improvision) and a lateral view is shown.

Supporting Information

Figure S1 Naive chemotaxis of wild-type and casy-1(tm718) mutants. Chemotaxis of naive animals to volatile attractants (Diacetyl and Isoamyl alcohol) and a repellent (2-Nonanone) was quantified as described in the methods and the legend to Fig. 1. The error bars show the SEM.
Found at: doi:10.1371/journal.pone.0004880.s001 (0.39 MB EPS)

Figure S2 Chemotaxis conditioning of casy-1(tm718) negative control lines. Chemotaxis conditioning transgenic of casy-1(tm718) carrying the unc-119 promoter-casy-1 3′UTR vector without cDNA insert (zhEx285.1 to zhEx285.3[unc-119p::no insert]). The average %LI of three independent control lines and their siblings without array is shown. The LI was calculated as described in the methods and the legend to Fig. 3 and is expressed as % value.
Found at: doi:10.1371/journal.pone.0004880.s002 (0.38 MB EPS)

Table S1 Supporting document
Found at: doi:10.1371/journal.pone.0004880.s003 (0.52 MB PDF)

Acknowledgments

We wish to thank all lab members for critical discussion of this work. We are grateful to Attila Stetak for help with primer design and behavioral assays, the Maricq, Mitani and Kaplan labs and the *C. elegans* Genetics Center for strains and the Fire lab for plasmid vectors and Gert Jansen for help with the salt chemotaxis assays.

Author Contributions

Conceived and designed the experiments: FH MW DJdQ AP AH. Performed the experiments: FH MW EFH AH. Analyzed the data: FH MW DJdQ AP AH. Wrote the paper: FH AP AH.

References

1. Kandel ER, Abrams T, Bernier L, Carew TJ, Hawkins RD, et al. (1983) Classical conditioning and sensitization share aspects of the same molecular cascade in Aplysia. Cold Spring Harb Symp Quant Biol 48 Pt 2: 821–830.
2. Malinow R, Malenka RC (2002) AMPA receptor trafficking and synaptic plasticity. Annu Rev Neurosci 25: 103–126.
3. Groc L, Choquet D (2006) AMPA and NMDA glutamate receptor trafficking: multiple roads for reaching and leaving the synapse. Cell Tissue Res 326: 423–438.
4. Choquet D, Triller A (2003) The role of receptor diffusion in the organization of the postsynaptic membrane. Nat Rev Neurosci 4: 251–265.
5. de Quervain DJ, Papassotiropoulos A (2006) Identification of a genetic cluster influencing memory performance and hippocampal activity in humans. Proc Natl Acad Sci U S A 103: 4270–4274.
6. Papassotiropoulos A, Stephan DA, Huentelman MJ, Hoerndli FJ, Craig DW, et al. (2006) Common Kibra alleles are associated with human memory performance. Science 314: 475–478.
7. Jacobsen LK, Picciotto MR, Heath CJ, Mencl WE, Gelernter J (2008) Allelic Variation of Calsyntenin 2 (CLSTN2) Modulates the Impact of Developmental Tobacco Smoke Exposure on Mnemonic Processing in Adolescents. Biol Psychiatry.
8. Zhang Y, Lu H, Bargmann CI (2005) Pathogenic bacteria induce aversive olfactory learning in *Caenorhabditis elegans*. Nature 438: 179–184.
9. Saeki S, Yamamoto M, Iino Y (2001) Plasticity of chemotaxis revealed by paired presentation of a chemoattractant and starvation in the nematode *Caenorhabditis elegans*. J Exp Biol 204: 1757–1764.
10. Rankin CH, Beck CD, Chiba CM (1990) *Caenorhabditis elegans*: a new model system for the study of learning and memory. Behav Brain Res 37: 89–92.

11. Mohri A, Kodama E, Kimura KD, Koike M, Mizuno T, et al. (2005) Genetic control of temperature preference in the nematode *Caenorhabditis elegans*. Genetics 169: 1437–1450.
12. Colbert HA, Smith TL, Bargmann CI (1997) OSM-9, a novel protein with structural similarity to channels, is required for olfaction, mechanosensation, and olfactory adaptation in *Caenorhabditis elegans*. J Neurosci 17: 8259–8269.
13. Spear NE, Kucharski D, Hoffmann H (1985) Contextual influences on conditioned taste aversions in the developing rat. Ann N Y Acad Sci 443: 42–53.
14. Ikeda DD, Duan Y, Matsuki M, Kunitomo H, Hutter H, et al. (2008) CASY-1, an ortholog of calsyntenins/alcadeins, is essential for learning in *Caenorhabditis elegans*. Proc Natl Acad Sci U S A 105: 5260–5265.
15. Konecna A, Frischknecht R, Kinter J, Ludwig A, Steuble M, et al. (2006) Calsyntenin-1 docks vesicular cargo to kinesin-1. Mol Biol Cell 17: 3651–3663.
16. Hintsch G, Zurlinden A, Meskenaite V, Steuble M, Fink-Widmer K, et al. (2002) The calsyntenins–a family of postsynaptic membrane proteins with distinct neuronal expression patterns. Mol Cell Neurosci 21: 393–409.
17. Nuttley WM, Atkinson-Leadbeater KP, Van Der Kooy D (2002) Serotonin mediates food-odor associative learning in the nematode *Caenorhabditis elegans*. Proc Natl Acad Sci U S A 99: 12449–12454.
18. Sawin ER, Ranganathan R, Horvitz HR (2000) *C. elegans* locomotory rate is modulated by the environment through a dopaminergic pathway and by experience through a serotonergic pathway. Neuron 26: 619–631.
19. Bernhard N, van der Kooy D (2000) A behavioral and genetic dissection of two forms of olfactory plasticity in *Caenorhabditis elegans*: adaptation and habituation. Learn Mem 7: 199–212.
20. Cassata G, Kuhn F, Witmer A, Kirchhofer R, Burglin TR (2000) A steep thermal gradient thermotaxis assay for the nematode *Caenorhabditis elegans*. Genesis 27: 141–144.
21. Araki Y, Tomita S, Yamaguchi H, Miyagi N, Sumioka A, et al. (2003) Novel cadherin-related membrane proteins, Alcadeins, enhance the X11-like protein-mediated stabilization of amyloid beta-protein precursor metabolism. J Biol Chem 278: 49448–49458.
22. Rongo C, Whitfield CW, Rodal A, Kim SK, Kaplan JM (1998) LIN-10 is a shared component of the polarized protein localization pathways in neurons and epithelia. Cell 94: 751–759.
23. Rose JK, Kaun KR, Chen SH, Rankin CH (2003) GLR-1, a non-NMDA glutamate receptor homolog, is critical for long-term memory in *Caenorhabditis elegans*. J Neurosci 23: 9595–9599.
24. Morrison GE, van der Kooy D (2001) A mutation in the AMPA-type glutamate receptor, *glr-1*, blocks olfactory associative and nonassociative learning in *Caenorhabditis elegans*. Behav Neurosci 115: 640–649.
25. Kano T, Brockie PJ, Sassa T, Fujimoto H, Kawahara Y, et al. (2008) Memory in *Caenorhabditis elegans* is mediated by NMDA-type ionotropic glutamate receptors. Curr Biol 18: 1010–1015.
26. Brenner S (1974) The genetics of *Caenorhabditis elegans*. Genetics 77: 71–94.
27. Hobert O (2002) PCR fusion-based approach to create reporter gene constructs for expression analysis in transgenic *C. elegans*. Biotechniques 32: 728–730.
28. Wicks SR, de Vries CJ, van Luenen HG, Plasterk RH (2000) CHE-3, a cytosolic dynein heavy chain, is required for sensory cilia structure and function in *Caenorhabditis elegans*. Dev Biol 221: 295–307.
29. Hukema RK, Rademakers S, Dekkers MP, Burghoorn J, Jansen G (2006) Antagonistic sensory cues generate gustatory plasticity in *Caenorhabditis elegans*. Embo J 25: 312–322.

3.3 PTEN negatively regulates MAPK signaling during *Caenorhabditis elegans* vulval development

The RAS/MAPK, NOTCH, and WNT signaling pathways determine an invariant pattern of cell fates during *C. elegans* vulval development, providing an excellent model to examine the crosstalk between different conserved signaling pathways that are deregulated in human cancer. Itay Nakdimon could identify in his PhD studies a novel form of crosstalk between components of the insulin pathway and the RAS/MAPK pathway during vulval development (Nakdimon et al., 2012). Thereby, the insulin receptor DAF-2 stimulates, while DAF-18 PTEN inhibits RAS/MAPK signaling in the VPCs. Genetic and biochemical analyses indicated that DAF-18 negatively regulates vulval induction by inhibiting MAPK activation.

My own contribution to this manuscript

In collaboration with Anina Schneider (who did her master thesis under my supervision), I was applying the previously established mass-spectrometry based approach for the identification of novel interaction partners to other GST-tagged fusion proteins such as ERM-1, MADD-2, LET-23, and DAF-18.
By performing pull-down experiments using the phosphatase domain of DAF-18 containing the substrate trapping mutation D137A, we identified by subsequent LC-MS/MS analyses the MAP kinase kinase MEK-2 (see master thesis of Anina Schneider). This led to the idea to investigate the phosphorylation level of MEK-2 in *let-60(gf)* animals and *let-60(gf) daf-18(lf)* double mutants. However, no further increase of pMEK-2 levels could be observed in *daf-18(lf) let-60(gf)* mutants compared to *let-60(lf)* animals (Fig. 2 A of the manuscript Nakdimon et al., 2012). In addition, I made co-immunoprecipitation experiments of DAF-18 with MEK-1 and ERK-2, but the results were contradictory and were thus not shown in the manuscript.

OPEN ACCESS Freely available online

PLOS | GENETICS

PTEN Negatively Regulates MAPK Signaling during *Caenorhabditis elegans* Vulval Development

Itay Nakdimon[1,2], Michael Walser[1,3], Erika Fröhli[1], Alex Hajnal[1]*

1 Institute of Molecular Life Sciences, University of Zürich, Zürich, Switzerland, **2** Cancer Network Zürich PhD Program, Institute of Molecular Life Sciences, University of Zürich, Zürich, Switzerland, **3** Molecular Life Sciences PhD Program, Institute of Molecular Life Sciences, University of Zürich, Zürich, Switzerland

Abstract

Vulval development in *Caenorhabditis elegans* serves as an excellent model to examine the crosstalk between different conserved signaling pathways that are deregulated in human cancer. The concerted action of the RAS/MAPK, NOTCH, and WNT pathways determines an invariant pattern of cell fates in three vulval precursor cells. We have discovered a novel form of crosstalk between components of the Insulin and the RAS/MAPK pathways. The insulin receptor DAF-2 stimulates, while DAF-18 PTEN inhibits, RAS/MAPK signaling in the vulval precursor cells. Surprisingly, the inhibitory activity of DAF-18 PTEN on the RAS/MAPK pathway is partially independent of its PIP_3 lipid phosphatase activity and does not involve further downstream components of the insulin pathway, such as AKT and DAF-16 FOXO. Genetic and biochemical analyses indicate that DAF-18 negatively regulates vulval induction by inhibiting MAPK activation. Thus, mutations in the PTEN tumor suppressor gene may result in the simultaneous hyper-activation of two oncogenic signaling pathways.

Citation: Nakdimon I, Walser M, Fröhli E, Hajnal A (2012) PTEN Negatively Regulates MAPK Signaling during *Caenorhabditis elegans* Vulval Development. PLoS Genet 8(8): e1002881. doi:10.1371/journal.pgen.1002881

Editor: Stuart K. Kim, Stanford University Medical Center, United States of America

Received February 3, 2012; **Accepted** June 19, 2012; **Published** August 16, 2012

Funding: This work was supported by a grant from the Swiss National Science Foundation to AH. The funders had no role in study design, data collection and analysis, decision to publish, or preparation of the manuscript.

Competing Interests: The authors have declared that no competing interests exist.

* E-mail: alex.hajnal@imls.uzh.ch

Introduction

PTEN (Phosphatase and TENsin homologue) is the second-most frequently somatically mutated tumor suppressor gene in human cancer. PTEN is often inactivated in glioblastoma, melanoma, prostate and endometrial neoplasia [1]. Germline mutations in PTEN are also known to cause a variety of rare syndromes, collectively known as the PTEN hamartoma tumor syndromes (PHTS) [2]. Cowden syndrome is the best-described syndrome within PHTS, with approximately 80% of patients carrying germline PTEN mutations [3]. The main reported function of PTEN is as a lipid phosphatase, which dephosphorylates PhosphatidylInositol(3,4,5)-trisphosphate (PIP_3) at position 3, thereby inhibiting the insulin pathway [4]. However, PTEN can also act as a dual-specificity tyrosine and serine/threonine protein phosphatase [5,6]. The catalytic phosphatase domain of PTEN (amino acids 123–131) contains several conserved amino acids, mutations of which affect the efficiency and specificity of the phosphatase activity [7]. One such mutation is G129E, which causes PTEN to lose its lipid phosphatase activity while retaining most of its protein phosphatase activity [4,5]. Using the G129E mutation, numerous reports have provided evidence for a crucial role of PTEN protein phosphatase activity in regulating cell migration, invasion and spreading independently of the canonical insulin signaling pathway. For example, PTEN G129E regulates cell migration, spreading, and the formation of focal adhesions [8]. Moreover, PTEN G129E binds and de-phosphorylates the Focal Adhesion Kinase FAK *in vitro* [8]. In glioblastoma cells injected into nude mice, PTEN G129E expression inhibits cell invasion, accompanied by decreased FAK phosphorylation without changing the activity of the AKT kinase [6,9]. Additionally, PTEN binds and dephosphorylates the adaptor protein Shc to modulate cell motility [10].

The *daf-18* gene encodes the single PTEN ortholog in *C. elegans* [11]. Under favorable growth conditions, *C. elegans* larvae pass through four distinct larval stages termed L1 to L4. However, under conditions of starvation or overcrowding, the L1 larvae enter a long-lived, stress resistant alternative developmental stage called the dauer larva stage. DAF-18 PTEN controls entry into the larval dauer stage, life span, neurite outgrowth and cell-cycle progression, mainly by inhibiting the insulin signaling pathway [12–14]. Human PTEN can functionally replace *C. elegans* DAF-18 to rescue the *daf-18(lf)* DAuer Formation defective (DAF-d) phenotype [15].

In the presence of abundant food, binding of various insulin ligands to the DAF-2 insulin receptor causes the activation of AGE-1, the only type I phosphatyidlinositol-3-kinase (PI3K) encoded by the *C. elegans* genome [11]. AGE-1 phosphorylates $PI(4,5)P_2$ to $PI(3,4,5)P_3$, which acts as a second messenger. PIP_3 then activates the AKT-1 and AKT-2 kinases that phosphorylate and thereby inhibit the FOXO transcription factor DAF-16 [16]. In the absence of the insulin signal, non-phosphorylated DAF-16 enters the nucleus and activates genes promoting entry into the dauer stage [17]. The main reported function of DAF-18 PTEN is to antagonize the insulin pathway by dephosphorylating PIP_3 [14]. Loss of *daf-18* thus leads to hyper-activation of the insulin pathway and a DAF-d phenotype, while loss of *daf-2* or *age-1* function leads to a DAuer Formation constitutive (DAF-c) phenotype.

Recent evidence indicates that similar to mammalian PTEN, *C. elegans* DAF-18 can also act as a protein phosphatase to regulate

Author Summary

The human tumor suppressor PTEN is mutated in many different types of cancer. Using the roundworm *C. elegans* as a model to study how cells communicate during animal development, we discovered a new mechanism by which PTEN inhibits the activity of the oncogenic RAS/MAPK signaling pathway. Focusing on the development of the vulva, the egg-laying organ of the hermaphrodite, as a model to investigate the regulation of RAS/MAPK signaling, we could distinguish between two distinct inhibitory activities of PTEN on the RAS/MAPK signaling pathway. On the one hand, PTEN acts as a lipid phosphatase that inhibits the production of PIP_3, which in turn stimulates RAS/MAPK signaling. On the other hand, PTEN acts as a protein phosphatase that negatively regulates RAS/MAPK signaling by inhibiting signal transduction at the level of the MAPK, which is a key component in the pathway. Understanding the detailed molecular mechanism by which the PTEN tumor suppressor homolog regulates signal transduction in *C. elegans* can help predict the consequences of mutations in human PTEN for cancer development in humans.

insulin-independent events. For example, DAF-18 PTEN directly binds and dephosphorylates the ephrin receptor tyrosine kinase VAB-1 to regulate oocyte maturation in the hermaphrodite germline [18]. Moreover, multiple genes causing synthetic lethality in combination with *daf-18(lf)* have been identified, pointing to additional functions of DAF-18 besides its role in insulin signaling [19].

The development of the *C. elegans* hermaphrodite vulva, the egg-laying organ, is one of the best-characterized models for organogenesis [20]. The interplay between the conserved RAS/MAPK, NOTCH, and WNT signaling pathways specifies two distinct vulval cell fates. Beginning in the L2 stage, the gonadal Anchor Cell (AC) releases the EGF ligand LIN-3, which activates the EGF receptor homolog LET-23 in the six Vulval Precursor Cells (VPCs). The VPC located nearest the AC (P6.p) receives most of the inductive LIN-3 EGF signal and hence exhibits the strongest activity of the RAS/MAPK pathway, allowing P6.p to adopt the primary (1°) vulval cell fate. Consequently, P6.p produces a lateral signal that activates the LIN-12 NOTCH signal in the neighboring VPCs P5.p and P7.p. Notch signaling in these two VPCs induces them to adopt the secondary (2°) cell fate and at the same time blocks transduction of the inductive LIN-3 signal by inhibiting MAPK activation. The 1° VPC P6.p and the 2° VPCs P5.p and P7.p each go through three rounds of cell division to generate 22 cells that form the vulva. The remaining three distal VPCs (P3.p, P4.p and P8.p) adopt the non-vulval 3° fate, which divide once and then fuse with the surrounding hypodermis (hyp7).

Mutations in genes encoding components of the RAS/MAPK, NOTCH, and WNT signaling pathways change the patterning of the VPC fates, which can readily be quantified. For example, mutations that hyperactivate the RAS/MAPK pathway cause the induction of more than three VPCs, resulting in a Multivulva (Muv) phenotype. On the other hand, mutations that cause a decrease in RAS/MAPK pathway activity, lead to the induction of fewer than three VPCs, a phenotype called Vulvaless (Vul).

In this work, we have discovered and characterized a new mode of crosstalk between components of the insulin and the RAS/MAPK pathways. Using genetic and biochemical epistasis analyses, we found that the insulin receptor DAF-2 stimulates while DAF-18 PTEN inhibits RAS/MAPK signaling in the VPCs. Surprisingly, part of the inhibitory activity of DAF-18 on the RAS/MAPK pathway is independent of its PIP_3 lipid phosphatase activity and does not involve further downstream components of the insulin pathway. Our results indicate that DAF-18 negatively regulates vulval induction most likely by inhibiting MAP kinase MPK-1 signaling.

Results

daf-18 inhibits vulval induction independently of the canonical insulin signaling pathway

In our previous work, we reported first evidence for a crosstalk between the DAF-2 insulin receptor and the RAS/MAPK signaling pathway during vulval development [21]. To further investigate this interaction, we performed a systematic epistasis analysis by combining various mutations in the insulin and RAS/MAPK signaling pathways and quantifying the levels of vulval induction (Table 1). As reported previously, a reduction-of-function *(rf)* mutation in the insulin receptor *daf-2* partially suppressed the Muv phenotype of *let-60 ras* gain-of-function *(gf)* animals (Table 1, rows 1, 2) [21]. Conversely, a *loss-of-function (lf)* mutation in the *PTEN* homolog *daf-18* strongly enhanced the *let-60(gf)* Muv phenotype (Table 1, row 3). Moreover, *daf-18(lf)* suppressed the vulvaless (Vul) phenotype caused by mutations in the EGF receptor *let-23* or in its cofactor *lin-2*, which activates the RAS/MAPK signaling pathway in the VPCs (Table 1, rows 4–7). Since DAF-18 PTEN counteracts the type I phosphatidyl-inositol-3 kinase (PI3K) AGE-1 that transduces the insulin signal downstream of DAF-2, we tested if an *age-1(lf)* mutation could revert the enhanced vulval induction caused by *daf-18(lf)*. Surprisingly, *age-1(lf)* only partially suppressed the increase in vulval induction caused by *daf-18(lf)*, both in the *let-60(gf)* and the *lin-2(lf)* backgrounds (Table 1, rows 8, 9). Also, the *daf-2(rf)* mutation only partially reverted the enhancement of the *let-60(gf)* Muv phenotype by *daf-18(lf)* (Table 1, row 10), suggesting that DAF-18 inhibits vulval induction to some extent independently of DAF-2 and AGE-1. However, mutations in further downstream components of the DAF-2 insulin pathway had no detectable effect on vulval induction. For example, a *gf* mutation in *akt-1*, which encodes one of the two AKT homologues transducing the insulin signal downstream of AGE-1 [16], did not suppress the *let-23(rf)* Vul phenotype (Table 1, row 11), and a *lf* mutation in *akt-1* did not suppress the *daf-18(lf) let-60(gf)* Muv phenotype (Table 1, row 12). To examine a possible redundancy between the two *akt* genes, we performed *akt-2* RNAi in *daf-18(lf) let-60(gf); akt-1(lf)* triple mutants, but observed no reduction in vulval induction compared to the RNAi controls (Table 2, rows 1, 2). Also, a *lf* mutation in *daf-16*, which encodes a FOXO transcription factor that is negatively regulated by the insulin pathway, did not enhance the *let-60(gf)* Muv phenotype (Table 1, row 13).

We further tested the role of AGE-1 during vulval development. Since *age-1(lf)* leads to a constitutive dauer phenotype (DAF-c) that is maternally rescued, homozygous *age-1(lf)* worms could only be analyzed in the F1 progeny of heterozygous *age-1(lf)*/+ parents or when rescued by the *daf-16(lf)* mutation. Our analysis indicated that *age-1* also exhibits a partial maternal rescue in vulval induction since the homozygous *age-1(lf); let-60(gf)* progeny obtained from heterozygous *age-1(lf)*/+ parents displayed similar levels of vulval induction as *let-60(gf)* single mutants (Table 1, row 14). In contrast, homozygous *age-1(lf); let-60(gf)* double mutants maintained in the *daf-16(lf)* background exhibited a partially suppressed Muv phenotype, though *age-1(lf)* suppressed the *let-60(gf)* Muv phenotype to a lesser extent than *daf-2(rf)* (Table 1, row 15, p-value$\leq$0.05 compared to row 2).

Table 1. Epistasis analysis between the insulin and RAS/MAPK pathways.

	genotype	Induction±SE	% Vul	% Muv	n
1	*let-60(gf)*	4.16±0.05	0.00	79.1	283
2	*daf-2(rf); let-60(gf)*	3.24±0.11$^{***(1)}$	0.00	19.3	31
3	*daf-18(lf) let-60(gf)*	4.99±0.05$^{***(1)}$	0.00	96.4	221
4	*let-23(rf)*	0.55±0.08	93.8	0.00	129
5	*let-23(rf); daf-18(lf)*	1.90±0.10$^{***(4)}$	63.9	6.8	133
6	*lin-2(lf)*	1.34±0.19	73.8	0.00	42
7	*daf-18(lf); lin-2(lf)*	2.50±0.12$^{***(6)}$	35.5	1.7	59
8	*age-1(lf); daf-18(lf) let-60(gf)*	4.61±0.08$^{***(1)}$	0.00	94.7	113
9	*age-1(lf); daf-18(lf); lin-2(lf)*	2.15±0.16$^{***(6)}$	53.1	6.1	49
10	*daf-2(rf); daf-18(lf) let-60(gf)*	4.40±0.17$^{(1)}$	0.00	88.0	25
11	*let-23(rf); akt-1(gf)*	0.36±0.13$^{(4)}$	94.9	0.00	39
12	*daf-18(lf) let-60(gf); akt-1(lf)*	4.80±0.29$^{(3)}$	0.00	80	15
13	*daf-16(lf); let-60(gf)*	4.18±0.11$^{(1)}$	0.00	77.5	80
14	*age-1(lf); let-60(gf)*†	4.08±0.06$^{(1)}$	0.00	76.2	164
15	*age-1(lf); daf-16(lf); let-60(gf)*	3.62±0.15$^{**(1)}$	0.00	54.1	24

SE indicates the standard error of the mean. % Vul indicates the fraction of animals with less than three induced VPCs. % Muv indicates the fraction of animals with more than three induced VPCs. Induction indicates the average number of induced VPCs per animal.
**indicates a p-value≤0.005;
***indicates a p-value≤0.0005. Numbers in brackets indicate the row against which a t-test was performed. Alleles used: LG I: *daf-16(mu86)*, LG II: *age-1(mg44), let-23(sy1)*, LG III: *daf-2(e1370)*, LG IV: *let-60(n1046), daf-18(ok480)*, LG V: *akt-1(ok525lf), akt-1(mg144af)*, LG X: *lin-2(n397)*.
†F1 progeny of heterozygous *age-1(lf)/+* parents.
doi:10.1371/journal.pgen.1002881.t001

Taken together, the genetic analysis indicates that the DAF-2 insulin receptor promotes and DAF-18 PTEN inhibits vulval induction. DAF-2 and DAF-18 both regulate vulval induction through AGE-1-dependent as well as AGE-1-independent pathways that do not utilize the canonical insulin pathway downstream of AGE-1.

DAF-18 inhibits vulval induction independently of other PI3Ks

AGE-1 is the only *C. elegans* member of the type I family of PI3Ks, which convert $PI(4,5)P_2$ into $PI(3,4,5)P_3$. To further investigate the AGE-1-independent effect of DAF-18 on vulval induction, we tested the roles of alternative PI3Ks that can phosphorylate PIs at position 3. *vps-34* encodes a type III PI3K, which catalyzes the production of $PI(3)P_1$, and *piki-1* encodes a type II PI3K involved in the engulfment of apoptotic cell corpses [22]. In order to examine the role of these alternative PI3Ks during vulval induction, we performed RNAi against *vps-34* and *piki-1* in *age-1(lf); daf-18(lf); lin-2(lf)* animals and tested for a further reduction of vulval induction. RNAi to *vps-34* and *piki-1* has been previously shown to be effective in different tissues [23,24]. Neither *vps-34* nor *piki-1* RNAi caused any significant reduction in the number of induced VPCs when compared to control (*gfp*) RNAi animals (Table 2, rows 3–5). Furthermore, *vps-34* and *piki-1* RNAi in an *age-1(lf); daf-18(lf) let-60(gf)* background did not cause a decrease in vulval induction (Table 2, rows 6–8). It thus seems unlikely that an alternative PI3K acts redundantly with AGE-1 during vulval induction, further supporting our observation that DAF-18 regulates vulval induction not only by regulating PIP_3 levels but also via a lipid phosphatase-independent activity.

Table 2. RNAi against *akt-2* and alternative PI3Ks.

	genotype	RNAi	Induction ±SE	% Vul	% Muv	n
1	*daf-18(lf) let-60(gf); akt-1(lf)*	*gfp*	5.41±0.12	0.00	100	17
2	*daf-18(lf) let-60(gf); akt-1(lf)*	*akt-2*	5.53±0.18	0.00	94.4	18
3	*age-1(lf);daf-18(lf);lin-2(lf)*	*gfp*	1.59±0.34	71	12	17
4	*age-1(lf);daf-18(lf);lin-2(lf)*	*vps-34*	1.60±0.28	65	0	20
5	*age-1(lf);daf-18(lf);lin-2(lf)*	*piki-1*	1.69±0.31	69	6	16
6	*age-1(lf);daf-18(lf);let-60(gf)*	*gfp*	5.14±0.20	0	94	17
7	*age-1(lf);daf-18(lf);let-60(gf)*	*vps-34*	5.40±0.16	0	100	15
8	*age-1(lf);daf-18(lf);let-60(gf)*	*piki-1*	5.44±0.12	0	100	17

SE indicates the standard error of the mean. % Vul indicates the fraction of animals with less than three induced VPCs. % Muv indicates the fraction of animals with more than three induced VPCs. Induction indicates the average number of induced VPCs per animal. Alleles used: LG II: *age-1(mg44)*, LG IV: *daf-18(ok480), let-60(n1046)*, LGV: *akt-1(ok525lf)*, LG X: *lin-2(n397)*.
doi:10.1371/journal.pgen.1002881.t002

daf-18 inhibits 1° vulval cell fate specification

To characterize the nature of the cell fate transformation caused by *daf-18(lf)*, we quantified the levels of the EGL-17::CFP reporter, whose expression is induced by RAS/MAPK signaling in the 1° vulval cell lineage [25] and of the LIP-1::GFP reporter whose expression is induced by LIN-12 NOTCH signaling in the 2° vulval cell lineage [26].

daf-18(lf) let-60(gf) double mutants showed an increased frequency of adjacent VPC descendants expressing high levels of EGL-17::CFP when compared to *let-60(gf)* single mutants (Figure 1A–1D). Specifically, in *daf-18(lf); let-60(gf)* double mutants 27% of adjacent VPC descendants showed strong EGL-17::CFP expression (i.e. at least 50% of the signal intensity seen in the P6.p lineage) versus 16% in *let-60(gf)* single mutants (Figure 1G). Furthermore, while the 2° P5.p and P7.p descendants in the wild-type displayed weak (i.e. less than 50% of the P6.px signal intensity) EGL-17::CFP expression in 22% of the cases, 52% of *daf-18(lf)* single mutants showed EGL-17::CFP expression in the 2° cells (Figure 1G).

Besides the slight increase in EGL-17::CFP expression, the morphology of the vulval invagination at the L4 larval stage was changed in *daf-18(lf) let-60(gf)* double mutants. The vulval invagination formed by the P5.p to P7.p descendants of most *let-60(gf)* single mutants resembles the single invagination formed in the wild-type (Figure 1E). In *daf-18(lf) let-60(gf)* double mutants, on the other hand, the P5.p to P7.p descendants were often completely detached from the cuticle, resulting in an abnormal shape of the vulval invagination (Figure 1F) (37% detached P5.p and/or P7.p descendants in *daf-18(lf) let-60(gf)* versus 3% detached in *let-60(gf)*, n = 54 and n = 35, respectively). A detachment of the P5.p and P7.p descendants from the cuticle is indicative of a 2° to 1° cell fate transformation as it has been observed in mutants exhibiting elevated MAPK activity in the 2° lineage [27].

In contrast to the 1° fate marker EGL-17::CFP, expression of the 2° fate marker LIP-1::GFP was not changed in *daf-18(lf)* mutants. In particular, LIP-1::GFP levels in the P5.p and P7.p

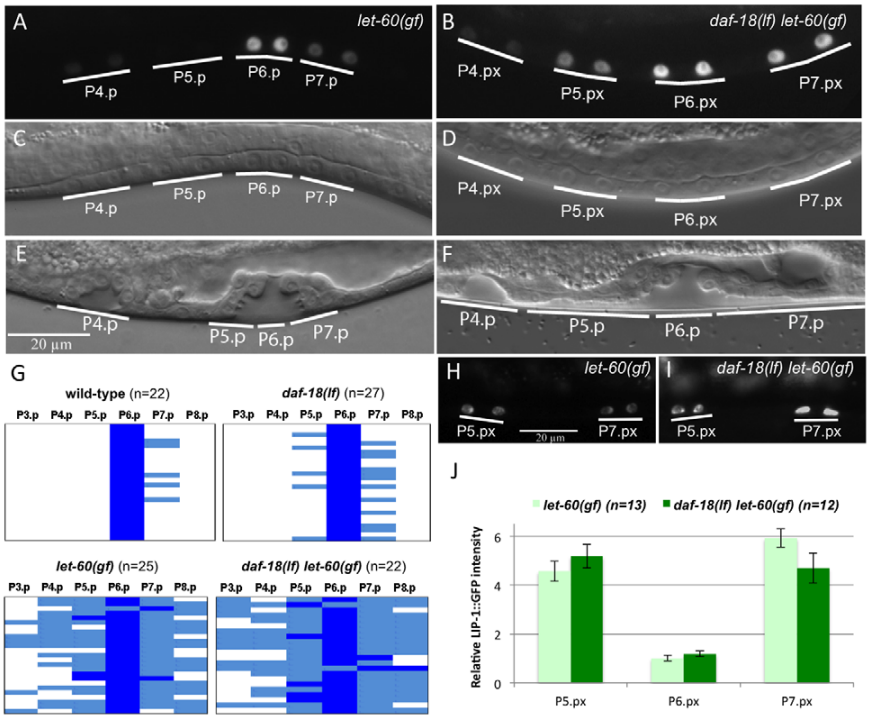

Figure 1. DAF-18 inhibits 1° vulval fate specification. (A) Expression of the 1° cell fate marker EGL-17::CFP in *let-60(gf)* single and (B) *daf-18(lf) let-60(gf)* double mutants at the Pn.px stage. (C and D) show the corresponding Nomarski images of the animals shown in (A) and (B), respectively. (E) Morphology of the vulval invagination in a *let-60(gf)* mutant at the Pn.pxxx stage. Note that the descendants of P5.p and P7.p remain attached to the cuticle, which is characteristic of the 2° cell fate. (F) P5.p and P7.p often detach from the cuticle in *daf-18(lf) let-60(gf)* animals, resulting in a broad invagination with abnormal morphology. (G) Quantification of the 1° fate marker EGL-17::CFP expression at the Pn.px and Pn.pxx stages in the indicated genetic backgrounds. Dark blue represents cells with high EGL-17::CFP expression, corresponding to at least 50% of the intensity observed in the P6.px(x) cells, light blue represents cells with clearly visible but less than 50% of the P6.px(x) signal, and white spaces represent cells with undetectable levels of EGL-17::CFP. (H) Expression of the 2° fate marker LIP-1::GFP in *let-60(gf)* and (I) *daf-18(lf) let-60(gf)* animals. (J) Quantification of LIP-1::GFP expression in the P5.p through P7.p descendants. Signal intensities are indicated relative to P6.px(x) in *let-60(gf)*.
doi:10.1371/journal.pgen.1002881.g001

descendants were unchanged in *daf-18(lf) let-60(gf)* double mutants compared to *let-60(gf)* single mutants (Figure 1H–1J).

Thus, *daf-18(lf)* enhances specification of the 1° cell fate and causes a partial 2° to 1° fate transformation in P5.p and P7.p without affecting the strength of the lateral LIN-12 NOTCH signal.

daf-18 negatively regulates vulval induction downstream of *sos-1* and upstream or at the level of *mpk-1*

Since EGFR/RAS/MAPK signaling induces the 1° vulval cell fate and *daf-18(lf)* mutants exhibited an increased expression of the 1° cell fate marker EGL-17::CFP, we sought to determine at what level DAF-18 inhibits the activity of the EGFR/RAS/MAPK signaling pathway. For this purpose, we performed further epistasis analysis combining *daf-18(lf)* with mutations in different components of the RAS/MAPK pathway. Even though *daf-18(lf)* single mutants showed no obvious changes in the vulval fate pattern (Table 3, rows 1, 2), *daf-18(lf)* increased the levels of vulval induction in most of mutants in the RAS/MAPK pathway tested, confirming that DAF-18 negatively regulates the RAS/MAPK signaling during vulval induction. For example, when combined with mutations in different positive regulators of the RAS/MAPK pathway such as *let-23(rf)*, *lin-2(lf)* or *lin-45(rf)*, *daf-18(lf)* significantly suppressed the Vul phenotype of these mutants (Table 3, rows 5–8 and 11–12). In particular, *daf-18(lf)* suppressed a *lf* mutation in the RAS-GEF *sos-1* when assayed in the *let-60(gf)* background to rescue the lethality caused by *sos-1(lf)*, placing *daf-18* function downstream of *sos-1* (table 3, rows 9–10). However, since vulval induction in *sos-1(lf); let-60(gf)* animals is partly sensitive to the inductive anchor cell signal [28], we cannot exclude the possibility that DAF-18 might inhibit RAS/MAPK signaling through a SOS-1 independent branch of the pathway. As an exception, *daf-18(lf)* did not suppress the Vul phenotype of *lin-3(rf)* mutants (Table 3, rows 3–4), suggesting that *daf-18(lf)* alone is not sufficient to activate the RAS/MAPK pathway in the absence of the inductive AC signal. Furthermore, *daf-18(lf)* did not affect the completely penetrant Vul phenotype caused by *mpk-1(lf)* (Table 3, rows 13–14). Taken together, our epistasis analysis indicates that DAF-18 inhibits RAS/MAPK signaling downstream of or in parallel with the RAS-GEF SOS-1 and upstream or at the level of the MAP kinase MPK-1.

DAF-18 negatively regulates MPK-1 but not MEK-2 phosphorylation

Activation of the RAS/MAPK pathway results in an increased phosphorylation and activity of the downstream effectors RAF, MAPK kinase (MEK) and MAPK. We thus examined if *daf-18(lf)* mutants exhibit elevated levels of MEK and MAPK phosphorylation. Western blots of extracts from L4 larvae were probed with antibodies against mono-phosphorylated MEK (pMEK-2) and di-phosphorylated MAPK (dpMPK-1). Although the *C. elegans* genome encodes two MEK genes, MEK-1 and MEK-2, the

Table 3. Epistasis analysis of *daf-18* with components of the RAS/MAPK pathway.

	genotype	Induction±SE	% Vul	% Muv	n
1	wild-type	3.00±0.00	0.0	0.0	many
2	*daf-18(lf)*	2.99±0.01	0.9	0.0	107
3	*lin-3(lf)*	0.81±0.19	95.2	0.0	21
4	*daf-18(lf) lin-3(lf)*	0.46±0.13	94.1	0.0	34
5	*let-23(rf)*	0.55±0.08	93.8	0.0	129
6	*let-23(rf); daf-18(lf)*	1.90±0.10***(5)	63.9	6.8	133
7	*lin-2(lf)*	1.34±0.19	73.7	0.0	42
8	*daf-18(lf); lin-2(lf)*	2.50±0.12***(7)	35.5	1.7	59
9	*let-60(gf); sos-1(lf)*#	2.60±0.17	16.7	0.0	30
10	*daf-18(lf) let-60(gf); sos-1(lf)*#	4.19±0.12***(9)	0.0	90.3	31
11	*lin-45(rf)*	1.81±0.15	57.3	0.0	68
12	*daf-18(lf) lin-45(rf)*	2.29±0.17*(11)	39.5	2.3	42
13	*mpk-1(lf)*	0.00±0.00	100	0.0	14
14	*mpk-1(lf); daf-18(lf)*	0.00±0.00	100	0.0	17
15	*let-60(gf)* - gonad	2.44±0.27	46	23	13
16	*daf-18(lf) let-60(gf)* - gonad	3.38±0.38	8	42	12

SE indicates the standard error of the mean. % Vul indicates the fraction of animals with three or less induced VPCs. % Muv indicates the fraction of animals with more than three induced VPCs. Induction indicates the average number of induced VPCs per animal.

*indicates a p-value<0.05.

***indicates a p-value<0.0005, numbers in brackets indicates the row number against which a t-test was performed. Alleles used: LG II: *let-23(sy1)*, LG III: *mpk-1(ga117)*, LG IV: *daf-18(ok480), let-60(n1046), lin-3(e1417), lin-45(sy96)*, LG V: *sos-1(s1031)*, LG X: *lin-2(n397)*.

#*sos-1(s1031)* is cis-linked to *unc-46(e177)*.

doi:10.1371/journal.pgen.1002881.t003

phosphorylation site in human MEK to which the phospho-MEK antibody was raised (S217/S221) is only conserved in *C. elegans* MEK-2. Thus, we were able to specifically detect phosphorylated MEK-2 in whole animal extracts. Wild-type and *daf-18(lf)* L4 larvae contained only low levels of pMEK-2 and dpMPK-1 that could not be reliably quantified. As expected, *let-60(gf)* single mutants contained significantly higher levels of pMEK-2 and dpMPK-1 than wild-type larvae (Figure 2A and 2C). However, we observed no further increase in pMEK-2 levels in *daf-18(lf) let-60(gf)* double compared to *let-60(gf)* single mutants (Figure 2B). In contrast, dpMPK-1 levels were around two-fold increased *daf-18(lf) let-60(gf)* compared to *let-60(gf)* mutants (Figure 2D). Together with the genetic epistasis data presented above, the increase in MPK-1 phosphorylation in the absence of a significant change in MEK-2 phosphorylation indicates that DAF-18 most likely inhibits vulval induction at the level of MPK-1. Finally, the fact that we observed increased MPK-1 phosphorylation in total worm lysates suggests a global regulation of the RAS/MAPK pathway by DAF-18, probably including the germline.

daf-18 expression in the VPCs inhibits vulval induction

To further investigate the role of DAF-18 during vulval induction, we constructed a translational reporter by inserting a *gfp* cassette at the 3′ end of the ORF in a genomic *daf-18* fragment (Figure 3). This DAF-18::GFP reporter rescued both the dauer defective (DAF-d) phenotype (data not shown) as well as the vulval phenotypes of *daf-18(lf)* with similar efficiency as a 6.5 kb genomic fragment spanning the entire *daf-18* locus (Figure 4). DAF-18::GFP expression was observed in many tissues during all larval stages, including the developing vulva, the uterus, the ventral nerve cord and the distal tip cells (data not shown). In particular, equal levels of DAF-18::GFP expression were detected in the six VPCs of L2 larvae, and expression persisted in the descendants of the induced VPCs until the Pn.pxxx stage (Figure 3). Interestingly, the sub-cellular localization of DAF-18::GFP changed over the course of vulval development. In the VPCs of L2 larvae prior to and during induction (Pn.p stage), DAF-18::GFP was predominantly localized in the cytoplasm and the nucleus (Figure 3A, 3B and 3B′). However, at the subsequent stages (Pn.px to Pn.pxx stages), DAF-18::GFP became increasingly localized to the plasma membrane of the vulval cells (Figure 2C, 2D and 2D′). Plasma membrane staining peaked at the "Christmas tree" (Pn.pxxx) stage, when almost all the protein appeared to be localized to the membranes and nuclear staining was reduced to very low levels (Figure 3E and 3F). Since the DAF-18::GFP reporter was also expressed in tissues surrounding the vulval cells, we examined whether tissue-specific expression of DAF-18 in the VPCs reduces vulval induction. For this purpose, we expressed *daf-18 cDNA* fused to *gfp* under the control of the Pn.p cell-specific *lin-31* promoter, which is active in the VPCs before and during vulval induction [29] (*Plin-31::daf-18 cDNA::gfp::unc-54 3′ UTR*). Indeed, introduction of the *lin-31::daf-18::gfp* transgene into *daf-18(lf); let-23(rf)* animals repressed vulval induction with similar efficiency as the *daf-18::gfp* reporter or a genomic *daf-18* rescue construct (Figure 4).

Besides the vulval cells, the DAF-18::GFP reporter was also expressed at the L3 to L4 larval stages in several cells of the uterus, which is part of the somatic gonad (Figure 3). We thus tested if the *daf-18*-mediated repression of vulval induction requires the gonad by ablating the Z1 to Z4 somatic gonad and germline precursor cells at the L1 stage. In gonad-ablated *daf-18(lf) let-60(gf)* double mutants, vulval induction was higher than in gonad-ablated *let-60(gf)* single mutants, indicating that DAF-18 represses vulval induction independently of a signal from the gonad (Table 3, rows 15, 16). Thus, DAF-18 probably acts predominantly in the VPCs to inhibit MAPK signaling during vulval induction.

Both lipid and protein phosphatase activities of DAF-18 inhibit vulval induction

Mammalian PTEN acts as a lipid phosphatase as well as a dual-specificity protein phosphatase [5,6]. Moreover, a recent report has shown that *C. elegans* DAF-18 can act as a protein phosphatase inhibiting signaling by the VAB-1 ephrin receptor during oocyte maturation [18]. The G129E mutation in the catalytic center of human PTEN eliminates the lipid phosphatase activity, while retaining the protein phosphatase activity [7]. The corresponding glycine 174 residue in *C. elegans* DAF-18 was therefore mutated to glutamic acid in the *daf-18 genomic* rescue construct. To quantify the rescuing activity of the *daf-18* wild-type (*daf-18 wt*) and the G174E mutated lipid phosphatase mutant (*daf-18 G174E*), these constructs were expressed in the *daf-18(lf) let-60(gf)* and *let-23(rf); daf-18(lf)* backgrounds, and vulval induction was quantified. As expected, expression of *daf-18 wt* rescued both the DAF-d (data not shown) and vulval phenotypes of *daf-18(lf)* (Figure 5). In contrast, *daf-18 G174E* did not rescue the DAF-d phenotype ([15] and own observation), yet exhibited a weaker, though significant rescuing activity of the vulval induction phenotype (Figure 5). These results indicate that the DAF-18 protein and lipid phosphatase activities each play independent roles in negatively regulating the RAS/MAPK pathway and that both activities are required for the full inhibition of vulval induction by DAF-18.

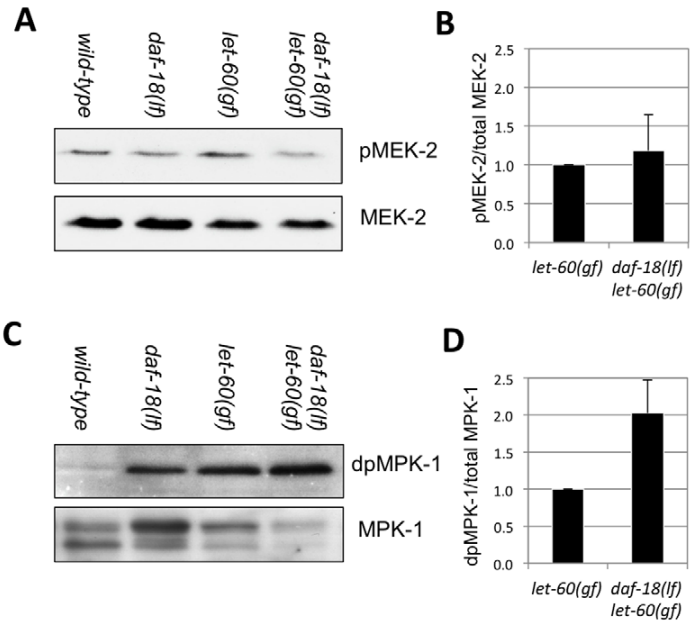

Figure 2. DAF-18 inhibits MPK-1 phosphorylation. Total extracts of wild-type, *daf-18(lf), let-60(gf)* and *daf-18(lf) let-60(gf)* larvae at the L4 stage were analyzed on Western blots using antibodies against (A) phosphorylated and total MEK-2 and (C) against di-phosphorylated (dp) and total MPK-1. Signal intensities were quantified in four (for MEK-2) and three (for MPK-1) independent experiments, and the average ratios of (B) pMEK-2 to total MEK-2 and (D) dpMPK-1 to total MPK-1 intensities were calculated.
doi:10.1371/journal.pgen.1002881.g002

Discussion

The Insulin pathway is a key regulator of development, reproduction, and life span in metazoans. In this study, we have discovered a new form of cross-talk between the Insulin and RAS/MAPK pathways during vulval development. Signaling by the Insulin receptor DAF-2 positively regulates MAPK activation. Surprisingly, the effect of DAF-2 on vulval development does not involve activation of the canonical Insulin pathway. DAF-2 signaling regulates vulval induction in at least two distinct manners, through AGE-1 dependent and independent pathways (Figure 6). One possible explanation for the AGE-1-independent branch of DAF-2 signaling is supported by mammalian data, which suggest that the Insulin receptor can directly stimulate RAS activation by recruiting GRB2 and the RAS-GEF SOS [30,31]. Also in *C. elegans*, LET-60 RAS was found to act downstream of the DAF-2 Insulin receptor to modulate the effects of Insulin signaling during entry into the Dauer stage [32].

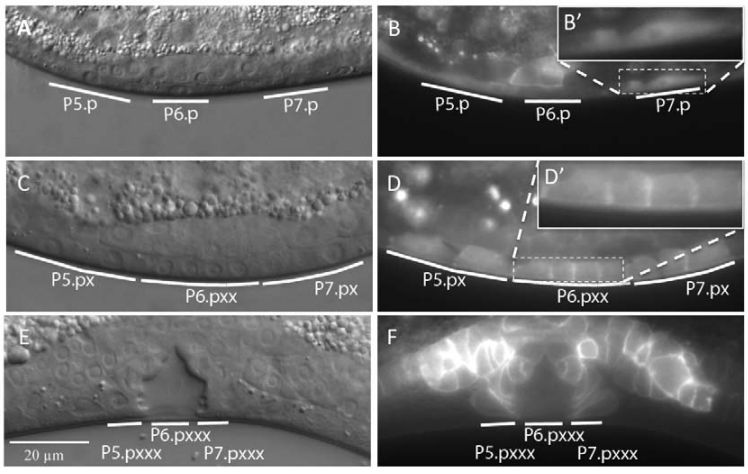

Figure 3. Expression pattern and sub-cellular localization of DAF-18::GFP. (A and B) Nomarski and fluorescence images of animals expressing the DAF-18::GFP translational reporter at the Pn.p cell stage, (C and D) the Pn.px(x) stage and (E and F) the Pn.pxxx "Christmas tree" stage. The insets in (B′) and (D′) show higher magnifications of the areas in (B) and (D) marked with dashed boxes.
doi:10.1371/journal.pgen.1002881.g003

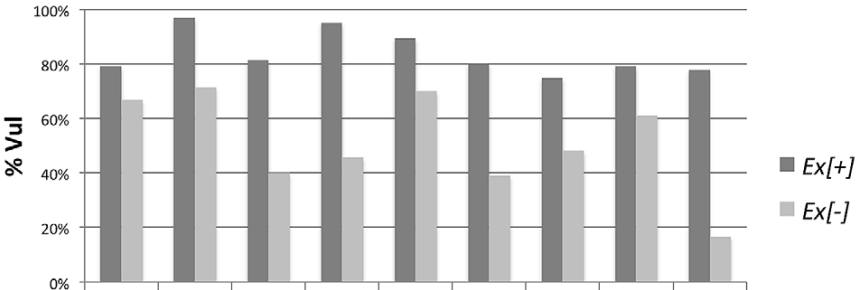

	Induction ±SE								
Ex[+]	0.98 ±0.25	0.44 ±0.14	1.07 ±0.23	0.60 ±0.19	0.84 ±0.25	1.50 ±0.31	1.54 ±0.19	1.06 ±0.26	1.28 ±0.29
Ex[-]	2.19 ±0.19	1.88 ±0.22	2.38 ±0.23	2.42 ±0.19	1.90 ±0.29	2.47 ±0.22	2.19 ±0.20	2.11 ±0.28	2.89 ±0.06
t-test	***	***	***	***	*	*	*	**	***

Figure 4. DAF-18 expression in the Pn.p cells inhibits vulval induction. Vulval induction was scored at the L4 stage comparing *let-23(rf); daf-18(lf)* animals carrying the different extra-chromosomal arrays (Ex[+]) to their siblings lacking the array (Ex[−]). Three independent lines were scored per construct and at least 20 Ex[+] and Ex[−] animals were counted per line. For each line, a t-test was performed comparing induction in Ex[+] and Ex[−] animals on the same plates. * indicates a p-value≤0.05, ** a p-value≤0.005, and *** a p-value≤0.0005.
doi:10.1371/journal.pgen.1002881.g004

Furthermore, we found that the PTEN ortholog DAF-18 strongly inhibits RAS/MAPK signaling. Vulval induction in *daf-18(lf) let-60(gf)* double mutants reaches levels similar to those seen in the strongest Muv mutants such as *lin-15AB(lf)* [33]. The increase in RAS/MAPK signaling in *daf-18(lf)* mutants could be partially reverted by loss of the PI3K activity, suggesting that elevated levels of PIP_3 do stimulate RAS/MAPK signaling but cannot explain all the functions DAF-18 exerts during vulval induction. Accordingly, the inhibitory activity requires both the lipid and protein phosphatase activities of DAF-18. PIP_3 acts as a second messenger that activates multiple downstream targets. One major PIP_3 target in the Insulin pathway is the AKT kinases, which phosphorylate and thereby inhibits the FOXO transcription factor DAF-16. However neither *akt-1*, *akt-2* nor *daf-16* mutations had any detectable effect on vulval induction. Thus, PIP_3 must act via other targets to stimulate RAS/MAPK signaling. Increased levels of PIP_3 in the plasma membrane could, for example, enhance the recruitment of an alternative GEF that activates RAS

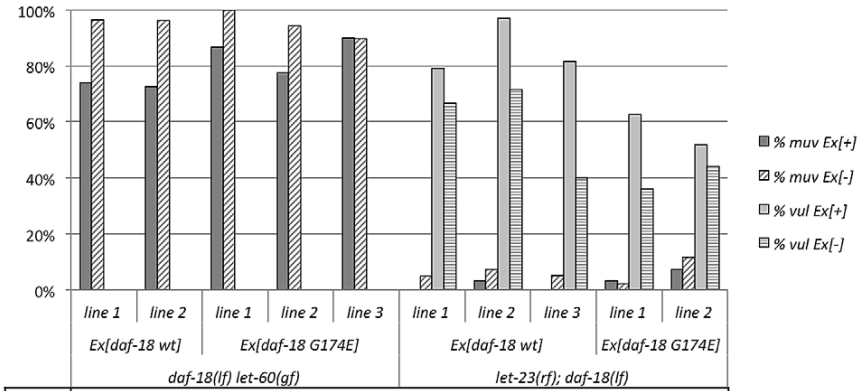

	Induction ±SE									
Ex[+]	3.85 ±0.14	3.82 ±0.15	4.52 ±0.18	4.42 ±0.15	4.65 ±0.19	0.98 ±0.25	0.44 ±0.14	1.07 ±0.23	1.84 ±0.21	2.10 ±0.16
Ex[-]	4.70 ±0.13	5.31 ±0.13	4.96 ±0.11	4.83 ±0.14	4.83 ±0.15	2.19 ±0.19	1.88 ±0.22	2.38 ±0.23	2.45 ±0.13	2.37 ±0.15
t-test	***	***	*			***	***	***	*	

Figure 5. A lipid phosphatase deficient mutant of DAF-18 remains partially active. Animals carrying the *daf-18 wt and daf-18 G174E* extra-chromosomal arrays were scored at the L4 stage as described in the legend to Figure 4.
doi:10.1371/journal.pgen.1002881.g005

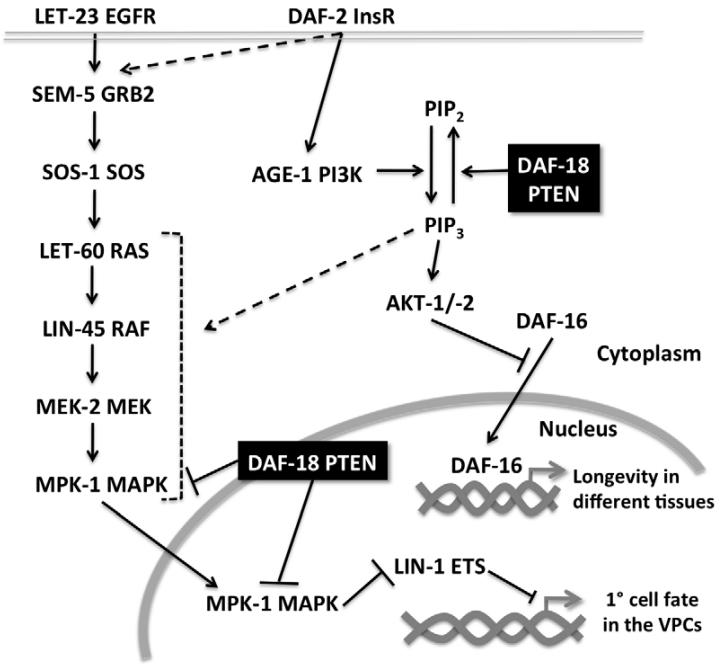

Figure 6. Multiple modes of crosstalk between the RAS/MAPK and insulin pathways during vulval development. Activation of LET-60 RAS in the VPCs causes phosphorylated MPK-1 to enter the nucleus where it phosphorylates transcription factors such as LIN-1 ETS, which represses 1° fate-specific gene expression. The insulin signaling pathway interacts with the RAS/MAPK pathway at several levels. Firstly, DAF-2 InsR activation enhances RAS/MAPK signaling by stimulating the PI3K AGE-1, which positively regulates RAS/MAPK signaling via increased PIP_3 production. In addition, DAF-2 signaling activates the RAS/MAPK signaling independently of AGE-1, possibly by recruiting SEM-5 to the plasma membrane. DAF-18 PTEN inhibits RAS/MAPK signaling in two distinct manners; by dephosphorylating PIP_3 and by negatively regulating MAPK activation.
doi:10.1371/journal.pgen.1002881.g006

signaling in parallel to the RAS-GEF SOS-1 [28] (Figure 6). However, we observed that prior to and at early stages of vulval induction, DAF-18::GFP was localized predominantly in the cytoplasm and nucleus of the VPCs, while membrane localization of DAF-18 only became apparent at later stages. Previous observations of mammalian PTEN localization suggested that PTEN performs different functions depending on its sub-cellular localization [34]. It has been proposed that the lipid phosphatase activity is important for the cytoplasmic and membrane functions of mammalian PTEN, while the protein phosphatase activity is rather required for its nuclear functions [34,35]. The nuclear localization of PTEN in mammalian cells is often associated with cell-cycle arrest in G1 and accompanied by decreased levels of ERK phosphorylation. Prior to vulval induction, the VPCs are maintained in a long G1 arrest lasting the entire L2 stage [36]. It is therefore possible that initially DAF-18 acts predominantly in the nucleus as a protein phosphatase that negatively regulates vulval induction. Indeed, Western blot analysis revealed elevated levels of dpMPK-1 in *daf-18(lf)* mutants, supporting our model that DAF-18 –directly or indirectly- blocks MAPK activation (Figure 6).

In humans, PTEN is one of the most frequently mutated tumor suppressor genes. However, not all disease phenotypes associated with loss of PTEN can be explained by hyper-activation of the Insulin pathway alone. Thus, PTEN must have other functions that are independent of its inhibitory activity in the Insulin pathway. Accordingly, Suzuki and Han [19] observed many synthetic phenotypes in *C. elegans daf-18(lf)* mutants, including embryonic lethality and sterility, which are independent of DAF-16 FOXO and do not involve DAF-2 InsR signaling. Our work highlights the importance of *C. elegans* DAF-18 PTEN in regulating a range of biological processes and may serve as a basis to better understand the multiple roles human PTEN plays during cancer initiation and progression. Thus, single mutations in the PTEN tumor suppressor may result in the simultaneous hyper-activation of several oncogenic signaling pathways.

Materials and Methods

General worm methods

Standard methods were used for maintaining and manipulating *Caenorhabditis elegans* [37]. Animals were cultured at 20°C and the wild-type strain is the Bristol N2 strain. Information regarding the mutants used in this study can be found on WormBase (http://www.wormbase.org). Mutations used according to their linkage group:

LG I: *daf-16(mu86)*, LG II: *age-1(mg44)*, *let-23(sy1)*, LG III: *daf-2(e1370)*, *mpk-1(ga117)*, LG IV: *let-60(n1046)*, *daf-18(ok480)*, *lin-3(e1417)*, *lin-45(sy96)*, LG V: *akt-1(mg144gf)*, *akt-1(ok525lf)*, LG X: *lin-2(n397)*, *sos-1(s1031)*, *unc-46(e177)* to cis link *sos-1(s1031)*, LG X: *lin-2(n397)*, *gap-1(ga133)*. Transgenes used: *syIs59[Pegl-17::cfp]*, *zhIs4[Plip-1::gfp]*, *zhEx382[daf-18 genomic]* *zhEx343[daf-18::gfp]*, *zhEx358[Plin-31::daf-18::gfp]*, *zhEx344[daf-18 G174E]*.

Plasmids and PCR fusion constructs

pIN05 (*daf-18 genomic wt*) was made by cloning the whole genomic fragment of *daf-18* starting 1.3 kb upstream of the ATG and ending 0.5 kb downstream of the STOP and cloning to pGEM-T. pIN03 (*daf-18 genomic G174E*) was made by fusion PCR [38] of two overlapping fragments of the whole genomic *daf-18* starting 1.3 kb upstream of the ATG and ending 0.5 kb

downstream of the STOP using primers which contain the mutation G174E (GGC to GAA) in the overlapping region and cloning to pGEM-T. pIN17 (*Plin-31::daf-18 cDNA::gfp::unc-54 3′UTR*) was made by amplifying *daf-18 cDNA::gfp* from a previously cloned plasmid with primers containing NotI sites on both ends, digestion with NotI and cloning into the NotI site of the pB253 plasmid containing the *lin-31* enhancer and promoter. The *daf-18 genomic* translational GFP reporter was made using fusion PCR of three parts by inserting a *gfp* cassette in frame between the last exon and the 3′ UTR into a genomic fragment encompassing 1.3 kb of 5′ regulatory sequences and the complete *daf-18* coding sequences. Sequences of the primers used for the different constructs can be found in Table S1.

Transgenic lines

Worms expressing extra-chromosomal transgenic arrays were generated by microinjection of DNA into young adult worms [39]. pIN03 (*zhEx344*), pIN05 (*zhEx382*) and pIN17(*zhEx358*) were injected at a concentration of 50 ng/µl. The fusion PCR *daf-18 genomic::gfp* (*zhEx343*) translational reporter was injected at a concentration of 30 ng/ul. Co-markers used were either pCFJ90 (Pmyo-2::mCherry) at a concentration of 2 ng/ul or pTJ1157 (Plin-48::gfp) at a concentration of 50 ng/ul. Final concentration of injected DNA was filled up to 150 ng/ul using the empty plasmid pBluescript-KS.

Fluorescence microscopy

DAF-18::GFP, P*lip-1*::GFP and P*egl-17*::CFP expression were observed under fluorescent light illumination with either a Leica DMRA microscope equipped with a cooled CCD camera (Hamamatsu ORCA-ER) or Olympus BX61 with Q Imaging Fast 1394 Retiga 2000R camera (Q Imaging Inc., Canada) controlled by the Openlab 5.x software (Improvision/PerkinElmer). Animals were mounted on 4% agarose pads in M9 solution with 20 mM tetramisole hydrochloride. Quantification of fluorescence levels was performed under the same picture acquisition settings for all conditions examined.

Vulval induction

Vulval induction was scored by examining worms at the L4 stage under Nomarski optics as described [40]. The number of VPCs that had adopted a 1° or 2° Vulval fate was counted for each animal and the induction index was calculated by dividing the number of 1° or 2° induced cells by the number of animals scored. Statistical analysis was performed using a t-test for independent samples.

RNA interference analysis

RNA interference analysis (RNAi) was performed by feeding animals dsRNA-producing bacteria as described previously [41]. Around 10 to 20 P0 animals at the L1 larval stage were transferred to plates containing RNAi bacteria grown on 3 mM IPTG. Vulval induction was scored in the F1 generation (or the P0 for *akt-2* RNAi) at the L4 larval stage to count the number of induced VPCs. *gfp*, *akt-2*, *piki-1* and *vps-34* RNAi clones were all taken from the Ahringer RNAi library.

Western blot analysis

Forty-five animals at the L4 stage were placed into 15 µl of 1× SDS sample buffer, lysed at 95°C for 5 min, centrifuged at 14,000 rpm for 2 min and the supernatant was loaded on 10% acrylamide gels, which were analyzed by Western blotting. Anti-phospho-MEK1/2 (S217/S221) and Anti-MEK1/2 (D1A5) antibodies were purchased from Cell Signaling Technology (Beverly, MA). Anti-di-phosphorylated ERK-1&2 (M8159) antibody was purchased from Sigma-Aldrich (St. Louis, MO), and anti-ERK 2 (K-23) antibody was purchased from Santa Cruz Biotechnology (Santa Cruz, CA). Quantification of the bands was performed using the gel quantification plugin in ImageJ software [42]. The ratios between phosphorylated and total MEK-2 and MPK-1 levels, respectively, were calculated and normalized for each independent experiment to the ratios measured in the *let-60(gf)* single mutants.

Supporting Information

Table S1 Primers used to generate the plasmids described in the manuscript.
(DOC)

Acknowledgments

We wish to thank members of our group for critical discussion and comments relating to this manuscript. We are also grateful to the *C. elegans* genetics center and S. Mitani (Japan Knockout Consortium) for providing strains, to Andrew Fire for GFP vectors, J. Ahringer for RNAi clones, Ian Chin-Sang for constructs, and David Reiner from Channing Der lab for constructs and discussion.

Author Contributions

Conceived and designed the experiments: IN MW AH. Performed the experiments: IN MW EF. Analyzed the data: IN MW AH. Contributed reagents/materials/analysis tools: IN MW EF. Wrote the paper: IN AH.

References

1. Li J, Yen C, Liaw D, Podsypanina K, Bose S, et al. (1997) PTEN, a putative protein tyrosine phosphatase gene mutated in human brain, breast, and prostate cancer. Science 275: 1943–1947.
2. Blumenthal GM, Dennis PA (2008) PTEN hamartoma tumor syndromes. Eur J Hum Genet 16: 1289–1300. doi:10.1038/ejhg.2008.162.
3. Liaw D, Marsh DJ, Li J, Dahia PL, Wang SI, et al. (1997) Germline mutations of the PTEN gene in Cowden disease, an inherited breast and thyroid cancer syndrome. Nat Genet 16: 64–67. doi:10.1038/ng0597-64.
4. Myers M, Pass I, Batty I, Van der Kaay J, Stolarov J, et al. (1998) The lipid phosphatase activity of PTEN is critical for its tumor supressor function. Proc Natl Acad Sci USA 95: 13513–13518.
5. Dey N, Crosswell HE, De P, Parsons R, Peng Q, et al. (2008) The protein phosphatase activity of PTEN regulates SRC family kinases and controls glioma migration. Cancer Res 68: 1862–1871. doi:10.1158/0008-5472.CAN-07-1182.
6. Cai X-M, Tao B-B, Wang L-Y, Liang Y-L, Jin J-W, et al. (2005) Protein phosphatase activity of PTEN inhibited the invasion of glioma cells with epidermal growth factor receptor mutation type III expression. Int J Cancer 117: 905–912. doi:10.1002/ijc.21251.
7. Myers MP, Stolarov JP, Eng C, Li J, Wang SI, et al. (1997) P-TEN, the tumor suppressor from human chromosome 10q23, is a dual-specificity phosphatase. Proc Natl Acad Sci USA 94: 9052–9057.
8. Tamura M, Gu J, Matsumoto K, Aota S, Parsons R, et al. (1998) Inhibition of cell migration, spreading, and focal adhesions by tumor suppressor PTEN. Science 280: 1614–1617.
9. Gildea J, Herlevsen M, Harding M, Gulding K, Moskaluk C, et al. (2004) PTEN can inhibit in vitro organotypic and in vivo orthotopic invasion of human bladder cancer cells even in the absence of its lipid phosphatase activity. Oncogene 23: 6788–6797. doi:10.1038/sj.onc.1207599.
10. Gu J, Tamura M, Pankov R, Danen EH, Takino T, et al. (1999) Shc and FAK differentially regulate cell motility and directionality modulated by PTEN. J Cell Biol 146: 389–403.
11. Hu PJ (2007) Dauer. Worm Book: 1–19. doi:10.1895/wormbook.1.144.1.
12. Christensen R, la Torre-Ubieta de L, Bonni A, Colón-Ramos DA (2011) A conserved PTEN/FOXO pathway regulates neuronal morphology during *C. elegans* development. Development 138: 5257–5267. doi:10.1242/dev.069062.

13. Fukuyama M, Rougvie A, Rothman J (2006) *C. elegans* DAF-18/PTEN mediates nutrient-dependent arrest of cell cycle and growth in the germline. Curr Biol 16: 773–779. doi:10.1016/j.cub.2006.02.073.
14. Mihaylova V, Borland C, Manjarrez L, Stern M, Sun H (1999) The PTEN tumor suppressor homolog in Caenorhabditis elegans regulates longevity and dauer formation in an insulin receptor-like signaling pathway. Proc Natl Acad Sci USA 96: 7427–7432.
15. Solari F, Bourbon-Piffaut A, Masse I, Payrastre B, Chan A, et al. (2005) The human tumour suppressor PTEN regulates longevity and dauer formation in Caenorhabditis elegans. Oncogene 24: 20–27. doi:10.1038/sj.onc.1207978.
16. Paradis S, Ruvkun G (1998) Caenorhabditis elegans Akt/PKB transduces insulin receptor-like signals from AGE-1 PI3 kinase to the DAF-16 transcription factor. Genes Dev 12: 2488–2498.
17. Cahill CM, Tzivion G, Nasrin N, Ogg S, Dore J, et al. (2001) Phosphatidylinositol 3-kinase signaling inhibits DAF-16 DNA binding and function via 14-3-3-dependent and 14-3-3-independent pathways. J Biol Chem 276: 13402–13410. doi:10.1074/jbc.M010042200.
18. Brisbin S, Liu J, Boudreau J, Peng J, Evangelista M, et al. (2009) A role for *C. elegans* Eph RTK signaling in PTEN regulation. Dev Cell 17: 459–469. doi:10.1016/j.devcel.2009.08.009.
19. Suzuki Y, Han M (2006) Genetic redundancy masks diverse functions of the tumor suppressor gene PTEN during *C. elegans* development. Genes Dev 20: 423–428. doi:10.1101/gad.1378906.
20. Sternberg PW (2005) Vulval development. Worm Book: 1–28. doi:10.1895/wormbook.1.6.1.
21. Battu G, Hoier E, Hajnal A (2003) The *C. elegans* G-protein-coupled receptor SRA-13 inhibits RAS/MAPK signalling during olfaction and vulval development. Development 130: 2567–2577.
22. Zou W, Lu Q, Zhao D, Li W, Mapes J, et al. (2009) Caenorhabditis elegans myotubularin MTM-1 negatively regulates the engulfment of apoptotic cells. PLoS Genet 5: e1000679. doi:10.1371/journal.pgen.1000679.
23. Ashrafi K, Chang FY, Watts JL, Fraser AG, Kamath RS, et al. (2003) Genome-wide RNAi analysis of Caenorhabditis elegans fat regulatory genes. Nature 421: 268–272. doi:10.1038/nature01279.
24. Kinchen JM, Doukoumetzidis K, Almendinger J, Stergiou L, Tosello-Trampont A, et al. (2008) A pathway for phagosome maturation during engulfment of apoptotic cells. Nat Cell Biol 10: 556–566. doi:10.1038/ncb1718.
25. Burdine RD, Branda CS, Stern MJ (1998) EGL-17(FGF) expression coordinates the attraction of the migrating sex myoblasts with vulval induction in *C. elegans*. Development 125: 1083–1093.
26. Berset T, Hoier E, Battu G, Canevascini S, Hajnal A (2001) Notch inhibition of RAS signaling through MAP kinase phosphatase LIP-1 during *C. elegans* vulval development. Science 291: 1055–1058. doi:10.1126/science.1055642.
27. Lackner MR, Kim SK (1998) Genetic analysis of the Caenorhabditis elegans MAP kinase gene mpk-1. Genetics 150: 103–117.
28. Chang C, Hopper N, Sternberg P (2000) Caenorhabditis elegans SOS-1 is necessary for multiple RAS-mediated developmental signals. EMBO J 19: 3283–3294. doi:10.1093/emboj/19.13.3283.
29. Tan PB, Lackner MR, Kim SK (1998) MAP kinase signaling specificity mediated by the LIN-1 Ets/LIN-31 WH transcription factor complex during *C. elegans* vulval induction. Cell 93: 569–580.
30. Sasaoka T, Kobayashi M (2000) The functional significance of Shc in insulin signaling as a substrate of the insulin receptor. Endocr J 47: 373–381.
31. Sasaoka T, Draznin B, Leitner JW, Langlois WJ, Olefsky JM (1994) Shc is the predominant signaling molecule coupling insulin receptors to activation of guanine nucleotide releasing factor and p21ras-GTP formation. J Biol Chem 269: 10734–10738.
32. Nanji M, Hopper N, Gems D (2005) LET-60 RAS modulates effects of insulin/IGF-1 signaling on development and aging in Caenorhabditis elegans. Aging Cell 4: 235–245. doi:10.1111/j.1474-9726.2005.00166.x.
33. Cui M, Chen J, Myers TR, Hwang BJ, Sternberg PW, et al. (2006) SynMuv Genes Redundantly Inhibit lin-3/EGF Expression to Prevent Inappropriate Vulval Induction in *C. elegans*. Dev Cell 10: 667–672. doi:10.1016/j.devcel.2006.04.001.
34. Planchon SM, Waite KA, Eng C (2008) The nuclear affairs of PTEN. J Cell Sci 121: 249–253. doi:10.1242/jcs.022459.
35. Weng LP, Brown JL, Eng C (2001) PTEN coordinates G(1) arrest by down-regulating cyclin D1 via its protein phosphatase activity and up-regulating p27 via its lipid phosphatase activity in a breast cancer model. Hum Mol Genet 10: 599–604.
36. Hong Y, Roy R, Ambros V (1998) Developmental regulation of a cyclin-dependent kinase inhibitor controls postembryonic cell cycle progression in Caenorhabditis elegans. Development 125: 3585–3597.
37. Brenner S (1974) The genetics of Caenorhabditis elegans. Genetics 77: 71–94.
38. Hobert O (2002) PCR fusion-based approach to create reporter gene constructs for expression analysis in transgenic *C. elegans*. Bio Techniques 32: 728–730.
39. Mello CC, Kramer JM, Stinchcomb D, Ambros V (1991) Efficient gene transfer in C.elegans: extrachromosomal maintenance and integration of transforming sequences. EMBO J 10: 3959–3970.
40. Sternberg PW, Horvitz HR (1986) Pattern formation during vulval development in *C. elegans*. Cell 44: 761–772.
41. Kamath RS, Fraser AG, Dong Y, Poulin G, Durbin R, et al. (2003) Systematic functional analysis of the Caenorhabditis elegans genome using RNAi. Nature 421: 231–237. doi:10.1038/nature01278.
42. Abramoff MD, Magalhães PJ, Ram SJ (2004) Image processing with ImageJ. Biophotonics international 11: 36–42.

4

General Discussion

4.1 Technical aspects

4.1.1 Optimization of protein complex purification from *C. elegans* extracts

In order to purify DEP-1 together with its physiological interaction partners, we initially used the Strep-Tactin-HA (SH) double affinity-purification technique that was recently developed at the ETH Zurich (Glatter et al., 2009). SH-purified DEP-1 was analyzed by LC-MS/MS, which led to the identification of an unexpected low number of proteins: From a total of 42 identified proteins, only three proteins are specific for DEP-1intraDA, and only seven for DEP-1full::HS. Further examination of these results showed that most of the identified proteins are highly abundant and they seem to be false-positive interactors of DEP-1. However, numerous peptides of DEP-1 were identified by LC-MS/MS analyses, why we conclude that the double affinity-purification of both DEP-1full::HS and DEP-1intraDA::HS was successful.

We assume that there are several reasons for these poor results. First, only a low amount of DEP-1 could be purified. The StrepTactin-purification led indeed to results as they were described in literature (Glatter et al., 2009), but a large amount of purified DEP-1::HS was lost during the subsequent HA-purification. This less efficient HA purification might be due to the fact that we were using an HS-tag in which the HA domain is not at the very end of the C-terminus but flanked by DEP-1 and StrepTactin, and thus less accessible to the monoclonal anti-HA-antibodies. Second, the molecular weight of DEP-1full::HS is with 158 kD relatively high, which complicated a purification of the intact protein. Third, the yield of purified proteins was too low to separate the samples by SDS-PAGE prior to tryptic digestion. Thus, the detergent originating form the lysis buffer could not be removed and attained to the mass spectrometer, which affected the measurements of LC-MS/MS. And fourth, proteins that have a weak binding affinity to DEP-1 might have been lost due to a too vigorous washing procedure.

To increase the yield of purified DEP-1 and thereby the number of interacting proteins which could be identified by LC-MS/MS, we performed single HA-purifications of DEP-1full::HS and DEP-1intraDA::HS instead of the StrepTactin-HA double affinity-purification. Thereby, the amount of purified DEP-1 was

increased dramatically, resulting in a three-fold increase in proteins detected by LC-MS/MS. Among the 332 proteins identified in two independent LC-MS/MS experiments, 50 proteins were not identified in the controls.
However, these results were still unsatisfactory. First, we had to use an enormous amount of protein extract (up to 100 mg) to get an adequate yield of purified DEP-1. This dramatically enhanced the risk of pulling-down high abundant proteins that would never interact with DEP-1 under physiological conditions. Second, loss of the second purification step made it even more difficult to remove all detergent from the sample. We tried to reduce the amount of detergent by extensive washing procedures, but its presence in the final eluate could not be avoided completely, resulting in suboptimal quality of the LC-MS/MS data. And third, proteins might have been lost due to this vigorous washing procedure and therefore could not be identified as DEP-1 interactors.
Taken together, both the StrepTactin-HA double and the HA-single purification methods of DEP-1intraDA and DEP-1full::HS worked in principle, but the yield of purified protein was not sufficient for a successful identification of DEP-1 interactors of by LC-MS/MS.

4.1.2 Identification of proteins by LC-MS/MS after GST purification of GST::DEP-1

We concluded from the previously described purification experiments that the success of the identification of interacting proteins by mass spectrometry depends on the yield of purified DEP-1. First, a higher amount of protein enables a fractionation by SDS-PAGE, which allows removing all detergent from the sample prior to tryptic digestion and analyses by LC-MS/MS. And second, increasing the yield of "bait" protein enhances the chance to identify lower abundant proteins because of its higher concentration in the sample.
Thus, we tried to further increase the amount of purified DEP-1 by expressing GST::DEP-1 fusion proteins in *E. coli* and to purify them with GST sepharose. Purification of GST-tagged proteins is a well-established method, and allows the purification of milligrams of proteins.
However, there are also a few drawbacks compared to the previously described method. First, the GST tag is with 26 kD much bigger than the HS-tag (5 kD) and might also modify DEP-1 and its activity. And second, a native expression of *C. elegans* DEP-1, a transmembrane protein with highly glycosylated extracellular domains, is not possible due to the lack of post-translational modification in bacteria. For this reason, we expressed not the full-length protein but only the intracellular domain of DEP-1 (DEP-1intrawt) as well as a version carrying the substrate trapping mutation D1241A (DEP-1intraDA) (Palka, 2002).
After extensive optimization of the conditions for protein expression and GST purification, we were able to receive high yields of purified DEP-1intra. Immobilized on GST-sepharose, DEP-1 was then incubated with total protein extract from mixed staged wild-type N2 worms to perform pull-down experiments. Since the high yield of DEP-1 allowed a fractionation by SDS-PAGE, we were able to use milder washing conditions without the risk of overloading the LC-MS/MS with too complex samples containing detergent.
As one would expect, Colloidal Coomassie Blue staining illustrated that more proteins bound to DEP-1intraDA rather than to DEP-1intrawt. In total, 585 proteins were identified, of which 97 were not present in the control fraction. Most prominent were three protein bands with a molecular weight of 90.1 kD, 135.9 kD, and 174.4 kD, which correspond to PAT-3, PAT-2, and NID-1 respectively.

By using GST- instead of HS-purified DEP-1, not only the quantity of identified proteins could be enhanced, but also its quality. On average, 5.07 peptides/protein were identified in the results of HA-purified DEP-1, whereas 10.93 peptides/protein were recognized in the GST-based approach. Furthermore, the average protein abundance decreased from 522.842 ppm (HA-purified DEP-1) to 378.8 ppm (GST-purified DEP-1), indicating that more low abundant proteins could be identified. We assume that this was due to milder washing conditions that were used during the GST-based pull-downs, and that no detergent was disturbing LC-MS/MS analyses.

4.1.3 LET-23 was not identified by LC-MS/MS

Although the EGF receptor LET-23 is a known substrate of DEP-1 (Berset, 2005; Jeon and Zinn, 2009; Tarcic et al., 2009) it was not identified by our MS-based approaches. This might be due to two reasons. First, LET-23 belongs with an abundance of 2.37 ppm to the lower abundant proteins of *C. elegans* proteome (average protein abundance = 75.62 ppm, PaxDB integrated dataset, pax-db.org). However, the average protein abundance of proteins identified in the GST pull-downs had a value of 378.8 ppm, indicating that it is more difficult to pull-down low-abundant proteins rather than high-abundant proteins, and especially to identify them by LC-MS/MS. The interaction of LET-23 and DEP-1 was performed with the same purified GST::DEP-1intraDA, but LET-23 was detected by a much more sensitive technique using antibodies (Berset, 2005).
Second, if two proteins with similar physical characteristics are simultaneously analyzed by LC-MS/MS, and if one of them exists in a much higher appearance than the other, only the more abundant protein is identified. Thus, the absence of a certain protein after LC-MS/MS analysis does not mean that it was not present in the sample.

4.1.4 Polyclonal DEP-1 antibodies

As an alternative to purify DEP-1 complexes, we performed co-immunoprecipitation using DEP-1 antibodies. Since there were no *C. elegans* DEP-1 antibodies available, we produced polyclonal DEP-1 antibodies that are directed against the intracellular domain of GST-tagged DEP-1.
First, immunoblot analyses with protein extracts of N2, *dep-1(lf);lip-1(lf)*, and *Peft-3::dep-1full::HS* worms as well as StrepTactin-purified DEP-1full::HS and DEP-1intraD1241A::HS showed that the affinity-purified antibodies derived from the rabbit 006-9AC-B07 were specific for DEP-1. However, in subsequent immunoblots that were done, the DEP-1 specific signal became weaker whereas other unspecific signals were enhanced (compare Fig. 3.10 A and B). We propose two reasons for these observations. First, the unspecific signals seems to correspond to proteins originating from *E. coli*, since the same signals also appear on immunoblots in which *E. coli* extracts were analyzed (data not shown). Because the protein extracts varies in their composition of *E. coli*, it could be possible that the samples used in the first western blot experiments contained less bacteria. To decrease the intensity of unspecific signal caused by *E. coli* proteins, it would be possible to perform pre-absorption with *E. coli* acetone powder, or to use worm protein extract from animals cleaned by sucrose-floating.
Another reason for the decrease in DEP-1 specific signal might be that the purified antibodies degraded

over time when they were stored at 4°C. Since other aliquots of affinity-purified DEP-1 antibodies are stored at -80°C, it would possible to thaw a new sample. In case the freshly thawed antibodies would as well not recognize DEP-1, a large amount of serum from the rabbit 006-9AC-B07 is stored at -80°C and could be processed again.

Immunostaining of *C. elegans* with DEP-1 antibodies led to the observation of a diffuse signal in some cells of the head region, in the vulva of a few L4 larvae, but never in the VPCs of Pn.px or Pn.pxx larvae. Since this expression pattern was very different from the expression pattern of DEP-1::GFP that was observed in the reporter line *zhEx112* (Berset, 2005), we assume that the expression is unspecific and stopped a further optimization of DEP-1 immunostainings. However, analyses of the reporter line *zhIs70* showed that DEP-1::GFP, which is not overexpressed, is also hardly visible in the VPCs prior to L4 larval stage, and strongly expressed in the head region.
Taken together, the polyclonal DEP-1 antibodies derived from the rabbit 006-9AC-B07 seem to work for western blot analysis, but it remains to be elucidated if they also work for immunostaining and Co-IPs.

4.1.5 Generation of endogenous DEP-1 reporters by using *MosTIC*

A novel transgene-instructed genome engineering technique called *MosTIC* (*Mos1* excision-induced transgene-instructed gene conversion) has been reported by (Robert et al., 2009), which allows the generation of endogenous reporters in *C. elegans*. Since this technique was not yet established in our laboratory, we tested three different approaches to build endogenous DEP-1::GFP and DEP-1::mCherry reporter lines.
In the first strategy A, we tried to identify *MosTic* engineered animals by a PCR-based screen in which the genomic DNA was extracted from half of the F2-F3 progeny and analyzed with primers specific for the inserted transgene. Although this approach was already performed in our laboratory to identify specific animals from a deletion mutant screen, it was not possible to identify *MosTic* engineered animals by this PCR-based screen. We assume that the complexity of genomic DNA increased so dramatically until the genomic DNA was extracted from the F2-F3 progeny, that a successful amplification by PCR was not possible.
To facilitate the identification of transgenic animals in our further approaches, we integrated in strategy B additionally to GFP or mCherry a *C. briggsae unc-119* rescue sequence as a co-injection marker. Screening for transgenic crawling animals under the dissecting scope allows the efficient identification of a single rescued worm among many others. Since *unc-119* was flanked by two FRT sites, the rescue sequence could be excised by FLP-FRT site directed recombination. Despite expressing FLPase under three different promoters, we were not able to identify a strain in which the *unc-119* rescue sequence was excised. This might be due to several reasons. First, the activity of *Phsp-16-48* in the germline might have been too low, why FLP-FRT mediated recombination was only promoted in somatic cells. Second, we have no evidence that the FLPase under *Pglh-2* (pMW26) and *Peft-3* (pMW27) was functional. Third, germ cells are very efficient in silencing genes present in multi-copy (Kelly et al., 1997). Thus, if the concentration of the micro-injected plasmids was too high, they might have been silenced. A strategy that might prevent silencing of the FLPase due to multi-copy arrays would be the creation of a transgenic line, in which a single-copy of *Peft-3::FLPase* is integrated into the genome of *C. elegans* by *MosSCI* (Frøkjær-Jensen et al., 2008).

Fourth, the efficiency of FLP-FRT site directed recombination in the germline might be in general very low. And fifth, we might not have been able to identify the respective animals among the large number of crawling siblings.
As in Strategy B, the repair construct used in strategy C contained a *C. briggsae unc-119* rescue sequence. However, *unc-119(+)* was not flanked by FRT sites and the *dep-1 3'UTR* was cloned in front of the rescue sequence. Micro-injection into *ttTi25065;unc-119(lf)* animals led immediately to the identification and isolation of strains in which a GFP- or mCherry- tag was integrated into the locus of *dep-1*. However, an insertion of the *unc-119* rescue construct is only possible if the position of the *Mos1* transposon is located at the *3'* end of the gene locus of interest. Otherwise the *unc-119* rescue sequence is affecting the gene of interest and prohibits the translation of a functional protein.
Tagging of DEP-1 with GFP and mCherry using *MosTIC* was ideal because the *Mos1* insertion was present at the *3'* end of *dep-1*. However, for many genes no *Mos1* insertions are available, or the position of the *Mos1* insertion does not allow the creation of a functional reporter line. In these cases a newly developed technique called CRISPR-Cas9 can be used, which allows the creation of customized double-strand breaks (Chen et al., 2013).

4.1.6 Expression patterns of DEP-1 reporter lines

To analyze the expression pattern of DEP-1, four different reporter lines have been built. First, a transcriptional *Pdep-1::GFP* reporter *zhIs10[Pdep-1Δpes::nls::gfp::lacZ, unc-119(+)]*. Second, the translational DEP-1::GFP reporter line *zhEx112* (Berset, 2005), in which the plasmid pTB24 is present as extrachromosomal repetitive structures. Third, the *MosTic* engineered DEP-1::GFP (*zhIs70*) reporter line, whereas the GFP tag was introduced directly into the endogenous *dep-1* locus. And fourth, the DEP-1::mCherry (*zhIs71*) reporter line, which was also made by *MosTIC* integration. In all three translational reporter lines, the GFP/mCherry tag was cloned in front of the stop codon at the 5' end of *dep-1*, resulting in a functional fusion protein.
Since DEP-1 is a transmembrane protein tyrosine phosphatase, we expected its expression predominantly at the cell membrane of the VPCs. However, most of the extrachromosomal DEP-1::GFP reporter *zhEx112* is expressed intracellularly with accumulations in the endoplasmatic reticulum (ER), but not at the cell membrane (Berset, 2005). This might be due to overexpression of DEP-1::GFP, leading to misfolding of the protein and therefore in accumulation in the ER.
In contrast, the endogenous reporter line *zhIs70* showed an expression of DEP-1::GFP at the cell membrane of the VPCs, particularly at the apical side as well as in intracellular vesicles. We have to clarify that a clear observation of DEP-1::GFP at the apical side was complicated by a strong auto fluorescence signal of the cuticle that could not be decreased by optical filters in the spinning-disc microscope that was used. However, an apical expression pattern of DEP-1::GFP stands in accordance with immunohistochemistry data performed in human cells, in which DEP-1 tends to be expressed specifically at the apical surface of polarized cells (Autschbach et al., 1999), such as in breast epithelia, in which PTPRJ is predominantly localized to the apical surface of luminal epithelial cells of alveoli and both small and large ducts (Smart et al., 2012).

In contrast to the apical expression of DEP-1::GFP in the VPCs of *zhIs70* animals, DEP-1::mCherry expression was clearly enhanced in intracellular punctae of both the VPCs and the head of *zhIs71* animals.

Since it has been reported that mCherry has the ability to aggregate when it is expressed within some fusions (Katayama et al., 2008), we assume that the size of these intracellular punctae are not physiological. An aggregation of mCherry enables the observation of very weak expression levels, which would not be detectable by analyzing GFP-tagged reporters. However, it is alarming how different mCherry and GFP behave, even if the copy number and loci of integration is the same.
Another difference in the expression of DEP-1 between the extrachromosomal (*zhEx112*) and endogenous (*zhIs70*) DEP-1::GFP reporter lines could be observed in the head and tail of *C. elegans*. In animals of the line *zhEx112*, DEP-1 is expressed in a few neuronal cells and in *hyp7* cells of the head, but also in the B and Y cells of the posterior hindgut. In contrast, the expression of endogenous DEP-1::GFP in the line *zhEx70* is much more multifaceted, particularly in numerous neurons in the head and the tail. Interestingly, expression of DEP-1 in these neuronal cells was clearly cytoplasmic.
The cause of these different expression patterns of DEP-1::GFP in the extrachromosomal and endogenous DEP-1 reporter lines might be the following. Although 4.5 kb of the *dep-1* upstream region were present in the extrachromosomal DEP-1::GFP reporter, several cis- and trans- regulatory elements as well as the native *dep-1 3' UTR* were only present and completely functional in the endogenous DEP-1::GFP reporter lines *zhIs70* and *zhIs71*. Thus, we assume that the expression pattern of DEP-1::GFP in the *MosTic* engineered lines *zhIs70* and *zhIs71* is closer to the real physiological expression of DEP-1, rather than the expression of DEP-1::GFP in *zhEx112*.

4.2 Role of DEP-1 in integrin regulation

4.2.1 Significance of integrins and EGFR signaling in cancer formation and metastasis

The ability of metastatic cells to spread throughout the body and to invade other tissues is one of the hallmarks of cancer (Hanahan and Weinberg, 2011). Metastasis premises several sequential and obligatory steps that must be completed, such as detachment of the cancer cell from its neighboring cells, degradation of the basement membrane, proliferation in foreign microenvironments, invasion into other tissues, and the ability to induce angiogenesis. To obtain these capabilities, cancer cells must degrade or remodel all the ECMs that impose barriers to their dissemination. This remodeling of the ECM, but also other cellular functions crucial to the initiation, progression and metastasis of solid tumors is controlled among others by integrins (Desgrosellier and Cheresh, 2010; Guo and Giancotti, 2004).
Specific integrin heterodimers are connecting the ECM to the cytoskeleton and mediate thereby the adherence to other cells. Hence, misexpression of integrins can render cancer cells more motile, invasive, and resistant to anticancer drugs (Desgrosellier and Cheresh, 2010; Makrilia et al., 2009).
In breast carcinoma, for example, it has been observed that overexpression of β1 integrins causes disruption of adherens junctions (Gimond et al., 1999). However, the expression levels of β1 and some other integrins can also be decreased in tumor cells which potentially increase tumor cell dissemination (Desgrosellier and Cheresh, 2010; Kren et al., 2007; Mattila et al., 2005; Ramirez et al., 2011).
Thus, expression of integrins is correlated with cancer progression in various tumor types and can be used as a molecular marker to improve diagnostic accuracy and to predict the metastatic potential of carcinomas (Friedrichs et al., 1995; Hieken et al., 1996; Liu et al., 2013; McCabe et al., 2007; Nip et al., 1992).

As discussed previously (see section 3.1.8), integrin trafficking by endosomal pathways influence their function and modulates integrin distribution and function (Pellinen, 2006). Several members of the Rab family, which regulate integrin and growth factor receptor recycling, are aberrantly expressed in various cancer types, resulting in enhanced growth factor signaling (Caswell et al., 2008).Thus, deregulation of integrin trafficking is closely related to cancer development and progression (Mosesson et al., 2008; Ramsay et al., 2007).
Another hallmark of cancer is induced angiogenesis, which enables the tumor to be provided with sufficient nutrients and oxygen (Hanahan and Weinberg, 2011). In the past years, some of the key molecular mechanisms that regulate angiogenesis have been specified. Several data implicate thereby that integrin signal transduction plays an important regulatory role in angiogenesis (Avraamides et al., 2008). These important contributions of integrins to the biology of cancer cells have made integrins appealing targets for cancer therapy. One drug that is currently tested in clinical trials is Cilengitide. This cyclic pentapeptide that inhibits ligand binding to αv integrins could inhibit tumor growth in patients with glioblastoma (Mas-Moruno et al., 2010). However, also other antagonists of several integrins, including αvβ3, αvβ5 and α5β1, are currently under investigations for cancer therapeutics (Avraamides et al., 2008).

Not only integrins contribute to tumor formation and metastasis, but also members of the epidermal growth factor family, including EGFR and ERBB2. In many carcinomas, including breast and pancreatic cancer, increased expression and hyperactivation of EGFR have been observed (Normanno et al., 2006), leading to enhanced activity of oncogenic signaling pathways. Different mechanisms can cause an oncogenic behavior of growth factors. For example, expression of a high number of receptors on the surface of tumor cells can increase their sensitivity to low concentrations of growth factors (Olayioye et al., 2000). Furthermore, mutations in the receptor or in proteins involved in intracellular signal transduction can explain the oncogenic role of growth factor receptors (Voldborg et al., 1997). Since aberrant activity of EGFR plays a key role in the development and growth of tumor cells, distinct therapeutic approaches, such as monoclonal antibodies, are currently employed for targeting EGFR in various human cancers (Ennis et al., 1991; Seshacharyulu et al., 2012).
There is increasing evidence supporting a central role of a crosstalk between integrins and growth factors, which is essential for many aspects of tumor progression (Desgrosellier and Cheresh, 2010). This interplay not only regulates tumor cell adhesion, migration, invasion and survival, but also affects many aspects of the host response to cancer (Desgrosellier and Cheresh, 2010). As discussed previously (see section 3.1.8), numerous mechanisms revealed a connection between integrins and RTKs playing a central role in many aspects of tumor progression in pancreatic, breast, colon, and hepatocellular carcinomas (Desgrosellier and Cheresh, 2010; Guo et al., 2006; Pouliot et al., 2001; Ricono et al., 2009; Yang et al., 2003).
For example, studies have shown that integrin ligation can induce EGFR phosphorylation independently of EGF, which crucially influences tumor cell susceptibility to treatment (Moro, 2001).

The receptor protein tyrosine phosphatase DEP-1 plays an essential role in regulating a variety of growth factor receptors, such as EGFR, VEGF, HGFR, and PDGFR, and regulates cell proliferation and differentiation (Grazia Lampugnani et al., 2003; Kovalenko et al., 2000; Takahashi et al., 2012; Tarcic et al., 2009). DEP-1 is down-regulated in numerous cancer cells in correlation with their malignant phenotype, and loss of heterozygosity at DEP-1 has been frequently observed in human cancers (Ruivenkamp et al., 2003;

Zhang et al., 1997). Data showing that restoration of DEP-1 expression in culture and *in vivo* suppresses tumor cell growth (Trapasso et al., 2006) further support the prominent role of DEP-1 as a tumor suppressor. In conclusion, both integrins, EGFR signaling and DEP-1 play essential roles in the modulation of tumorigenesis. By showing that DEP-1 activates PAT-3 by dephosphorylation and that activated integrins negatively regulate RAS/MAPK during vulval development, we could identify a so far unknown mechanism that contributes to a further knowledge of how these pathways are regulated. This basic research is premise for a further understanding of cancer formation and tumor invasion, but also for the development of novel cancer therapeutic drugs. However, our observations also emphasize the need for further research focused on the molecular mechanisms connecting DEP-1, the integrins, and RAS/MAPK signaling.

4.2.2 Outlook: Characterizing the exact role of PAT-2/PAT-3 in RAS/MAPK signaling

In section 3.1 we report the identification of the *C. elegans* β-integrin subunit PAT-3 in a mass spectrometry-based approach as a novel substrate of the tyrosine phosphatase DEP-1. Using biochemical and genetic epistasis analyses, we found that PAT-3 acts as a negative regulator of RAS/MAPK signaling during vulval development, and that DEP-1 binds to the highly conserved NPxY motif of the PAT-3 cytoplasmic tail to regulate its activity. However, there are still several open questions to be answered, and further research on the molecular mechanisms connecting DEP-1, the integrins, and RAS/MAPK signaling is needed.

One of the most important questions to be solved is how the integrins PAT-2/PAT-3 are connected to the RAS/MAPK signaling pathway. As discussed previously, there are numerous possibilities how integrins can be linked to RAS/MAPK signaling (see section 3.1.8). However, the complexity of the two multifaceted pathways complicates the identification of the connecting molecular mechanism. A central question is if integrins do regulate the EGF receptor LET-23 themselves, or if they regulate downstream components of the RAS/MAPK pathway affected such as RAS/LET-60.
One possibility to answer this question is to perform more epistasis analysis, for example by vulva-specific knock-down of PAT-2 or PAT-3 by RNAi in *let-23(gf)* animals. If this led to an enhanced vulval induction, it would show that integrins act in parallel or downstream of LET-23.
A similar conclusion could be drawn when *dep-1* is knocked-down by RNAi in *let-23(gf);pat-3(lf)* animals, in which *pat-3* with disrupted NPxY motifs is expressed. If this altered the induction of VPCs compared to control RNAi treated mutants, it would suggest that integrins negatively regulate EGFR/RAS/MAPK signaling via DEP-1 activity. However, if *dep-1* RNAi did not change the number of induced vulval cells, it would indicate that the integrins negatively regulate more downstream components of the RAS/MAPK pathway.
Another way to test if integrins inhibit the EGF receptor is to analyze the intracellular dynamic of LET-23. If RNAi against the integrins altered the localization and/or dynamic of LET-23::GFP, it would give evidence that PAT-2/PAT-3 regulate the activity of LET-23. As an alternative to RNAi, one could also test if *pat-3* with disrupted NPxY motifs alters the dynamic of LET-23.

Talin is one of the most important adaptor proteins of PAT-3 and binds with high affinity to the non-phosphorylated NPxY motif to trigger integrin activation (Critchley, 2000; Tadokoro et al., 2003). Since

C. elegans talin (TLN-1, UNC-35) co-localizes with PAT-2 and PAT-3 (Moulder et al., 1996), and because reduction of talin leads to phenotypes that are also observed with depletion of *pat-2* and *pat-3* (Cram et al., 2003), it would be conceivable that talin is a linker of activated integrin and the RAS/MAPK signaling pathway.
To test this hypothesis, one could knock-down *tln-1/unc-35* specifically in the vulva of *let-60(gf)* animals and examine the number of induced vulval cells. If the same increase in vulval induction was observed as when PAT-3 is knocked-down, it would suggest that TLN-1/UNC-35 is downstream of PAT-3 and a linker of integrins and RAS/MAPK signaling.

Another important question is if DEP-1 regulates integrin trafficking. As described earlier, we hypothesize that loss off *dep-1* causes enhanced apical and intracellular expression of PAT-3::GFP. However, due to the limits of optical resolution we have not yet been able to quantify these changes. A method that should enable the quantification of putative differences in integrin trafficking caused by DEP-1 is fluorescence recovery after photobleaching (FRAP) analysis, which one could perform in *pat-3*::GFP (*qyIs43*) and *pat-3::GFP;dep-1(lf)* (AH2916) animals.
In addition, we plan to analyze animals that express PAT-3::GFP with disrupted NPxY motifs. If mutated NPxY altered the localization of PAT-3::GFP, it would give further evidence that they play a crucial role in integrin trafficking.

Finally, it would be of big interest to determine if the interaction between DEP-1 and PAT-3 is also conserved in human. To determine this, it first has to be tested in which cell lines DEP-1/CD148 and β1 or β3 are expressed. Subsequently, one could perform pull-down experiments to confirm a possible interaction of human DEP-1/CD148 with β-integrins. Furthermore, it would be worth to test if reduction of β1 or β3 by siRNA affects the level of RAS/MAPK signaling in human cell lines. However, the analyses of integrins in cell culture might not be that trivial since 24 distinct α/β heterodimer combinations are formed by 18 α-subunits and 8 β-subunits, which all differ in their functionality.

5

Materials and Methods

5.1 DNA Methods

5.1.1 PCR

Amplification of PCR fragments was performed with Phusion® High-Fidelity DNA Polymerase (NEB), Taq DNA Polymerase (Invitrogen), or LongAmp® Taq DNA Polymerase (NEB) according to the manufacturer's protocol using the following PCR-mixes and cycle programs.

Phusion® High-Fidelity DNA Polymerase (NEB)

Component	20 µl reaction
5X Phusion HF Buffer	4 µl
2 mM dNTPs	2 µl
2 mM forward Primer	2 µl
2 mM reverse Primer	2 µl
Template DNA	variable
Phusion DNA Polymerase	0.2 µl
dH_2O	to 20 µl

Cycles	Temperature	Time
1x	98°C	30 sec
30x	98°C	10 sec
	58°C	30 sec
	72°C	30 sec/kb
1x	72°C	5-10 min
	12°C	∞

Taq DNA Polymerase (Invitrogen)

Component	20 µl reaction
10X PCR Buffer (minus Mg)	4 µl
2 mM dNTPs	2 µl
50 mM $MgCl_2$	0.8 µl
2 mM forward Primer	2 µl
2 mM reverse Primer	2 µl
Template DNA	variable
Taq DNA Polymerase	0.8 µl
dH_2O	to 20 µl

Cycles	Temperature	Time
1x	94°C	3 min
30x	94°C	45 sec
	58°C	30 sec
	72°C	1 min/kb
1x	72°C	10 min
	12°C	∞

LongAmp® Taq DNA Polymerase (NEB)

Component	20 µl reaction
5X LongAmp Taq Reaction Buffer	4 µl
2 mM dNTPs	2 µl
2 mM forward Primer	2 µl
2 mM reverse Primer	2 µl
Template DNA	variable
LongAmp Taq Polymerase	0.8 µl
dH_2O	to 20 µl

Cycles	Temperature	Time
1x	94°C	2 min
30x	94°C	30 sec
	58°C	30 sec
	65°C	50 sec/kb
1x	65°C	10 min
	12°C	∞

PCRs were run in 0.2 ml Multiply®Pro Tubes (Sarstedt) or sealed 96-well plates on the BioRad MyCycler Termocycler. Thereafter, 2-4 µl of the PCR product was loaded together with 4 µl of PCR-loading buffer on a 1% agarose gel (containing 50 µl 2 µg/ml Ethidium bromide per 50 ml agarose solution) and was run for approximately 20 minutes at 120 V. With a UV-light picture, the quality of the PCR was determined.

5.1.2 Oligonucleotides

The primers, ordered from Microsynth AG (www.microsynth.ch), were kept in a 100 µM stock solution diluted in TE at -20°C. For the PCR reactions, the primers were further diluted with dH_2O to a final concentration of 2 µM. All primers mentioned below are listed from 5' to 3'.

bar-1

OMW 71	CCTTCTAGGAATAGTCGATTTCCTGCAGGTCGACTCTAGAGGATC
OMW 72	GGAATGTGCAACAAATATCCGACTG
OMW 185	GTAACGCATCCCAGTTTTCTG

dep-1

OMW 42	TTTGGCCGGCCGATTCACTGACAACATCGGCTGAGC
OMW 43	AAATTAATTAACTATAGCAATGGGATTGCTGGAGTTGC
OMW 44	TTTGGCCGGCCAATCGAACAAAGAAAGCGAGACTCGC
OMW 45	AAATTAATTAATCAAAATCCCGATTCGACAATCAT
OMW 46	GGCGCTTTCGTAAAGCGTTTTCC
OMW 47	CTGATATTCAAGTCGCTGAGCAC
OMW 48	GTTTCAGCTTCGTCCCCTTCCAC
OMW 49	CCCGTATTCGCGAAGAATCTTG
OMW 50	CGCATTACGCAGTTAATGTGAC
OMW 51	CGGAAACCACAGCTGACGAATC
OMW 52	CTGTAGCTGCATCGGAATTGCC
OMW 53	GGAAAACGCTTTACGAAAGCGCC
OMW 54	GTGCTCAGCGACTTGAATATCAG
OMW 55	GTGGAAGGGGACGAAGCTGAAAC
OMW 56	CAAGATTCTTCGCGAATACGGG
OMW 57	GTCACATTAACTGCGTAATGCG
OMW 58	GATTCGTCAGCTGTGGTTTCCG
OMW 59	GGCAATTCCGATGCAGCTACAG
OMW 60	GAGAACGTTTCGATTTTTCGATTTCTTCGATGGCAAATGAG
OMW 61	CATATCAAATTATTGCGACTGTTCAAAAAGGCGGTCAAG
OMW 62	GAAGCATATCAAATTATTGCGACTGTTCAAAAAGGCGGTCAAGTCTCTG
OMW 65	TTTGGCGCGCCAGGATGATACGCTGGAAGTACGAAC
OMW 66	AAAGGCCGGCCAAATCCCGATTCGACAATCATTTG
OMW 67	AAAGAGCTCTCAAAATCCCGATTCGACAATCATTTG
OMW 68	GGTCAAATGATTGTCGAATCGGGATTTGGCCGGCCACCAGCACAGTGGCGGCC
OMW 69	AAAGGCCGGCCTAGCAATGGGATTGCTGGAGTTGC
OMW 70	GGCGCGCCAGGATGAATCGAACAAAGAAAGCGAGACTCGC
OMW 77	GCATTATATGGCATGGCCTGCTTTTGGAGCCCCGTCTCATCC
OMW 78	GCTCCAACGATAGTGCATTCCAGTGCTGGAGTTGGTCGTTC
OTB 94	GTCGACGGATTTTGAACCATTGGGTCG
OMW 121	TTTTTCTACCGGTACCCTCCAAGGG
OMW 128	GAATTCCTAAAACGTGAGTGATCAG
OMW 129	GAGAGCTTAGAACTGGCGAAGTCAC
OMW 130	GCTTACAGACAAGCTGTGACCGTCTC
OMW 131	CATTTTTTCTACCGGTACCCTCCAAGGGTCCTCC
OMW 132	GGAGGACCCTTGGAGGGTACCGGTAGAAAAAATGGTCTCAAAGGGTGAAGAAG
OMW 188	CAAATTGCAGACTCGCAGCGGCAG
OMW 189	GTTGAAGTAGATGTTGGAGACGGAG
OMW 190	CAAAAATGTAGAGAAGGGGTTTCTCTCTATTTGTATAGTTCATCCATGCC
OMW 191	CTCCGTCTCCAACATCTACTTCAAC
OMW 192	GACACTTGTGGCTGGACGACTTGC
OMW 193	GAACCTGACTTACCAGTGTATCGG
OMW 194	AGAGAAACCCCTTCTCTACATTTTTG
OMW 195	CTCCGGATACTTACCTCTTTCTAGTC
OMW 196	CTGTAAGATCCCTAGGTTACCCTC

OMW 197	CTCGAAAGAGAAAGAGTCGCAGTGG
OMW 198	GCAGGAAATCCTATAGAGCTTGTGGG
OMW 199	CAAAAATGTAGAGAAGGGGTTTCTCTCTACTTATACAATTCATCCATGCCACCTGTCG
OMW 200	CAAAAATGTAGAGAAGGGGTTTCTCTG
OMW 203	GTATATCAAATTGCAGACTCGCAGCG
OMW 204	CCATGACAGTACTTGCAGCTGATTCG
OMW 205	GATGATGGCAGAGAGAGCCGCTG
OMW 206	GAGGACGACTTCCGACACTTGTGG
OMW 208	GCCTGCAAATGTCTTCGGAACATTC
OMW 210	CTGCCTACCGCTAACTTAATCCTGG
OMW 211	CATCGACGACGAGTTCCAACTCGC
OMW 217	CACATGTTCTTTCCTGCGTTATCCC
OMW 218	CCTTTGAGTGAGCTGATACCGCTC
OMW 219	GGACTTGGATAAATTGGCTCAAAGCTGTAAGATCCCTAGGTTACCCTCC
OMW 222	CTACTTATACAATTCATCCATGCCACCGTAAGATCCCTAGGTTACCCTCCTG

dpy-19

OMW 223	GCAGTAGAGAATGGAATCAGATCC
OMW 224	CTTGCATTTCTGTACCGCCCATTC

eft-3

OMW 161	GCTTGCATGCCTGCAGGTCGACG
OMW 162	CCGCTAGCCAAGGGTCCTCCTG

FLP recombinase

OMW 212	GGTTAGTTCAGCAGCACATAATGC
OMW 213	CAATACCTGATCACTACTTCGCAC
OMW 214	CAGGAGGACCCTTGGCTAGCGGATGCCACAATTTGGTATATTATG
OMW 215	GTGCGAAGTAGTGATCAGGTATTG

gfp

OMW 73	TTTGGCGCGCCAGGATGAGTAAAGGAGAAGAACTTTTCAC
OMW 74	AAAGGCCGGCCTTTGTATAGTTCATCCATGCCATGTG
OMW 75	GGCATGGATGAACTATACAAAGGCCGGCCACCAGCACAGTGGCGGCCGCTCG
OMW 79	CTACGATATTGCATCAAGACAGCG
OMW 80	CATTTTTTCTACCGGTACCCTCCAAG
OMW 83	CCGCAGTTCGAAAAAGCGGCCGATATGAGTAAAGGAGAAGAACTTTTCAC
OMW 84	GTGGGCAGATCTTCGAATGCATCG
OMW 86	CATTTGGAGTCACATGTTGGGAG
OMW 87	CTAGTTGAACGCTTCCATCTTC
OMW 116	CAATCAGGGACGTCACGGACAAATGATGAGTAAAGGAGAAGAACTTTTCAC
OMW 117	GTAAAGAATAAGGAACAAAAAATGGAAAATACTATTTGTATAGTTCATCCATGCCATGTG
OMW 125	GTTATTGTCTCATGAGCGGATAC
OMW 209	CAGACAACCATTACCTGTCCACAC

HA-Strep-III

OMW 63	TTTGGCCGGCCACCAGCACAGTGGCGGCCGCTCG
OMW 64	AAATTAATTAATCAATCGGCCGCTTTTTCGAACTGCG
OMW 81	CTTGGAGGGTACCGGTAGAAAAAATGGGCCGGCCACCAGCACAGTGGCGGCCGC
OMW 82	ATCGGCCGCTTTTTCGAACTGCGG

let-60

OTS 38	TCATTCTCCGTCGTCTTC
OTS 39	CATTTTTTTCAGTTCCAGCC

lin-31

OMW 155	CTTCCCAATTACCGTACCAGTGTC
OMW 156	GACACTGGTACGGTAATTGGGAAG
OMW 157	GGGTCCTTTGGCCAATCCCGGG
OMW 158	CTGAGCTCAGAGCGAATTCTGATC
OMW 159	CATTACAATTTCCGATCACATTGC
OMW 160	GCAATGTGATCGGAAATTGTAATGGATTAGGGTGAATGGAGGGTGTTTG
OMW 175	GTCATTCAACGACTGCTTCATCAAG
OMW 176	CTTCTAAGGCTTGGCTTCTCAAAC

lip-1

OIR 4	CTCACCTACCGAGCACATC
OIR 5	CTCGTCTTGTTCACTGTCG
OIR 6	GAGGTGACGCCGAACAGC

mCherry

OMW 122	CCCTTGGAGGGTACCGGTAGAAAAAATGGTCTCAAAGGGTGAAGAAG
OMW 123	TAGCATTCGTAGAATTCCAACTGAGC
OMW 124	GCTCAGTTGGAATTCTACGAATGCTACTTATACAATTCATCCATGCCACCTGTCG
OMW 201	GGTGGCATGGATGAATTGTATAAGTAGGAAGTTCCTATTCTCTAGAAAGTATAGGAACTTCCTTTGAGCCAATTATC-CAAGTCC
OMW 202	CTACTTATACAATTCATCCATGCCACC

mos1

OJL 115	GCTCAATTCGCGCCAAACTATG
OJL 116	GAACGAGAGGCAGATGGAGAGGC

myo-3

OMW 37	TTCCGGCTCGTATGTTGTGTGG
OMW 38	GGGTGCAGACAGACATACGGACTCTACCGGTACCCTCCAAGGG

nid-1

OMW 139	GGAGCAATATCAGGAAGAGTTCCC
OMW 140	CAGCTACAGCCTGCATTCTTCCG
OMW 141	GCCCTCTCCACTCAATTACCCATC
OMW 142	GTGCAGTTAAGTCAATATTGGGCG
OMW 143	CATTTCACCTGAAATACCAATATTC
OMW 144	CAGAGAATTGCCGCAGATGCTAG
OMW 145	GCATCCCTTCACTTTGACATTGTC
OMW 146	CCTGACACAACCTAAAGTTCAGTC
OMW 147	AGAGCTTTAATTTTCTCCCTCATTTGC
OMW 148	GGACAATGTCAAAGTGAAGGGATGCAGCTTGCATGCCTGCAGGTCGAC
OMW 149	GCAAATGAGGGAGAAAATTAAAGCTCTCTATTTGTATAGTTCATCCATGCC
OMW 150	GCAGCTTTCGATGTAATCGTTAGAG
OMW 151	GATTGTCCGTGTTGGCGACGATCG
OMW 152	GAATATTGGTATTTCAGGTGAAATGAGTAAAGGAGAAGAACTTTTCACTG

pat-2

OMW 88	GGTTACTGTAGCTCCAAAATTCTG
OMW 89	CTGATCAAGTATAGATCAAGACCGG
OMW 90	CATTTGTCCGTGACGTCCCTGATTG
OMW 91	CAATCAGGGACGTCACGGACAAATG
OMW 92	CAATCAGGGACGTCACGGACAAATGCTAATGGTCTCAAAGGGTGAAGAAG
OMW 93	GAATAAGGAACAAAAAATGGAAAATATTACTTATACAATTCATCCATGCCACC
OMW 94	CGAATCATCTCAGCCAATTGCTTG

OMW 95	GATGGTCAGATTCAAGCAATTGGC
OMW 118	TATTTTCCATTTTTTGTTCCTTATTCTTTAC
OMW 119	CTACTGGAAATTTGGAATTCGG
OMW 120	CCGAATTCCAAATTTCCAGTAGATGCGAGAGGGTAGTTTTCCGCG
OMW 163	CAGGAGGACCCTTGGCTAGCGGATGCGAGAGGGTAGTTTTCCGCGAAGG
OMW 164	GGAGCAAGCATAAACTGCTCCAGG
OMW 165	GTTACCAGCCATGTGATGAACCAC
OMW 166	GTGGTTCATCACATGGCTGGTAACGCAATTGCTTCTGAAGAAGGAAGAG
OMW 167	GTGGTTCATCACATGGCTGGTAACAGGTGTGGTTTCTTCAAACGTAATCGTC
OMW 173	CAATCAGGGACGTCACGGACAAATGCTAGCGGCCGCCATCTTTTACCC
OMW 179	GAGCTCATGCGAGAGGGTAGTTTTCCGCG
OMW 180	GGTCGACCATGGAACAGGTAGTTTTCCAG
OMW 187	GGTCAGATTCAAGCAATTGGCTGAG

pat-3

dnI-F 1	TCCTCTTCATTCGCCGTCCAAGATGCG
dnI-R 1	TCACCTTCCACTGAGCCTCAAACC
OMW 96	CGTTTGACAGCAAGATATAGCCCG
OMW 97	GCAGGTTTTGGTGGAGAATTCTGC
OMW 98	GTTGGCTTTTCCAGCGTATACTGG
OMW 99	CCAGTATACGCTGGAAAAGCCAACATGGTCTCAAAGGGTGAAGAAG
OMW 100	GGGAAAATTATTAAAATATAAGGATAAAAACTATCTTATACAATTCATCCATGCCACC
OMW 101	ATAGTTTTTATCCTTATATTTTAATAATTTTCCC
OMW 102	CATGTCTTCTCAGATAGTTATGGC
OMW 103	GAATGCTTTCTGTGCACTTGGATG
OMW 104	GTTGCCACCTGTTGAAAGCAG
OMW 105	CGACGAGAAGAAGCCATATGCC
OMW 106	GACCGCTGCGACTCGAAAACTTG
OMW 107	GGCGTTGGCTTGTAATGTAAGTGG
OMW 108	CAAATGCTTCAGAAGGACTCAAGC
OMW 109	CTACAATATTGCCCTCGCCGTGC
OMW 110	GACCTGGAATGAGTACTGCTGC
OMW 111	CTAACGAATCAGCAATCTGTGAGG
OMW 112	CCTGTTGAGGAATTACCCAGTAAG
OMW 113	GAGGCCACAGATAATGCAACAGTC
OMW 114	CTTAATTCGGTATCTGCAGGCACAC
OMW 115	CGTTTCGAGTTGTTTGGATGGAG
OMW 126	GAACGAGAACCCAATCGCCAAACAGGCCACGACAAC
OMW 127	CAACATTTAAAAATCCAGTAGCCGCTGGAAAAGCCAAC
OMW 133	CCAGAGCAACAAGAGAAGAATTCCGAGG
OMW 134	CCTCGGAATTCTTCTCTTGTTGCTCTGGGCGGCCGCCATCTTTTACCCATACGATGTTC
OMW 135	CAGTACTTCATGATAGATCCGAAGCCGCTACTTTCAATAACGAAAGGC
OMW 136	GAACCCAATCTACAAACAGGCCGCGGCAGCATTTAAAAATCCAGTATACGCTGG
OMW 137	GCTTGAGTCCTTCTGAAGCATTTG
OMW 138	CTTCATGATAGATCCGAAGCCGCTACTTTCAATAACG
OMW 153	GCACGGCGAGGGCAATATTGTAG
OMW 154	CCCGGGATTGGCCAAAGGACCCTCCTCTTCATTCGCCGTCCAAGATGC
OMW 168	ATGCCACCTTCAACATCATTGCTGC
OMW 169	GTCCTTGATCGGAGAGTTTACTGTC
OMW 170	GTCACGTGACAGACTGTAGCATGG
OMW 171	CCATGCTACAGTCTGTCACGTGACGAGGCCACAGATAATGCAACAGTCTG
OMW 172	CCCATGCTACAGTCTGTCACGTGACTGGAAATTGCTCACAGTACTTCATG
OMW 174	CAGGAGGACCCTTGGCTAGCGGATGCCACCTTCAACATCATTGCTGC
OMW 177	GGAACGTCATATGGATAGGATCC
OMW 178	CCTCTTCATTCGCCGTCCAAGATGCGTTACGCTCTTGCCGCTTGTCTCC
OMW 181	CGTATCCCATTTGGCCATAAGCC
OMW 182	GGCTTATGGCCAAATGGGATACGAACGAGAACCCAATCTACAAACAG
OMW 183	GAGCTCATGCCACCTTCAACATCATTGCTG

OMW 184	GGGTACCCATGGAACAGGTAGTTTTCCAG
OMW 229	CATGTCAAAGTGTCCGCTTCACGG
OMW 230	GTCCTCTAGTGAATGGGAATTGACC
OMW 231	GATTTACGCAGCTCGTGTACTCCC
OMW 232	GCATATTCGAACATCCGACAACTGC

rde-1

OLM 6	CCTGGACATTCGATCATCTGAAG
OLM 7	CGTTTCACGATCCAAACAGATTCG

unc-119

OMW 216	GAGGGTAACCTAGGGATCTTACAGCTTTGAGCCAATTTATCCAAGTCCTTG
OMW 220	CAGCTTTGAGCCAATTTATCCAAGTCCTTG
OMW 221	GGTGGCATGGATGAATTGTATAAGTAG
OMW 226	GAACGTCACTTCTTCAAAGATCGCC
OMW 227	GGGATGAATTGGCTCAAAGTTAGG
OMW 228	CCTAACTTTGAGCCAATTCATCCC

5.1.3 PCR purification

DNA samples were diluted with 5x Binding solution and purified using the "GenElute™ PCR Clean-Up Kit" (Sigma-Aldrich) according to the manufacturer's protocol.

5.1.4 Ligation of DNA into pGEM®-T Easy vector

PCR fragments were purified using the "GenElute™ PCR Clean-Up Kit" (Sigma-Aldrich) and ligated according to the manufacturer's protocol into pGEM®-T Easy Vectors (Promega). If the PCR fragments were amplified with the Phusion® High-Fidelity DNA Polymerase (NEB), a poly-A tailing was performed prior to ligation using the GoTaq® DNA Polymerase. Therefore, a mix containing:

5 µl	PCR (purified)
2 µl	5x GoTaq PCR Buffer
0.2 µl	dATPs (10 µM)
0.2 µl	GoTaq® Polymerase
2.6 µl	H_2O

was incubated at 70°C for 30 min in a PCR machine (BioRad MyCycler). *E. coli* were transformed with the whole mix as described in 6.2.10 with the difference that 40 µl of 1 M IPTG and 40 µl of X-Gal were plated on the petri dishes.

5.1.5 Ligation of DNA into plasmid vector

Depending on the DNA concentration, plasmid backbone and insert were ligated with T4 DNA ligase (Roche) for 2 hours at room temperature in:

2 µl	T4 DNA ligase buffer
1 µl	T4 DNA ligase
H_2O	to a total volume of 20 µl

5.1.6 Restriction enzyme digestion

Plasmids were digested using restriction enzymes from Roche or NEB according to the manufacturer's protocol. If necessary, digested fragments were dephosphorylated by adding 1/10 of 10X Antarctic Phosphatase Reaction Buffer / 1 µl of Antarctic Phosphatase (NEB) and incubated at 37°C for 1 h. The Antarctic Phosphatase was then heat inactivated for 5 min at 70°C.
Digested DNA fragments that were excised from agarose gels were extracted using the GenElute™ Gel Extraction Kit (Sigma-Aldrich) according to the manufacturer's protocol.

5.1.7 Transformation of *E. coli*

Competent *E. coli* were thawed on ice before adding 100 µl to the plasmid of interest. After 10-20 minutes incubation on ice, the bacteria were heat shocked for 90 seconds at 42°C. 800 µl of 2xTY buffer were added before incubating the sample for 30 minutes at 37°C. After centrifugation for 2 minutes at 4'000 rpm, the supernatant was discarded, and the pellet was resuspended in 100 µl of 2xTY and the whole volume was plated on petri dishes.

5.1.8 Miniprep

A single bacteria colony was added to 2 ml of 2xTY containing ampicillin and incubated at 37°C over night. The next day, the liquid culture was transferred to a 1.5 ml Eppendorf tube and centrifuged for 2 minutes at 4'000 rpm. The supernatant was discarded and 350 µl of STET were added before vortexing to dissolve the pellet. 25 µl of Lysozyme were added and the sample was incubated at 95°C for one minute. Next, the sample was centrifuged at 4°C for 8 minutes at 14'000 rpm, the pellet was removed with a forceps and 30 µl of 3 M NaAc pH=5.2 and 300 µl of Isopropanol were added to the supernatant. After another centrifugation step using the same conditions, the supernatant was discarded and the pellet was resolved in 40 µl of TE.

5.1.9 Midiprep

MidiPreps were performed using the "QIAfilter Plasmid Midi Kit" (Qiagen) according to the manufacturer's protocol with the following changes. After step 13, the pellet was resolved in 400 µl of TE, transferred to a 1.5 ml Eppendorf tube, and the DNA was precipitated with 40 µl of 3M NaAc and 800 µl of 100% ice-cold EtOH. After incubation at -80°C for 10 minutes, the sample was centrifuged for 10 minutes at 14'000 rpm at 4°C. The supernatant was discarded and the pellet was resuspended in 100 µl of TE.

5.1.10 Site directed mutagenesis

To mutate one specific site on a plasmid, a ~50 bp long primer was designed with the desired mutation in the center. A mix containing:

2.5 µl	10x PfuUltra™ HF reaction buffer
2 µl	dNTPs (10 µM)
100 ng	Plasmid
100 ng	Primer (50 bp long)
0.2 µl	PfuUltra™ HF DNA polymerase
H_2O	to a total volume of 25 µl

was incubated in a PCR machine (BioRad MyCycler) with the following program:

Cycles	Temperature	Time
1x	95°C	1 min
35x	95°C	1 min
	55°C	1 min
	65°C	2 min/kb
	12°C	∞

After incubation, 1 µl of DpnI (NEB) was added to the mix and incubated at 37°C for 1 hour. 10 µl were then used for transformation of DH10B competent *E. coli*.

5.1.11 Plasmids

pMW4 *Peft-3::dep-1full::HS*
Fusion PCR of *dep-1minigene* (amplified from pTB18 with OMW65/66) with HA-StrepIII (amplified from pTO_HA with OMW68/64) and cloned into the AscI/PacI site of pLN022.

pMW5 *Peft-3::dep-1intraD1241A::HS*
dep-1 intracellular domain with substrate trapping mutation D1241A amplified from pTB30 with OMW70 and OMW66 and cloned into the AscI/FseI site of pMW4.

pMW6 *Peft-3::gfp::HS*
Fusion PCR of *gfp* (amplified from pPD95.75 with OMW73/76) with HA-StrepIII (amplified from pMW4 with OMW75/64) and cloned into the AscI/PacI site of pLN022.

pMW7 *let-23::GFP::HS* (entry clone)
Fusion PCR of OJE54/OMW80 (amplified from pJE5-02) with OMW81/OMW82 (amplified from pMW4) and OMW83/OJE55 (amplified from pJE5-02). PCR construct was amplified with adaptor primers OCH40/OCH41 and cloned by BP reaction into pDONR P2r-P3.

pMW8 *Peft-3::dep-1fullD1241A::HS*
Site directed mutagenesis of pMW4 with OMW77.

pMW10 *pat-3::GFP* (translational reporter)
Amplification of *pat-3::gfp* from NK358 worm lysate with OMW96 and OMW102 and subcloned into pGEM®-T Easy.

pMW11 *pat-3::GFP Y792A* (translational reporter)
Site directed mutagenesis of pMW10 with OMW126.

pMW12 *pat-3::GFP Y804A* (translational reporter)
Site directed mutagenesis of pMW10 with OMW127.

pMW13 *pat-3::GFP TTT796-798AAA* (translational reporter)
Site directed mutagenesis of pMW10 with OMW136.

pMW14 *pat-3::GFP Y792A Y804A* (translational reporter)
Site directed mutagenesis of pMW10 with OMW126.

pMW15 *pat-3::GFP Y772A* (translational reporter)
Site directed mutagenesis of pMW10 with OMW138.

pMW16 *pat-3::GFP Y772A Y792A* (translational reporter)
Site directed mutagenesis of pMW11 with OMW138.

pMW21 *Plin-31::pat-3 HA* (B-tail)
Fusion PCR of OMW175-OMW159 (amplified from pPG2) with OMW160-OMW177 (amplified from genomic DNA from the strain *qyIs15*)

pMW23 *dep-1::gfp::dep-1* (resque construct for *MosTic* line *ttTi25067*)
Fusion PCR of OMW197-OMW189 (amplified from genomic DNA) with OMW191-OMW190 (amplified from pTB24) and OMW194-OMW198 (amplified from genomic DNA) and subcloned into pGEM®-T Easy.

pMW24 *dep-1::mCherry::FRTunc-119(+)FRT::dep-1* (resque construct for *MosTic ttTi25067*)
Fusion PCR of OMW211-OMW189 (amplified from genomic DNA) with OMW191-121 (amplified from pTB24), OMW122-OMW202 (amplified from pWD200), OMW201-OAH378 (amplified from pCFJ150) and OMW194-OMW210 (amplified from genomic DNA). The final PCR product was cloned into pGEM®-T Easy.

pMW25 *dep-1::gfp::FRTunc-119(+)FRT::dep-1* (resque construct for *MosTic ttTi25067*)
Fusion PCR of OMW211-OAH375 (amplified from pMW23) with OAH377-OMW210 (amplified from pMW24). The final PCR product was cloned into pGEM®-T Easy.

pMW26 *Pglh-2::FLPase*
FLPase was cut out of pWD79 with MluI/NheI (NEB) and cloned into the MluI/NheI site of pJL43.1 (replacement of Transposase with FLPase)

pMW27 *Peft-3::FLPase*
Fusion PCR of OMW161-OMW162 (amplified from pLN22) with OMW214-M13rev (amplified from pMW26) and cloned into pGEM®-T Easy.

pMW28 *dep-1::gfp::dep-1 3'UTR::unc-119(+)::dep-1 3'UTR*
PCR fragment amplified from pMW24 with OMW216-M13rev was digested with AvrII (NEB) and cloned into the AvrII site of pMW23.

pMW29 *dep-1::mCherry::dep-1 3'UTR::unc-119(+)::dep-1 3'UTR*
Fusion PCR of M13f-OMW199 (amplified from pMW24) with OMW194-OSN63 (amplified from pMW28) was digested with SacII (NEB) and cloned into the SacII site of pMW28.

5.1.12 DNA sequencing

DNA samples of interest were first purified using the "GenElute™ PCR Clean-Up Kit" (Sigma-Aldrich). The final sample were then sequenced by in-house sequencing service and had a total volume of 10 µl containing:

PCR-Primer:	1 µl (10 µM)
Plasmid:	500 – 1'000 ng DNA
PCR:	10-20 ng DNA per 100 bp

5.1.13 DNA micro-injection

The injection mix (20 µl total volume containing a total amount of 150 ng DNA) was filtered (Coxtar, SPIN-X Centrifuge Tube Filter, 0.45 µm Cellulose Acetate) and then injected into young adult hermaphrodites that were sticked on slides with 2 % agarose pads and Halocarbon oil (700) as described by (Mello, Kramer, Stinchcomb, & Ambros, 1991). The injected animals were rescued from the slides with M9 buffer, transferred to a fresh plate with OP50 *E. coli*, and later on screened for transgenic progeny.

5.1.14 Lysis of worms

Genomic DNA was prepared by lysis of young adult hermaphrodites and served as template for PCR assays. 1-10 worms were picked and placed into individual tubes containing 10 µl of lysis mix (see 5.5 for content) and incubated in a thermocycler. The cycle program on PCR machine (BioRad MyCycler) was as follows:

Temperature	Time
60°C	1 hour
95°C	10 min
12°C	∞

5.1.15 Genotyping PCR assays

Genotyping was performed by 2 primers flanking the correspondgin mutation or deletion. PCR reactions were done with Invitrogen Taq Polymerase or NEB LongAmp Taq DNA Polymerase in 20 µl of reactions. For point-mutations, PCR products were purified prior to sequencing.

Genotyping of	5' Primer	3' Primer	Size	Sequencing Primer
lip-1	OIR4	OIR5 OIR6	920 bp (mut) / 560 bp (wt)	-
dep-1(zh34)	OMW197	OMW189	1.8 kb	OMW52
dep-1(ttTi25067)	OMW194	OMW196	500 bp (-Mos) / 1.8 kb (+Mos)	-
let-60	OTS38	OTS39	700 bp	OTS49
rde-1(ne219)	OLM6	OLM7	800 bp (mut) / 2.5 kb (wt)	-
pat-3 NPxY motifs	OMW112	OMW102	1.3 kb	OMW113
pat-3(st564)	OMW232	OMW229	12.3 kb	OMW111
nid-1(cg119)	OMW139	OMW140	2.8 kb (mut) / 5.8 kb (wt)	-

5.1.16 Generation of endogenous *dep-1::gfp* and *dep-1::mCherry* reporters

Endogenous single copy reporters of *dep-1::GFP* and *dep-1::mCherry* were created by *MosTIC* insertion as reported by (Robert et al., 2009). The repair templates were cloned by PCR fusion of the last 1.8 kb of the *dep-1* locus to *GFP* or *mCherry*, followed by 500 bp of the *dep-1* 3' UTR, the *C. briggsae unc-119* rescue construct, and 1.9 kb of the genomic *dep-1* downstream region. The final construct was subcloned into pGEM®-T Easy (Promega) and 50 ng/µl of the created plasmid (pMW28 or pMW29) was micro-injected together with 50 ng of the Mos1-transposase pJL43.1, 2.5 ng of *myo-2::mCherry*, 5 ng of pCFJ104, and 10 ng of pGH8 into the Mos insertion line *ttTi25067; unc-119(e2498)*. *MosTIC* engineered animals were identified by screening the F2 progeny for crawlers that lost the *myo-2::mCherry* marker, and confirmed by sequencing.
For FLP-FRT site directed recombination of animals in which *mCherry::FRT::unc-119(+)::FRT* was integrated into the locus of *dep-1*, 50 ng/µl of *Phsp-16-48::flp* (pWD79-2RV) were injected into 30 animals, which were incubated directly after micro-injection for 35 minutes at 33°C. Next morning, the animals were again heat-shocked again for 20 minutes at 33°C. As further approaches, 50 ng/µl or 100 ng/µl of pMW26 (*Pglh-2::FLPase*), or 100 ng/µl pMW27 (*Peft-3::FLPase*) were injected.

5.1.17 PAT-3::GFP reporter constructs

For the *pat-3::GFP* translational reporters, a 8.7-kb fragment was PCR-amplified from *pat-3::GFP* expressing worms (*qyIs43*; kindly provided by David Sherwood) with the primers OMW96 and OMW102 and subcloned into pGEM®-T Easy (Promega) according to the manufacturer's protocol. The Y-to-A mutations were introduced by site directed mutagenesis (see 6.2.7).

5.2 Protein Methods

5.2.1 SDS-PAGE

Polyacrylamide gels were prepared according to standard protocols (see Molecular Cloning – A Laboratory Manual by Maniatis). SDS gels were run at 100 V in fresh SDS running buffer. After running, the gel was either stained with Coomassie Blue (see below), or further used for Western blot experiments.

2x SDS loading buffer:	1 ml 1 M Tris pH=6.8, 2 ml 1 M DTT, 2 ml 20% SDS, 20 ml Bromophenol Blue, 2 ml 100% Glycerol, 3 ml H_2O
5x Laemmli buffer:	60 mM Tris-Cl pH=6.8, 2% SDS, 10% Glycerol, 5% β-mercaptoethanol, 0.01% bromophenol Blue
1x SDS running buffer:	8 l H_2O, 30.2 g Tris, 188 g Glycine, 50 ml 20% SDS
Running gel 8%:	2.3 ml H_2O, 1.3 ml 30% acrylamide mix, 1.5 ml Tris pH=8.8, 25 µl 20% SDS, 50 µl 10% APS, 5 µl TEMED
Running gel 12%:	50 ml 1 M Tris, 150 ml 5 M NaCl, 2.5 ml Tween 20, 5l H_2O, 25 µl 20% SDS, 50 µl 10% APS, 5 µl TEMED
Stacking gel:	13.6 ml H_2O, 3.4 ml 30% acrylamide mix, 2.5 ml 1.5M Tris pH=8.8, 0.1 ml 20% SDS, 0.2 ml 10% APS, 20 µl TEMED

5.2.2 Coomassie Blue staining

For Coomassie Blue staining, the SDS-PAGE gel was removed from the glass and transferred to a staining box. Enough Coomassie stain was added to cover the gel by 1.5 cm. The Coomassie stain was boiled in the microwave on high power, before the gel was incubated in the Coomassie stain for 5 to 10 minutes on a rocking table. The Coomassie stain was poured off and could be recycled a couple of times when it was stored at 4°C. The gel was rinsed twice in dH_2O before fresh destain solution is boiled up in the microwave. A folded Kimwipe is added, and after incubation for 10 minutes, the step with the Coomassie destain solution is repeated. The gel can be stored at the end in dH_2O.

Coomassie Blue Stain:	0.25 g Coomassie Brillant Blue, 45 ml Methanol, 45 ml H_2O, 10 ml Glacial acetic acid
Coomassie Blue Destain:	100 ml MetOH, 75 ml Glacial acetic acid, 825 ml H_2O

5.2.3 Colloidal Coomassie Blue staining

For Colloidal Coomassie Blue staining, the SDS-PAGE gel was removed from the glass and transferred to a staining box. Enough fixing solution was added to cover the gel and incubated on a rocking table for 30 minutes before incubation over-night with staining solution. The gel was then transferred to a clean staining box and incubated with enough washing solution for not more than 5 minutes. Thereafter the gel was again transferred to a clean staining box and stored in dH_2O.

Fixing solution:	20% (v/v) Methanol, 1% (v/v) 85% phosphoric acid, 79% H_2O
Staining solution:	20% (v/v) Methanol, 20% (v/v) Roti Blue concentrate, 60% H_2O
Washing solution:	25% (v/v) Methanol, 75% H_2O

5.2.4 Western Blot

Proteins that were previously separated by SDS-PAGE were blotted onto a PVDF membrane by the MiniProtean® Electrophoresis System from BioRad. Thereby, the PVDF membrane, which was previously activated with 100% Methanol, was placed on the SDS gel to form a gel sandwich and placed to the Trans-blot cell. The chamber was filled with freshly prepared transfer buffer before the proteins were blotted with 100V during 1 hour. Thereafter, the membrane was blocked with 5% milk in TBS-T for 4 hours to avoid unspecific binding of the antibodies, before the primary antibody, which was diluted in the blocking solution, was applied to the membrane over-night at 4°C. Excess antibody was removed by three washes of 30 minutes with TBS-T rocking at room temperature. Secondary antibodies conjugated with horseradish peroxidase (HRP) were diluted and applied onto the membrane for 1h at room temperature. Afterwards, the same washing conditions were used as to remove the excess primary antibodies. The activation of the HRP was done by applying the Amersham™ ECL™ Wester blotting detection reagents (GE Healthcare) onto the membrane for 4 minutes, before the membrane was illuminated on a Western blot imaging system.

Transfer Buffer:	160 ml Methanol, 640 ml H_2O, 2.42 g Tris, 11.528 g Glycine
Blocking Buffer:	5% milk powder (Coop) in TBS-T

5.2.5 Antibodies

αAJM-1	Monoclonal mouse MH27		
αGFP	Monocolonal mouse Anti-Green Fluorescent Protein	Roche	11 814 460 001
αHA	Monocolonal mouse Anti-HA (12CA5)	Roche	11 583 816 001
αIgG	Goat Anti-Mouse IgG Horseradish Peroxidase (HRP)	Jackson Immuno Research	115-035-003
αIgG	Goat Anti-Rabbit IgG Horseradish Peroxidase (HRP)	Jackson Immuno Research	111-035-003
FITC	Fluorescein FITC Donkey Anti-Rabbit IgG (H+L)	Jackson Immuno Research	711-096-152
Cy5	Cyanine Cy5 Donkey Anti-Mouse IgG (H+L)	Jackson Immuno Research	715-175-151

5.2.6 GST purification of GST::DEP-1

A single colony of *E. coli* BL21, previously transformed with pTB29 or pTB30, was grown in a 20 ml 2xTY liquid culture containing ampicillin at 37°C over-night. The next day, 2x 9 ml were transferred to two Erlenmeyer flasks containing 150 ml 2xTY (without ampicillin) and grown until the OD600=1 was reached (measured with a photometer). The culture was cooled down to <18°C, before 0.2 mM IPTG (final concentration) was added. After incubation for 4 hours at 18°C, the liquid culture was centrifuged at 4'000 rpm for 10 minutes at 4°C. After discarding the supernatant, the pellet was resuspended in 10 ml of cold PBS (containing 250 µl of 50x complete and 1.2 ml of 10 % Triton-X (endconcentration=1%)), and transferred to a 15 ml falcon tube. Keeping the sample on ice, protein extraction was conducted by sonication. Sonication was done 5 times for 30 seconds with 20 % intensity, followed by a break of 30 seconds (Bandelin Sonopuls). The sample was transferred to 2 ml Eppendorf tubes and centrifuged for 10 minutes at 10'000 rpm at 4°C.

The supernatant was incubated for 1 hour at 4°C with 200 µl of GST sepharose (Sigma) which has previously been equilibrated in cold PBS. Thereafter, the sample was washed three times with cold GST washing buffer for 15 minutes at 4°C.

For quality control, 50 µl of the purified GST-bound protein were transferred to a new 1.5 ml Eppendorf tube where the whole liquid was taken away with a deformed Pasteur pipette. 30 µl of 2xSDS binding buffer were added and the samples were heated up to 95°C for 5 minutes. 15 µl were loaded on a 10 % SDS gel and stained with Coomassie Blue.

5.2.7 Preparation of *C. elegans* protein extract

To prepare *C. elegans* protein extract, mixed-stage liquid cultures were cleaned by sucrose flotation and stored in aliquots at -80°C. After thawing 400 µl of packed worms in 800 µl lysis buffer (100 mM Tris pH=8.0, 150 mM NaCl, 1 mM EDTA, 1 mM DTT, 0.5% NP-40, 1x protease inhibitor cocktail; Roche) at 4°C, the suspension was dropped into liquid nitrogen. Then, the frozen droplets were transferred to a grinding beaker that was previously cooled in liquid nitrogen, and homogenized in a mixer mill (MM300; Retsch). The frozen powder was thawed slowly at 4°C before the soluble protein extract was optained by centrifugaation the whole mixture for 10 minutes at 4°C and 10,000 g.

5.2.8 StrepTactin-HA double purification of DEP-1::HS

Strep-III purification

200 µl of StrepTactin® Sepharose® (IBA 2-1201-010) were equilibrated twice with 1 ml of lysis buffer. *C. elegans* protein extract was added to the sepharose and incubated for 30 min at 4°C. After washing six times with 1 ml of lysis buffer, the sample was transferred to a Micro Bio-Spin column (Biorad) and eluted by gravity flow four times with 250 µl of elution buffer (100 mM Tris pH=8.0, 150 mM NaCl, 1 mM EDTA, 10 mM Biotin).

HA-Purification

100 µl of HA-Agarose (Monoclonal Anti-HA-Agarose antibody produced in mouse, A2095, Sigma) was equilibrated twice with 1 ml of washing buffer (100 mM Tris pH=8.0, 150 mM NaCl, 1 mM NaCl, 1 mM EDTA). Eluate from Strep-III purification was incubated with the HA-Agarose for 4 hours at 4 °C. After six washing steps with washing buffer, the sample was transferred to a Micro Bio-Spin column (Biorad) and eluted three times with 150 µl of 0.2 M Glycine pH=2.5 into Eppendorf tubes containing 80 µl of 1M NH_4HCO_3.

5.2.9 HA purification of DEP-1::HS

180 µl of HA-Agarose (Monoclonal Anti-HA-Agarose antibody produced in mouse, A2095, Sigma) were equilibrated twice with 1 ml of washing buffer (100 mM Tris pH=8.0, 150 mM NaCl, 1 mM NaCl, 1 mM EDTA). *C. elegans* protein extract was incubated with the HA-Agarose for 4 hours at 4 °C. After washing once with lysis buffer and six times with washing buffer, the sample was transferred to a Micro Bio-Spin column (Biorad) and eluted three times with 150 µl of 0.2 M Glycine pH=2.5 into Eppendorf tubes containing 100 µl of 1M NH_4HCO_3.

5.2.10 GST pull-down experiments for Western blot experiments

Approximately 10 µg of purified GST::DEP-1 (wild-type and D1241A) and 40 µg of GST (negative control) were incubated with ca. 800 µg total worm extract over night at 4°C for each binding reaction. Followed by washing with lysis buffer, bound proteins were eluted by boiling the beads for 5 minutes in Laemmli buffer. GFP tagged proteins were detected on Western blots using 10% acrylamide gels with monoclonal Anti-GFP antibody (Roche, Cat. No. 11 814 460 001). For phosphatase inhibitor experiments, 5 mM Na_3VO_4 was added to the lysis buffer.

5.2.11 GST pull-down experiments for LC-MS/MS analyses

Approximately 50 µg of purified GST::DEP-1 (wild-type and D1241A) and 100 µg of GST (negative control) were used for each binding reaction. To prepare N2 worm extracts, mixed-stage liquid cultures were cleaned by sucrose flotation, resuspended in lysis buffer (100 mM Tris pH=8.0, 150 mM NaCl, 1 mM EDTA, 1 mM DTT, 0.5% NP-40, 1x protease inhibitor cocktail; Roche), shock frozen in liquid nitrogen, and homogenized in a mixer mill (MM300; Retsch). Thawed worm extract was then centrifuged for 10 minutes at 4°C and 10'000g to remove insoluble components. About 2.5 mg of total protein extract was used for each reaction. Binding was performed at 4°C over night, followed by three washes with lysis buffer. Bound proteins were eluted by boiling the beads for 5 minutes in 30 µl of laemmli buffer and separated on a 4-15% linear gradient SDS-gel (Biorad Nr. 161-1104), followed by Colloidal Coomassie Blue staining according to the manufacturer's protocol (Roti Blue; Roth).

5.2.12 In-solution tryptic digestion

After HA purification, the volume of the purified proteins was reduced to ~10 µl by speedvac drying before 140 µl of 25 mM AmBic pH=8.0 were added. Disulphide bridges were reduced by adding DTT with a final concentration of 10 mM (in 25 mM AmBic pH=8.0) and by incubating for 45 minutes at 50°C. Iodacetamide (IAM) was added with a final contentration of 50 mM (in 25 mM AmBic pH=8.0) and the sample was incubated for 1 hour at room temperature in the dark to alkylate cysteines. Tryptic digestion was performed by adding 20 ng trypsin and incubation at 37°C over-night. Next morning, the samples were speedvac dried, resuspended in 10 µl of 3% acetonitrile, 0.2% of formic acid and desalted with C18 ZipTip® (Millipore) before being analyzed on a calibrated LTQ-Orbitrap mass spectrometer (Thermo Scientific).

5.2.13 In-gel tryptic digestion

After GST pull-down, separation by SDS-PAGE and Colloidal Coomassie Blue staining, differential protein bands were excised with a scalpel into small pieces and prepared for in-gel tryptic digestion. Thereby, the gel pieces were washed and dehydrated three times in 50% Acetonitrile and dried in speedvac. 10 mM DTT (in 25 mM Ammonium bicarbonate pH=8.0) was added to cover gel pieces and incubated for 45 minutes at 56°C. After DTT was removed, 50 mM IAM (in 25 mM Ammonium bicarbonate pH=8.0) was added to cover gel pieces and incubated for 1 hour at room temperature in the dark. IAM

was removed and gel pieces were washed twice with 50% Acetonitrile before dried in Speed Vac. 25 mM Ammonium bicarbonate pH=8.0 containing 50 ng trypsin was added to be absorbed by the gel pieces and incubated over night at 37°C. To extract the peptides, gel pieces were incubated three times for 15 minutes with 50% Acetonitrile /5% TFA and once with 100% Acetonitrile. The peptides were speedvac dried before resuspended in 5 µl of 3% Acetonitrile/0.1% formic acid. Samples were desalted with C18 ZipTip® (Millipore) before being analyzed on a calibrated LTQ-Orbitrap mass spectrometer (Thermo Scientific).

5.2.14 ZipTip C18 sample clean-up

Speedvac dried samples were taken up in about 20 µl washing solution. Then, the tip was prewet three times by aspirating 10 µl of wetting solution into the tip and subsequent dispension to waste. Thereafter, the tip was equilibrated for binding by aspirating 10 µl equlibration solution. The peptides were then bound to the ZipTip by aspiration and dispension of the sample during 10 cycles. The tip was washed three times by aspirating 10 µl washing solution, before the peptides were eluted twice with 10 µl of elution solution. The elutions were pooled and speedvac dried before being analyzed by LS-MS/MS.

Wetting solution:	100% Acetonitrile (ACN)
Washing solution:	3-5% ACN; 0.1% TFA
Elution solution:	50-60% ACN; 0.1% TFP

5.2.15 Protein identification by LTQ-Orbitrap

Desalted peptides were resovled in 15 µl of 3 % Acetonitrile/0.2 % formic acid and loaded on a 10 cm fused silica column packed with 3 µm 200 Å pore size C18 resin. Peptides were eluted from the column via an ACN gradient of 5-45% (v/v) over 80 minutes and 40-80% ACN over the subsequent 15 minutes in a buffer containing 0.2% formic acid (v/v) at a flow rate of 200 nl/min.
The range of MS scan was m/z 450-1500. LC-MS/MS spectra were exported to the MASCOT generic format (mgf) and proteins were identified by searching the MASCOT database search engine version 2.2 (Perkins et al., 1999). The MASCOT search parameters were as follows: set-off threshold at 0.05 in the expectation value cutoff, peptide tolerance at 5 ppm, MS/MS tolerance at 0.8 Da, peptide charge of 2+ or 3+, trypsin as enzyme allowing up to one missed cleavage, carbamidomethylation on cysteines as a fixed modification and oxidation on methionine as a variable modification. Only peptides with a maximum of 2 (3 for semi-tryptic digest) missed cleavage sites were allowed in database searches. Further comparisons and analyses of the proteins were performed using Scaffold 3.0 (Proteome Software).

In-solution tryptic digestioon, in-gel tryptic digestion, ZipTip clean-up, and LC-MS/MS analysis were performed in the Functional Genomic Center Zurich, University of Zurich, Switzerland. The project run under the name "p726 - A Mass Spectrometry-Based Approach to Identify New Interaction Partners of the Tyrosine Phosphatase DEP-1" and was supervised by Dr. Paolo Nanni. The instrument methods were saved under the name p726_20101101_95min and the MS data of the DEP-1::GST-pull down experiments as:

LC-MS/MS data of DEP-1::HS pull-downs

20100809_03_dep1intra_0727.mgf	20100809_04_dep1fullwt_0727.mgf	20100809_01_gfp_0727.mgf
20100809_08_dep1intra_0720.mgf	20100809_09_dep1fullwt_0720.mgf	20100809_06_gfp_0720.mgf
20100907_04_dep1intra_1.mgf	20100907_05_dep1full_1.mgf	20100907_02_N2_1.mgf
20100907_09_dep1intra_2.mgf	20100907_10_dep1full_2.mgf	20100907_07_N2_2.mgf
20101011_09_dep1intra_1.mgf	20101011_10_dep1full_1.mgf	20101011_07_N2_1.mgf
20101011_14_dep1intra_2.mgf	20101011_15_dep1full_2.mgf	20101011_12_N2_2.mgf

LC-MS/MS data of GST::DEP-1 pull-downs

20101101_01_pTB29_1.mgf	20101101_07_pTB30_1.mgf	20101101_14_pGEX_1.mgf
20101101_02_pTB29_2.mgf	20101101_08_pTB30_2.mgf	20101101_15_pGEX_2.mgf
20101101_03_pTB29_3.mgf	20101101_09_pTB30_3.mgf	20101101_16_pGEX_3.mgf
20101101_04_pTB29_4.mgf	20101101_10_pTB30_4.mgf	20101101_17_pGEX_4.mgf
20101101_05_pTB29_5.mgf	20101101_11_pTB30_5.mgf	20101101_18_pGEX_5.mgf
	20101101_12_pTB30_6.mgf	
20101117_01_pTB29_1.mgf	20101117_07_pTB30_1.mgf	20101117_19_pGEX_1.mgf
20101117_02_pTB29_2.mgf	20101117_08_pTB30_2.mgf	20101117_20_pGEX_2.mgf
20101117_03_pTB29_3.mgf	20101117_09_pTB30_3.mgf	20101117_21_pGEX_3.mgf
20101117_04_pTB29_4.mgf	20101117_10_pTB30_4.mgf	20101117_22_pGEX_4.mgf
20101117_05_pTB29_5.mgf	20101117_11_pTB30_5.mgf	20101117_23_pGEX_5.mgf
	20101117_12_pTB30_6.mgf	
	20101117_13_pTB30_7.mgf	
	20101117_14_pTB30_8.mgf	
20101220_07_pTB29_1.mgf	20101220_14_pTB30_1.mgf	20101220_01_pGEX_1.mgf
20101220_08_pTB29_2.mgf	20101220_15_pTB30_2.mgf	20101220_02_pGEX_2.mgf
20101220_09_pTB29_3.mgf	20101220_16_pTB30_3.mgf	20101220_03_pGEX_3.mgf
20101220_10_pTB29_4.mgf	20101220_17_pTB30_4.mgf	20101220_04_pGEX_4.mgf
20101220_11_pTB29_5.mgf	20101220_18_pTB30_5.mgf	20101220_05_pGEX_5.mgf
20101220_12_pTB29_6.mgf	20101220_19_pTB30_6.mgf	

5.2.16 Polyclonal DEP-1 Antibodies

Immunization of rabbits

An adequate amount of the intracellular domain of wild-type DEP-1 (expressed by pTB29) was GST-purified (see 6.3.1) with the exception that the purified protein was eluted from the GST sepharose at the end. This was achieved by washing the beads three times with GST elution buffer (50 mM Glutathion, pH=8). The elution fractions were combined and dialyzed with PBS over night. Ca. 200 µg of purified DEP-1 protein was aliquoted in six Eppendorf tubes and sent to the "Institute of Laboratory Animal Sciences, UZH" for the immunization of two rabbits. Protein concentration was measured by performing Amido Black assay.

Purification of antibodies

The sera of the two rabbits (006-9AB-1D2 and 006-9AC-B07) containing the DEP-1 antibodies were affinity-purified by using HiTrap NHS(N-hydroxysuccinimide)-Activated HP columns (Ge Healthcare Life Sciences) according to the manufacturer's protocol. Columns were packed with either 1 mg of purified GST or with 1 mg of the intracellular domain of wild-type DEP-1 (expressed by pTB29), which were previously dialyzed over night in two liters of coupling buffer (0.2 M $NaHCO_3$, 0.5 M NaCl, pH=8.3) and concentrated to 1 ml using 10 kD Millipore filters. 1 ml of the sera was diluted 1:10 in 10 mM Tris-HCl pH=7.5 and firstly flowed through the DEP-1-column. Washing buffer (10 mM Tris, 500 mM NaCl pH=7.5) was used to remove unspecific bound molecules. Elution of antibodies was performed using 100 mM Glycine pH=2.5 and 100 mM Triethylamine pH=11.5. The eluted fractions were neutralized with 1 M Tris pH=8 and tested for protein content by performing a dotblot that was stained with Ponceau S. The first four fractions of the acidic eluation were pooled and dialyzed with 10 mM Tris pH=7.5 before they were flowed three times through the GST-column. The buffer of the affinity-purified antibodies was changed to 1x PBS using 10 kD Millipore filters, aliquoted and stored at -80°C.

Examination of DEP-1 antibodies by Western blot analysis

50 young adult animals from the strains N2, *dep-1;lip-1*, and *zhIs027[Peft-3::dep-1minigene::HA-StrepIII; unc-119(+)]* were picked to 50 µl of Laemmli buffer, boiled for 5 minutes at 95°C, centrifuged at 14'000 rpm for 2 minutes and loaded on 12% acrylamide gels. Purified DEP-1 antibodies were diluted 1:500 and 1:1'000 and incubated for 2 hours at room-temberature. After washing, secondary antibodies conjugated with HRP were diluted 1:10'000 and applied onto the membrane for 1 hour at RT.

Immunostaining

The immunostaining method used in this study is based on the protocol established by Finney and Ruvkun (1990). Mixed staged worms of a confluent plate were transferred with 1x PBS to an Eppendorf tube. The worm suspension was washed with 1x PBS until the remaining OP50 was removed and the supernatant was clear. The spinning steps were henceforth performed at 2'000 rpms for 1 minute. The volume was adjusted to 450 µl before 500 µl of 2x RFB buffer were added. The tubes were shock frozen in liquid nitrogen and stored at -80°C.

To fix animals, 50 µl of paraformaldehyde (1% end concentration) was added. Afterwards, the tubes were subjected to three rounds of freeze-thaw cracking in liquid nitrogen and hand warm tap water to

allow the paraformaldehyde to penetrate the cuticle of the worms. After incubation for 30 minutes at 4°C on a rocker, the fixation reaction was stopped by washing the worms three times with 1x TTB.
The cuticle was permeabilized by reducing the disulfide bonds of the cuticle collagen with 1 ml of 1x TTB, 40 µl of Triton X-100 (10%) and 10 µl of β-Mercaptoethanol for 6 h at 37°C. Finally, the worms were washed twice with 4x BO_3 buffer. The reduced disulfide bonds were modified and sealed by incubating the worms in 990 µl of 4x BO_3 buffer and 10 µl DTT (1 M) for 15 minutes rocking at RT. The reaction was stopped by two washes with 4x BO_3 buffer, followed by incubation in 990 µl of 4x BO_3 buffer and 10 µl of H_2O_2 for 15 minutes. This oxidation step was stopped by two washes with 4x BO_3.
To minimize unspecific binding of the antibodies, permeabilized worms were blocked with 1 ml ABA-buffer during 15 minutes rocking at RT. Worms were incubated over-night at 4°C with the primary antibodes that were diluted in 200 µl of ABA-buffer. After three washing steps (15 minutes rocking at RT) with PBS-T, the secondary antibodies were diluted 1:100 in 200 µl of ABA-buffer and incubated with the worms for 2 h rocking at RT in the dark. To stain the DNA, worms were incubated with 1 ml of PBS-T containing 1 µl of Hoechst dye (10 mg/ml) for 5 minutes rocking at RT, followed by two washes with PBS-T for 5 minutes.
The supernatant was removed to an approximate final end volume of 20 µl. 20 µl of Mowiol were added and mixed, and then immediately distributed by 2 drops on one slide. The drops were covered with a coverslip and dried overnight at RT in the dark. Long-term storage was done at 4°C.

Paraformaldehyde	100 mg Paraformaldehyde, 450 µl dH_2O, and 0.5 µl 12 M NaOH was vortexed and incubated at 60°C for 10 min (vortexed shortly every 2 minues) before 5 µl 1 M HCl and 50 µl 10xPBS were added.
2x RFB "Ruvkun Fixation Buffer"	160 mM KCl, 40 mM NaCl, 20 mM Na2EGTA, 10 mM Spermidine HCl, 30 mM PIPES pH=7.4, 50% Methanol. Store at -20°C.
1x TTB "Tris Triton Buffer"	100 mM Tris HCl, pH=7.4, 1 mM EDTA, 0.1% Triton X-100.
100x BO_3 Buffer	5 M H_3BO_3, 2.5 M NaOH. (Crucial: pH should not be lower than 9.5).
4x BO_3 Buffer	Dilute 100x BO_3 Buffer 1:25. Add 0.01% Triton X-100.
1x PBS-T	1x PBS, 0.05% Triton X-100.
ABA-buffer	2% BSA in 1xPBS-T (1.4 ml per sample and staining)
Mowiol	2.4 g Mowiol 4-88, 6 g Glycerol, 6 ml H_2O, 12 ml 0.2 M Tris pH=8.5, 2.5% (w/v) DABCO.

5.3 Animal methods

5.3.1 *C. elegans* strains and general handling

The strains used for the experiments and crosses were derivates of Bristol strain N2 of *Caenorhabditis elegans*. The animals were cultivated under standard conditions at 20°C as described in (Brenner, 1974). Unless noted otherwise, the mutations used have been described previously and are listed below by their linkage group.

LGII: *dep-1(zh34)* (Tarcic et al., 2009)
unc-4(e120) (Brenner, 1974)
rrf-3(pk1426) (Simmer et al., 2002)
ttTi25067 (*dep-1* transposon insertion, Université Lyon 1, Villeurbanne, France)

LGIII: *unc-119(ed3)* (Maduro & Pilgrim, 1995)
unc-119(ed4) (Maduro & Pilgrim, 1995)
unc-119(e2498) (Maduro & Pilgrim, 1995)
pat-3(st564) (Williams & Waterston, 1994)
glp-1(q339) (Troemel et al., 1999)

LGIV: *lip-1(zh15)* (Berset et al., 2001)
let-60(n1046) (Ferguson & Horvitz, 1985)

LGV: *rde-1(ne219)* (Pavelec et al., 2009)
nid-1(cg119) (Trzebiatowska et al., 2008)

Integrated transgenic arrays:

LGII: *zhIs70[dep-1::gfp::unc-119(+)]*
zhIs71[dep-1::mCherry::unc-119(+)]

LGIV: *qyIs15[zmp-1 > HA-ßtail]* (Hagedorn et al., 2009)
zhIs038[let-23::GFP; unc-119(+)] (Haag et al., unpublished data),

LG unknown: *qyIs43 [pat-3::GFP, ina-1(genomic), unc-119(+)]* (Hagedorn et al., 2009)
qyIs110[egl-17>dnPat-3] (Hagedorn et al., 2009)
zhIs396[*Pdlg-1::lifeact::gfp::unc-54 3'UTR,Plin-48::gfp*] (Farooqui et al., 2012)
jeIs2222[pat-2::GFP rol-6(su1006)] (Meighan & Schwarzbauer, 2007)
zhIs021[Peft-3::taptag::dep-1 intracellular domain(wt)/unc-119(+)]
zhIs022[Peft-3::taptag::dep-1 intracellular domain (D1241A) / unc-119(+)]
zhIs027[Peft-3::dep-1minigene::HA-StrepIII; unc-119(+)]
zhIs028[Peft-3::dep-1intraD1241A::HA-StrepIII; unc-119(+)]
zhIs020[Peft-3::taptag::dep-1 extracellular domain / unc-119(+)]

Extrachromosomal transgenic lines:

zhEx419[pat-3::gfp Y792A Y804A]
zhEx420[pat-3::gfp Y772A]
zhEx432[pat-3::gfp Y772A Y804A]
zhEx433[pat-3::gfp Δintra]
zhEx456[pat-3::gfp Y792A]
zhEx457[pat-3::gfp Y804A]
zhEx458[pat-3::gfp TTT796-798AAA]
mwEx31[pat-3 Y804F] (Lee et al., 2001)
mwEx32[pat-3 Y792F Y804F] (Lee et al., 2001)
zhEx477[dep-1::mCherry]
zhEx479[Pnid-1::gfp, myo-2::mCherry]
zhEx524[pat-3::gfp,myo-2::mCherry]
zhEx528[pat-3::gfp Y804A, myo-2::mCherry]
zhEx338[Peft-3::gfp::HA-StrepIII]
zhEx418[Plin-31::rde-1;myo-2::mCherry]

For Nomarski analysis, animals were mounted on 4% agarose pads in M9 solution containing 20 mM tetramisole hydrochloride.

5.3.2 Crosses

To generate *C. elegans* males by heat-shock, four plates containing 20 L4 hermaphrodites were incubated at 30°C for 5 hours.
Twelve males and four hermaphrodites were kept on a NGM plate containing only a small drop of OP50 food. Two days later, the hermaphrodites were singled out and screened for male F1 offspring. F1 animals males were either used for further crosses or singled out prior to F2 generation genotyping.

5.3.3 Worm liquid cultures

Three small agar plates confluent with *C. elegans* were used to inoculate one liquid culture consistent of:

100 ml	S-Basal
300 µl	1M $MgSO_4$
300 µl	1M $CaCl_2$
1 ml	K-Citrate pH=6
1 ml	100x trace metals
1 ml	Pen/Strep 100x
100 µl	Nystatin 1'000x
100 µl	Cholesterol (5 mg/ml)
4 ml	Worm food

Two to three days later, the worms were cleaned by sucrose floating.
The worm food media was autoclaved, consisting of:

24 g	Bacto tryptone
48 g	Yeast extract
16 ml	50 % Glycerol
2 l	dH_2O

Next, 100 ml autoclaved 1 M KPO_4 and 100 µl of *E. coli* Na22 bacteria were added to the mixture in a 3 liter Erlenmeyer flask and grown at 37°C. The following day, the liquid culture was centrifuged at 4'000 rpm for 10 minutes, the supernatant discarded and the pellet resolved in 15 ml of 2xTY. The worm food was then kept at -20°C.

5.3.4 Cleaning of *C. elegans* by sucrose floating

Worms from the liquid culture were centrifuged at 2'000 rpm for 1 minute. The supernatant was discarded and the worms were washed twice with 50 ml of cold 0.1 M NaCl. Subsequently, the 0.1 M NaCl was removed until 25 ml were left, and 25 ml of ice-cold 60 % Sucrose were added. After centrifugation at 1'100 rpm for 5 minutes, the floating worms were transferred with a Pasteur pipette in another 50 ml falcon tube and washed twice with 0.1 M NaCl. ~ 400 µl of packed worms were aliquoted in a 1.5 ml Eppendorf tube, shock frozen in liquid nitrogen and kept frozen at -80°C.

5.3.5 Freezing worms

Preferentially L1 worms were frozen and stored at -80°C. Worms of three confluent plates were washed with M9 media and centrifuged for 1 minute at 1'100 rpm. The supernatant was discarded until 1 ml was left and 1 ml of freezing solution was added. The 2 ml liquid were distributed to four cryotubes, labeled with the freezing number and A, B, C or D. The cryotubes were put in freezing boxes, filled with Isopropanol and kept on -80°C. Two days later, the D probe was thawed to check if the worms survived the freezing.

5.3.6 RNAi

For RNAi, the feeding method described by (Kamath et al., 2001) was used. RNAi plates consisting of NGM agar including 3 mM IPTG, 50 µg/ml ampicillin and 50 µg/ml tetracycline were poured and dried for 2-4 days at room temperature. RNAi bacterial clones were grown over night at 37°C in 2xTY and subsequently spotted on the RNAi plates. Induction of the dsRNA production was performed by incubating the RNAi plates for 24 hours at room temperature. The worms were synchronized with hypochloride solution and L1 larvae were placed on growth media plates (P0) and allowed to grow at 20°C. Unless noted otherwise, the F2 generation was analyzed.

RNAi NGM plates:

1.5 g	NaCl
1.25 g	Peptone (Tryptone Peptone)
9.5 g	Agar (Bacto Agar)
0.5 ml	Cholesterol (5 mg/ml)
0.5 l	H_2O
12.5 ml	KPO_4 pH=6
0.5 ml	1M $MgSO_4$
0.5 ml	1M $CaCl_2$
1.5 ml	1M IPTG
0.5 ml	Ampicillin

5.3.7 Worm bleaching

Two plates confluent with adult worms were transferred with H_2O to a 15 ml falcon tube. The falcon tube was centrifuged for 1 minute at 1'100 rpm and the supernatant was discarded. After adding 2 ml of bleaching solution, the worms were vortexed until no floating bodies were detected. The bleach was attenuated to 14 ml with H_2O and washed four times with H_2O.

5.4 Instruments

DNA experiments

PCR machine:	BioRad MyCycler™
Photometer:	Eppendorf Bio Photometer
Nanodrop:	NanoDrop® ND-1'000 Spectrophotometer

Protein experiments

Western blot:	Mini Trans-Blot® Electrophoretic Transfer Cell PowerPac™ Basic Power Supply
Mass Spectrometer:	LTQ-Orbitrap Thermo Scientific
HPLC Pump:	Eksigent 1D plus
Sonicator:	Bandelin Sonopuls

Microscopes

Fluorescent and Nomarski microscope:	Leica DMRA, equipped with a cooled CCD camera (Hamamatsu ORCA-ER)
Dissecting scope:	Leica MS5
Fluorescence dissecting scope:	Leica MZDLIII
Injection scope:	Leica DM-IRB
Spinning Disk Confocal scope:	Andor Revolution Spinning Disk confocal microscope inverted, Zeiss Axio Observer A1. Focus: Piezo Z-Stage. Scanner: Yokogawa CSU-X1 Spinning Disk Unit. Detector: Andor iXon3 EMCCD-Camera, 512 x 512 pixels, Andor Neo sCMOS-Camera 2560 x 2160 pixels.

Other instruments

Centrifuges:	Eppendorf Centrifuge 5804 Eppendorf Centrifuge 5417 R
SpeedVac:	Thermo Savant SpeedVac 121P

5.5 General buffers

S-Basal:	5.85 g NaCl, 50 ml KPO_4, 1 l H_2O
STET:	8% Sucrose, 5% Triton-X 100%, 50 mM EDTA, 50 mM Tris pH=8
TE:	2 ml 1 M Tris pH=7.5, 0.4 ml 0.5M EDTA, 197.6 ml H_2O
TBS-T:	50 ml 1 M Tris, 150 ml 5 M NaCl, 2.5 ml Tween 20, 5 l H_2O
1x TBE:	108 g Tris, 55 g Boric acid, 40 ml 0.5 M EDTA pH=8, 10 l H_2O
Bleaching solution:	1 ml 10 M NaOH, 3ml $NaClO_2$ 13%, 10 ml H_2O
M9:	3 g KH_2PO4, 6 g Na_2HPO_4, 5 g NaCl, 1 ml 1 M $MgSO_4$, 1 l H_2O
Worm lysis buffer:	50 mM KCl, 10 mM Tris 8.2, 2.5 mM $MgCl_2$, 0.45% NP-400, 45% Tween-200®, 0.01% Gelatine
Electrophoresis Buffer:	0.8 g TrisBase, 55 g Boracid, 40 ml EDTA (0.5 M, pH=8), 10 l H_2O
2xTY:	16 g Bacto Tryptone, 10 g Yeast extract, 5 g NaCl, 1 l H_2O

5.6 Kits

PCR Purification:	GenElute™ PCR Clean-Up (Sigma)
Gel Extraction:	GenElute™ Gel Extraction Kit (Sigma)
MidiPrep:	QIAfilter Plasmid Midi Kit (Qiagen)

5.7 Software used for data analysis

Control software for Leica microscope: Openlab 5.0.1

Processing pictures:	Adobe Photoshop CS 5.5 Adobe Illustrator CS 5.5, ImageJ 1.47q Imaris 7.6.1
DNA analysis:	Sequencher 4.8 DNA Strider 1.4f6 CLC Main Workbench 5 EnzymeX 3.1
Massspectrometry analysis:	Scaffold 3 Mascot (www.matrixscience.com)

6

References

Alonso, A., Sasin, J., Bottini, N., Friedberg, I., Friedberg, I., Osterman, A., Godzik, A., Hunter, T., Dixon, J., and Mustelin, T. (2004). Protein tyrosine phosphatases in the human genome. Cell 117, 699–711.

Ambros, V. (1999). Cell cycle-dependent sequencing of cell fate decisions in Caenorhabditis elegans vulva precursor cells. Development 126, 1947–1956.

Arora, D., Stopp, S., Böhmer, S.-A., Schons, J., Godfrey, R., Masson, K., Razumovskaya, E., Rönnstrand, L., Tänzer, S., Bauer, R., et al. (2011). Protein-tyrosine phosphatase DEP-1 controls receptor tyrosine kinase FLT3 signaling. J. Biol. Chem. 286, 10918–10929.

Aumailley, M., Battaglia, C., Mayer, U., Reinhardt, D., Nischt, R., Timpl, R., and Fox, J.W. (1993). Nidogen mediates the formation of ternary complexes of basement membrane components. Kidney Int. 43, 7–12.

Autschbach, F., Palou, E., Mechtersheimer, G., Rohr, C., Pirotto, F., Gassler, N., Otto, H.F., Schraven, B., and Gayá, A. (1999). Expression of the membrane protein tyrosine phosphatase CD148 in human tissues. Tissue Antigens 54, 485–498.

Avraamides, C.J., Garmy-Susini, B., and Varner, J.A. (2008). Integrins in angiogenesis and lymphangiogenesis. Nat Rev Cancer 8, 604–617.

Baum, P.D., and Garriga, G. (1997). Neuronal migrations and axon fasciculation are disrupted in ina-1 integrin mutants. Neuron 19, 51–62.

Beitel, G.J., Tuck, S., Greenwald, I., and Horvitz, H.R. (1995). The Caenorhabditis elegans gene lin-1 encodes an ETS-domain protein and defines a branch of the vulval induction pathway. Genes & Development 9, 3149–3162.

Berset, T.A. (2005). The C. elegans homolog of the mammalian tumor suppressor Dep-1/Scc1 inhibits EGFR signaling to regulate binary cell fate decisions. Genes & Development 19, 1328–1340.

Berset, T., Hoier, E.F., Battu, G., Canevascini, S., and Hajnal, A. (2001). Notch inhibition of RAS signaling through MAP kinase phosphatase LIP-1 during C. elegans vulval development. Science 291, 1055–1058.

Blanchetot, C., Chagnon, M., Dubé, N., Hallé, M., and Tremblay, M.L. (2005). Substrate-trapping techniques in the identification of cellular PTP targets. Methods 35, 44–53.

Borges, L.G., Seifert, R.A., Grant, F.J., Hart, C.E., Disteche, C.M., Edelhoff, S., Solca, F.F., Lieberman, M.A., Lindner, V., Fischer, E.H., et al. (1996). Cloning and characterization of rat density-enhanced phosphatase-1, a protein tyrosine phosphatase expressed by vascular cells. Circ. Res. 79, 570–580.

Brenner, S. (1974). The genetics of Caenorhabditis elegans. Genetics 77, 71–94.

C. elegans Sequencing Consortium (1998). Genome sequence of the nematode C. elegans: a platform for investigating biology. Science 282, 2012–2018.

Calderwood, D.A. (2004). Integrin activation. J. Cell. Sci. 117, 657–666.

Calderwood, D.A., Fujioka, Y., de Pereda, J.M., García-Alvarez, B., Nakamoto, T., Margolis, B., McGlade, C.J., Liddington, R.C., and Ginsberg, M.H. (2003). Integrin beta cytoplasmic domain interactions with phosphotyrosine-binding domains: a structural prototype for diversity in integrin signaling. Proc. Natl. Acad. Sci. U.S.a. 100, 2272–2277.

Calderwood, D.A., Yan, B., de Pereda, J.M., Alvarez, B.G., Fujioka, Y., Liddington, R.C., and Ginsberg, M.H. (2002). The phosphotyrosine binding-like domain of talin activates integrins. J. Biol. Chem. 277, 21749–21758.

Caswell, P.T., Chan, M., Lindsay, A.J., McCaffrey, M.W., Boettiger, D., and Norman, J.C. (2008). Rab-coupling protein coordinates recycling of alpha5beta1 integrin and EGFR1 to promote cell migration in 3D microenvironments. J. Cell Biol. 183, 143–155.

Chabot, C., Spring, K., Gratton, J.-P., Elchebly, M., and Royal, I. (2009). New role for the protein tyrosine phosphatase DEP-1 in Akt activation and endothelial cell survival. Molecular and Cellular Biology 29, 241–253.

Chen, C., Fenk, L.A., and de Bono, M. (2013). Efficient genome editing in Caenorhabditis elegans by CRISPR-targeted homologous recombination. Nucleic Acids Res.

Chen, H., Zou, Z., Sarratt, K.L., Zhou, D., Zhang, M., Sebzda, E., Hammer, D.A., and Kahn, M.L. (2006). In vivo beta1 integrin function requires phosphorylation-independent regulation by cytoplasmic tyrosines. Genes & Development 20, 927–932.

Chen, N., and Greenwald, I. (2004). The lateral signal for LIN-12/Notch in C. elegans vulval development comprises redundant secreted and transmembrane DSL proteins. Developmental Cell 6, 183–192.

Chen, W.J., Goldstein, J.L., and Brown, M.S. (1990). NPXY, a sequence often found in cytoplasmic tails, is required for coated pit-mediated internalization of the low density lipoprotein receptor. J. Biol. Chem. 265, 3116–3123.

Chen, Z., and Han, M. (2001). C. elegans Rb, NuRD, and Ras regulate lin-39-mediated cell fusion during vulval fate specification. Curr. Biol. 11, 1874–1879.

Chiu, S.-J., Jiang, S.-T., Wang, Y.-K., and Tang, M.-J. (2002). Hepatocyte growth factor upregulates alpha2beta1 integrin in Madin-Darby canine kidney cells: implications in tubulogenesis. J. Biomed. Sci. 9, 261–272.

Chowdhury, S.K., Katta, V., and Chait, B.T. (1990). Electrospray ionization mass spectrometric peptide mapping: a rapid, sensitive technique for protein structure analysis. Biochem. Biophys. Res. Commun. 167, 686–692.

Clark, E.A., and Brugge, J.S. (1995). Integrins and signal transduction pathways: the road taken. Science 268, 233–239.

Coller, B.S., and Shattil, S.J. (2008). The GPIIb/IIIa (integrin alphaIIbbeta3) odyssey: a technology-driven saga of a receptor with twists, turns, and even a bend. Blood 112, 3011–3025.

Cox, D., Brennan, M., and Moran, N. (2010). Nat Rev Drug Discov 2010 Cox. 1–17.

Cram, E.J., Clark, S.G., and Schwarzbauer, J.E. (2003). Talin loss-of-function uncovers roles in cell contractility and migration in C. elegans. J. Cell. Sci. 116, 3871–3878.

Cram, E.J., Shang, H., and Schwarzbauer, J.E. (2006). A systematic RNA interference screen reveals a cell migration gene network in C. elegans. J. Cell. Sci. 119, 4811–4818.

Critchley, D.R. (2000). Focal adhesions - the cytoskeletal connection. Curr. Opin. Cell Biol. 12, 133–139.

Crowe, D.T., Chiu, H., Fong, S., and Weissman, I.L. (1994). Regulation of the avidity of integrin alpha 4 beta 7 by the beta 7 cytoplasmic domain. J. Biol. Chem. 269, 14411–14418.

Cui, M., Chen, J., Myers, T.R., Hwang, B.J., Sternberg, P.W., Greenwald, I., and Han, M. (2006). SynMuv genes redundantly inhibit lin-3/EGF expression to prevent inappropriate vulval induction in C. elegans. Developmental Cell 10, 667–672.

Datta, A., Shi, Q., and Boettiger, D.E. (2001). Transformation of chicken embryo fibroblasts by v-src uncouples beta1 integrin-mediated outside-in but not inside-out signaling. Molecular and Cellular Biology 21, 7295–7306.

Datta, A., Huber, F., and Boettiger, D. (2002). Phosphorylation of beta3 integrin controls ligand binding strength. J. Biol. Chem. 277, 3943–3949.

Desgrosellier, J.S., and Cheresh, D.A. (2010). nrc2748. Nat Rev Cancer 10, 9–22.

Ennis, B.W., Lippman, M.E., and Dickson, R.B. (1991). The EGF receptor system as a target for antitumor therapy. Cancer Invest. 9, 553–562.

Evans, R., Patzak, I., Svensson, L., De Filippo, K., Jones, K., McDowall, A., and Hogg, N. (2009). Integrins in immunity. J. Cell. Sci. 122, 215–225.

Fantl, W.J., Johnson, D.E., and Williams, L.T. (1993). Signalling by receptor tyrosine kinases. Annu. Rev. Biochem. 62, 453–

481.

Farooqui, S., Pellegrino, M.W., Rimann, I., Morf, M.K., Müller, L., Fröhli, E., and Hajnal, A. (2012). Coordinated lumen contraction and expansion during vulval tube morphogenesis in Caenorhabditis elegans. Developmental Cell 23, 494–506.

Fay, D.S., and Yochem, J. (2007). The SynMuv genes of Caenorhabditis elegans in vulval development and beyond. Developmental Biology 306, 1–9.

Felding-Habermann, B. (2003). Integrin adhesion receptors in tumor metastasis. Clin. Exp. Metastasis 20, 203–213.

Ferguson, E.L., and Horvitz, H.R. (1985). Identification and characterization of 22 genes that affect the vulval cell lineages of the nematode Caenorhabditis elegans. Genetics 110, 17–72.

Félix, M.-A. (2012). Caenorhabditis elegans vulval cell fate patterning. Phys Biol 9, 045001.

Finehout, E.J., and Lee, K.H. (2004). An introduction to mass spectrometry applications in biological research. Biochem Mol Biol Educ 32, 93–100.

Flint, A.J., Tiganis, T., Barford, D., and Tonks, N.K. (1997). Development of "substrate-trapping" mutants to identify physiological substrates of protein tyrosine phosphatases. Proc. Natl. Acad. Sci. U.S.a. 94, 1680–1685.

Fox, J.W., Mayer, U., Nischt, R., Aumailley, M., Reinhardt, D., Wiedemann, H., Mann, K., Timpl, R., Krieg, T., and Engel, J. (1991). Recombinant nidogen consists of three globular domains and mediates binding of laminin to collagen type IV. Embo J. 10, 3137–3146.

Friedrichs, K., Ruiz, P., Franke, F., Gille, I., Terpe, H.J., and Imhof, B.A. (1995). High expression level of alpha 6 integrin in human breast carcinoma is correlated with reduced survival. Cancer Res. 55, 901–906.

Frøkjær-Jensen, C., Davis, M.W., Hopkins, C.E., Newman, B.J., Thummel, J.M., Olesen, S.-P., Grunnet, M., and Jorgensen, E.M. (2008). Single-copy insertion of transgenes in Caenorhabditis elegans. Nat. Genet. 40, 1375–1383.

Gettner, S.N., Kenyon, C., and Reichardt, L.F. (1995). Characterization of beta pat-3 heterodimers, a family of essential integrin receptors in C. elegans. J. Cell Biol. 129, 1127–1141.

Giancotti, F.G., and Tarone, G. (2003). Positional control of cell fate through joint integrin/receptor protein kinase signaling. Annu. Rev. Cell Dev. Biol. 19, 173–206.

Gimond, C., van Der Flier, A., van Delft, S., Brakebusch, C., Kuikman, I., Collard, J.G., Fässler, R., and Sonnenberg, A. (1999). Induction of cell scattering by expression of beta1 integrins in beta1-deficient epithelial cells requires activation of members of the rho family of GTPases and downregulation of cadherin and catenin function. J. Cell Biol. 147, 1325–1340.

Girard, L.R., Fiedler, T.J., Harris, T.W., Carvalho, F., Antoshechkin, I., Han, M., Sternberg, P.W., Stein, L.D., and Chalfie, M. (2007). WormBook: the online review of Caenorhabditis elegans biology. Nucleic Acids Res. 35, D472–D475.

Glatter, T., Wepf, A., Aebersold, R., and Gstaiger, M. (2009). An integrated workflow for charting the human interaction proteome: insights into the PP2A system. Mol Syst Biol 5.

Golemis, E.A., and Adams, P.D. (2005). Protein-Protein Interactions (CSHL Press).

Grazia Lampugnani, M., Zanetti, A., Corada, M., Takahashi, T., Balconi, G., Breviario, F., Orsenigo, F., Cattelino, A., Kemler, R., Daniel, T.O., et al. (2003). Contact inhibition of VEGF-induced proliferation requires vascular endothelial cadherin, beta-catenin, and the phosphatase DEP-1/CD148. J. Cell Biol. 161, 793–804.

Guo, W., and Giancotti, F.G. (2004). Integrin signalling during tumour progression. Nat. Rev. Mol. Cell Biol. 5, 816–826.

Guo, W., Pylayeva, Y., Pepe, A., Yoshioka, T., Muller, W.J., Inghirami, G., and Giancotti, F.G. (2006). Beta 4 integrin amplifies ErbB2 signaling to promote mammary tumorigenesis. Cell 126, 489–502.

Hagedorn, E.J., Yashiro, H., Ziel, J.W., Ihara, S., Wang, Z., and Sherwood, D.R. (2009). Integrin Acts Upstream of Netrin Signaling to Regulate Formation of the Anchor Cell•s Invasive Membrane in C. elegans. Developmental Cell 17, 187–198.

Haj, F.G., Markova, B., Klaman, L.D., Böhmer, F.-D., and Neel, B.G. (2003). Regulation of receptor tyrosine kinase signaling by protein tyrosine phosphatase-1B. J. Biol. Chem. 278, 739–744.

Hanahan, D., and Weinberg, R.A. (2011). Hallmarks of cancer: the next generation. Cell 144, 646–674.

Harroch, S., Palmeri, M., Rosenbluth, J., Custer, A., Okigaki, M., Shrager, P., Blum, M., Buxbaum, J.D., and Schlessinger, J. (2000). No obvious abnormality in mice deficient in receptor protein tyrosine phosphatase beta. Molecular and Cellular Biology 20, 7706–7715.

Hertog, den, J., Blanchetot, C., Buist, A., Overvoorde, J., van der Sar, A., and Tertoolen, L.G. (1999). Receptor protein-tyrosine phosphatase signalling in development. Int. J. Dev. Biol. 43, 723–733.

Hieken, T.J., Ronan, S.G., Farolan, M., Shilkaitis, A.L., and Gupta, Das, T.K. (1996). Beta 1 integrin expression: a marker of lymphatic metastases in cutaneous malignant melanoma. Anticancer Res. 16, 2321–2324.

Hirsch, E., Barberis, L., Brancaccio, M., Azzolino, O., Xu, D., Kyriakis, J.M., Silengo, L., Giancotti, F.G., Tarone, G., Fässler, R., et al. (2002). Defective Rac-mediated proliferation and survival after targeted mutation of the beta1 integrin cytodomain. J. Cell Biol. 157, 481–492.

Hoerndli, F.J., Walser, M., Fröhli Hoier, E., de Quervain, D., Papassotiropoulos, A., and Hajnal, A. (2009). A Conserved Function of C. elegans CASY-1 Calsyntenin in Associative Learning. PLoS ONE 4, e4880.

Holsinger, L.J., Ward, K., Duffield, B., Zachwieja, J., and Jallal, B. (2002). The transmembrane receptor protein tyrosine phosphatase DEP1 interacts with p120(ctn). Oncogene 21, 7067–7076.

Hood, J.D., and Cheresh, D.A. (2002). Role of integrins in cell invasion and migration. Nat Rev Cancer 2, 91–100.

Horvitz, H.R., and Sternberg, P.W. (1991). Multiple intercellular signalling systems control the development of the Caenorhabditis elegans vulva. Nature 351, 535–541.

Howe, A., Aplin, A.E., Alahari, S.K., and Juliano, R.L. (1998). Integrin signaling and cell growth control. Curr. Opin. Cell Biol. 10, 220–231.

Hughes, P.E., O'Toole, T.E., Ylänne, J., Shattil, S.J., and Ginsberg, M.H. (1995). The conserved membrane-proximal region of an integrin cytoplasmic domain specifies ligand binding affinity. J. Biol. Chem. 270, 12411–12417.

Hunter, T. (1999). 1-s2.0-S0092867400816888-main. Cell 100, 113–127.

Huyer, G., Liu, S., Kelly, J., Moffat, J., Payette, P., Kennedy, B., Tsaprailis, G., Gresser, M.J., and Ramachandran, C. (1997). Mechanism of inhibition of protein-tyrosine phosphatases by vanadate and pervanadate. J. Biol. Chem. 272, 843–851.

Hynes, R.O. (1992). Integrins: versatility, modulation, and signaling in cell adhesion. Cell 69, 11–25.

Hynes, R.O. (2002). Integrins: bidirectional, allosteric signaling machines. Cell 110, 673–687.

Iuliano, R., Trapasso, F., Le Pera, I., Schepis, F., Samà, I., Clodomiro, A., Dumon, K.R., Santoro, M., Chiariotti, L., Viglietto, G., et al. (2003). An adenovirus carrying the rat protein tyrosine phosphatase eta suppresses the growth of human thyroid carcinoma cell lines in vitro and in vivo. Cancer Res. 63, 882–886.

Ivaska, J., and Heino, J. (2011). Cooperation between integrins and growth factor receptors in signaling and endocytosis. Annu. Rev. Cell Dev. Biol. 27, 291–320.

Jacobson, J.W., and Hartl, D.L. (1985). Coupled instability of two X-linked genes in Drosophila mauritiana: germinal and somatic mutability. Genetics 111, 57–65.

Jacobson, J.W., Medhora, M.M., and Hartl, D.L. (1986). Molecular structure of a somatically unstable transposable element in Drosophila. Proc. Natl. Acad. Sci. U.S.a. 83, 8684–8688.

Jeon, M., and Zinn, K. (2009). Receptor tyrosine phosphatases control tracheal tube geometries through negative regulation of Egfr signaling. Development 136, 3121–3129.

Jeon, M., Scott, M.P., and Zinn, K. (2012). Interactions between Type III receptor tyrosine phosphatases and growth factor receptor tyrosine kinases regulate tracheal tube formation in Drosophila. Biol Open 1, 548–558.

Jia, Z., Barford, D., Flint, A.J., and Tonks, N.K. (1995). Structural basis for phosphotyrosine peptide recognition by protein tyrosine phosphatase 1B. Science 268, 1754–1758.

Johansson, M.W., Larsson, E., Lüning, B., Pasquale, E.B., and Ruoslahti, E. (1994). Altered localization and cytoplasmic domain-binding properties of tyrosine-phosphorylated beta 1 integrin. J. Cell Biol. 126, 1299–1309.

Kamath, R.S., Martinez-Campos, M., Zipperlen, P., Fraser, A.G., and Ahringer, J. (2001). Effectiveness of specific RNA-mediated interference through ingested double-stranded RNA in Caenorhabditis elegans. Genome Biol. 2, RESEARCH0002.

Kang, S.H., and Kramer, J.M. (2000). Nidogen Is Nonessential and Not Required for Normal Type IV Collagen Localization in Caenorhabditis elegans. Mol. Biol. Cell Vol. 11, 3911–3923.

Kappert, K., Paulsson, J., Sparwel, J., Leppänen, O., Hellberg, C., Östman, A., and Micke, P. (2007). Dynamic changes in the expression of DEP-1 and other PDGF receptor-antagonizing PTPs during onset and termination of neointima formation. Faseb J. 21, 523–534.

Katayama, H., Yamamoto, A., Mizushima, N., Yoshimori, T., and Miyawaki, A. (2008). GFP-like proteins stably accumulate in lysosomes. Cell Struct. Funct. 33, 1–12.

Keane, M.M., Lowrey, G.A., Ettenberg, S.A., Dayton, M.A., and Lipkowitz, S. (1996). The protein tyrosine phosphatase DEP-

1 is induced during differentiation and inhibits growth of breast cancer cells. Cancer Res. 56, 4236–4243.

Kelly, W.G., Xu, S., Montgomery, M.K., and Fire, A. (1997). Distinct requirements for somatic and germline expression of a generally expressed Caernorhabditis elegans gene. Genetics 146, 227–238.

Kishihara, K., Penninger, J., Wallace, V.A., Kündig, T.M., Kawai, K., Wakeham, A., Timms, E., Pfeffer, K., Ohashi, P.S., and Thomas, M.L. (1993). Normal B lymphocyte development but impaired T cell maturation in CD45-exon6 protein tyrosine phosphatase-deficient mice. Cell 74, 143–156.

Kornfeld, K. (1997). Vulval development in Caenorhabditis elegans. Trends Genet. 13, 55–61.

Kovalenko, M., Denner, K., Sandström, J., Persson, C., Gross, S., Jandt, E., Vilella, R., Böhmer, F., and Östman, A. (2000). Site-selective dephosphorylation of the platelet-derived growth factor beta-receptor by the receptor-like protein-tyrosine phosphatase DEP-1. J. Biol. Chem. 275, 16219–16226.

Kren, A., Baeriswyl, V., Lehembre, F., Wunderlin, C., Strittmatter, K., Antoniadis, H., Fässler, R., Cavallaro, U., and Christofori, G. (2007). Increased tumor cell dissemination and cellular senescence in the absence of beta1-integrin function. Embo J. 26, 2832–2842.

Krueger, N.X., Streuli, M., and Saito, H. (1990). Structural diversity and evolution of human receptor-like protein tyrosine phosphatases. Embo J. 9, 3241–3252.

la Fuente-García, de, M.A., Nicolás, J.M., Freed, J.H., Palou, E., Thomas, A.P., Vilella, R., Vives, J., and Gayá, A. (1998). CD148 is a membrane protein tyrosine phosphatase present in all hematopoietic lineages and is involved in signal transduction on lymphocytes. Blood 91, 2800–2809.

Law, D.A., DeGuzman, F.R., Heiser, P., Ministri-Madrid, K., Killeen, N., and Phillips, D.R. (1999). Integrin cytoplasmic tyrosine motif is required for outside-in alphaIIbbeta3 signalling and platelet function. Nature 401, 808–811.

Lee, H.-J., Kim, S.-Y., Koh, J.-M., Bok, J., Kim, K.-J., Kim, K.-S., Park, M.-H., Shin, H.-D., Park, B.L., Kim, T.-H., et al. (2007). Polymorphisms and haplotypes of integrinalpha1 (ITGA1) are associated with bone mineral density and fracture risk in postmenopausal Koreans. Bone 41, 979–986.

Lee, M., Cram, E.J., Shen, B., and Schwarzbauer, J.E. (2001). Roles for beta(pat-3) integrins in development and function of Caenorhabditis elegans muscles and gonads. J. Biol. Chem. 276, 36404–36410.

Li, L., and Dixon, J.E. (2000). Form, function, and regulation of protein tyrosine phosphatases and their involvement in human diseases. Semin. Immunol. 12, 75–84.

Li, M., Wu, X., Wang, J., and Pan, Y. (2012). Towards the identification of protein complexes and functional modules by integrating PPI network and gene expression data. BMC Bioinformatics 13, 109.

Liu, S., Calderwood, D.A., and Ginsberg, M.H. (2000). Integrin cytoplasmic domain-binding proteins. J. Cell. Sci. 113 (Pt 20), 3563–3571.

Liu, S., Liang, B., Gao, H., Zhang, F., Wang, B., Dong, X., and Niu, J. (2013). Integrin αvβ6 as a novel marker for diagnosis and metastatic potential of thyroid carcinoma. Head Neck Oncol 5, 7.

Lu, C.F., and Springer, T.A. (1997). The alpha subunit cytoplasmic domain regulates the assembly and adhesiveness of integrin lymphocyte function-associated antigen-1. J. Immunol. 159, 268–278.

Lu, C., Takagi, J., and Springer, T.A. (2001). Association of the membrane proximal regions of the alpha and beta subunit cytoplasmic domains constrains an integrin in the inactive state. J. Biol. Chem. 276, 14642–14648.

Maduro, M., and Pilgrim, D. (1995). Identification and cloning of unc-119, a gene expressed in the Caenorhabditis elegans nervous system. Genetics 141, 977–988.

Makrilia, N., Kollias, A., Manolopoulos, L., and Syrigos, K. (2009). Cell adhesion molecules: role and clinical significance in cancer. Cancer Invest. 27, 1023–1037.

Mallick, P., and Kuster, B. (2010). Proteomics: a pragmatic perspective. Nat. Biotechnol. 28, 695–709.

Margadant, C., Monsuur, H.N., Norman, J.C., and Sonnenberg, A. (2011). Mechanisms of integrin activation and trafficking. Curr. Opin. Cell Biol. 23, 607–614.

Mas-Moruno, C., Rechenmacher, F., and Kessler, H. (2010). Cilengitide: the first anti-angiogenic small molecule drug candidate design, synthesis and clinical evaluation. Anticancer Agents Med Chem 10, 753–768.

Matozaki, T., Suzuki, T., Uchida, T., Inazawa, J., Ariyama, T., Matsuda, K., Horita, K., Noguchi, H., Mizuno, H., and Sakamoto, C. (1994). Molecular cloning of a human transmembrane-type protein tyrosine phosphatase and its expression in gastrointestinal cancers. J. Biol. Chem. 269, 2075–2081.

Mattila, E., Auvinen, K., Salmi, M., and Ivaska, J. (2008). The protein tyrosine phosphatase TCPTP controls VEGFR2 signalling. J. Cell. Sci. 121, 3570–3580.

Mattila, E., Marttila, H., Sahlberg, N., Kohonen, P., Tähtinen, S., Halonen, P., Perälä, M., and Ivaska, J. (2010). Inhibition of receptor tyrosine kinase signalling by small molecule agonist of T-cell protein tyrosine phosphatase. BMC Cancer 10, 7.

Mattila, E., Pellinen, T., Nevo, J., Vuoriluoto, K., Arjonen, A., and Ivaska, J. (2005). Negative regulation of EGFR signalling through integrin-alpha1beta1-mediated activation of protein tyrosine phosphatase TCPTP. Nat. Cell Biol. 7, 78–85.

McCabe, N.P., De, S., Vasanji, A., Brainard, J., and Byzova, T.V. (2007). Prostate cancer specific integrin alphavbeta3 modulates bone metastatic growth and tissue remodeling. Oncogene 26, 6238–6243.

Meighan, C.M., and Schwarzbauer, J.E. (2007). Control of C. elegans hermaphrodite gonad size and shape by vab-3/Pax6-mediated regulation of integrin receptors. Genes & Development 21, 1615–1620.

Mello, C.C., Kramer, J.M., Stinchcomb, D., and Ambros, V. (1991). Efficient gene transfer in C.elegans: extrachromosomal maintenance and integration of transforming sequences. Embo J. 10, 3959–3970.

Miller, L.M., Gallegos, M.E., Morisseau, B.A., and Kim, S.K. (1993). lin-31, a Caenorhabditis elegans HNF-3/fork head transcription factor homolog, specifies three alternative cell fates in vulval development. Genes & Development 7, 933–947.

Mitra, S.K., and Schlaepfer, D.D. (2006). Integrin-regulated FAK-Src signaling in normal and cancer cells. Curr. Opin. Cell Biol. 18, 516–523.

Mohri, A., Kodama, E., Kimura, K.D., Koike, M., Mizuno, T., and Mori, I. (2005). Genetic control of temperature preference in the nematode Caenorhabditis elegans. Genetics 169, 1437–1450.

Mori, I. (1999). Genetics of chemotaxis and thermotaxis in the nematode Caenorhabditis elegans. Annu. Rev. Genet. 33, 399–422.

Moro, L. (2001). Integrin-induced Epidermal Growth Factor (EGF) Receptor Activation Requires c-Src and p130Cas and Leads to Phosphorylation of Specific EGF Receptor Tyrosines. Journal of Biological Chemistry 277, 9405–9414.

Morrison, G.E., Wen, J.Y., Runciman, S., and van der Kooy, D. (1999). Olfactory associative learning in Caenorhabditis elegans is impaired in lrn-1 and lrn-2 mutants. Behav. Neurosci. 113, 358–367.

Mosesson, Y., Mills, G.B., and Yarden, Y. (2008). Derailed endocytosis: an emerging feature of cancer. Nat Rev Cancer 8, 835–850.

Moulder, G.L., Huang, M.M., Waterston, R.H., and Barstead, R.J. (1996). Talin requires beta-integrin, but not vinculin, for its assembly into focal adhesion-like structures in the nematode Caenorhabditis elegans. Mol. Biol. Cell 7, 1181–1193.

Murata, Y., Mori, M., Kotani, T., Supriatna, Y., Okazawa, H., Kusakari, S., Saito, Y., Ohnishi, H., and Matozaki, T. (2010). Tyrosine phosphorylation of R3 subtype receptor-type protein tyrosine phosphatases and their complex formations with Grb2 or Fyn. Genes Cells 15, 513–524.

Nakdimon, I., Walser, M., Fröhli, E., and Hajnal, A. (2012). PTEN negatively regulates MAPK signaling during Caenorhabditis elegans vulval development. PLoS Genet. 8, e1002881.

Nip, J., Shibata, H., Loskutoff, D.J., Cheresh, D.A., and Brodt, P. (1992). Human melanoma cells derived from lymphatic metastases use integrin alpha v beta 3 to adhere to lymph node vitronectin. J. Clin. Invest. 90, 1406–1413.

Nooren, I.M.A., and Thornton, J.M. (2003). Diversity of protein-protein interactions. Embo J. 22, 3486–3492.

Normanno, N., De Luca, A., Bianco, C., Strizzi, L., Mancino, M., Maiello, M.R., Carotenuto, A., De Feo, G., Caponigro, F., and Salomon, D.S. (2006). Epidermal growth factor receptor (EGFR) signaling in cancer. Gene 366, 2–16.

O'Toole, T.E., Ylänne, J., and Culley, B.M. (1995). Regulation of integrin affinity states through an NPXY motif in the beta subunit cytoplasmic domain. J. Biol. Chem. 270, 8553–8558.

Ohno, H., Stewart, J., Fournier, M.C., Bosshart, H., Rhee, I., Miyatake, S., Saito, T., Gallusser, A., Kirchhausen, T., and Bonifacino, J.S. (1995). Interaction of tyrosine-based sorting signals with clathrin-associated proteins. Science 269, 1872–1875.

Olayioye, M.A., Neve, R.M., Lane, H.A., and Hynes, N.E. (2000). The ErbB signaling network: receptor heterodimerization in development and cancer. Embo J. 19, 3159–3167.

Oxley, C.L., Anthis, N.J., Lowe, E.D., Vakonakis, I., Campbell, I.D., and Wegener, K.L. (2008). An integrin phosphorylation switch: the effect of beta3 integrin tail phosphorylation on Dok1 and talin binding. J. Biol. Chem. 283, 5420–5426.

Ozbabacan, S.E.A., Engin, H.B., Gursoy, A., and Keskin, O. (2011). Transient protein-protein interactions. Protein Eng. Des. Sel. 24, 635–648.

Östman, A., Yang, Q., and Tonks, N.K. (1994). Expression of DEP-1, a receptor-like protein-tyrosine-phosphatase, is enhanced with increasing cell density. Proc. Natl. Acad. Sci. U.S.a. 91, 9680–9684.

Page, A.P., and Johnstone, I.L. (2007). The cuticle. WormBook 1–15.

Palka, H.L. (2002). Hepatocyte Growth Factor Receptor Tyrosine Kinase Met Is a Substrate of the Receptor Protein-tyrosine Phosphatase DEP-1. Journal of Biological Chemistry 278, 5728–5735.

Papassotiropoulos, A., Stephan, D.A., Huentelman, M.J., Hoerndli, F.J., Craig, D.W., Pearson, J.V., Huynh, K.D., Brunner, F., Corneveaux, J., Osborne, D., et al. (2006). Common Kibra Alleles Are Associated with Human Memory Performance. Science 314, 475–478.

Pavelec, D.M., Lachowiec, J., Duchaine, T.F., Smith, H.E., and Kennedy, S. (2009). Requirement for the ERI/DICER complex in endogenous RNA interference and sperm development in Caenorhabditis elegans. Genetics 183, 1283–1295.

Pellinen, T. (2006). Integrin traffic. J. Cell. Sci. 119, 3723–3731.

Pellinen, T., Tuomi, S., Arjonen, A., Wolf, M., Edgren, H., Meyer, H., Grosse, R., Kitzing, T., Rantala, J.K., Kallioniemi, O., et al. (2008). Integrin trafficking regulated by Rab21 is necessary for cytokinesis. Developmental Cell 15, 371–385.

Petermann, A., Haase, D., Wetzel, A., Balavenkatraman, K.K., Tenev, T., Gührs, K.-H., Friedrich, S., Nakamura, M., Mawrin, C., and Böhmer, F.-D. (2010). Loss of the Protein-Tyrosine Phosphatase DEP-1/PTPRJ Drives Meningioma Cell Motility. Brain Pathology 21, 405–418.

Pouliot, N., Nice, E.C., and Burgess, A.W. (2001). Laminin-10 mediates basal and EGF-stimulated motility of human colon carcinoma cells via alpha(3)beta(1) and alpha(6)beta(4) integrins. Exp. Cell Res. 266, 1–10.

Puig, O., Caspary, F., Rigaut, G., Rutz, B., Bouveret, E., Bragado-Nilsson, E., Wilm, M., and Séraphin, B. (2001). The tandem affinity purification (TAP) method: a general procedure of protein complex purification. Methods 24, 218–229.

Pytela, R., Pierschbacher, M.D., and Ruoslahti, E. (1985). A 125/115-kDa cell surface receptor specific for vitronectin interacts with the arginine-glycine-aspartic acid adhesion sequence derived from fibronectin. Proc. Natl. Acad. Sci. U.S.a. 82, 5766–5770.

Ramirez, N.E., Zhang, Z., Madamanchi, A., Boyd, K.L., O'Rear, L.D., Nashabi, A., Li, Z., Dupont, W.D., Zijlstra, A., and Zutter, M.M. (2011). The $\alpha_2\beta_1$ integrin is a metastasis suppressor in mouse models and human cancer. J. Clin. Invest. 121, 226–237.

Ramsay, A.G., Keppler, M.D., Jazayeri, M., Thomas, G.J., Parsons, M., Violette, S., Weinreb, P., Hart, I.R., and Marshall, J.F. (2007a). HS1-associated protein X-1 regulates carcinoma cell migration and invasion via clathrin-mediated endocytosis of integrin alphavbeta6. Cancer Res. 67, 5275–5284.

Ramsay, A.G., Marshall, J.F., and Hart, I.R. (2007b). Integrin trafficking and its role in cancer metastasis. Cancer Metastasis Rev. 26, 567–578.

Ricono, J.M., Huang, M., Barnes, L.A., Lau, S.K., Weis, S.M., Schlaepfer, D.D., Hanks, S.K., and Cheresh, D.A. (2009). Specific cross-talk between epidermal growth factor receptor and integrin alphavbeta5 promotes carcinoma cell invasion and metastasis. Cancer Res. 69, 1383–1391.

Robert, V.J.P., Katic, I., and Bessereau, J.-L. (2009). Mos1 transposition as a tool to engineer the Caenorhabditis elegans genome by homologous recombination. Methods 49, 263–269.

Rose, J.K., and Rankin, C.H. (2001). Analyses of habituation in Caenorhabditis elegans. Learn. Mem. 8, 63–69.

Rose, J.K., and Rankin, C.H. (2006). Blocking Memory Reconsolidation Reverses Memory-Associated Changes in Glutamate Receptor Expression. Journal of Neuroscience 26, 11582–11587.

Ruivenkamp, C.A.L., van Wezel, T., Zanon, C., Stassen, A.P.M., Vlcek, C., Csikós, T., Klous, A.M., Tripodis, N., Perrakis, A., Boerrigter, L., et al. (2002). Ptprj is a candidate for the mouse colon-cancer susceptibility locus Scc1 and is frequently deleted in human cancers. Nat. Genet. 31, 295–300.

Ruivenkamp, C., Hermsen, M., Postma, C., Klous, A., Baak, J., Meijer, G., and Demant, P. (2003). LOH of PTPRJ occurs early in colorectal cancer and is associated with chromosomal loss of 18q12–21. Oncogene 22, 3472–3474.

Sacco, F., Tinti, M., Palma, A., Ferrari, E., Nardozza, A.P., van Huijsduijnen, R.H., Takahashi, T., Castagnoli, L., and Cesareni, G. (2009). Tumor Suppressor Density-enhanced Phosphatase-1 (DEP-1) Inhibits the RAS Pathway by Direct Dephosphorylation ofERK1/2 Kinases. J. Biol. Chem. VOL.284, pp.22048–pp.22058.

Sadiq, M.W., Salehpour, M., Forsgard, N., Possnert, G., and Hammarlund-Udenaes, M. (2011). Morphine brain pharmacokinetics at very low concentrations studied with accelerator mass spectrometry and liquid chromatography-tandem mass spectrometry. Drug Metab. Dispos. 39, 174–179.

Saeki, S., Yamamoto, M., and Iino, Y. (2001). Plasticity of chemotaxis revealed by paired presentation of a chemoattractant and starvation in the nematode Caenorhabditis elegans. J. Exp. Biol. 204, 1757–1764.

Sakai, T., Jove, R., Fässler, R., and Mosher, D.F. (2001). Role of the cytoplasmic tyrosines of beta 1A integrins in transformation by v-src. Proc. Natl. Acad. Sci. U.S.a. 98, 3808–3813.

Sakai, T., Zhang, Q., Fässler, R., and Mosher, D.F. (1998). Modulation of beta1A integrin functions by tyrosine residues in the beta1 cytoplasmic domain. J. Cell Biol. 141, 527–538.

Sallee, J.L., and Burridge, K. (2009). Density-enhanced phosphatase 1 regulates phosphorylation of tight junction proteins and enhances barrier function of epithelial cells. J. Biol. Chem. 284, 14997–15006.

Schindler, A.J., and Sherwood, D.R. (2013). Morphogenesis of the C. elegans vulva. Wiley Interdiscip Rev Dev Biol 2, 75–95.

Schlaepfer, D.D., and Hunter, T. (1998). Integrin signalling and tyrosine phosphorylation: just the FAKs? Trends Cell Biol. 8, 151–157.

Schlessinger, J. (2000). Cell signaling by receptor tyrosine kinases. Cell 103, 211–225.

Schwartz, M.A., Schaller, M.D., and Ginsberg, M.H. (1995). Integrins: emerging paradigms of signal transduction. Annu. Rev. Cell Dev. Biol. 11, 549–599.

Senis, Y.A., Tomlinson, M.G., Ellison, S., Mazharian, A., Lim, J., Zhao, Y., Kornerup, K.N., Auger, J.M., Thomas, S.G., Dhanjal, T., et al. (2009). The tyrosine phosphatase CD148 is an essential positive regulator of platelet activation and thrombosis. Blood 113, 4942–4954.

Seshacharyulu, P., Ponnusamy, M.P., Haridas, D., Jain, M., Ganti, A.K., and Batra, S.K. (2012). Targeting the EGFR signaling pathway in cancer therapy. Expert Opin. Ther. Targets 16, 15–31.

Sharma-Kishore, R., White, J.G., Southgate, E., and Podbilewicz, B. (1999). Formation of the vulva in Caenorhabditis elegans: a paradigm for organogenesis. Development 126, 691–699.

Shattil, S.J., Kim, C., and Ginsberg, M.H. (2010). The final steps of integrin activation: the end game. Nat. Rev. Mol. Cell Biol. 11, 288–300.

Shaye, D.D., and Greenwald, I. (2002). Endocytosis-mediated downregulation of LIN-12/Notch upon Ras activation in Caenorhabditis elegans. Nature 420, 686–690.

Shultz, L.D., Schweitzer, P.A., Rajan, T.V., Yi, T., Ihle, J.N., Matthews, R.J., Thomas, M.L., and Beier, D.R. (1993). Mutations at the murine motheaten locus are within the hematopoietic cell protein-tyrosine phosphatase (Hcph) gene. Cell 73, 1445–1454.

Silva, R., D'Amico, G., Hodivala-Dilke, K.M., and Reynolds, L.E. (2008). Integrins: the keys to unlocking angiogenesis. Arterioscler. Thromb. Vasc. Biol. 28, 1703–1713.

Simmer, F., Tijsterman, M., Parrish, S., Koushika, S.P., Nonet, M.L., Fire, A., Ahringer, J., and Plasterk, R.H.A. (2002). Loss of the putative RNA-directed RNA polymerase RRF-3 makes C. elegans hypersensitive to RNAi. Curr. Biol. 12, 1317–1319.

Sims, P.J., Ginsberg, M.H., Plow, E.F., and Shattil, S.J. (1991). Effect of platelet activation on the conformation of the plasma membrane glycoprotein IIb-IIIa complex. J. Biol. Chem. 266, 7345–7352.

Smart, C.E., Askarian Amiri, M.E., Wronski, A., Dinger, M.E., Crawford, J., Ovchinnikov, D.A., Vargas, A.C., Reid, L., Simpson, P.T., Song, S., et al. (2012). Expression and function of the protein tyrosine phosphatase receptor J (PTPRJ) in normal mammary epithelial cells and breast tumors. PLoS ONE 7, e40742.

Smith-Garvin, J.E., Koretzky, G.A., and Jordan, M.S. (2009). T cell activation. Annu. Rev. Immunol. 27, 591–619.

Spencer, T.E., Johnson, G.A., Bazer, F.W., and Burghardt, R.C. (2004). Implantation mechanisms: insights from the sheep. Reproduction 128, 657–668.

Springer, T.A. (1994). Traffic signals for lymphocyte recirculation and leukocyte emigration: the multistep paradigm. Cell 76, 301–314.

Sternberg, P.W. (1988). Lateral inhibition during vulval induction in Caenorhabditis elegans. Nature 335, 551–554.

Sternberg, P.W., and Han, M. (1998). Genetics of RAS signaling in C. elegans. Trends Genet. 14, 466–472.

Sternberg, P.W., and Horvitz, H.R. (1986). Pattern formation during C. elegans vulval induction. Cell 44, 761–772.

Sternberg, P.W., and Horvitz, H.R. (1989). The combined action of two intercellular signaling pathways specifies three cell fates during vulval induction in C. elegans. Cell 58, 679–693.

Sternberg, P.W. (2005). Vulval development. WormBook 1–28.

Stewart, P.L., and Nemerow, G.R. (2007). Cell integrins: commonly used receptors for diverse viral pathogens. Trends Microbiol. 15, 500–507.

Stinchcomb, D.T., Shaw, J.E., Carr, S.H., and Hirsh, D. (1985). Extrachromosomal DNA transformation of Caenorhabditis elegans. Molecular and Cellular Biology 5, 3484–3496.

Sulston, J.E., and Horvitz, H.R. (1977). Post-embryonic cell lineages of the nematode, Caenorhabditis elegans. Developmental Biology 56, 110–156.

Sulston, J.E., and White, J.G. (1980). Regulation and cell autonomy during postembryonic development of Caenorhabditis elegans. Developmental Biology 78, 577–597.

Tadokoro, S., Shattil, S.J., Eto, K., Tai, V., Liddington, R.C., de Pereda, J.M., Ginsberg, M.H., and Calderwood, D.A. (2003). Talin binding to integrin beta tails: a final common step in integrin activation. Science 302, 103–106.

Takagi, J., Petre, B.M., Walz, T., and Springer, T.A. (2002). Global conformational rearrangements in integrin extracellular domains in outside-in and inside-out signaling. Cell 110, 599–511.

Takahashi, K., Mernaugh, R.L., Friedman, D.B., Weller, R., Tsuboi, N., Yamashita, H., Quaranta, V., and Takahashi, T. (2012). Thrombospondin-1 acts as a ligand for CD148 tyrosine phosphatase. Proc. Natl. Acad. Sci. U.S.a. 109, 1985–1990.

Takahashi, T. (2006). A monoclonal antibody against CD148, a receptor-like tyrosine phosphatase, inhibits endothelial-cell growth and angiogenesis. Blood 108, 1234–1242.

Tamkun, J.W., DeSimone, D.W., Fonda, D., Patel, R.S., Buck, C., Horwitz, A.F., and Hynes, R.O. (1986). Structure of integrin, a glycoprotein involved in the transmembrane linkage between fibronectin and actin. Cell 46, 271–282.

Tan, P.B., Lackner, M.R., and Kim, S.K. (1998). MAP kinase signaling specificity mediated by the LIN-1 Ets/LIN-31 WH transcription factor complex during C. elegans vulval induction. Cell 93, 569–580.

Tangye, S.G., Phillips, J.H., Lanier, L.L., de Vries, J.E., and Aversa, G. (1998). CD148: a receptor-type protein tyrosine phosphatase involved in the regulation of human T cell activation. J. Immunol. 161, 3249–3255.

Tarcic, G., Boguslavsky, S.K., Wakim, J., Kiuchi, T., Liu, A., Reinitz, F., Nathanson, D., Takahashi, T., Mischel, P.S., Ng, T., et al. (2009). An Unbiased Screen Identifies DEP-1 Tumor Suppressor as a Phosphatase Controlling EGFR Endocytosis. Current Biology 19, 1788–1798.

Tax, F.E., Thomas, J.H., Ferguson, E.L., and Horvitz, H.R. (1997). Identification and characterization of genes that interact with lin-12 in Caenorhabditis elegans. Genetics 147, 1675–1695.

Thomas, P.E., Wharram, B.L., Goyal, M., Wiggins, J.E., Holzman, L.B., and Wiggins, R.C. (1994). GLEPP1, a renal glomerular epithelial cell (podocyte) membrane protein-tyrosine phosphatase. Identification, molecular cloning, and characterization in rabbit. J. Biol. Chem. 269, 19953–19962.

Tonks, N.K. (2003). PTP1B: from the sidelines to the front lines! FEBS Letters 546, 140–148.

Tonks, N.K. (2006). Protein tyrosine phosphatases: from genes, to function, to disease. Nat. Rev. Mol. Cell Biol. 7, 833–846.

Trapasso, F., Iuliano, R., Boccia, A., Stella, A., Visconti, R., Bruni, P., Baldassarre, G., Santoro, M., Viglietto, G., and Fusco, A. (2000). Rat protein tyrosine phosphatase eta suppresses the neoplastic phenotype of retrovirally transformed thyroid cells through the stabilization of p27(Kip1). Molecular and Cellular Biology 20, 9236–9246.

Trapasso, F., Drusco, A., Costinean, S., Alder, H., Aqeilan, R.I., Iuliano, R., Gaudio, E., Raso, C., Zanesi, N., Croce, C.M., et al. (2006). Genetic ablation of Ptprj, a mouse cancer susceptibility gene, results in normal growth and development and does not predispose to spontaneous tumorigenesis. DNA Cell Biol. 25, 376–382.

Trapasso, F., Yendamuri, S., Dumon, K.R., Iuliano, R., Cesari, R., Feig, B., Seto, R., Infante, L., Ishii, H., Vecchione, A., et al. (2004). Restoration of receptor-type protein tyrosine phosphatase eta function inhibits human pancreatic carcinoma cell growth in vitro and in vivo. Carcinogenesis 25, 2107–2114.

Troemel, E.R., Sagasti, A., and Bargmann, C.I. (1999). Lateral signaling mediated by axon contact and calcium entry regulates asymmetric odorant receptor expression in C. elegans. Cell 99, 387–398.

Trzebiatowska, A., Topf, U., Sauder, U., Drabikowski, K., and Chiquet-Ehrismann, R. (2008). Caenorhabditis elegans teneurin, ten-1, is required for gonadal and pharyngeal basement membrane integrity and acts redundantly with integrin ina-1 and dystroglycan dgn-1. Mol. Biol. Cell 19, 3898–3908.

Tsuboi, N., Utsunomiya, T., Roberts, R.L., Ito, H., Takahashi, K., Noda, M., and Takahashi, T. (2008). The tyrosine phosphatase CD148 interacts with the p85 regulatory subunit of phosphoinositide 3-kinase. Biochem. J. 413, 193.

Ulmer, T.S., Yaspan, B., Ginsberg, M.H., and Campbell, I.D. (2001). NMR analysis of structure and dynamics of the cytosolic tails of integrin alpha IIb beta 3 in aqueous solution. Biochemistry 40, 7498–7508.

Upla, P., Marjomäki, V., Kankaanpää, P., Ivaska, J., Hyypiä, T., Van Der Goot, F.G., and Heino, J. (2004). Clustering induces a lateral redistribution of alpha 2 beta 1 integrin from membrane rafts to caveolae and subsequent protein kinase C-dependent internalization. Mol. Biol. Cell 15, 625–636.

Voldborg, B.R., Damstrup, L., Spang-Thomsen, M., and Poulsen, H.S. (1997). Epidermal growth factor receptor (EGFR) and EGFR mutations, function and possible role in clinical trials. Ann. Oncol. 8, 1197–1206.

Wang, M., and Sternberg, P.W. (2001). Pattern formation during C. elegans vulval induction. Curr. Top. Dev. Biol. 51, 189–220.

Wen, J.Y., Kumar, N., Morrison, G., Rambaldini, G., Runciman, S., Rousseau, J., and van der Kooy, D. (1997). Mutations that prevent associative learning in C. elegans. Behav. Neurosci. 111, 354–368.

White, D.J., Puranen, S., Johnson, M.S., and Heino, J. (2004). The collagen receptor subfamily of the integrins. Int. J. Biochem. Cell Biol. 36, 1405–1410.

Whiteford, J.R., Xian, X., Chaussade, C., Vanhaesebroeck, B., Nourshargh, S., and Couchman, J.R. (2011). Syndecan-2 is a novel ligand for the protein tyrosine phosphatase receptor CD148. Mol. Biol. Cell 22, 3609–3624.

Willard, H.H. (1988). Instrumental Methods of Analysis (Wadsworth Publishing Company).

Williams, B.D., and Waterston, R.H. (1994). Genes critical for muscle development and function in Caenorhabditis elegans identified through lethal mutations. J. Cell Biol. 124, 475–490.

Wood, W.B. (1988). The Nematode Caenorhabditis elegans (Cold Spring Harbor Laboratory Pr).

Woodside, D.G., Liu, S., and Ginsberg, M.H. (2001). Integrin activation. Thromb. Haemost. 86, 316–323.

Xiao, T., Takagi, J., Coller, B.S., Wang, J.-H., and Springer, T.A. (2004). Structural basis for allostery in integrins and binding to fibrinogen-mimetic therapeutics. Nature 432, 59–67.

Xiong, J.P., Stehle, T., Diefenbach, B., Zhang, R., Dunker, R., Scott, D.L., Joachimiak, A., Goodman, S.L., and Arnaout, M.A. (2001). Crystal structure of the extracellular segment of integrin alpha Vbeta3. Science 294, 339–345.

Xu, X., Ahn, J.H., Tam, P., Yu, E.J., Batra, S., Cram, E.J., and Lee, M. (2010). Analysis of conserved residues in the betapat-3 cytoplasmic tail reveals important functions of integrin in multiple tissues. Dev. Dyn. 239, 763–772.

Yamada, K.M., and Even-Ram, S. (2002). Integrin regulation of growth factor receptors. Nat. Cell Biol. 4, E75–E76.

Yang, C., Zeisberg, M., Lively, J.C., Nyberg, P., Afdhal, N., and Kalluri, R. (2003). Integrin alpha1beta1 and alpha2beta1 are the key regulators of hepatocarcinoma cell invasion across the fibrotic matrix microenvironment. Cancer Res. 63, 8312–8317.

Ye, F., Hu, G., Taylor, D., Ratnikov, B., Bobkov, A.A., McLean, M.A., Sligar, S.G., Taylor, K.A., and Ginsberg, M.H. (2010). Recreation of the terminal events in physiological integrin activation. J. Cell Biol. 188, 157–173.

Ylänne, J., Chen, Y., O'Toole, T.E., Loftus, J.C., Takada, Y., and Ginsberg, M.H. (1993). Distinct functions of integrin alpha and beta subunit cytoplasmic domains in cell spreading and formation of focal adhesions. J. Cell Biol. 122, 223–233.

Yochem, J., Weston, K., and Greenwald, I. (1988). The Caenorhabditis elegans lin-12 gene encodes a transmembrane protein with overall similarity to Drosophila Notch. Nature 335, 547–550.

Yoo, A.S., Bais, C., and Greenwald, I. (2004). Crosstalk between the EGFR and LIN-12/Notch pathways in C. elegans vulval development. Science 303, 663–666.

Zaidel-Bar, R., Milo, R., Kam, Z., and Geiger, B. (2007). A paxillin tyrosine phosphorylation switch regulates the assembly and form of cell-matrix adhesions. J. Cell. Sci. 120, 137–148.

Zhang, L., Martelli, M.L., Battaglia, C., Trapasso, F., Tramontano, D., Viglietto, G., Porcellini, A., Santoro, M., and Fusco, A. (1997). Thyroid cell transformation inhibits the expression of a novel rat protein tyrosine phosphatase. Exp. Cell Res. 235, 62–70.

Zhang, X., and Greenwald, I. (2011). Spatial regulation of lag-2 transcription during vulval precursor cell fate patterning in Caenorhabditis elegans. Genetics 188, 847–858.

Zhang, Y., Lu, H., and Bargmann, C.I. (2005). Pathogenic bacteria induce aversive olfactory learning in Caenorhabditis elegans. Nature 438, 179–184.

Zhu, J.W., Brdicka, T., Katsumoto, T.R., Lin, J., and Weiss, A. (2008). Structurally distinct phosphatases CD45 and CD148 both regulate B cell and macrophage immunoreceptor signaling. Immunity 28, 183–196.

7

Appendix

7.1 Abbreviations

1°	Primary
2°	Secondary
3°	Tertiary
A	Alanin
AC	Anchor cell
APF	Adjacent primery fate
C. elegans	*Caenorhabditis elegans*
cDNA	complementary DNA
D	Aspartic acid
DEP-1	Density enhanced phosphatase 1
DN	Dominant-negative
DNA	Desoxyribonucleic acid
dNTP	Desoxyribonukleosidtriphosphate
Dpy	dumpy (shortened body)
DSB	Double strand break
DTT	Dithiothreitol
ECM	Extra eellular matrix
E. coli	*Escherichia coli*
ETA	Ethylendiamine tetraacetic acid
EGF	Epidermal growth factor
EGFR	Epidermal growth factor receptor
EMS	Ethyl methyl sulfonate
ER	Endoplasmatic reticulum
EtOH	Ethanol
F	Phenylalanine
F1	first filial generation
F2	second filial generation
FAK	Focal adhesion kinase
FLP	Flippase
FRT	FLP recognition targets
FRAP	Fluorescence recovery after photobleaching
gf	gain of function
GFP	Green fluorescent protein
GFR	Growth factor receptor
GST	Gluthatione S-transferase
HA	Haemagglutinin
HPLC	High performance liquid chromatography
HRP	Horse radish peroxidase
HS	Haemagglutinin-StrepTactin-III
IPTG	Isopropyl-β-D-thiogalactopyranosid
kD	kilo dalton
l	Liter

LC-MS/MS	Liquid chromatography-tandem mass spectrometry
LET	Lethal
lf	loss of function
LIN	Lineage defective
L1-4	larval stages 1-4
µl	Microliter
µm	Micrometer
M	Molar
mm	Milimeter
MAPK	Mitogen-activated protein kinase
MosTic	*Mos1* excision-induced transgene-instructed gene conversion
MS	Mass spectrometry
Muv	Multivulva
N2	*C. elegans* wild-type strain
ng	Nanogramm
NPxY	Asp-Pro-X-Tyr
P0	parental generation
PAGE	polyacrylamide gel electrophoresis
PAT	Paralysed arrest at two-fold
PCR	Polymerase chain reaction
PI3K	Phosphoinositide 3-kinase
PTP	Phosphotyrosine phosphatase
Pvl	Protruding vulva
RAS	Rat sarcoma
rf	reduction of function
RT	Room temperature
RNAi	RNA interference
Rol	Roller (rolling movement)
Strep	StrepTactin
SDS	Sodium dodecyl sulfate
TAP	Tandem affinity-purification
TBE	Tris-Borat-EDTA
TBS	Tris Buffered Saline
TM	Transmembrane
Tris	Tris[hydroxymethyl]aminomethane
Unc	Uncoordinated
UTR	Untranslated region
VPC	Vulval precursor cell
Vul	Vulvaless
wt	wild-type
Y	Tyrosine

7.2 Curriculum vitae

Personal Data

Name:	Michael Simon WALSER
Day of birth:	October 21, 1981
Nationality:	Swiss
Hometown:	Teufen AR (CH)
Matriculation No.:	02-701-738

Education

2007 - 2013	**PhD Dr. sc. nat.** Doctoral thesis: "Mass Spectrometry-Based Approaches to Identify Novel Interaction Partners of the Tyrosine Phosphatase DEP-1". Carried out under the supervision of Prof. Dr. Alex Hajnal, Institute of Molecular Life Sciences, University of Zurich, Switzerland.
Summer 2007	Project work at Wenner-Gren-Institute Project title: "Localization and Function of PPK11 in the Drosophila melanogaster Trachelal System". Carried out in the laboratory of Prof. Dr. Christos Samakovlis, Stockholm University, Sweden.
2005 - 2007	**Master of Science in Developmental Biology** Master's Thesis: "Sensitized Screens for Genes Mediating Lateral Signaling During Vulval Development in *C. elegans*". Carried out under the Supervision of Prof. Dr. Alex Hajnal, Institute of Zoology, University of Zurich, Switzerland.
2002 - 2005	**Bachelor of Science in Biology** University of Zurich, Switzerland.
1997 - 2002	**Matura Typus L** (Music, French, English) at Seminar Unterstrass, Zurich, Switzerland.
1995 - 1997	Secondary School, Zurich, Switzerland.
1989 - 1995	Primary School, Zurich, Switzerland.

Publications

"A conserved function of *C. elegans* CASY-1 calsyntenin in associative learning"
Frédéric J. Hoerndli, Michael Walser, Erika Fröhli Hoier, Dominique de Quervain, Andreas Papassotiropoulos and Alex Hajnal.
PLoS ONE. 2009; 4(3): e4880

"PTEN Negatively Regulates MAPK Signaling during *Caenorhabditis elegans* Vulval Development"
Itay Nakdimon, Michael Walser, Erika Fröhli, Alex Hajnal.
PLoS Genetics, 2012 August; 8(8): e1002881

Poster presentations

"Sensitized screens for genes mediating lateral signaling during vulval development".
Michael Walser, Sara Vassalli, Ivo Rimann, Alex Hajnal.
International *C. elegans* Meeting in Los Angeles, USA, 2007

"Analysis of *C. elegans* behavior in mutants of genes associated with human episodic memory performance"
Michael Walser, Frédéric J. Hoerndli, Dominique de Quervain, Andreas Papassotiropoulos, Alex Hajnal.
European *C. elegans* Meeting in Seville, Spain, 2008

"Mass Spectrometry Based Approach to Identify Physiological Substrates of the Tyrosine Phosphatase DEP-1"
Michael Walser, Alex Hajnal.
5th annual retreat of the MLS PhD in Flumserberg Tannenboden, Switzerland, 2008

"Two Mass Spectrometry Based Approaches to Identify Physiological Substrates of the Tyrosine Phosphatase DEP-1"
Michael Walser, Alex Hajnal.
6th annual retreat of the MLS PhD program in Interlakenn, Switzerland, 2008

"A Mass Spectrometry-Based Approach to Identify New Interaction Partners of the Tyrosine Phosphatase DEP-1"
Michael Walser and Alex Hajnal.
International *C. elegans* Meeting in Los Angeles, USA, 2009

"A Mass Spectrometry-Based Approach to Identify New Interaction Partners of the Tyrosine Phosphatase DEP-1"
Michael Walser and Alex Hajnal.
EMBO Conference Series – *C. elegans*: Development and Gene Expression 2010 in Heidelberg, Germany, 2010.

"PAT-2/PAT-3 – Two Novel Substrates of the Tyrosine Phosphatase DEP-1"
Michael Walser and Alex Hajnal.
The 4th EMBO Meeting in Nice, France, 2012.

"The *C. elegans* β-Integrin PAT-3 is a substrate of the Tyrosine Phosphatase DEP-1"
Michael Walser and Alex Hajnal
The 5th EMBO Meeting in Amsterdam, Netherlands, 2013.

Teaching experiences

2003 - 2004	Undergraduate course assistant in "Practical Course in Chemistry" Institute of Chemistry, University of Zurich
2006 - date	Assistant in various courses for M.Sc. biology and medical student Bio 323: "Modern genetic and genomic" Bio 326: "Experimental Development Biology" Medical course: "Zellwachstum und Zelltod in *C. elegans*"
2009	Supervision of a "Maturarbeit" "Aufreinigen und Testen von Antikörpern im Fadenwurm *C. elegans* – ein Forschungsprojekt an der Universität Zürich". Martina Kalt, Kantonsschule Wettingen, Switzerland.
2011 - 2012	Supervision of a M.Sc. project "Identification of ERM-1/MADD-"/DAF-18 interaction partners by mass spectrometry in *C. elegans*". Anina Schneider, Institute of Molecular Life Sciences, University of Zurich, Switzerland.
2009 - date	Teacher at the Life Science Learning Center "*C. elegans* – Ein kleiner Wurm ganz gross". Life Science Learning Center, University of Zurich, Switzerland.

7.3 Acknowledgements

First of all, I would like to thank Prof. Dr. Alex Hajnal for his supervision of this study, for his interest and confidence in my work, and for his moral support. He was an excellent boss, having the perfect mix of giving me the freedom to work independently, but also setting boundaries to drive my work in a successful direction.
Also I would like to give thanks to all the former and present members of the Hajnal- and Hengartner lab – especially to Erika Fröhli, Claudia Walser and Tobias Schmid – for the support and discussions they shared with me throughout the last years, for the great atmosphere in the lab and for all the coffe breaks, barbeques and collective activities outside the university.
Further thanks also goes to the members of my thesis committee, Prof. Dr. Fritz Müller, Prof. Dr. Michael Hengartner and Prof. Dr. Gert Jansen, for their support, good discussions and helpful suggestions during my PhD studies.
I also thank Irene for her support and all organizational issues, and Franziska Pfistner, Louisa Müller, Daniel Widmer, and Juan Escobar for their help with this thesis.
Further, I am very grateful for the help and support from Paolo Nanni during the MS analyses, and Claudia Fortes and Bernd Roschitzki from the FGCZ for their advice and help.
I thank Werner Boll for his help with the confocal spinning disc microscope, Flora Nicholls for the immunization of the rabbits, Martina Kalt for helping me with the DEP-1 antibody purification, Elisabeth Fischer , Charlotte Lambert and Christoph Umricht for their assistance with the *MosTic* experiments, Jonas Hartmann for his help making the histograms, and Anina Schneider for working with me during her master studies.
Further, I would like to thank Dane for the great time we spent at the university and for the wonderful experiences during scubadiving, to Sabine for being such a great friend for so many years and for the support in all situations, to Lorenz, Claudia, Adrian, Bianca for the great adventures, and several others who made my life happier outside the lab.
A special thanks goes to my parents and my brother Kaspar, who always supported and encouraged me in what I did. A very warm thanks also goes to Franziska for her tireless motivation, for accepting me as I am, and for sharing the past couple of years with me. And last but not least I would like to thank my Cello, the SJSO, AOZ and ALSO, and all the great composers enabling me to experience all the magical moments on stage that gave me the power to do this work.

«*Zurück vom Ring!*»